CRANFIELD UNIVERSITY

ROBERTA D'AURELIO

DEVELOPMENT OF NANOMIP BASED SENSORS FOR DRUGS OF ABUSE DETECTION

SCHOOL OF AEROSPACE, TRANSPORT AND MANUFACTURING

PhD Thesis
Academic Year: 2016 - 2018

Supervisors: Prof Ibtisam E. Tothill
Dr Iva Chianella

February 2018

CRANFIELD UNIVERSITY

SCHOOL OF AEROSPACE, TRANSPORT AND MANUFACTURING

PhD Thesis

Academic Year 2016 - 2018

ROBERTA D'AURELIO

DEVELOPMENT OF NANOMIP BASED SENSORS FOR DRUGS OF ABUSE DETECTION

Supervisors: Prof Ibtisam E. Tothill
Dr Iva Chianella
February 2018

This thesis is submitted in partial fulfilment of the requirements for the degree of Doctor of Philosophy

ABSTRACT

This work presents the development of portable, yet highly sensitive and specific, sensor based on NanoMIPs EIS for the detection of cocaine and morphine at trace levels (sub-ppm). The molecularly imprinted polymer nanoparticles (nanoMIPs) were synthesised as the sensing elements using solid-phase synthesis approach at the University of Leicester. Cocaine nanoMIPs and morphine nanoMIPs particle size (d_H) were measured using Dynamic Light Scattering (DLS) and were found to be 168.80±68.73 nm and 170.09±54.75 nm for cocaine nanoMIP and morphine nanoMIP respectively, thus highlighting a small batch to batch variations.

The nanoMIPs were then covalently attached to the conventional screen-printed electrode (SPE), thus yielding a nanoMIP EIS sensor. The Faradic Electrochemical Impedance Spectroscopy (EIS) was applied to detect the analyte binding events, having 10 mM $[Fe(CN)_6]^{3-/4-}$ in MOPS (10 mM, pH 7.4) as redox couple solution. The EIS was recorded at a 0.12 V potential over the frequency range from 0.1 Hz to 50 kHz with a modulation voltage of 10 mV.

The cocaine nanoMIP EIS sensor, fabricated onto SPE, was optimised and was able to detect cocaine hydrochloride (salt form) dissolved in 10 mM MOPS (pH 7.4) in the linear range of 0.1 – 50 ng mL^{-1} (R^2=0.984) and with a LOD equal to 0.24 ng mL^{-1}. The optimisation studies on the surface blocking agents guaranteed the absence of cross-reactivity towards other drugs, such as morphine and other cocaine adulterants, such as levamisole, caffeine and, partially, mannitol. The optimised sensor and assay conditions were replicated using interdigitated electrode (IDE), achieving an LOD (2.5 ng mL^{-1}), which will requires further optimisation.

Analogously, the morphine nanoMIP EIS sensor, fabricated onto SPE, was optimised and tested against morphine salt dissolved in MOPS (pH 7.4) (0.1 – 50 ng mL^{-1}). The sensor was able to detect morphine in the linear range of 0.1- 10 ng mL^{-1} (R^2 = 0.977) and achieving a LOD as low as 0.109 ng mL^{-1}. The optimised sensor was replicated using IDE, placed in a custom-made 3D printed IDE cable holder. The sensor achieved an LOD of 0.114 ng mL^{-1} in a linear range of 0.01 to 5 ng mL^{-1}.

Furthermore, a QCM platform with a fully automated microfluidic system was employed in this work to develop a multiplexing nanoMIPs QCM sensor for cocaine and morphine detection. The morphine nanoMIPs and cocaine nanoMIPs were respectively immobilised on spot 1 and spot 2 of a QCM sensor chip. Due to the required QCM signal enhancement, morphine and cocaine were separately adsorbed onto 40 nm gold nanoparticles (AuNPs). Increasing concentration (250 ng mL^{-1} to 50 µg mL^{-1}) of each drug conjugated AuNPs were prepared in PBS (pH 7.4) and injected onto the nanoMIP QCM sensor. The nanoMIPs QCM sensor was able to detect morphine-AuNPs and cocaine-AuNPs, without any detectable cross-reactivity events, with the respective LOD equal to 0.191 µg mL^{-1} and 0.360 µg mL^{-1}. The morphine-AuNPs and cocaine-AuNPs detection binding data were fitted to 1:1 Langmuir binding model and the average (±SD) values of the K_D were equal to 0.647±0.340 µM and 0.225±0.197 µM respectively, thus providing insight on the affinity binding.

All the nanoMIPs sensors developed in this work are cheap, easy-to-use and portable (in the case of EIS) screening methods for drugs of abuse detection, thus being a valuable competitor to the current on-site screening methods

Keywords:

Electrochemical Impedance Spectroscopy (EIS), Molecularly Imprinted Polymers Nanoparticles (nanoMIPs), Drugs of Abuse, Gold nanoparticles (AuNPs), Quartz Cristal Microbalance (QCM).

To all the victims of criminal activities.

To my cat, Mojito.

ACKNOWLEDGEMENT

I would like to thank with all my heart Prof Sam Tothill for giving me the opportunity to enrol in this PhD, for the excellent supervision, for all the support, friendship and trust she gave me, especially in the critical moments of this challenging PhD. Her positive attitude and wise advices helped me to achieve a dream I put in stand-by long time ago and to enrich my professional career. I would like to acknowledge Dr Iva Chianella for her supervision, support and friendship throughout the whole PhD.
The financial support received for this research is gratefully acknowledged from the European Commission, HORIZON 2020 - Innovation Action (ID: 653839).

I would like to thank Dr Jack Goode for the helpful introduction on IES biosensor platform. I would like to thanks Dr Kimpton and Dr Liu for their help with the surface analysis. I would also like to thank the lab manager Dr Sofia Foukaraki for her friendship, support and guidance in the lab risk assessment.

My special thanks goes to my PhD mates Noor Masdor, Shas Wignarajah, Antonio Rendon Romero, who have been always friendly and supportive and with whom I had excellent exchange of ideas and knowledge. A special thanks goes to Antonio for his help with the 3D printing cable holder, which was developed in this work.

I would also like to thanks Dima, Paulina, Maria, Francesca, Tymėle, Dimitris and all the other Cranfield friends who always supported and encouraged me throughout my PhD.

Above all, my biggest thanks goes to my Family, including my cat, Mojito, for their understanding, patience, support and encouragement in all the personal and professional decisions I took before and during the PhD course.

TABLE OF CONTENTS

LIST OF FIGURES

LIST OF TABLES

LIST OF EQUATIONS

LIST OF ABBREVIATIONS

2,4-DNT	2,4-dinitro toluene
AA	Allyl amine
AAS	Anabolic androgen steroids
AC	Alternating current
ADHD	Attention deficit hyperactivity disorder
AFM	Atomic-force microscopy
ANOVA	Analysis of variance
APTES	(3-aminopropyl)triethoxysilane
AS	Anabolic steroids
ATS	Amphetamine-type stimulant
AuNP	Gold Nanoparticles
AuNPs	gold colloidal nanoparticles
AV	Alternating voltage
BMK	Benzyl methyl ketone
BSA	bovine serum albumin
CBD	cannabidiol
CBDA	cannabidiolic acid
CBG	cannabigerol;
CBGA	cannabigerolic acid
CBN	cannabinol
CDTPA	4-cyano-4-[(dodecylsulfanylthiocarbonyl)sulfanyl]pentanoic acid
CE	Capillary electrophoresis
CL	Control line
CNS	Central nervous system
CP	Carbon paste
CPE	Constant phase element
CT	Computed tomography
CV	Cyclic voltammetry
DA*HCl	Dopamine hydrochloride
DALYs	Disability-Adjusted Life Years
DART	Direct Analysis in Real Time
DCC	Diclyclohexylcarbodiimide
DLS	Dynamic light scattering
DMF	N,N-dimethylformamide
DMSO	Dimethylsulfoxide
ECL-AB	electrogenerated chemiluminescence aptamer-based
EDC	1-ethyl-3-(3-dimethylaminopropyl) carbodiimide
EIS	Electrochemical impedance Spectroscopy
ELISA	Enzyme-linked immunosorbent assay
EMCDDA	European Monitoring Centre for Drugs and Drug Addiction
EMIT	Enzyme multiplied immunoassay technique
EtOH	Ethanol
FPIA	Fluorescence Polarization Immunoassay

FRA	Frequency response analyser
FRET	Fluorescence resonance energy transfer
GC	Gas chromatography
GlyMO	(3-glycidyloxypropyl)trimethoxysilane
HPLC	High-performance liquid chromatography
HPLC	High-Performance Liquid Chromatography
HPLC-DAD	High-Performance Liquid Chromatography with Diode-Array Detection
IA	Immuno Assay
IDE	Interdigitated electrode
IMS	Ion Mobility Spectroscopy
INN	International Non-proprietary Name
IUPAC	International Union of Pure and Applied Chemistry
KOH	Potassium Hydroxide
LC	Liquid chromatography
LEA	Law enforcement agencies
LOD	Limit of detection
MAm	Methacrylamide
MeOH	Methanol
MES	2-(N-morpholino)ethanesulfonic acid
MIP	Molecularly imprinted polymer
MO	Morphine
MOPS	3-(N-Morpholino)propanesulfonic acid
MS	Mass spectrometry
MUDA	11-mercaptoundecanoic acid
NanoMIP	Molecular Imprinted Polymers nanoparticles
NFI	Netherlands Forensic Institute
NHS	N-hydroxysuccinimide
NIP	Non-imprinted polymers
NMR	Nuclear Magnetic Resonance
NOSY	New Operational Sensing sYstem
NP	Nanoparticle
NPS	New psychoactive substance
NPV	Negative predictive value
OF	Oral fluid
PBS	phosphate buffered saline
pDA	Poly(dopamine)
PDCA	plan–do–check–adjust
PDI	polydispersity index
PE	Peak current enhancement
PPV	Positive predictive value
QCM	Quartz Crystal Microbalance
QD	Quantum dots
RIA	RadioImmunoAssay
RT	Real Time
SAM	Self-assembly monolayer
SD	Standard deviation
SE	Surfaceenhanced

SEM	Scanning Electron Microscopy
SORS	Spatially offset Raman spectroscopy
SPE	Screen-printed electrode
SPR	Surface Plasmon Resonance
SWGDRUG	Scientific Working Groups Analysis of Seised Drug
TEM	Transmission Electron Microscope
TEOS	Tetraethyl orthosilicate
THC	tetrahydrocannabinol
THCA	tetrahydrocannabinolic acid
TL	Test line
TLC	Thin-layer chromatography
TLC	Thin-layer chromatography
TMA	Trimesic acid
TRIM	Trimethylolpropane trimethacrylate
ULEIC	University of Leicester
UNODC	United Nations Office on Drugs and Crime
UV	Ultraviolet-visible
VOC	Volatile organic compounds
WADA	World Anti-Doping Association
WE	Working electrode

Chapter 1

Literature Review

1.1 Introduction

Drugs of abuse are all psychoactive illegally used for recreational or criminal activities. Drugs related crimes are illicit activities committed FOR manufacturing, supply, possess and use of drugs of abuse (EMCDDA, 2016). These crimes are of great concern nowadays due to their implications for human security and health. Although illegal and persecuted by law, these activities are anything but decreasing due to the significant money profits behind their smugglings. The profit of illicit drugs black market has been estimated to range around $320 billion per year (EMCDDA; Europol, 2013; UNODC, 2017b). Furthermore, illicit drugs trade are linked to criminal organisations, among which organised terroristic groups (UNODC, 2017b). According to the latest statistics, globally 5% of the adult population (an average of 255 million people), aged between 15 and 64, have been using illicit drugs in 2015. Furthermore, it has been reported that around 11% of drugs users (equal to 29.5 million people) are suffering from drug use disorders worldwide. The impact of drugs use on health corresponds to a global loss of 28 million "healthy" years of life (UNODC, 2017b). Overall, these figures bespeak how many clients belong to the drugs market and, consequently, to criminal organisations business.

To limit criminal organisation profits and related criminal activities, to increase the global security as well as to indirectly reduce the impact on the healthcare system and the law enforcement agencies (LEAs), it is imperative to “catch and destroy” illicit activities related to illegal drugs trafficking, manufacturing and possession. To achieve this aim, investigators have to collect explicit evidence of illicit drug activities. Within this contest, both “sniffer” dogs and forensic drug chemistry play a key role. Thanks to the outstanding olfactory system, “sniffer dogs” are useful in detecting illicit drugs concealed in various items/packages/containers (Leitch *et al.*, 2013; Jezierski *et al.*, 2014; Cerreta and Furton, 2015). On the other side, forensic drug chemistry can provide evidence on whether a suspected substance contains illegal drugs using reproducible scientific methods, which may be used as unequivocal information (evidence) of the drug-related offence in Court of Law (UNODC, 2012; Harper, Powell and Pijl, 2017). Once the suspected drugs substances have been seised in the contest of an inspection, they are usually analysed using presumptive and confirmatory tests. The former comes in the form of screening detection kit/devices which indicates whether illegal drugs may be present or not

(Musshoff et al., 2014; Cuypers, Bonneure and Tytgat, 2016; Forbes and Najarro, 2016; Krauss et al., 2016; Veitenheimer and Wagner, 2017). Confirmatory analyses are performed in forensic laboratories through several complex procedures and expensive analytical tools such as GC-MS, LC-MS, HPLC-MS (Arroyo *et al.*, 2013; Smith *et al.*, 2014; Stephanson *et al.*, 2015; Harper, Powell and Pijl, 2017). They can simultaneously identify and quantify the seised substance. Only when one or more illegal drugs have been detected in the seised substance (preferably, at least by two methods), there is the evidence of drug-related crimes, which can be persecuted in the Court of Justice (ENFSI, 2014).

Unfortunately, illicit drugs market patterns and pathways constantly change to escape the law enforcement controls. In the light of this scenario, European Commission and United Nations Office on Drugs and Crime (UNODC) have recently expressed the need of cutting-edge technologies to fight illicit goods trafficking, among which illicit drugs. Therefore, a fast reacting, cheap and accurate monitoring system should be implemented to tackle illicit drugs trafficking, manufacturing and possession. An elegant and convenient way to meet these needs is offered by biosensors, based on different sensing receptors (such as antibodies, affibodies, aptamers, MIPs, nanoMIPs, aptamers -nanoMIP hybrids) and different transducers (such as electrochemical, optical, and piezoelectric) (Yáñez-Sedeño *et al.*, 2014; Neves *et al.*, 2015; Poma *et al.*, 2015; Ansari and Karimi, 2017; Smolinska-Kempisty *et al.*, 2017).

This work aims to develop a fast, easy to use and portable sensor to detect illicit drugs and is developed within the NOSy (New Operational Sensing sYstem) project, funded under EU Horizon 2020 scheme. The selected illicit drugs for this work are cocaine and morphine in salt form. The work focuses on two different biosensor platform, namely, electrochemical impedance spectroscopy (EIS) and quartz crystal microbalance (QCM). Furthermore, a specific nanoMIPs (nano molecularly imprinted polymers) for each selected drug is used as the sensing receptors. For the nanoMIPs EIS sensor development, both screen-printed (SPEs) and interdigitated electrodes (IDEs) are considered as a transducer. In particular, the goal is to develop a nanoMIP based sensor able to detect traces of drugs of abuse with performances comparable or higher to sniffer dogs and

identify them with the same or higher performance provided by the current screening tests.

This chapter sets the background for this work by providing a comprehensive literature review on the state of the art of the conventional and innovative methods for detecting the selected drugs. Briefly, the first part provides information about the selected illegal drugs and an overview of the drugs of abuse legal framework. The second part provides state of the art on current presumptive and confirmatory tests. The third part provides an overview on the available biosensors for the detection of the selected drugs of abuse. The last part explores the application of nanotechnology to improve the drugs of abuse detection, focusing on the use of nanoMIPs as drugs of abuse sensing receptors.

1.2 Drugs of Abuse

Illicit drugs are "psychoactive or psychotropic substances able to change individual's mood, thinking processes or consciousness by acting on physiological mechanisms that normally regulate those functions" (WHO, 2004). The psychoactive activities are due to the induced communication dysfunction between neurons located in the central nervous system (CNS). Indeed, illicit drugs can inhibit or enhance the communication between neurons (WHO, 2004; Korpi *et al.*, 2015). A useful drugs classification for the Law Enforcement Agency (LEA) is based on the effects on individual's behaviour induced by the illicit drugs. As reported in **Table 1-1**, illicit drugs can be grouped into the following categories: narcotics, central nervous system (CNS) stimulants, CNS depressants, hallucinogens, steroid and inhalants (Caddy, 2003).

Table 1-1: Drugs of abuse classification based on their induced behaviour effects (data were sourced from DEA, 2017).

Class	Examples	Common Effects
Narcotics	Opium, heroin, morphine, methadone, Oxycodone.	Induce stupor, coma, or insensitivity to pain.
CNS Stimulants	Amphetamine-type stimulants, cocaine, caffeine, nicotine.	Activates, enhances, or increases neural activity.
CNS Depressants	Alcohol, barbiturates, benzodiazepines, methaqualone, cannabis, meprobamate, opiates.	Suppresses, inhibits, or decreases some aspects of CNS activity.
Hallucinogens	LSD, phencyclidine (PCP), mescaline, psilocybin, some hallucinogenic amphetamine.	Induce illusions, hallucinations, delusions, paranoid ideations, and other alterations of mood and thinking.
Steroids	Human growth steroids, anabolic steroids, testosterone.	Induce mood swings, hostility, Impaired judgment, aggression.
Inhalants	Ether, nitrous oxide, butane, cyclohexylnitrite, amyl nitrite.	Induce loss of inhibition, intoxication, slurred speech, decreased coordination, euphoria, disorientation.

CNS= central nervous system; LSD = Lysergic acid diethylamide; PCP= phencyclidine.

Other than the psychoactive substances, the composition of the illicit drug may include also cutting agents, which are divided into agents adulterants or diluents (Broséus,

Huhtala and Esseiva, 2015). Adulterants (such as levamisole, paracetamol, phenacetin, caffeine) are usually added to enhance the drug effect or to make the administration easier (Cole et al., 2011). Diluents (e.g., mannitol, lactose) are added to increase their profit. On the other hand, the involuntary adulterants occurrence into the drugs is usually a sign of poor manufacturer product (Stojanovska et al., 2013). However, the cutting agents used may vary across time and countries (Broséus, Gentile and Esseiva, 2016).

To develop a biomimetic sensor able to detect the selected psychoactive substances is advantageous to know the chemical structure, the physical properties and the primary cutting agents. Therefore, a summary of the selected drugs of abuse is provided in the following sections.

1.2.1 Cocaine

Cocaine is alkaloid obtained from coca leaves or synthesised from ecgonine or its derivatives (UNODC, 2003). Illicit cocaine comes in several forms and is trafficked mainly as cocaine hydrochloride and free-base (**Figure 1-1**).

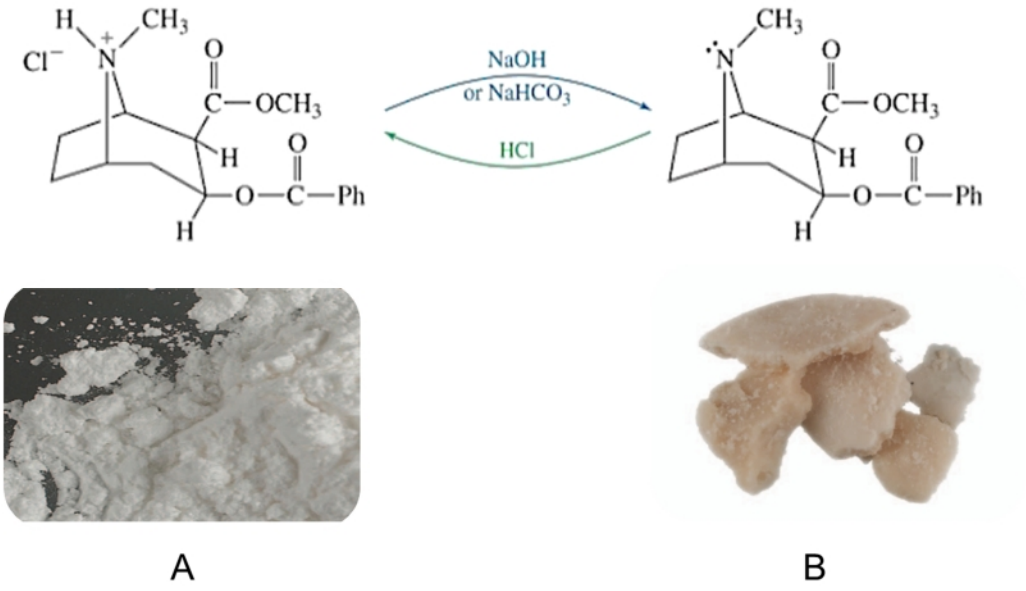

Figure 1-1: 2D chemical structure and image of (A) cocaine hydrochloride (HCl) and (B) cocaine "free-base". Ph= aromatic ring. (2D chemical structure were sourced from Wade, 2010 and images were sourced from DEA, 2017).

The coca paste appears as a white sticky paste and contains from 30 to 80% cocaine (UNODC, 2003). Since coca paste has a limited "shelf-life" drugs traffickers turn coca paste into cocaine hydrochloride (salt form) (Casale and Klein, 1993). Cocaine salt appears as a white powder, which can be snorted or injected (Emcdda, 2010). When cocaine hydrochloride is converted into the base form, crack (or freebase cocaine) is obtained (Wade, 2010). Crack appears as small, irregularly shaped white chunks (or "rocks") or flaky material, which is suitable for smoking (Caddy, 2003). Cutting agents occur in both the salt and freebase cocaine. Specifically, levamisole and caffeine occur as adulterants, while mannitol is often used as a diluent of the cocaine hydrochloride (Grobério *et al.*, 2015). However, drug dealer may change the adulterant used over the time.

In medical and research settings, cocaine salt is used as a local anaesthetic. According to the purity and the types of impurities, it is possible to discriminate the pharmaceutical cocaine from the illicit cocaine. Indeed, the pharmaceutical cocaine has a purity grade higher than 99.5%. on the other hand, the European Monitoring Centre for Drugs and Drug Addiction (EMCDDA) estimated that the purity for street cocaine can range between 22 and 57% (2016)

The map presented in **Figure 1-2** shows the number of cocaine seizures performed in 2015 in EU countries, thus highlighting the pressure posed on boarders and police in counteracting the drug trafficking (EMCDDA, 2016). Notably, for some countries data were not available. According to the statistic of the United Nations Office on Drugs and Crime (UNODC, 2017b), cocaine (864 tons) was the most seised drugs worldwide in 2015, after cannabis (7.317 tons). Concerning the cocaine use, the European Monitoring Centre for Drugs and Drug Addiction (2016) reported that cocaine (17.5 million) is also the most used drug by the European adult population (15-64 year old), after cannabis (87.5 million).

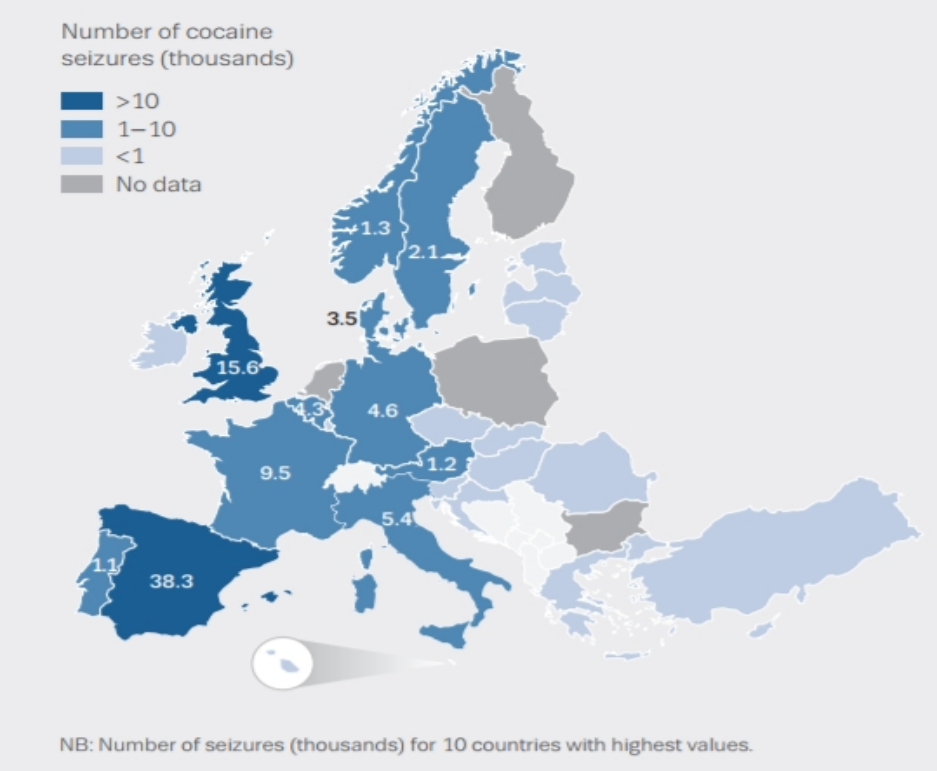

Figure 1-2: Number of cocaine seizures expressed in thousands and clustered in 4 classes per each European countries (EU Member States, Turkey and Norway.). Data for The Netherland, Poland, Bulgaria and Finland were not available. Numbers of seizures (thousands) are reported for the 10 countries with highest values (EMCDDA, 2016).

1.2.2 Morphine and Heroin

Morphine and its derivative heroine are alkaloids obtained from opium poppy and formerly belonging to opioid drugs class (Caddy, 2003). Opioids include both the semi- or fully-synthesised opioids (such as fentanyl, hydrocodone) and opiates, which are drugs derived from poppy plant (UNODC, 2017b). In clinical settings, pharmaceutical morphine is used for the treatment of pain and during surgical procedures.

Illicit morphine can be smuggled as it is or converted to heroine by acetylation reaction using acetic anhydride (EMCDDA, 2016; UNODC, 2017b). Illicit morphine and heroin are often adulterated with paracetamol and caffeine, while mannitol or lactose are commonly used as diluents, although the morphine purity and adulteration may change over the time (Broséus *et al.*, 2015). Morphine is either swallowed, smoked, sniffed, or injected. Heroin is usually injected, smoked, or sniffed/snorted, with the latter two

methods being mostly used for high purity heroin (Caddy, 2003). Morphine and heroin can induce physical addiction and, when injected, can also contribute to the spread of infectious diseases if infected needles are shared among drugs users (UNODC, 2017b).

According to World Drug Report 2017, the opium production has increased by 87% compared to 2016. Consequently, the price of the opiates has dropped, while the purity increased, thus boosting the opiates illicit trafficking worldwide. The map shown in **Figure 1-3** displays the number of seizures carried out at European level in 2015. Furthermore, opioids are sold in two forms in the EU countries, i.e. the brown powder form is the heroin base imported from Afghanistan; white powder form is less common and is mainly smuggled from South-East Asia. The EMCDDA reported that opioids were found in 81% of fatal overdoses, thus highlighting the life-threating risk associated to the use of these drugs (EMCDDA, 2016).

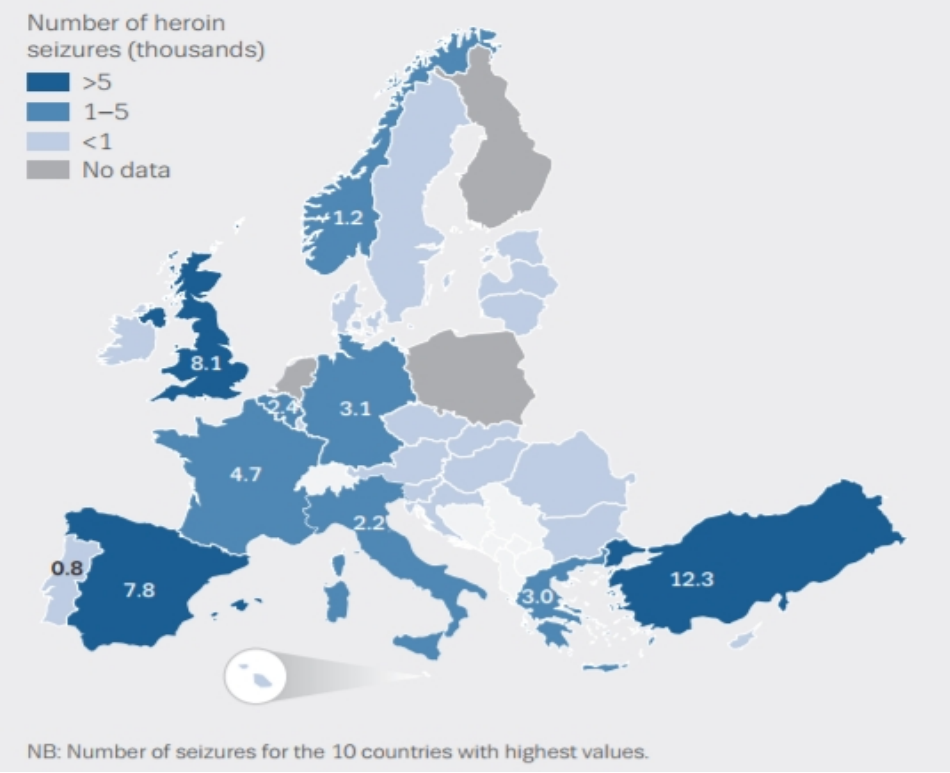

Figure 1-3: Number of heroin seizures expressed in thousands and clustered in 4 classes per each European countries (EU Member States, Turkey and Norway). Data for The Netherland, Poland, Bulgaria and Finland were not available. Numbers of seizures (thousands) are reported for the 10 countries with highest values (EMCDDA, 2016).

1.3 Legal Framework

Despite their potential addiction and psychoactive effects, some of the illicit drugs can be used for medicine and veterinary medicine purposes (like morphine, methadone and ketamine) and, therefore, their possession, manufacture, distribution, and sale are under international and national legislation control. Consequently, these drugs are also named "controlled substances". Both illicit drugs and controlled substances may be used for recreational purposes. Regulations set out worldwide punish the illegal use, possession, manufacture or trafficking of controlled and illicit drugs (Caddy, 2003; UNODC, 2013, 2015, 2017b; EMCDDA, 2016).

However, not all the illegal drugs are banned. It is a matter of reality that online supply systems of new psychoactive substance (NPS), better known as "legal high", is proliferating and is poorly controlled by the law enforcement since they can be sold "legally" as "substance not for human consumption", until they are formally banned by the law (Emcdda and Union, 2015). Furthermore, any NPS are legal until officially classified as forbidden substances.

At international legal framework, the following three United Nation Conventions have been set in place to fights drugs related crimes:

1. Single Convention on Narcotic Drugs Of 1961 as amended by the 1972 Protocol (UN 61/72).
2. Convention on Psychotropic Substances of 1971 (UN 71).
3. United Nations Convention against Illicit Traffic in Narcotic Drugs and Psychotropic Substances of 1988 (UN 88).

Overall, around 250 substances are listed according to their monitored harmfulness, and the degree of control required. Specifically, the UN 61/72 lists all the narcotic substances in four schedules and allows the possession, use, production, manufacturing, trade, export and import of such substances only for medical and scientific purposes. The UN 71 classifies the illicit drugs in four schedules and limits their use only for medical and research purpose (**Table 1-2**). The UN 88 convention lists the precursors and solvents under trade control in two different tables, respectively, while providing measures against illicit drug trafficking.

Table 1-2: Illicit drugs classifications established by international legislation (UN 61/72 and UN 71).

Illicit Drugs	Schedules	
	UN 61/72	UN 71
Cocaine	I	
Heroin	I,IV	
Morphine	I	
Cannabis and cannabis resin and extracts and tinctures of cannabis	I	
Cannabis and Cannabis resin	IV	
THC (Tetrahydrocannabinol, isomers and their stereochemical variants)	-	I
Amphetamines	-	II

"Schedule I", "Schedule II", "Schedule III" and "Schedule IV" mean the correspondingly numbered list of drugs or preparations annexed to the respective United Nation convention (UN 61/72 or UN 71) and as amended from time to time.

1.3.1 EU Regulations

At European level, the classification and anti-trafficking rules of substances related to drugs of abuse are limited to the following Decision and Directive:

- Council Framework Decision 2004/757/JHA of 25 October 2004 laying down minimum provisions on the constituent elements of criminal acts and penalties in the field of illicit drug trafficking.
- Proposal for a Directive of the European Parliament and of the Council amending Council Framework Decision 2004/757/JHA of 25 October 2004 laying down minimum provisions on the constituent elements of criminal acts and penalties in the field of illicit drug trafficking, as regards the definition of drug.

Although European harmonised lists of narcotic and psychoactive substances are missing, each Member States have regulations that classify these substances and establish the penalties for supply and possession for personal use. The possession for personal use may be strictly banned for some drugs, while, for other drugs (i.e. cannabis), it is allowed below a threshold that varies according to the specific national regulation. On the other hand, the term "supply" refers to illicit drugs "production, trafficking, offering, selling,

or possession with intent to distribute" and the related offence may or may not be linked to an established quantity of drugs. Each EU country has established thresholds for the supply and personal use of cocaine and opioids (morphine and heroin). Where a threshold has not been established, a zero tolerance is applied, or punishment may vary on a case by case basis (EMCDDA, 2005). Nevertheless, the thresholds and punishment widely vary across countries leading to jurisdictions across the EU Member States, thus posing limitations over control on illicit drug trafficking, production and use.

1.3.2 UK regulations

The following two regulations are in place in the United Kingdom to control illicit drugs crimes:

1. Misuse of Drugs Act (1971)
2. Misuse of Drugs Regulations (2001)

As the UN 61/72, the Misuse of drugs Act classifies the controlled drugs in three categories, namely Class A, Class B and Class C, where the former is the most harmful. All injectable Class B drugs are treated as Class A. The same Act establishes the penalties for the illicit drugs use, possession, manufacturing and supply. The Misuse of Drugs Regulations is as the UN 71 and it sets the rules for possession, use, production, manufacturing, trade, export and import of the controlled drugs for medical and scientific purposes. Concerning this work, the classification of selected drugs of abuse according to the different international and UK regulations are reported in **Table 1-3**.

The UK penalties related to illicit drugs dealing and possession are reported in **Table 1-4**, as established by Misuse of Act (2001). Notably, according to the Misuse of Drugs Act 1971, s.9, Sch. 4, the only use of prepared opium is explicitly prohibited and punished by imprisonment for a variable length of time (up to 14 years) (EMCDDA). Recently the UK government have issued the Psychoactive Substances Act 2016, which has entered into force on the 26th May 2016. According to this Act, it is an offence to produce, supply, offer to supply, possess with intent to supply, possess on custodial premises, import or export psychoactive substances. A psychoactive substance is also defined as "any substance intended for human consumption that is capable of producing a psychoactive

effect". Though some substances are excluded, such as alcohol, tobacco, nicotine, caffeine and medical products as well as controlled drugs, which are regulated by the Misuse of Drugs Act 1971.

Table 1-3: Controlled drugs classifications established by UK legislations (Misuse of Drugs Regulations 2001 and Misuse of Drugs Act 1971).

	Misuse of Drugs Regulations 2001	Misuse of Drugs Act 1971
Illicit drugs	**Schedule**	**Class**
Cocaine	1(coca leaf), 2 (cocaine)	A
Heroin	2	A
Morphine	2	A
Cannabis and cannabis resin and extracts and tinctures of cannabis	1	B
Cannabis and Cannabis resin	1	B
THC (Tetrahydrocannabinol, isomers and their stereochemical variants)	1	B
Amphetamines	2	B
Methamphetamine	2	A
Anabolic steroids	4 (part 2)	C

Schedule 1 covers drugs that have no therapeutic value and are usually used mainly in research under a Home Office licence.
Schedule 2 covers drugs that have therapeutic value, but are highly addictive. These are strictly controlled and subject to special requirements relating to their prescription, dispensing, recording and safe custody.
Schedule 3 covers drugs that have therapeutic value, but have slightly lighter control, special requirements relating to their prescription, dispensing, recording and safe custody.
Schedule 4 is divided in two parts. Part 1- benzodiazepines and Part 2 anabolic and androgenic steroids, which is subject to lighter regulation with no possession offence.
Schedule 5 covers weaker preparations (in less than 0.2% concentration) of Schedule 2 drugs that present little risk of misuse and can be sold over the counter as a pharmacy medicine (without prescription).
"Class A drug", "Class B drug" and "Class C drug" mean any of the substances and products for the time being specified respectively in Part I, Part II and Part III of Schedule 2 of Misuse of Drugs Act as amended.

Table 1-4: Penalties for possession, supply and production according to the Misuse of Drugs Act 1971.

Class	**Penalties**	
	Supply and Production	**Possession**
A	Up to life in prison	Up to 7 years in prison
B	Up to 14 years in prison	Up to 5 years in prison
C	Up to 14 years in prison	Up to 2 years in prison, none for personal use of anabolic steroids
Temporary class drugs*	Up to 14 years	None

***Includes all banned drugs not yet classified.

1.4 Forensic Investigation and Chemistry

Investigations activities on illicit drugs crimes performed by LEA follow a specific route that aims to turn the suspect of illicit drug offences into evidence, as shown in **Figure 1-4**.

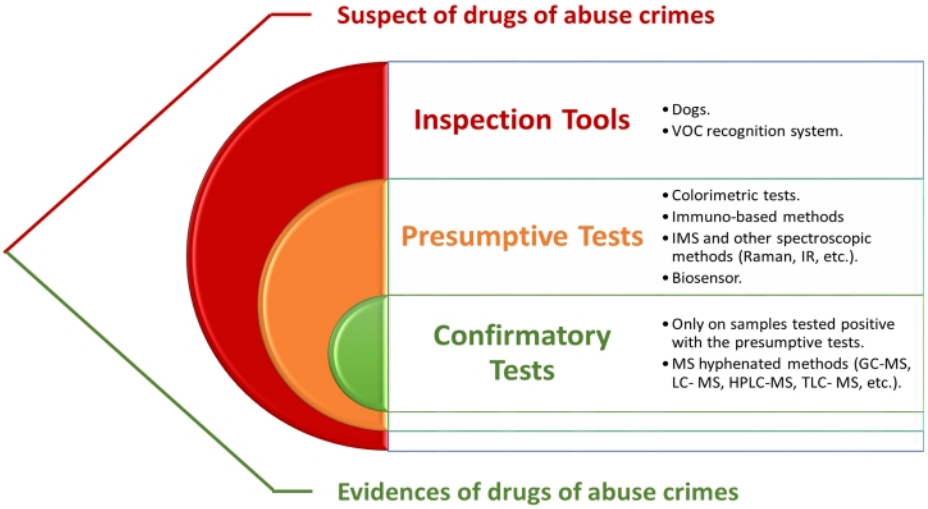

Figure 1-4: Overview of the Investigative activities on drugs of abuse crimes performed by LEA.

On the first instance, the suspected items or places are inspected. This is achieved using sniffer dogs, which have an outstanding olfactory system able to detect drugs of abuse concealed by drugs traffickers in several unpredictable ways (Bell, 2009; Jezierski *et al.*, 2014). As part of the investigative activities, the investigator collects biological or environmental samples (**Figure**).

Tools for the biological sample are quite standardised, often provided within on-site kit and devices. They include oral fluid swab or brush, sponge, urine collector, syringe and blood vials, breath collector (Moore, Kelley-Baker and Lacey, 2013; Christodoulides *et al.*, 2015). Tools for collecting environmental sample vary from swabs, pads to cartridges. Swab and pad are used to collect drugs from any surfaces where the drugs might have been in contact with (i.e., money, tables, clothes,). The cartridges are specifically designed to collect samples of illicit drugs in the form of airborne particulates in the outdoor and indoor environment (Cecinato *et al.*, 2014; Mastroianni *et al.*, 2015; Cecinato, Balducci and Perilli, 2016).

Figure : Classification of different types of illicit drug-related samples.

Polypropylene, polycarbonate, and polyethene are the recommended materials for the manufacturing of plastic tools for sampling purposes, since any others materials may absorb the analyte of interest (i.e. drugs of abuse), thus preventing their detection (Swiss Guidelines Committee for Drugs of Abuse Testing, 2012).

Subsequently, the seized substance is conveyed to forensic chemistry analysis, which can provide information on whether a suspected substance contains illegal drugs by applying reproducible scientific methods (Bell, 2009). More in detail, this information can be divided into:

1. Investigative information, which resulted from presumptive tests and are used by forensic intelligence to quickly leading to further lab confirmatory analysis. Presumptive tests are chromatic methods, such as Marquis Test assay, immune-based methods, such as immunoassay, or spectrometric methods, such as Ion Mobility Spectroscopy (IMS). When a presumptive test gives a positive response, the result needs to be corroborated by a confirmatory test (Kerrigan *et al.*, 2011; Lesiak *et al.*, 2014; Yáñez-Sedeño *et al.*, 2014). In other case, investigators may directly forward

the seized suspected materials to the forensic laboratories for confirmatory analysis (Tsai and Lin, 2005; Agius and Kintz, 2010).

2. Prosecutorial information, which resulted from the confirmatory tests and are used to persecute drug-related crimes in a court of Justice. Indeed, only when one or more illegal drugs are detected in the seized substance (preferably, at least by two detection methods), there is the evidence of a drug-related crime, which can be persecuted in the Court of Justice (Bell, 2009).

To evaluate the performance of both on-site and in-lab methods, at least the following parameters have to be considered: sensitivity, specificity, accuracy (Bottarelli and Ostanello, 2011). The sensitivity is associated with the limit of detection (LOD) of the methods. Nevertheless, if the methods is designed to provide qualitative results, the sensitivity is related to the "cut-off" of the methods rather than on the limit of detection (LOD). The "LOD" and "cut-off" definitions according to the UNODC (2009a) are reported in **Figure 1-5**. The "cut-off" limit leads to a decrease of false positive results, but also to a possible increase of false negative results, if the "cut-off" value has been set too high. As shown in **Figure 1-6**, samples can be grouped into positives and negatives. The performance parameters (sensitivity, specificity and accuracy) assess the ability of analytical methods (test) in allocating the samples in the correct group.

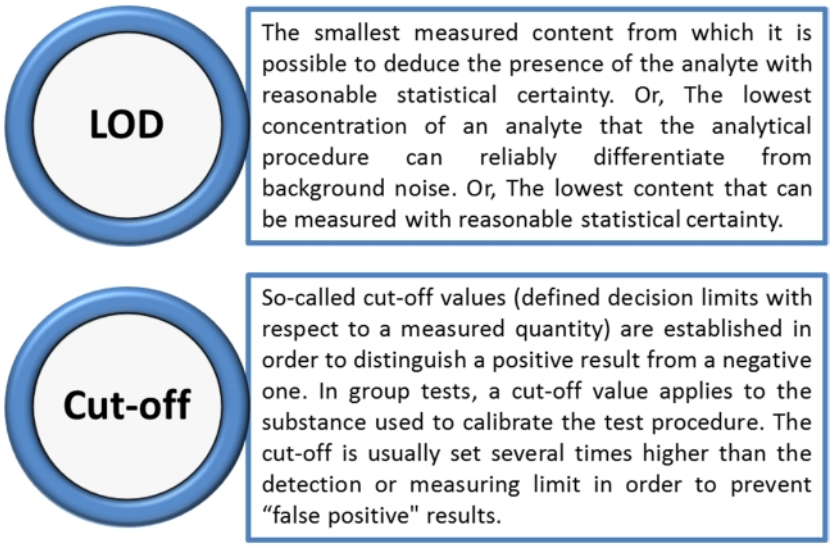

Figure 1-5: "LOD" and "cut-off" definitions as provided by UNODC (2009).

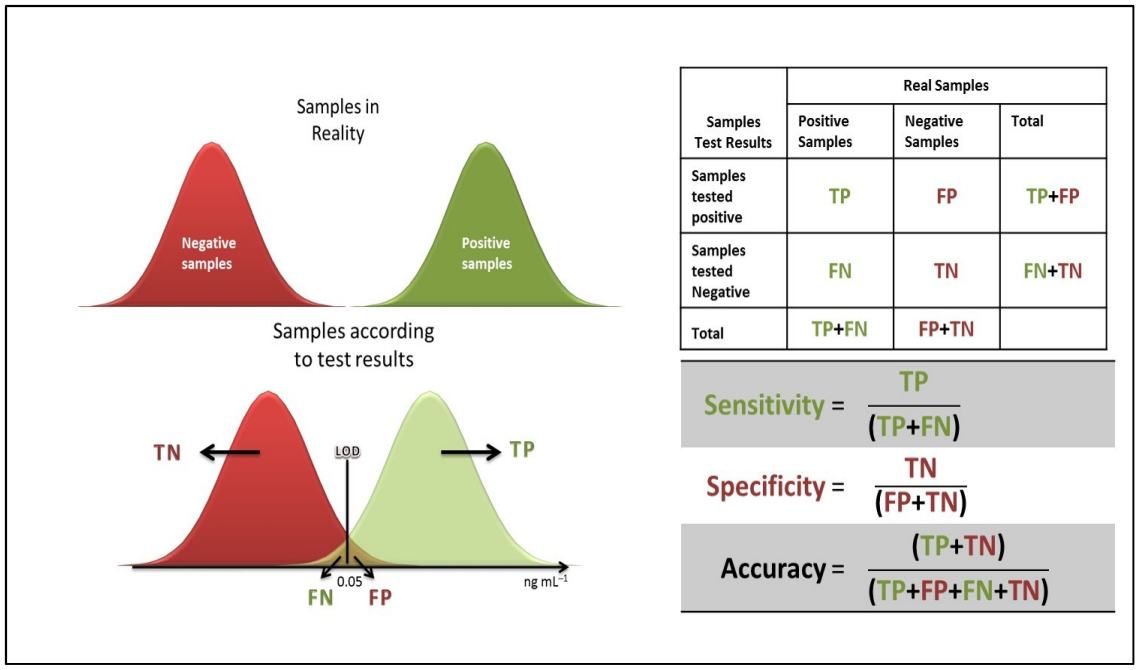

Samples Test Results	Real Samples		
	Positive Samples	Negative Samples	Total
Samples tested positive	TP	FP	TP+FP
Samples tested Negative	FN	TN	FN+TN
Total	TP+FN	FP+TN	

$$\text{Sensitivity} = \frac{TP}{(TP+FN)}$$

$$\text{Specificity} = \frac{TN}{(FP+TN)}$$

$$\text{Accuracy} = \frac{(TP+TN)}{(TP+FP+FN+TN)}$$

Figure 1-6: Analytical detection methods performance parameters. TN = true negative sample, TP = true positive sample, FN = false negative sample, FP = false positive sample (modified from Bottarelli and Ostanello, 2011).

1.5 Biological Organisms as Investigative Tools

In nature, there are several animals provided with exceptional sensing systems, which may be employed to rapidly investigate the occurrence of hidden illicit drugs in vast areas, such as harbour, airport, train and metro stations, public parks/squares/streets, public institutes. In particular, the olfactory systems are specialised to detect, recognised, discriminate and locate materials via volatile organic compounds (VOCs) released from the materials (Leitch *et al.*, 2013). Having over 300 million of olfactory sensory cells (Fenton, 1992; Chandler, 2005; Craven, Paterson and Settles, 2010), the most well-known animal used by LEA for illicit drugs detection are dogs (*Canis lupus var. familiaris*.) (Jezierski *et al.*, 2014). The most important advantages are the canine agility, ability to search in large areas, ability to detect and discriminate between target and non-target VOCs, even if the illicit drugs occur at low concentrations (Lorenzo *et al.*, 2003; Leitch *et al.*, 2013; Cerreta and Furton, 2015). However, their efficacy have been questioned due to:

1. Long and expensive training required;
2. The olfactory fatigues, i.e. decreased sensitivity and specificity of dogs detecting ability upon prolonged exposure to the same target;
3. Decreasing performances due to handler and environmental factor;
4. Inter individual variability in detecting illicit drugs (Leitch *et al.*, 2013);
5. The lack of scientific evidence on their detection capabilities (Hickey *et al.*, 2012);
6. Their reported failure to detect some drugs, such as ecstasy (Dunn and Degenhardt, 2009);
7. The poor performances achieved when dogs are trained with surrogate illicit drugs scents (Rice and Koziel, 2015).

In order to contrast the scepticism in dog's abilities, some studies on canine performances were carried out. These studies aimed to investigate the dog failure rate and the dog performances (Lorenzo *et al.*, 2003; Macias *et al.*, 2010; Jezierski *et al.*, 2014; Cerreta and Furton, 2015). As recently reported by Jezierski and co-authors (2014) and sum up in **Table 1-5**, fully trained police dogs are successfully employed to detect illicit drugs.

Table 1-5: Detection parameters depending per each selected drugs (modified from Jezierski et al., 2014).

Drugs	Amount of drug hidden (g)	% correct indications	% misses	% false alerts
Marijuana	10–15	91.8	4.4	3.8
Hashish	10–15	82.4	5.7	11.9
Amphetamine	10–15	78.3	5.0	16.7
Cocaine	10–15	74.0	12.6	13.4
Heroin	10–15	70.3	12.0	17.7

Canine specificity (i.e. proportion of the number of hits samples by the dog to the sum of the number of hits and missed samples) are estimated to range between 70% and 100%. Concerning the limit of detection (LOD), various LOD values have been reported for police dogs (16 ppb for methyl benzoate vapour and 0.03 ppb for illicit cocaine vapour)

(Waggoner et al., 1997) and 3,4-methylenedioxy-methamphetamine (MDMA) (1 ng) (Macias et al., 2010). Although these studies attempt to evaluate the detection limit of police dogs nose, a LOD has not been established yet (Jezierski *et al.*, 2014). Other vertebrate and invertebrate animals may be employed to detect VOCs related to illicit drugs, such as mice, honeybees (*Apis mellifera*), wasps, moths. Rats (*Sprague-Dawley rats*) showed a better ability to reach very narrow spaces compared to dogs. On the other hand, their training is more time consuming: their working time is shorter (up to 40 minutes) while the studies on their efficacy, specificity and accuracy are still lacking (Leitch *et al.*, 2013; He *et al.*, 2015). Honeybees, wasp and other invertebrates have been explored as new biological organism detectors, for both explosives and drugs (Schott, Klein and Vilcinskas, 2015). Interestingly, their antennas have been successfully incorporated into living sensor devices due to the remarkable capability to detect illicit drugs (Schott *et al.*, 2013; Schott, Klein and Vilcinskas, 2015). However, the short life of invertebrates limits the efficiency of these devices (Leitch *et al.*, 2013).

1.6 Presumptive Methods

Presumptive methods are rapid test applied to rapidly screen for drugs of abuse offences. They can be used either on-site or in-lab. To date, the mostly used presumptive tests are:

1. Immune-based methods;
2. Colorimetric methods;
3. Spectroscopic methods.

The ideal on-site presumptive method should have a high detection rate and a low false alarm rate: a high true positive rate will discourage smugglers and prevent smuggling activities, whereas a low false alarm rate will prevent unnecessary law enforcement workload as well as avoid innocent travellers to be exposed to unnecessarily control (Wetter, 2013). They should have an accuracy higher than 95% with selectivity and specificity higher than 90% (Wille *et al.*, 2010).

1.6.1 Immune-Based Methods

Among the several screening devices available in commerce, the immune-based are the most popular. They are based on lateral flow immunoassay devices (among which, lateral flow device) and enzyme-linked immunosorbent assay (ELISA), enzyme multiplied immunoassay technique (EMIT), radioimmunoassay (RIA), and fluorescence polarisation immunoassay (FPIA) (Mali, Karpe and Kadam, 2011; Musshoff *et al.*, 2014; Harper, Powell and Pijl, 2017). The assay format is based on indirect competitive inhibition immunoassay (Kadehjian, 2005). Recently, other ligands have been explored to replace the use of the antibody in the lateral flow assay. Examples of these ligands are molecularly imprinted polymers (MIPs) and aptamers or a combination of them (Chianella *et al.*, 2013; Chen and Yang, 2015; Poma *et al.*, 2015; Smolinska-Kempisty *et al.*, 2017). Different labelling can be used, such as coloured latex beads, magnetic particles, carbon nanoparticles, gold nanoparticles, silver nanoparticles, selenium nanoparticles, quantum dots, textile dyes, organic fluorophores, enzymes, liposomes (Eltzov *et al.*, 2015; Chantada-Vázquez *et al.*, 2016). Among them, gold nanoparticles are often conjugated to the antibodies to visualise the signal (Quesada-González and Merkoçi, 2015). Furthermore, the immune-based test strip can be embedded in a plastic case, thus constitute a lateral flow device. The result is read by naked eyes user or the reading can be performed by a detector (such as, VIS/UV spectrometer) (Eltzov *et al.*, 2015; Ma *et al.*, 2015). The test results are semi-quantitative and are based on a "cut-off" limit rather than on the limit of detection (LOD). A summary of the immune-based screening kits and devices currently in used to detect drugs of abuse are reported in Appendix A. Immune-based assays have been mostly developed for biological samples, although their application can also be extended to environmental samples (such as, Alere™ Rapid Solids Cassette Test). Disadvantages of immune-based methods are: 1) the possible occurrence of cross-reactivity in the immune-based tests which leads to false positive results (Nieddu *et al.*, 2014); 2) interpretation errors (D'Elia, Montalvo García and García Ruiz, 2015); and 3) the use of animal antibodies which production is costly, time-consuming, while posing animal welfare concerns.

1.6.1.1 Lateral Flow Device

The lateral flow device for drugs of abuse detection is based on competitive inhibition immunoassay (Musshoff *et al.*, 2014). The structure of lateral flow strips is shown in **Figure 1-7** (Miočević *et al.*, 2017). The competitive inhibition immunoassay is designed to generate the competitive binding for a specific ligand between the free drug present in the sample and the derivatives drug immobilised onto the test line. Specifically, the sample, which may contain or not a specific drug (for instance cocaine), is placed in the sample pad. Due to the capillary force, the sample diffuses through the cellulose thus reaching the conjugate pad. The conjugate pad, usually made of glass fibre, contains an optimised amount of labelled-antibody with a specific affinity for the tested drug (for instance, cocaine antibody). Then, antibodies and the sample will flow into the detection pad, which is made of nitrocellulose and where the test line (TL) and control line (CL) are printed. In the competitive inhibition immunoassay, the test line contains immobilised cocaine derivative drug. If the sample contains cocaine molecules, they will bind to the antibodies, which will not be free to bind to the derivatives drugs present in the test line. The absence of signal in the test line means that the test is positive. When the cocaine is not present in the sample, the labelled antibodies are free to bind the derivatives drugs present in the test line, thus giving the signal. Therefore, the test is negative. The control line is made up of anti-antibodies, which capture or the free antibodies or the drug antibodies complex, thus showing that the assay has appropriately worked (Mark *et al.*, 2010; Eltzov *et al.*, 2015; Miočević *et al.*, 2017).

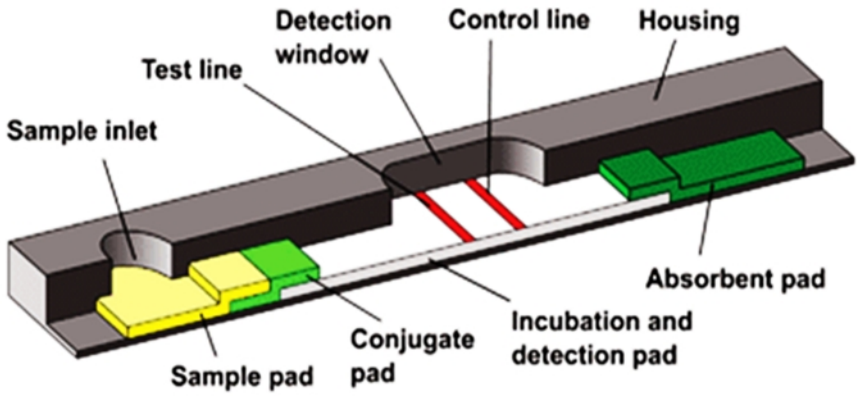

Figure 1-7: Typical structure of a lateral flow strip (Mark *et al.*, 2010).

A wide array of specimens can be tested using lateral flow devices, such as blood, saliva (oral fluid), urine or drugs in powder form after dissolution into a liquid medium. Most of the lateral flow devices are currently in use by the LEA, and some have also been approved by the UK Home Office (Table_Apx A-1). As shown in **Table 1-6**, several studies have evaluated the lateral flow devices performance parameters in comparison with confirmatory methods (such as GC-MS) (Wille *et al.*, 2010; Blencowe *et al.*, 2011; Strano-Rossi *et al.*, 2012; Musshoff *et al.*, 2014). The reported performances parameters widely differ in each study probably due to the inconsistent methodology applied. Most of the devices were tested on oral fluid samples. However, the same device may be used for detecting illicit drugs in solid seized substances, blood, urine or other types of specimens.

Table 1-6: Performance parameter of some on-site lateral flow devices in use for cocaine and opiates (morphine and heroin) detection.

Test kit	Drugs	Sample	Cut-off (ng mL^{-1})	Sens. (%)	Spec. (%)	Acc. (%)	Ref.
Drαäger Drug Test®5000	Cocaine	plasma samples	20	67	60	63	Sarah M.R. Wille 2010
	Cocaine	oral fluids	20	76	74	75	Musshoff 2014
	Opiates		20	95	91	93	
Mavand Rapid STAT®	Cocaine	oral fluids	10	100	100	100	
	Opiates		10	100	100	100	
Securetec Drugwipe-5+®	Cocaine	oral fluids	30/50	63	99		(Strano-Rossi *et al.*, 2012)
	Opiates		10\20	10	99		
	Cocaine	oral fluids	15	100	40	63	Musshoff 2014
	Opiates		10	100	50	67	
	Cocaine	biological specimen	50	99	98		DRUIT 2010
	Opiates		20	99	97		
	Cocaine	plasma samples	50	78	100	88	Sarah M.R. Wille 2010

Sens.= sensitivity; Spec.= specificity; Acc.= accuracy; Ref.= reference.

1.6.1.2 Enzyme-Linked Immunosorbent Assay (ELISA)

Due to its popularity in other sectors (i.e., medical diagnosis), ELISA is extensively used to screen biological specimens and seized drugs materials in the forensic laboratories. ELISA allows a fast screening by excluding negative samples from further analysis when a significant amount of samples has to be analysed (Temerdashev, Grigoriev and Rybalchenko, 2015). The ELISA test relies on the same principle of the lateral flow device, i.e. competitive assay. In this instance, the enzyme label is linked to the drug derivatives included in the test kit. The drug in the sample and the labelled drug derivatives will compete for binding to antibodies immobilised onto a solid phase (micro-wells strips or plates). As in the on-site lateral flow devices, a positive result gives no colour signal, while a negative result gives a strong colour signal (due to the enzymatic activities) (Pujol *et al.*, 2007; Arntson *et al.*, 2013; Mohr *et al.*, 2014). The sample absorbance provide an indication of the illicit drug concentration in the analysed materials. ELISA tests are easy to use and a highly sensitive, but require experienced personnel to be performed. The cut-off of the commercially available ELISA assay is 0.1 ng mL^{-1} and the sensitivity and the specificity range s are 80-99 % and 50-91 %, respectively (Musshoff *et al.*, 2012).

1.6.2 Colorimetric Test

Colorimetric tests are based on the chemical reaction between the suspected substances and a chosen reagent. The reaction between a mixture of reagents (either in liquid, powder or aerosol form) and the suspected substance lead to a coloured product which is indicative of a particular illicit drug. They are the first example of quick on-site presumptive tests to screen for both illicit drugs and their precursors occurrence in a suspected seized material (UNODC, 1995).

The most popular colour test is the Marquis test, although other colour tests have been used for qualitative screening on the occurrence of illicit drugs in seized substances, as listed in **Table 1-7**. Notably, Cuypers and co-authors (2016) recently proposed the combined use of three commercially available colour tests as a presumptive test to detect new psychoactive substance (NPS). Limitations of these tests are the need for trained and

experienced staff able to mix the reagents in the field and to read the resulting colour correctly. Usually, more than one test should be applied to detect the illicit drug (Verkouteren and Staymates, 2011). Furthermore, they suffer from a high false positive rate due to the production of the same colour by two different illicit substances. With this respect, Favretto and co-authors (2013) recently reported a Marquis false positive results on blue tablet seized in Italy.

Table 1-7: Overview of the most popular colour tests currently applied to seize substances.

Colour test	Reagents	Illicit drugs	Colour (positive results)	Ref
Marquis reagent	Mixture of formaldehyde and concentrated sulfuric acid	Opium alkaloids	Purple	(UNODC, 1995; Choodum and Daeid, 2011)
		Amphetamines	Orange	
Mecke's reagent	Mixture of selenous acid and concentrated sulfuric acid	Opium alkaloids	Yellowish-brown colour	
		Phenethylamines	Green brownish	
Mandelin reagent	A mixture of ammonium vanadate and concentrated sulfuric acid	Phenethylamines		
Simon's reagent	Mixture of sodium nitroprusside, sodium carbonate and acetaldehyde	Amphetamine	Orange/brown	
		Methamphetamine	Blue	
Scott's reagent	Cobalt thiocyanate	Cocaine	Blue	
Duquenois–Levine colour test	Mixture of acetaldehyde, vanillin, concentrated hydrochloric acid and chloroform	Tetrahydrocannabinol (THC)	Violet	(UNODC, 2009b)
Fast Blue B salt test	Mixture of petroleum ether, fast Blue B salt, sodium bicarbonate	Tetrahydrocannabinol (THC)	Red	
		Cannabinol (CBN)	Purple	
		Cannabidiol (CBD)	orange	
Fast Corinth V salt test	Mixture of petroleum ether, Fast Corinth V salt, sodium bicarbonate	THC CBD and CBN	purple red	

Briefly, the Marquis test showed a positive result for the presence of amphetamine in a seized blue tablet. When the same tablet was analysed by GC–MS, it resulted to be composed by two anabolic steroids (AS), namely, methandienone and methyltestosterone, whereas no amphetamines were detected. Thanks to recent

technology advancement, these colour tests have been coupled with image software (Choodum and Daeid, 2011) or with smartphone technology (Choodum *et al.*, 2014; Krauss *et al.*, 2016), thus achieving quantitative or semi-quantitative colourimetric assay with promising results.

1.6.3 Ion Mobility Spectroscopy (IMS)

Ion mobility spectroscopy (IMS) is frequently used for on-site detection of illicit drugs in both biological and environmental specimens (Liuni *et al.*, 2014; Sonnberg *et al.*, 2015). Ion mobility spectroscopy is a method able to separate ions in a gaseous phase according to their mobility in an electric field (Cumeras *et al.*, 2015). The components of IMS are illustrated in **Figure 1-8**.

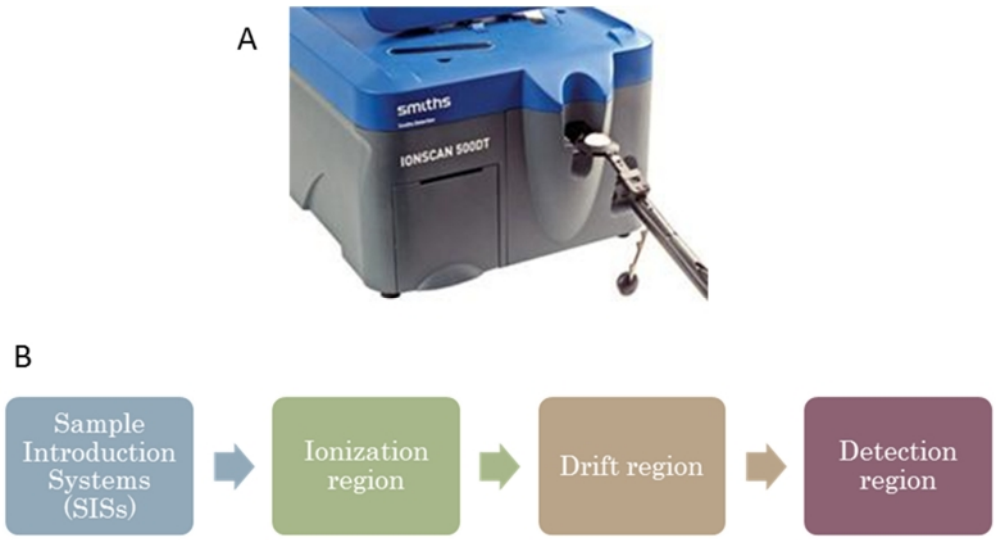

Figure 1-8: (A) Commercially available IMS (IONSCAN500DT - Smiths Group plc., UK) and (B) illustration of the principal IMS components.

Briefly, the sample introduction system aims to convert solid or liquid substances into volatile compounds and to introduce them onto the IMS machine with a gas carrier. The ionisation region enables the ionisation of sample molecules into a positive or negative charged molecules, which may participate in different reactions with the ionised gaseous

carrier, thus leading to the formation of the ionic cluster. Afterwards, the ionic clusters moved into the core part of IMS, which is the separation region, or better known as drift region or drift tube. Here the ions will move in a gas phase carrier under an electric field effect. The final component is the detector, which detects the ionised molecule according to their drift time and intensity. Ionisation of illicit drugs yields positive ionic cluster ($(M + H)^+$). Therefore, the detector operates in positive mode (Weyermann *et al.*, 2011). The signals reach an automated recorder and, then, a software, which processes the data for results visualisation (Rouessac and Rouessac, 2013; Cumeras *et al.*, 2015). Since IMS is prone to saturation, small and representative sample has to be introduced to the machine. This is one of the major IMS drawbacks in analysing seized bulk materials for illicit drugs detection and identification (Weyermann *et al.*, 2011). However, a chromatographic separation column may be coupled to IMS to improve the separation of the molecule before entering into the IMS.

The IMS is user-friendly and can detect illicit drugs in trace amount (Verkouteren and Staymates, 2011). Furthermore, the IMS analyser does not need any particular ambient condition and can identify a broad range of substances, providing quick, reliable results (high sensitivity and specificity) and detection limits in the order of ppm (Borsdorf and Eiceman, 2006). These advantages along with low price compared with conventional mass spectrometry have promoted IMS as the favoured on-site method for illegal substances detection (Cumeras *et al.*, 2015). Indeed, IMS is the technique mostly applied for chemical weapon detection at airport and borders and, recently has also been applied for drugs of abuse detection. A commercially available example is the IONSCAN 500D (Smiths Group plc., UK) and is shown in **Figure 1-8A**. Interestingly, this device obtained the Official Government Product Certifications/Accreditations in many countries, among which United Kingdom, Italy, French, China, and Canada.

To speed up and reduce the cost of ionisation procedure, IMS has been coupled to ambient ionisation method, such as the ion spray paper, which generates ion molecules in a cheap, fast and simple method. A recent study investigated the application of paper spray IMS in detecting cocaine residues in liquid or solid samples collected from different surfaces (e.g. marble, glass, wood, skin, fingernails) (M. Li *et al.*, 2014). Briefly, the solid samples were collected by wiping with a chromatography paper, while liquid samples were

directly dropped onto the chromatography paper. Then, 20 mL of solvent (70% methanol: 30% water: 0.1% formic acid) was dripped onto the paper. A high voltage (3.0 kV) was then applied to ionise the sample. IMS analysis was carried out in positive ion mode. The attained LOD for liquid samples was 2 μg mL^{-1}, while for surface samples was as low as 5 ng per sampled surface area.

Illicit environmental samples are often a mixture of several compounds which may compete with the target compound during the ionization process. For instance, a mixture of cocaine and heroin hampers the detection of the latter compound. For the same reason, IMS performs poorly in detecting cannabinoids since these drugs are composed of several substances. Therefore, colour tests and thin layer chromatography are applied as presumptive tests in this instances (UNODC, 2009b). Furthermore, IMS is prone to environmental contamination and may give false positive results (Weyermann *et al.*, 2011). Another limitation is the lack of illicit drugs reference materials, which leads to a high uncertainty of the whole analysis result (Verkouteren and Staymates, 2011).

1.6.4 Other *in-situ* Spectroscopy Methods

Fourier transform infrared spectroscopy (FT-IR) has been employed as on-site presumptive test at police custom offices. FT-IR may be used to quantify illicit drugs, such as methamphetamine, although performance limitations in detecting illicit drugs have been reported when analysing complex matrices (Harper, Powell and Pijl, 2017). Other *in situ* spectroscopy methods have been recently proposed, such as the near infrared (NIR) absorption spectroscopy and Raman spectroscopy. They allow for non-destructive and non-invasive identification and quantification of suspected materials included in plastic containers, paper envelopes, glass bottles and clothes (Buckley and Matousek, 2012). Although, NIR is a powerful method to detect different compounds in a mixture, its application is limited since common packaging materials interfere with the NIR absorption. For this investigation, a better performance can be achieved by Raman spectroscopy, which is an easy to use, fast, non-invasive, and non-destructive method. Raman spectroscopy does not require sample preparation, is suitable for large amount of seized materials, which include oil and alcohol based liquids.

Weyermann et al. (2011) successfully used a transportable Raman Spectrometer to detect and discriminate cocaine, heroin and amphetamine in street samples, achieving a limit of detection equal to 5 mg mL^{-1}. However, Raman spectroscopy is not suitable for trace analysis and dark coloured or opaque packaging can still hamper the analysis. Moreover, exposure to daylight and neon light may affect the results. Glass and brown coloured containers may affect the analysis. Better results can be achieved by means of spatially offset Raman spectroscopy (SORS). Buckley and Matousek (2012) were able to detect cocaine concealed in various containers, such as opaque plastic containers, coloured glass bottles, paper envelopes and clothes. The authors achieved an LOD equal to 12 g/0.7 L of adulterated cocaine (75% pure cocaine) of seised materials. Notably, SORS is fast, portable non-invasive and non-destructive technique, which can discriminate between cutting agent and illicit drugs. Although, it is not suitable for trace analysis and the application is limited to non-metallic containers. Other major limitations are the cost and the complex signal interpretation.

1.7 Confirmatory Methods

When a presumptive test results is positive, it has to be confirmed by confirmatory methods. Due to the high sensitivity, specificity and accuracy, separation methods coupled to Mass Spectrometry (MS) detectors are considered the "golden standard" methods for illicit drugs detection and quantification in environmental and biological samples. Therefore, their results are often used as a proof in criminal court trials (Erol Öztürk, Yeter and Alpertunga, 2015; Mastroianni *et al.*, 2015; D'Avila, Limberger and Fröehlich, 2016; Jain and Singh, 2016; Polet *et al.*, 2016) and for new methods validation (Strano-Rossi *et al.*, 2012; Arntson *et al.*, 2013; Mohr *et al.*, 2014; Erol Öztürk, Yeter and Alpertunga, 2015).

Separation methods aim to separate the target compound from other compounds present in the suspected material (i.e. seized drugs or biological samples) (Kadehjian, 2005). This step is crucial for the detection and identification of illicit drugs since they never occur as pure substance in the seized materials. They are part of a mixture, which may contain more than one drug, adulterants, impurities and, sometimes, precursor's residues. The

most common separation methods are gas chromatography (GC), liquid chromatography (LC), high-performance liquid chromatography (HPLC), capillary electrophoresis (CE), capillary electrochromatography, and thin-layer chromatography (TLC) (Cruces-Blanco and García-Campaña, 2012; Meyer, 2014). Although widely used, GC and LC are not suitable for highly polar, thermally-unstable and non-volatile illicit drugs. Derivatisation techniques can be applied to overcome this issue. However, they may introduce new variables and increase the cost of the analysis. The HPLC is a widely used separation method as it does not require a derivatisation steps for the drugs analysis, thus saving time and resource (Cruces-Blanco and García-Campaña, 2012).

Capillary electrophoresis (CE) and capillary electrochromatography (CEC) methods have recently been applied as a separation method of illicit drugs since they share the same advantages held by HPLC, i.e. no derivatisation step needed, suitable for automation, high efficiency, flexibility, and low consumption of samples and reagents. They can be coupled with several detection systems, such as MS (Cruces-Blanco and García-Campaña, 2012). HPLC and capillary electrophoresis (CE) methods are the most reported separation methods for plant-based drugs (marijuana, poppy seed, and raw opium) (Temerdashev, Grigoriev and Rybalchenko, 2015).

Thin-layer chromatography (TLC), also known as planar chromatography allows the separation of substances while they migrate on a thin layer (100–200 μm) of stationary phase (usually made by silica). Compared to HPLC, TLC is cheaper and allows processing more than one sample at the same time, even though more laborious and time-consuming (Rouessac and Rouessac, 2013). TLC is one of the screening methods of choice for cannabinoids analysis suggested by UNODC (2009b).

In order to identify and quantify illicit drugs, separation methods can be combined to a detection method, such as:

1. Mass spectrometry (MS) and tandem mass spectrometry (MS/MS),
2. Ion mobility spectroscopy (IMS),
3. Raman spectroscopy,
4. Surface-enhanced Raman spectroscopy (SERS),
5. Infrared (IR) spectroscopy,

6. NMR (Nuclear Magnetic Resonance),

An overview of the relevant hyphenated methods for drugs of abuse detection is provided in **Table 1-8**.

Table 1-8: Overview of some relevant hyphenated methods used for illicit drugs detection reported in the scientific literature.

Methods	Sample	Drugs	LOD	Ref.
Various Hyphenated MS Methods	Indoor and outdoor air	Cocaine	From 0.001 to 29.4 ng m^{-3}	(Cecinato, Balducci and Perilli, 2016)
		Δ^9-THC		
		Cannabinol		
		Amphetamine		
Paper Spray Ionisation MS	blood samples	Cocaine	5 ng mL^{-1}	(Su *et al.*, 2013)
DART-MS	commercially available herbal incense samples (synthetic cannabinoids)	AM-2201		(Lesiak *et al.*, 2014)
		JWH-122		
		JWH-203		
		JWH-210		
		RCS-4		
DART- Time-Of-Flight- MS	Surfaces (glass table, floor tile, kitchen table, wood door, paint, cloth quilt, rug)	Methamphetamine	0.025 µg 100 cm^{-2}	(Grange and Sovocool, 2011) (Gross, 2013)
		Amphetamine		
		Heroin		
		Cocaine		
		Morphine	0.1 µg 100 cm^{-2}	
		THC		
HPLC-DAD	Poppy seed	Morphine	1.8 µg mL^{-1}	(Acevska *et al.*, 2012)
		Oripavine	0.3 µg mL^{-1}	
		Codeine	0.6 µg mL^{-1}	
		Papaverine	0.3 µg mL^{-1}	
		Thebaine	0.2 µg mL^{-1}	
		Noscapine	0.5 µg mL^{-1}	

Among them, GS-MS, LC-MS, HPLC-MS, NMR and IR are the equipment commonly used as confirmatory methods (Meyer, 2014). While the MS based analyses are destructive, IR and NMR are non-destructive thus allowing further reanalysis of the sample (D'Elia, Montalvo García and García Ruiz, 2015).

Among the hyphenated MS methods, LC coupled with tandem MS (LC-MS/MS), the direct analysis in real time MS (DART-MS), and the desorption electrospray ionization MS (DESI MS) are becoming popular detection methods for conventional and new illicit

drugs (Mackuľak *et al.*, 2015). Several samples can be analysed by hyphenated methods, such as oral fluids (D'Elia, Montalvo García and García Ruiz, 2015), urine and blood (Erol Öztürk, Yeter and Alpertunga, 2015; Ozturk *et al.*, 2015), exhaled breath (Stephanson *et al.*, 2015), street drugs (Leffler *et al.*, 2014; Gambaro *et al.*, 2015), illicit drugs concealed in carrier solutions (Burnett *et al.*, 2011), contaminated surfaces (Grange and Sovocool, 2011), wastewater (Heuett *et al.*, 2015), air (Cecinato, Balducci and Perilli, 2016), banknotes (Mackuľak *et al.*, 2015), adhesive tapes (Moreno *et al.*, 2014).

Nevertheless, standard materials are still not fully available especially for the new psychoactive substances (NPSs), which limits hyphenated methods application for NPSs detection and identification (Meyer, 2014). While confirmatory tests provide unequivocal evidence, they are not suitable for fast on-site application; time-consuming due to the lengthy sample preparation procedures. Indeed, extraction, digestion, pre-concentration and derivatisation processes may be required (Mali, Karpe and Kadam, 2011; Leffler *et al.*, 2014; Meyer, 2014; Heuett *et al.*, 2015; Jain and Singh, 2016).

1.8 Biosensors

The International Union of Pure and Applied Chemistry (IUPAC) defines biosensor as a *"device that uses specific biochemical reactions mediated by isolated enzymes, immunosystem, tissues, organelles or whole cells to detect chemical compounds usually by electrical, thermal or optical signals"* (Nagel, Dellweg and Gierasch, 1992). A more practical definition of biosensor has been provided by Tothill and Turner (2003), who defined a biosensor as *"a bioanalytical device incorporating a molecular recognition element associated or integrated with a physicochemical transducer"*. Briefly and as shown in **Figure 1-9**, a biosensor consist of:

- a molecular receptor (also known as sensing receptors), able to bind or recognise the analyte of interest;
- a transducer, able to convert the binding event into a signal;
- a signal processor, able to process the signal in electrical signals which can be visualised in a video interface and processed throughout a dedicated software (Analysis, 2011; Altintas, Gittens, *et al.*, 2015; Justino *et al.*, 2015).

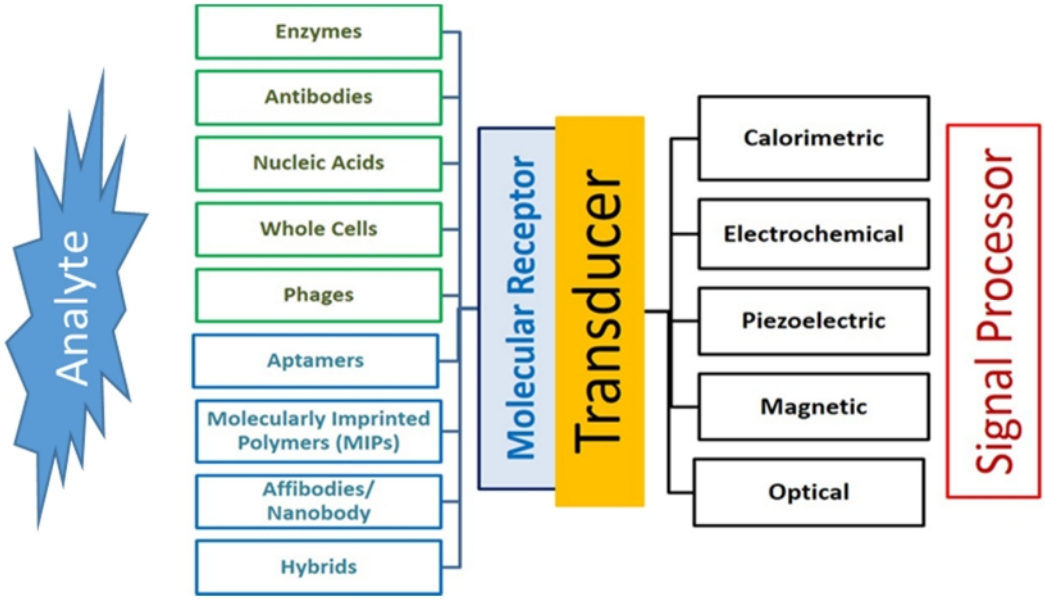

Figure 1-9: Biosensors components.

Several transducers have been developed and they can be classified into the following general category: calorimetric (thermistor), electrochemical (amperometry, potentiometry, conductimetry and impedimetry), mass sensitive (piezoelectric or acoustic wave, mechanical), magnetic or optical (colorimetry, fluorescence, luminescence, interferometry, spectroscopy of optical waveguides and surface plasmon resonance) (Tothill and Turner, 2003; Analysis, 2011; Altintas, Fakanya and Tothill, 2014; Altintas, Kallempudi and Gurbuz, 2014). Biosensors applications covers medical, food, environmental (Ahmed, J. V Rushworth, *et al.*, 2013; Abdin, Altintas and Tothill, 2015; Pawula, Altintas and Ibtisam E Tothill, 2016; Masdor, Altintas and Tothill, 2017) and forensic fields (Yáñez-Sedeño *et al.*, 2014; Gandhi *et al.*, 2015). Biosensors are promising tools for detection and identification of illicit drugs either in trace or bulk forms. According to recent reviews (Yáñez-Sedeño *et al.*, 2014; Gandhi *et al.*, 2015), the most studied transducers to detect illicit drugs belongs to the electrochemical category, followed by SPR and piezoelectric and micromechanical ones. Each transducer can be coupled with different biological or bio-inspired sensing receptors, such as peptides (Tothill, 2010; Heurich, Altintas and Tothill, 2013), antibodies (Masdor, Altintas and Tothill, 2017), whole cells (Mcquillan and Shaw, 2013), bacteriophages (Han *et al.*, 2016; Kim, Moon and Oh, 2016), DNA (Altintas and Tothill, 2012), nanobodies (Goode, Dillon

and Millner, 2016), affibodies (Ilkhani, Ravalli and Marrazza, 2016), aptamers (Piro *et al.*, 2016), molecularly imprinted polymers nanoparticles (nanoMIPs) (Abdin, Altintas and Tothill, 2015; Altintas, Pocock, *et al.*, 2015), and aptamer-MIP hybrid receptors (Turner, 2013; Justino *et al.*, 2015; Poma *et al.*, 2015).

The biosensors platform applications offers several advantages, such as the real-time and on-site result visualisation (Ashley *et al.*, 2017), miniaturisation and portability opportunities (Zhang *et al.*, 2015; Wen *et al.*, 2017), the user friendly and automated procedures (Salam, Uludag and Tothill, 2013), outstanding limit of detection (Farka *et al.*, 2017), reusability through surface regeneration (Goode, Rushworth and Millner, 2015). As shown in **Figure 1-10**, the scientific community has explored the application of biosensor in detecting illicit drugs in recent times.

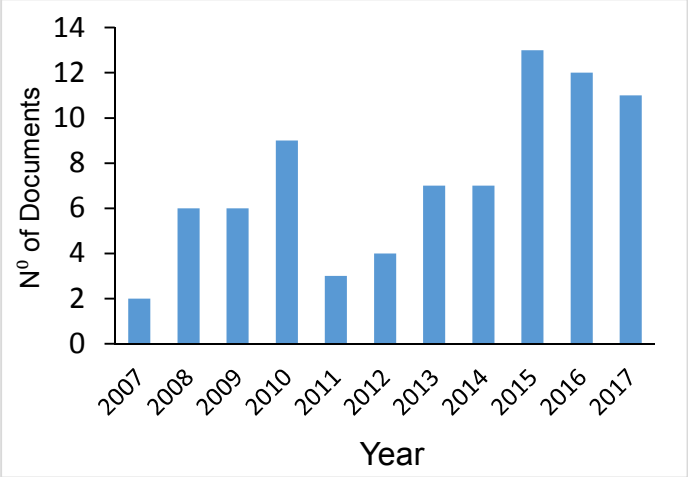

Figure 1-10: Results obtained by searching on Scopus ("TITLE-ABS-KEY" ("sensor")"AND" TITLE-ABS-KEY"(drugs" AND"of" AND"abuse")").

Outstanding performances have been achieved using antibodies (Gandhi *et al.*, 2015), aptamers (Mokhtarzadeh *et al.*, 2015), MIPs or their hybrids as sensing receptors (Piletska *et al.*, 2008; Poma *et al.*, 2015; Garcia *et al.*, 2017; Smolinska-Kempisty *et al.*, 2017). The following sections provide an overview on the biosensors and the nanotechnology application to detect illicit drugs, focusing on the biosensor platforms (EIS and QCM) and the sensing receptor (NanoMIP) used within this work.

1.8.1 Optical Biosensor

Optical sensors measure the variation in optical properties (e.g., intensity, wavelength, polarisation, and phase) arising at the transducer surface when a ligand-binding event occurs (Analysis, 2011). Optical sensors are mainly divided into two types:

1. label based, among which chemiluminescence and fluorescence,
2. Label-free, which includes light absorption and scattering, reflectance and SPR.

Label based optical biosensors are extremely sensitive, but the bias in the fluorescence signal limits its application in quantitative analysis (i.e., it is almost impossible to define the number of fluorophores attached on each molecule, thus possibly resulting in the same signal irrespective to the number of molecules detected). Moreover, the labelling process is time-consuming and can alter the biomolecule activity (Guo, 2012).

Among the label-free optical sensors, Surface Plasmon Resonance (SPR) is the most employed to detect illicit drugs. SPR is a real-time label-free optical biosensor used to study molecular binding interaction, where the optical signal derives and is proportional to the degree of binding between the sensing receptor and the target occurring at the biosensor surface (Tothill, 2011; Altintas, Fakanya and Tothill, 2014; Chardin *et al.*, 2014; Nguyen *et al.*, 2015). As shown in **Figure 1-11**, the SPR biosensor platform relies on the changes of the refractive index the light induced by ligand-analyte binding occurring at the gold sensor surface and probed by the surface plasmon wave (SPW) (Nguyen *et al.*, 2015).

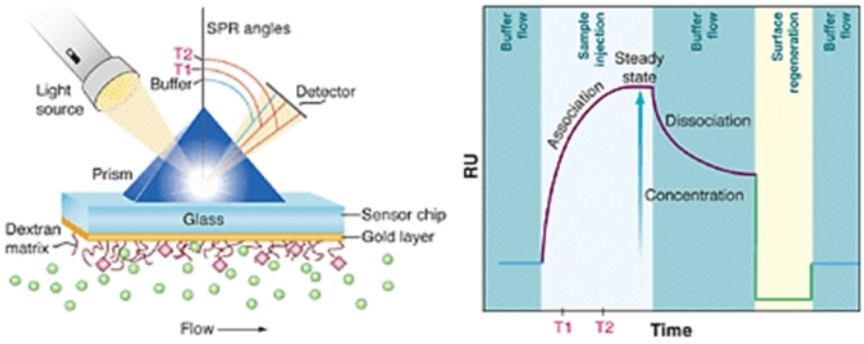

Figure 1-11: SPR operating principle and SPR signal at sample injection and regeneration steps generated by the change of the refractive index (Wilson, 2002).

The components of a SPR platform are a light source light, light detector and the glass prism coated by a 50 nm gold layer, which is functionalised with a bioreceptors (such as antibodies). The SPW is induced as the light passes through the glass prism and probes the materials in contact with the sensor surface. Any change occurring at the boundary induce a change in the propagation of the SPW and in the reflectivity of the coupled light wave (Hinman, McKeating and Cheng, 2018). Recently, SPR based biosensors for detecting the selected illicit drugs have been developed achieving a LOD in the order of pg μL^{-1}, as reported in **Table 1-9**.

Biolayer interferometry (BLI) is a well-established label-free optical biosensor platform able to provide results in real-time (D. Yang *et al.*, 2016). The core principle of BLI relies on the use of white light interferometry to detect and quantify different analyte, ranging from small molecule to cells (Gao, Zheng and Wu, 2017). The BLI measures the interference of the reflected light occurring at the two surfaces of the end of an optical fibre. The first surface act as an internal reference surface (e.g., surface functionalised with antibodies) and the second surface occurred upon the analyte-receptor binding event. The light travelling along the optical fibre will be reflected at the two different surfaces inducing two reflected beams, which interfere with each other thus inducing a shift in the wavelength. The shift is directly related to the amount of the analyte binding or dissociating at the functionalised tip surface (Petersen and L., 2017). Compared to the SPR, BLI does not require a microfluidic system and commercially available BLI enable to operate simultaneously on 384-wells (Octet RED384, FortéBio® Menlo Park, CA, USA).

Dynamic light scattering (DLS) coupled with gold nanoparticles (AuNPs) is an innovative, yet cheap, optical biosensor platform. DLS has been recently proposed for the detection of small analytes (such as toxic metal ions and DNA) as well as on microorganism, such as *Listeria monocytogenes* (Huang *et al.*, 2015). The AuNP DLS-biosensor principle combines the high light scattering ability of the gold nanoparticles with the ability of the DLS to detect the aggregation of antibody functionalised AuNPs upon analyte binding. Indeed, the AuNPs aggregation results in a changing in colour, an enhanced absorption and an increase of the of the average particle size which is detected by DLS (Zheng, Bott and Huo, 2016). The DLS technique is described in Section 2.3.7.1.

1.8.2 Piezoelectric Biosensor

Piezoelectric sensor belongs to acoustic wave based sensors and can monitor in real-time a biological event (i.e. ligand-analyte binding) occurring at the sensor surface and which induces a change in the physical properties of an acoustic wave. Piezoelectric sensor relies on the piezoelectric effect exhibited by quartz (SiO_2) and other similar materials. Quartz is the mostly common material used to fabricate acoustic sensors, which are grouped in: bulk acoustic wave (BAW) and surface acoustic wave (SAW) sensors (Fogel, Limson and Seshia, 2016). Both of them rely on the piezoelectric effect which is the ability of quartz crystal to generate an electrical voltage when it is compressed or stretched. Also, the opposite is true, meaning that the quartz crystal can be shortened or lengthened by applying an electrical voltage. When a voltage, generated by alternating current (AC) is applied, the quartz repeats the compression-stretching cycle at a particular oscillating frequency (*f*). A description of the generation of the acoustic wave in BAW and SAW sensor is provided in **Figure 1-12**. The Quartz Crystal Microbalance (QCM), one of the sensor platform used in this work, is a BAW sensor and is widely applied in biosensors development in several areas, such as biomedical, environmental and food safety sectors (Halámek *et al.*, 2002; Uludag and Tothill, 2012; Masdor, Altintas and Tothill, 2016).

The QCM chip is made by a thin disk of AT-cut quartz crystal (i.e. the disk is cut out from the quartz at 35.25^0 orientation from its optical axis) and it is sandwiched between two metal electrodes (usually gold). The piezoelectric effect occurs as a shear (tangential) deformation which is induced by the application of an alternating voltage.

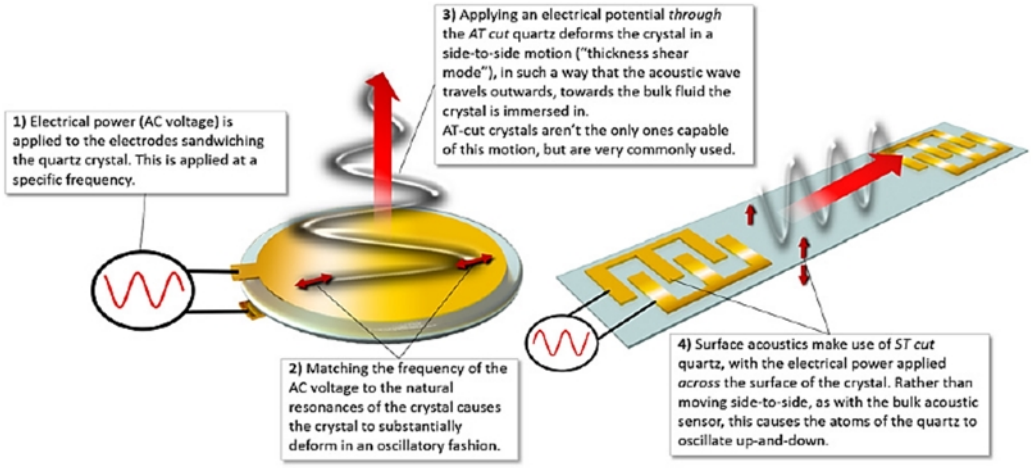

Figure 1-12: Description of the general process to induce acoustic wave in SAW and BAW sensor (from Fogel et al., 2016).

This deformation induces a side to side and opposite directed movement of the two surfaces, thus creating an acoustic wave which propagates perpendicularly from the bulk crystal toward the sensor surface (Ferreira, da-Silva and Tomé, 2009; Chen, Penn and Xi, 2018). Thus the QCM sensor, also named acoustic resonator, resonates at a particular frequency (f, Hz), which is sensitive to the mass changes at the sensor surface (Fogel, Limson and Seshia, 2016). When the sensor operates in an unaltered ambient environment and the bonded material is rigid, thin and uniformly distributed onto the QCM sensor, the Sauerbrey's equation (1-1) is used to relate the change of the oscillation (or resonant) frequency of the quartz crystal (Δf) to the change in the mass at the QCM surface (Δm_q).

$$\Delta f = \left(\frac{-2f_{r0}^2}{A\sqrt{\rho_q G_q}}\right)\Delta m_q \tag{1-1}$$

Where:

f_{r0} *is the resonant frequency of the quartz crystal;*
A *is the active surface area;*
ρ_q *is the density of the quartz;*
G_q *is the share modulus of the quartz crystal.*

When the resonator is immersed in a fluid (as in the QCM biosensor platform) and the viscoelastic materials (such as biomolecules) are attached onto the sensor surface, the

frequency changes is not anymore related to only the mass changes, but rather proportional to the changes of the viscosity (η_L) and density (ρ_L) of the fluid and is described by Kanazawa and Gordon equation (1-2) (Ferreira, da-Silva and Tomé, 2009). Under this circumstance, the oscillation frequency is dissipated by the damping effect induced by the changes in viscosity and density of the soft layer at the sensor surface boundaries.

$$\Delta f = -f_{r0}^{3/2}\sqrt{\frac{\Delta(\rho_L \eta_L)}{\pi \rho_q G_q}} \quad (1\text{-}2)$$

Where:

ρ_L *is the density of the liquid;*
η_L *is the viscosity of the liquid.*

If the buffer composition constant kept constant throughout the cumulative assay, the viscosity of the liquid (buffer solution) is considered constant whereas the concentration of the analyte dissolved in the buffer solution changes the density and the viscosity at the sensor surface, thus yielding the frequency changes of the QCM signal response. As reported in **Table 1-9**, different QCM based sensors have been explored to detect illicit drugs, and some reached already the market stage. Most of them rely on a competitive immunoassay. Though, Romero Guerra et al. (Romero Guerra *et al.*, 2009) developed a QCM sensor having a molecularly imprinted polymer film against methamphetamine. Even though the achieved LOD was 1 µg mL^{-1}, this can be a good starting point in the development of a fast, cheap and on-site MIP based biosensor for illicit drug detection.

Notably, the BIOSENS®600 (Biosensor Applications Sweden AB, Sweden) is a commercially available piezoelectric SAW biosensor using a monoclonal antibody as a sensing receptor. It is designed to detect methamphetamine and MDMA, D9-THC, cocaine, opiates and benzodiazepines in liquid, powder, tablet and on items which have been in contact with the drugs (such as steering wheels, bags or wallet), human skin and oral fluid. Blencowe et al. (2011) assessed the BIOSENS® (Biosensor Applications Sweden AB, Sweden) (older devices release) performances in comparison with the confirmatory test (GC-MS). While the specificity and accuracy values were notable for

amphetamine, cocaine and opiates, the BIOSENS® poorly performed in detecting cannabis. Nevertheless, the BIOSENS® manufacturer declares that the latest devices analysis time takes only 30 seconds and that it has to be considered a presumptive test.

1.8.3 Electrochemical Biosensors

Electrochemical biosensors are able to detect the change of an electrical property (i.e., current, potential, resistance) upon the binding event between a target analyte and its specific bio or bio-inspired receptor occurring at the transducer interface (Bănică, 2012; Jaffrezic-Renault, 2013; Yoon, 2013). The binding event is detected at the working electrode (Li *et al.*, 2015). Usually, the working electrode surface is coated with a sensing layer (e.g., antibodies, molecularly imprinted polymers, and aptamers). Furthermore, the working electrode surface is in contact with an electrolyte solution. Upon binding events, ions or electrons may be supplied or withdrawn, thus inducing some change in the measurable electrical properties (Monošík, Stred'anský and Šturdík, 2012). Thus, electrochemical biosensors are grouped according to the measured electrical property, i.e. the measurement of the change in current intensity (amperometric/ voltammetric), electric potential energy (potentiometric), electrolytic conductivity (conductimetric), current resistance in circuit (impedance) or in the amount of electric charge (capacitance) (Ahmed *et al.*, 2014; Gandhi *et al.*, 2015).

The amperometric biosensor records the change in the current at a fixed voltage, whereas the potentiometric biosensors monitor the change in the voltage at zero current. Finally, the impedance-based biosensors monitor the change in the total electrical resistance to the flow of an alternating current while it passed through an electrochemical system (Tothill, 2001; Jaffrezic-Renault, 2013; Uygun, 2013; Goode, Dillon and Millner, 2016). In potentiometric and amperometric biosensors, the electric signal is due only to an electrochemical reaction, and it is correlated to the reaction rate through the Faraday's Law. The glucose sensor based on the ferrocyanide mediated glucose oxidase (GO_x) is a typical example of an amperometric sensor and was firstly developed by a joint collaboration between Cranfield and Oxford University in 1987 (Turner, 2013). The sensor detects the amount of glucose occurring in a sample by firstly converting the

glucose in gluconic acid by the GO_x enzyme. The reduced GO_x is then oxidised again by the ferricyanide ion $(CN_6)^{3-}$, which is reduced into the ferrocyanide ion $(CN_6)^{4-}$. The ferrocyanide ion gives the ion to the electrodes, thus generating the electrical current. Therefore, the amperometric sensor measures the change or the generation of a current induced by the redox reaction of electroactive species occurring at the electrodes surface (Hammond *et al.*, 2016). The amperometric biosensor was then developed using a sandwich assay format, where the secondary antibody is labelled an enzyme (such as horseradish peroxidase). The analyte binding is then detected and quantified by adding the specific enzyme mediator/substrate, which generates the electrical current(Yoon, 2013). Amperometric biosensors were successfully developed to detect a wide range of analytes, such as cancer biomarkers, narcotics, food allergens and contaminants (Eissa *et al.*, 2012; Altintas and Tothill, 2013; Altintas, Fakanya and Tothill, 2014; Gandhi *et al.*, 2015).

The potentiometric sensor measures the ion activity by detecting the difference in the potential between the RE and the WE due to the occurrence of charged species at the cathodic interface. Lai et al. (2017) recently developed a potentiometric biosensor able to detect urea at 5 M concentration. The biosensor consisted of urease enzyme immobilised onto an ITO glass electrode, previously modified with a conductive polymer poly(3-hexylthiophene-co-3-thiopheneacetic acid 1:1) (P(3HT-co-3TAA). The sensor detected and quantified the increase in $p[OH^-]$ in the sampled solution due to the urea hydrolysis caused by the urease. Other potentiometric biosensors were also developed to detect Bovine Herpes Virus-1 (Adnane, 2011) and cocaine (Smolinska-Kempisty *et al.*, 2017).

Instead, the impedance biosensor measures the resistive and capacitive properties of the system by applying a fluctuating potential as a function of frequency (Ronkainen, Halsall and Heineman, 2010). Examples of electrochemical biosensor developed per each selected drugs of abuse have been reported in **Table 1-9**.

Table 1-9: Non-exhaustive list of biosensors for drugs of abuse detection.

Biosensor	Transducer	Sensing receptor	Assay Principle	Drugs	Samples	LOD	Linear range	Ref
Optical	SPR	Antibodies	Indirect	Amphetamine		5 pg μL^{-1} (37 nM)		(Klenkar and Liedberg, 2008)
	SPR	Antibody	Indirect	Heroin		0.5 pg μL^{-1} (1.4 nM)		
	SPR	Antibodies	Indirect	Cocaine		2.5 pg μL^{-1} (7.4 nM)		
	fluorescence based sensors	aptamer	Direct	Cocaine	spiked serum	COC: 0.07 ng mL^{-1} - 209 pM ; COC in spiked serum: 293 pM (0.1 ng mL^{-1})	0.5–20 nM 0.17 – 6.8 ng mL^{-1}	(Emrani *et al.*, 2016)
	fluorescence based sensors	MIP	Direct	Cocaine	diluted cocaine		500 and 1000 µM 169.91 – 339.81 µg mL^{-1}	(Wren *et al.*, 2014)
	Fluorescence Microscope	aptamer	Direct	cocaine	diluted cocaine	10 pM - 3.4 pg mL^{-1}	-	(Hilton *et al.*, 2011)
Piezoelectric	QCM	MIP film	Direct	Methamphetamine	Methamphetamine	1 µg mL^{-1} – 6.7 µM	-	(Romero Guerra *et al.*, 2009)
	QCM	Monoclonal antibody	Competitive	Cocaine	oral fluids	-	17-1847 ng mL^{-1} 0.05 – 5.4 µM	(Blencowe *et al.*, 2011)
	QCM	Monoclonal antibody	Competitive	Opiates (morphine)	oral fluids	-	20-8259 ng mL^{-1} 0.05 - 21.8 µM	(Blencowe *et al.*, 2011)
	electromagnetic piezoelectric acoustic sensor (EMPAS)	Aptamer	Direct	Cocaine	diluted cocaine	0.9 µM 0.31 µg mL^{-1}	2 - 50 µM 0.68 – 17 µg mL^{-1}	(Neves *et al.*, 2015)

Biosensor	Transducer	Sensing receptor	Assay Principle	Drugs	Samples	LOD	Linear range	Ref
Electrochemical	Electrochemiluminiscence	Aptamer	Direct	Cocaine	diluted cocaine	10 pM - 3.4 pg mL^{-1}		(Sun *et al.*, 2010)
	Electrochemiluminiscence	Aptamer	Sandwich	Cocaine	spiked banknotes	3.7 x 10^{-12} mol L^{-1}/ banknotes 1.26 pg mL^{-1}	1.0 x 10^{-11} to 1.0 x 10^{-9} mol L^{-1} 3.4 – 339.81 pg mL^{-1}	(Cai *et al.*, 2011)
	Electrochemiluminescence	Aptamer conjugated HRP	Direct	Cocaine	Serum	0.48 nM 163 pg mL^{-1}	10^{-9}–10^{-8} M 339.81 – 3398 pg mL^{-1}	(Li, Ji and Liu, 2011)
	Amperometric	CYP 450 (enzyme)	Direct	Cocaine	street samples	23.05 nM 7.8 ng mL^{-1}		(Asturias-Arribas *et al.*, 2013)
	Amperometric	MIP film	Direct	Morphine	morphine	0.2 mM (57.0 µg mL^{-1})		(Yeh and Ho, 2005)
	Voltammetric	Aptamer	Direct	Cocaine	serum, saliva,	<10 mM < 3.39 mg mL^{-1}		(Baker *et al.*, 2006).
	Voltammetric	Aptamer	Direct	Cocaine	spiked serum	100 pM 34 pg mL^{-1}	1 nM to 11 µM 0.34 – 3738 ng mL^{-1}	(Roushani and Shahdost-fard, 2016)
	EIS	Aptamer	Direct	Cocaine	spiked serum	200 pM 68 pg mL^{-1}	2–8 nM 0.68 – 2.72 ng mL^{-1}	

1.9 Electrochemical Impedance Spectroscopy (EIS)

As a powerful tool to detect interfacial events, EIS (one of the investigated technique in this work) has been applied for a long time to study the corrosion mechanism, the membrane charge and to develop batteries (Santos et al. 2014). EIS measures the electrical impedance, which indicates the opposition that an electrical circuit presents to the flow of an alternating current (AC). The AC is generated by applying a small alternating voltage (AV), typically between 2 to 10 mV, and is measured as a function of frequency (Daniels and Pourmand, 2007; Rushworth *et al.*, 2013; Santos, 2014; Muñoz, Montes and Baeza, 2017). This perturbation induces a current response characterised by an impedance measurement (Z), which is expressed as:

$$Z = \frac{V_{(t)}}{I_{(t)}} = \frac{V_0 \sin(2\pi f t)}{I_0 \sin(2\pi f t + \varphi)} = \frac{1}{Y} \tag{1-3}$$

Where:

- V_t *is the voltage-time function;*
- I_t *is the current–time function;*
- V_0 *is the maximum voltage signal;*
- I_0 *is the maximum current signal;*
- f *is the frequency;*
- t *is the time;*
- φ *is the phase shift between the voltage-time and current–time functions;*
- Y *is the complex conductance or admittance.*

The applied alternating voltage should be small enough, usually below 10 mV, for two reasons (Daniels and Pourmand, 2007):

8. Within this perturbation, the current-voltage response will be linear.
9. At this voltage, the bonds between the electrode surface and the sensor receptor as well as between the sensor receptor and the analyte will not be affected. Indeed the covalent bound energies occurring between the sensing receptor and the electrode is usually in the order of 2-3 eV, whilst the one between the sensing receptor and the analyte may be much lower.

Since the impedance measurements are recorded at different frequencies, usually between 10^6 and 10^{-4} Hz, EIS is defined as a spectroscopic technique (Lisdat and Schäfer, 2008; Rushworth *et al.*, 2013; Santos, 2014).

The impedance measurement is expressed by a complex value, i.e. the real value and the imaginary value ($j = \sqrt{-1}$). Hence, the impedance measurement can be broken down into its components (Rushworth *et al.*, 2013):

1. The in-phase current response which is the real (resistive) component of the impedance;
2. The out-of-phase current response which constitutes the imaginary (capacitive) component of the impedance.

Two different plots are used to illustrate the impedance values (Z) (Prodromidis, 2010; Rushworth *et al.*, 2013):

1. Nyquist plot, where the capacitive component (Z_i) is plotted against the resistive one (Z_r) at each excitation frequency;
2. Bode plot, where both the logarithm of the impedance module, |Z| and the phase shift, φ, are plotted against the logarithm of the excitation frequency.

The Bode plot highlights the relationship between the impedance and the frequency, whereas the Nyquist plot highlights the relationship between the resistance (real value) and the capacitance (imaginary value) (Lisdat and Schäfer, 2008; Muñoz, Montes and Baeza, 2017).

1.9.1 EIS Equipment

EIS equipment requires an electrode which is immersed into an electrolyte solution, and connected to a potentiostat/galvanostat and a frequency response analyser (FRA) (Jaffrezic-Renault, 2013). Generally, three different electrodes are used in the electrochemistry, namely, working electrode (WE), counter or auxiliary electrode (CE or AE), and reference electrode (RE). The WE is generally made of inert materials, such as gold, platinum or glassy carbon, and is where the reaction of interest takes place. The CE is made of inert material and is used to close the circuit of the electrochemical cell, thus

allowing the measurement of the current flowing between the WE to the CE. The RE is made of Ag/AgCl and allows to control the potential at the working electrode (Harris, 2010).

The electrochemical cell is composed of the electrodes and the electrolyte solution. In the EIS biosensor, the electrochemical cell can have a two or three electrodes configurations. The two electrodes configuration (only WE and CE) is used when the whole system is under investigation and no potential control at reference electrodes is needed. The three electrodes configuration (WE, CE and RE) is used when only the reaction occurring at the WE has to be investigated (Jaffrezic-Renault, 2013). The EIS can be performed with or without an electrochemical reaction occurring in the solution, thus resulting in the faradaic process and the non-faradaic process, respectively (Santos, 2014; Goode, Dillon and Millner, 2016; Arya *et al.*, 2018). In the former instance, a redox probe (redox couple), such as potassium ferricyanide/ferrocyanide $[Fe(CN_6)]^{3-/4-}$, is added into the solution. The FRA/potentiostat system introduces desired voltage between the WE and the electrolyte solution and, concurrently records the current flowing between them (Jaffrezic-Renault, 2013; Santos, 2014).

1.9.2 Electrical Elements and Equivalent Circuits Modelling

The impedance spectrometry measurements provide information about:

1. the electric resistance of the cell (ohmic resistance);
2. the double layer capacitance (capacitance);
3. the diffusion process (Warburg impedance).

Solution resistance (Rsol) and the charge transfer resistance (Rct) contributes to the overall system resistance. The Rsol depends on the ions concentration, the conductivity of the solution, temperature and the area among which the current is carried out. The Rct, sometimes referred as electron transfer resistance (Ret) (Santos, 2014; Uygun and Ertuğrul Uygun, 2014), is one of the electrical components of the EIS biosensor and refers to the resistance against the charge transfer from the metal electrode to the solution. Indeed, when a metal is immersed in an electrolyte, it spontaneously dissolves into the

electrolyte, thus diffusing metal ions. The charge transfer is due to the ions diffusion and promoting the redox reaction according to the forward reaction:

$$\text{Red} \leftrightarrow Ox + ne^-$$

This reaction depends on the concentration of the reaction products, the applied potential and the temperature. When the imposed potential is small, the system is at equilibrium, and the relation between the Rct and the current can be expressed as (Randviir and Banks, 2013):

$$R_{ct} = \frac{RT}{nF\ i_0} \tag{1-4}$$

Where:

- *R* *is the gas constant;*
- *T* *is the temperature;*
- *n* *is the number of electron involved;*
- *F* *is the Faraday constant;*
- i_0 *is the exchange current density.*

Double-layer capacitance is due to electrical double layer effect. When a voltage is applied to the working electrode surface immersed into an electrolyte, the electrons are withdrawn or supplied thus changing the overall electron distribution at the electrode surface. Consequently, the ions in the solution migrate from or to the surface to compensate the surface charge, until zero charges is achieved at the electrode surface. This charges flow gives rise to current flow. Also, a thin insulating layer (in the order of few angstroms) separate the charged electrode from the charged ion, thus creating a capacitor (Santos, 2014).

As schematically illustrated in **Figure 1-13**, when a negative charge is applied at the electrode surface, an electrical double layer is formed. The first layer in direct contact with the electrode is the compact ion layer, which is due to the migration of the positively charged ions present in the solution towards the negative electrode surface. More in details, they are hydrated ions, and therefore the hydrogens are oriented towards the electrode surface. The second layer is named "diffusion layer" and consists of ions

randomly distributed, although even in this layer the cation ions are more abundant compared to anion ions since weak electrostatic forces still exist. As moving away from the electrode surface, the charges start to balance until reaching the neutral solution area. In the compact ion layer, the potential energy decreases linearly as the distance from the electrode increase. In the diffusive layer, the potential energy slowly and asymptotically decrease. The thickness of the two layers (compact and diffusive) varies by increasing or decreasing the electrolyte concentration. If the electrolyte is highly concentrated, the compact layer increases, while the diffusive layer decreases. The contrary occurs when the electrolyte less concentrated. Warburg impedance (W) is due to the mass-transfer limitation and describes the impedance of the current caused by the bulk diffusion to the interface (Lvovich, 2012).

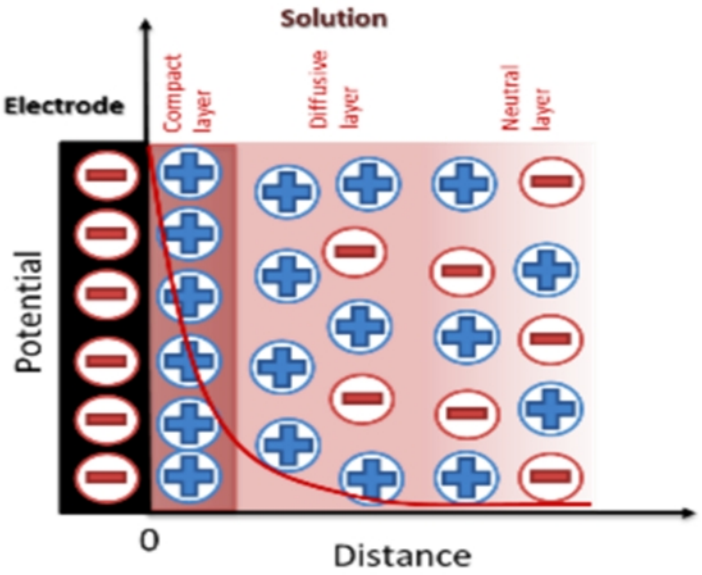

Figure 1-13: Double layer at the electrode/solution interface in the case of a negatively polarised electrode (adapted from Bănică 2012).

To get the value of each electrical elements (Rct, Rsol, Cdl) EIS experimental data are fitted into an equivalent circuit (Uygun and Ertuğrul Uygun, 2014; Muñoz, Montes and Baeza, 2017). The Randles circuit coupled with the Nyquist plot is often used in EIS biosensors data analysis, as shown in **Figure 1-14**.

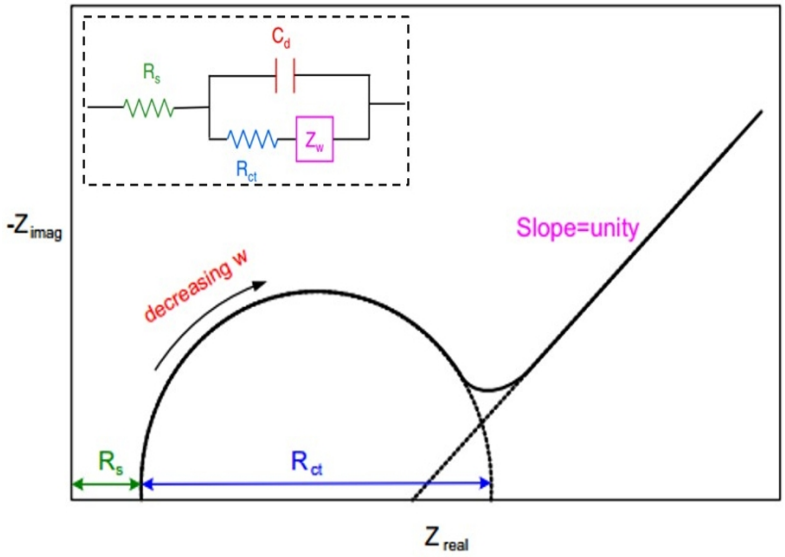

Figure 1-14: Nyquist plot and Randles circuit (inserted dash frame). w (ω) is the frequency; R_s is the solution-phase resistance; Cdl is the double-layer capacitance; Rct is the charge-transfer resistance (inversely proportional to the rate of electron transfer); Z_w is the Warburg impedance, arising from mass-transfer limitations (from Suni, 2008).

1.10 Electrodes Used in EIS Measurement

When the surface of the working electrode is coated with a sensing layer, electrochemical impedance spectroscopy (EIS) biosensor arises. The electrodes used in EIS technique can be either round shaped electrode screen-printed electrode (SPE) or interdigitated electrode (IDE), as shown in **Figure 1-15**.

The three electrodes configuration is used in the first option. Furthermore, the sensing layer covers the working electrode surface, and the binding event is controlled against to a reference electrode (Santos, 2014; Muñoz, Montes and Baeza, 2017). In the second option, the twin electrodes (WE and CE) are assembled in an interdigitated way. The sensing layer may either lay down between the electrodes, over the electrodes or the whole electrodes (Lisdat and Schäfer, 2008; Jaffrezic-Renault, 2013).

As the voltage is applied, the current flow across both the sensing layer and the bulk solution and the impedance signal is generated upon the binding event occurring at the surface of both the working and counter electrodes.

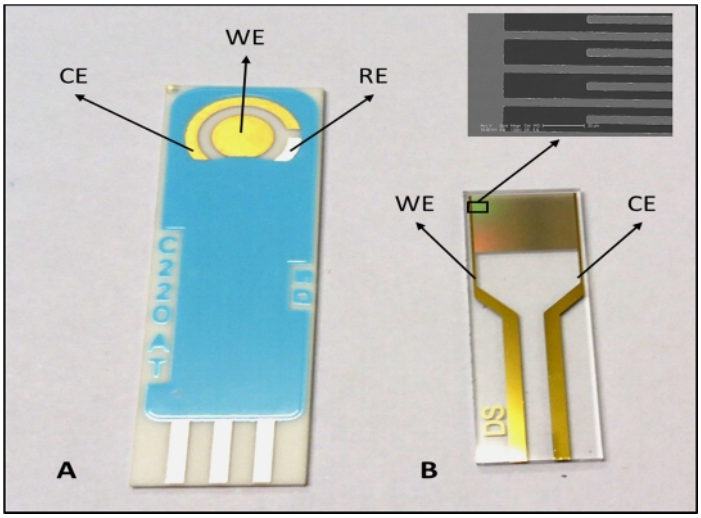

Figure 1-15: Commercially available (A) round shape electrodes screen-printed electrode (SPE) and (B) interdigitated electrode (IDE). WE = working electrode; CE = counter electrode; RE = reference electrode.

The use of a reference electrode to control the signal background is not required (Arya *et al.*, 2018) , although it has been suggested by Bănică (2012). The change in the impedance components (Rct and Cdl) directly expresses the solution composition or the binding occurring at the electrode/solution interface. When the EIS technique is applied for quantitative purposes, the impedance can be related to different concentrations (Lisdat and Schäfer, 2008).

The EIS biosensor can be classified in two main formats: non-Faradaic (or capacitive) and Faradic (or Faradaic impedimetric). In both cases, the coating of the working electrode surface, the signal amplification and the functionalization to allow sensing receptors attachment play a key role in the success of the biosensor development.

1.10.1 Faradaic EIS Biosensor

The impedance spectroscopy can be performed with an electrochemical reaction occurring in the solution, thus gathering the faradaic process. To this aim, a redox probe (redox couple) is added to the electrolyte solution. Usually, $[Fe(CN)_6]^{3-/4-}$ ions are used as a negatively charged redox probe, while the hexaammineruthenium III/II ions are used as positively charged redox probes (Bănică, 2012; Muñoz, Montes and Baeza, 2017). In

this format, the biosensor signal relies on the current generated from the charges transfer across the interface (Santos, 2014). Indeed, the working electrode surface is covered entirely by a non-insulating or partially covered by an insulating layer. The working electrode can catalyse the redox reaction of the redox probe, which is added to the solution. Thus an electron transfer from and to the working electrode is generated by the alternating reduction and oxidation of the redox probe.

The change in Rct gives the signal of the binding event occurring at the electrode surface. Indeed, the binding events induce an increase in the thickness of the sensing layer, thus hindering the contact between the electrolyte solution and the electrode surface. As can be inferred, the larger the analyte, the thicker the sensor layer become. As a consequence, the charge transfer resistance increases. Nevertheless, also the analyte or the sensing layer charges, if any, may influence the Rct signal since it can induce repulsive or attractive force according to the charge of the solution ions. Overall, the charge transfer resistance (Rct) is the measured parameter, which is the real component of the impedance, as shown in **Figure 1-16**.

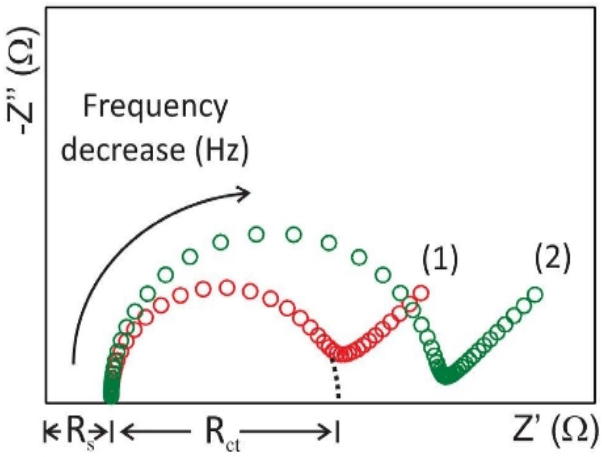

Figure 1-16: Nyquist plot for non-faradic EIS biosensor, before (1) and after ligand analyte binding (From Santos et al., 2014).

Furthermore, the diffusion of the redox probe towards the electrode surface may affect the current flow and is quantified by the Warburg impedance Z_w. The Rct and the Z_w are coupled in series in the equivalent circuit. Although, the current can also flow along the

double layer capacitance (C_{dl}), which therefore is coupled in parallel with the Rct. Finally, the solution resistance also may impede the current flow, which therefore is placed in series with all the previous impedance components.

The resulting circuit model is the Randles circuit, shown in the **Figure 1-17A**. When the Warburg impedance is not visible, the simplified Randles circuit is applied (**Figure 1-17B**). The measurement is taken at the frequency values, typically 0.1–1.0 Hz, while the AC voltage is kept very low (usually ≤ 10mV) (Bănică, 2012). Compared to the non-Faradic, the Faradaic EIS biosensor has higher sensitivity, though the redox probe may affect the electrode coating layer (Prodromidis, 2010). Since this work aims to develop an EIS sensor to detect drugs of abuse in trace level, the Faradic EIS format will be applied.

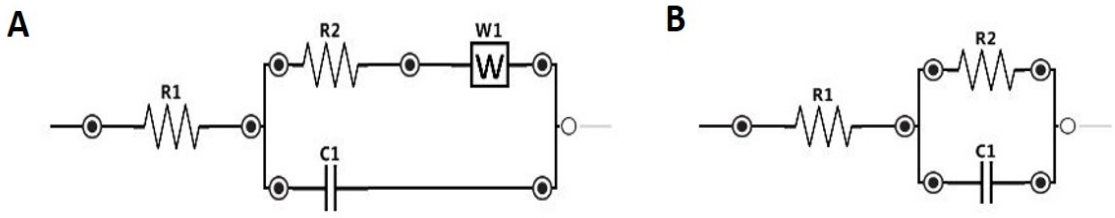

Figure 1-17: Screenshot sourced from PalmSens PS5 software. (A) Randles circuit and (B) simplified Randles circuit, where R1 = Rsol, R2 = Rct and C1= Cdl.

1.10.2 Non-Faradaic (Capacitive) EIS Biosensor

In the non-Faradaic biosensor, the redox probe is not required, and the electrode surface is entirely covered by a dielectric layer and behaves as an insulator. However, a saline solution (such as phosphate buffer, or sodium chloride solution) is still required (Arya *et al.*, 2018). In the non-Faradaic EIS biosensor, the electrode/solution interface behaves like an electrical capacitor, which can store the electric energy. The binding event between the sensing receptor and the target analyte is expected to decrease the capacitance. Once a receptor layer covers the working electrode, the distance between the electrode surface and the compact ion layer increases. Furthermore, the dielectric constant

of a biomolecule (ε_r~ 2-5) is considerably lower compared to the water one (ε_r = 80), thus decreasing the ability to store electrical energy (Davis, 2009). As illustrated in **Figure 1-18**, the capacitance of the electrode layer is the sum of the following capacitances:

- The capacitance of the insulating layer (C_m), which includes the self-assembled monolayer (SAM) and the electrical double layer.
- The sensing receptor layers (C_{rec}).
- The layer arising upon the binding between the sensing layer and the analyte (C_a).

To achieve a good signal, the insulating layer should be impermeable to ions from the solution, while being as thin as possible.

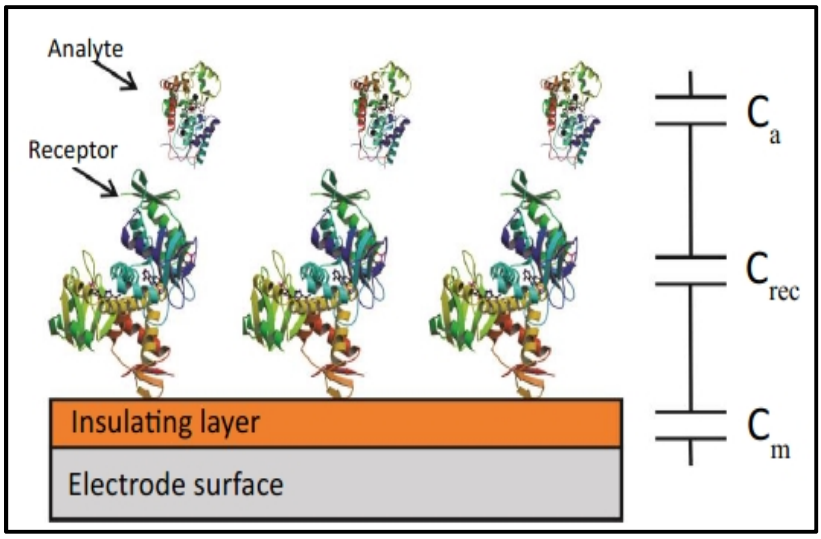

Figure 1-18: Schematic representation of a non-faradaic EIS biosensor (from Santos et al., 2014).

1.10.3 EIS Biosensor Advantages and Drawbacks

In comparison with other electrochemical technique, EIS provides detailed information on the resistive and capacitive properties of the recognition surface (Jaffrezic-Renault, 2013). Furthermore, EIS popularity has been recently increasing due to the many advantages over others biosensors, i.e. the miniaturisation feasibility, easiness to use, the low-cost production, the on-site application opportunity and the low limit of detection (in the order of nM/pM) (Rushworth *et al.*, 2013; Santos, 2014; Muñoz, Montes and Baeza,

2017; Arya *et al.*, 2018).

Compared to amperometric biosensors, EIS has some advantages. Whereas amperometric sensors rely on the Faradaic current which is generated only by the electrochemical reactions, the impedance-based biosensor takes into consideration also the capacitive current (also known as Non-Faradaic currents or charging current) which is triggered by electric charges (electrons and ions) rearrangement at the electrode solution interface. Therefore, while all amperometric biosensors should be designed to reduce the capacitive current as low as possible thus to reduce the noise effect, the EIS biosensors measure the impedance at the electrode/solution interface and takes into account both types of currents (capacitive and resistance) (Bănică, 2012; Jaffrezic-Renault, 2013; Rushworth *et al.*, 2013). EIS spectrometry is not affected by the mass-transfer, and can directly detect the binding between the sensing receptor and its analyte, while preserving the sample (Ram *et al.*, 2016). Another key advantage is that the small voltage applied does not damage the biosensing receptors layer (Daniels and Pourmand, 2007).

These advantages bestow EIS biosensors as fast, sensitive and accurate electrochemical biosensors. The EIS drawbacks include the complex and not automated data processing, occurrence of non-specific binding, reproducibility (Daniels and Pourmand, 2007; Ahmed *et al.*, 2014). However, both recent advance in technology and the application of nanotechnology allow minimising the aforementioned limitations.

1.10.4 EIS Biosensors for Drugs of Abuse Detection

EIS biosensors have been already explored as a tool to detect drugs of abuse in biological samples (e.g., blood, urine) and having aptamers or antibodies as sensing receptor. A summary of the most recent and relevant EIS based biosensors for drugs of abuse detection have been reported in **Table 1-10.**

The most investigated EIS biosensor is the Faradaic one. Although good LOD has been reached, the Faradaic EIS biosensors developed so far are not suitable as on-site, fast and portable tools. Indeed Faradaic EIS biosensors still need reagents addition and data processing. Therefore, further development of EIS biosensor is needed.

Table 1-10: Summary of relevant studies on EIS biosensor for drugs of abuse detection.

Drugs	Samples	Sensing Receptor	LOD	Redox Probe	Scan	Ref.
Cocaine	Cocaine hydrochloride (sewage)	Aptamer	10 nM 3.4 ng mL^{-1}	2 mM $[Fe(CN)_6]^{3-/4-}$ in 50 mM PBS (pH 7.0)	100 kHz to 1 Hz; AV= 10 mV	(Z. Yang *et al.*, 2016)
	spiked serum	Aptamer-conjugated with PtNPs	200 pM 68 pg mL^{-1}	5 mM $Fe(CN_6)^{3-/4-}$in 0.1 M KCl.	-	(Roushani and Shahdost-fard, 2016)
	Cocaine (real sample)	Aptamer	0.3 µM 0.1 µg mL^{-1}	5 mM $[Fe(CN)_6]^{3-/4-}$ in 0.1 M KCl	10 mHz to 10 kHz; AV= 220 mV	(Hua *et al.*, 2010)
	Cocaine solution	Aptamer	0.1 nM 34 pg mL^{-1}	1 mM $[Fe(CN)_6]^{3-/4-}$ and 0.1 M NaCl	AV= 179 mV 0.1–10 kHz.	(Sheng *et al.*, 2014)
Morphine	Human urine and plasma	MIP film	qualitative study	5 mM $[Fe(CN)_6]^{3-/4-}$ in 0.1 M KCl	5 mHz to 100 kHz AV = 5 mV	(Rezaei, Foroughi-Dehnavi and Ensafi, 2015)
	Morphine spiked blood samples	Antibody	0.7 fM 0.27 pg L^{-1}	1x 10^{-3} mol L^{-1} $[Fe(CN)_6]^{3-/4-}$ in 0.01 mol L^{-1} KCl^-	AV=:5 mV; 1 Hz to 100 kHz	(Yang *et al.*, 2014)
	Morphine spiked urine samples	Carbon paste (CP) electrode with ferrocene /gold nanoparticles GNFMCPE	3.507 nM 1.33 ng mL^{-1}	$[Fe(CN)_6]^{3-/4-}$	0.1Hz to 100 kHz	(Atta *et al.*, 2012)
Methamphetamine	Methampheta mine solution	Aptamer	n.a,	5 mM $[Fe(CN)_6]^{3-/4-}$ in 10 mM Tris buffer (pH 7.4)	0.1 Hz to 100 kHz; AV = 5 mV	(Ebrahimi *et al.*, 2012)
	Methampheta mine Spiked blood samples	Antibody	10.1 pg L^{-1} 67.68 fM	1x 10^{-3} mol L^{-1} of $[Fe(CN)_6]^{3-/4-}$ in 0.01 mol L^{-1} KCl	1 Hz to 100 kHz; AV=:5 mV.	(Yang *et al.*, 2014)

1.11 The Use of Nanotechnology for Drugs of Abuse Detection

The advent of nanotechnology has prompt the development of a new sub-class of biosensors, i.e. the nano-biosensor. Specifically, the prefix “nano” commonly refers to the use of nanomaterials to improve the biosensor sensitivity and specificity, thus improving the overall biosensor performances (Tothill, 2011; Abdin, Altintas and Tothill, 2015; Quesada-González and Merkoçi, 2015; Fenzl, Hirsch and Baeumner, 2016;

Masdor, Altintas and Tothill, 2016; Farka *et al.*, 2017; Yüce and Kurt, 2017). Examples are carbon nanotubes, graphene oxide, golden nanoparticles, nano molecularly imprinted polymers (nanoMIPs). As nanoMIPs were applied in this work, they are discussed separately in Section 1.12.

Quantum dots (QDs) are semiconductor nanocrystals, which shown significant advantages over conventional dye, such as high quantum yield, exceptional photochemical stability, and broad absorption. Concerning biosensors for illicit drugs detection, they have been mostly applied as fluorescence resonance energy transfer (FRET) donors in combination with aptamers and antibodies (Mokhtarzadeh *et al.*, 2015). Due to QDs nanosize, they can provide a distinct fluorescent signal from any individual molecular receptor, thus overcoming the major drawback of conventional fluorophores. As an example, Zhang and Johnson functionalised the surface of 605QD with aptamer/Cy5 complexes to develop a single QD based optical sensor. Briefly, upon binding between the cocaine and the aptamer, the dissociation of the Cy5 oligonucleotide from the aptamer/Cy5 complexes is induced, thus decreasing the Cy5 fluorescence. The LOD achieved was as low as 5 μM (Zhang and Johnson, 2009). Later, Fei and co-authors (2013) developed an electrochemiluminescent immunoassay to detect morphine. They coated a gold electrode with a nanocomposite film containing self-assembled polyamidoamine (PAMAM) CdS quantum dots and electrodeposited gold nanoparticles (Au-NPs). The binding between the antibodies and morphine induces a steric hindrance, thus decreasing the electrochemiluminescent signal. The Authors applied the sensor to detect morphine in real blood samples, achieving a LOD equal to 67 pg mL^{-1}.

Nanotechnology allows the synthesis of carbon-based nanomaterials in different shape and size. Among them, the most widely explored are single- and multi-walled carbon nanotube (SWCNT and MWCNT, respectively), fullerene, carbon dots, and graphene oxide (Ramachandran *et al.*, 2015). Some of the properties that make them attractive for biosensor application are the large surface area, chemical stability, fast electron transfer kinetics, and an excellent electrical conductivity (Gandhi *et al.*, 2015). Different carbon nanomaterials have been used to enhance biosensor sensitivity in detecting drugs of abuse, either alone or in combination with others nanomaterials. Taghdisi and co-authors (2015) developed an electrochemical aptasensor using SWCNTs. The achieved LOD in

serum was as low as 136 pM. Voltammetric sensor based on MWNTs-doped GO (ER-MWNTs-dopedGO) composite film was developed by Li and co-authors to detect morphine (2014). The reported detection limit was 5.0 ×10−8 mol L^{-1}. Another rapid voltammetric sensor for the detection of morphine was recently developed using graphene–palladium-hybrid-modified glassy carbon electrode (Atta, Hassan and Galal, 2014). Briefly, the modified carbon electrode had an excellent electrochemical response toward the electrochemical oxidation of morphine in PBS pH 7.4, achieving a LOD equal to 39.9 nmol L^{-1}.

Gold nanoparticle (Au NPs) have been extensively studied in biosensor application due to their unique electrical and optical properties such as high intensity SPR, scattering flux, luminescence, conductivity high surface area to volume ratio (Salam, Uludag and Tothill, 2013; Mokhtarzadeh *et al.*, 2015; Masdor, Altintas and Tothill, 2016). All these properties allow for signal amplification thus improving the biosensors sensitivity. Recently Au NPs have been applied even in drugs of abuse biosensors development. Shi and co-authors (2013) developed a fluorescence aptasensor based on AuNPs and graphene oxide, which act as electron acceptor and donor, respectively. When cocaine occurs in the sample aptamers change conformation in a way that brings AuNPs close to the graphene oxide surface. Consequently, the fluorescence quenching of graphene oxide occurs. Authors achieved a LOD 0.1 nM. Furthermore, the high surface area to volume ratio enables Au NPs to adsorb several bio-macromolecules onto their surface. This property has been applied to develop similar high sensitive fluorescence aptasensors, having a LOD in the order of nM (He *et al.*, 2010; Ma *et al.*, 2011).

1.12 Molecularly Imprinted Polymers (MIPs)

Molecularly imprinted polymer (MIP) is stereochemical complementary polymer structure, able to covalently or non-covalently bind to a selected analyte (**Figure 1-19**). To this aim the analyte (or the analyte's analogous), often referred as "template", is introduced during the polymerisation process (Wackerlig and Lieberzeit, 2015). Many research groups developed MIPs with different purposes, such as to replace biological receptors; to improve the selective binding in chromatography and in solid phase

extraction; to design "plastic" antibodies for immunoassays; and to build up a selective sensing receptor for biosensor development (Wulff, 2013).

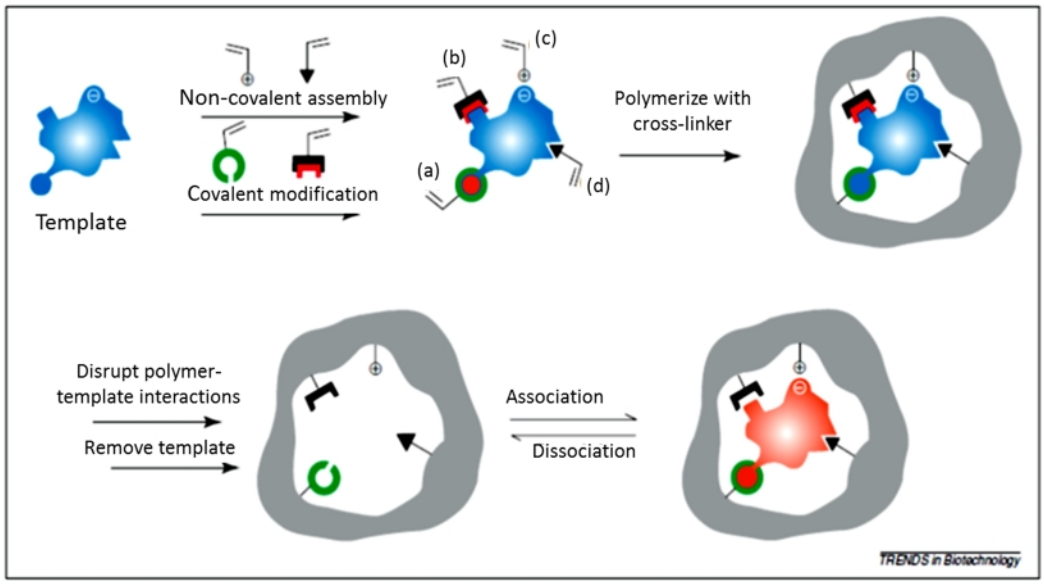

Figure 1-19: Basic concept beyond MIP synthesis (Poma et al., 2010).

1.12.1 MIPs Synthesis Methods

As defined by Whitcombe and co-authors (2011), the molecular imprinting is *"the formation of specific recognition sites (with binding or catalytic properties) in a material through its interaction with a template, where the template directs the positioning and orientation of the material's structural components by a self-assembly mechanism"*. The MIPs synthesis requires the following steps:

1. Preparation of the pre-polymerisation solution, by dissolving functional monomer(s), cross-linker(s) and initiator in a suitable solvent (also named "porogen"). Functional monomer(s) have complementary functional groups to the template molecule. Their selection is crucial to produce high MIP affinity to the template. A standard way to select them is achieved by applying molecular modelling simulation (Abdin, Altintas and Tothill, 2015; Altintas *et al.*, 2016; Cowen, Karim and Piletsky, 2016; Smolinska-Kempisty *et al.*, 2017).

2. Spontaneous self-assembly of the functional monomer(s) around the selected template, thus forming the so-called "pre-polymerisation complex".
3. Polymerisation and stabilisation of the "pre-polymerization complex" elicited by means of initiator and cross-linker(s), respectively. Briefly, the initiator, activated by either UV (in organic solvent) or persulfate-initiated polymerisation (in water), triggers the polymerisation reaction. Then, one or more cross-linker(s) stabilise the formed complementary cavities inside the polymer matrix, induce mechanical stability and control the MIP morphology and the size.
4. Template removal is induced by several washing steps, when non-covalent imprinting process has been performed, or by hydrolysis, when a covalent imprinting process has been applied.
5. Affinity rebinding study is carried out to evaluate the success of the molecular imprinting process.

Traditionally, MIPs have been produced by grinding the imprinted polymer monolith obtained at point 4 and, then sieving to select the MIP with the desired particle size (Piletska *et al.*, 2008; Whitcombe *et al.*, 2011). However, monolith grinding often resulted in the damage of the imprinted sites, while sieving resulted in poor yielding. Another major drawback is the incomplete removal of the template, which imparted the subsequent MIPs application. All these weaknesses have prevented the scale-up of MIP in industry production process and, therefore, their success in many manufacturing fields, such as biosensors (Poma, Turner and Piletsky, 2010; Tothill, 2011; Wackerlig and Lieberzeit, 2015).

The recent advent of nanotechnology helped in overcoming most of the above-mentioned drawbacks. Nanotechnology has enabled the synthesis of MIP at the nanoscale (nanoMIP), thus increasing their surface-to-volume ratio and a better conductivity, whenever MIP monomers have this property. The MIPs nanoscale synthesis improves the binding site formation as well as the accessibility of the template onto the recognition sites. Furthermore, it enhances the template removal during the MIP synthesis process (Madhuri et al., 2014; Li et al., 2014; Poma et al., 2013; Whitcombe et al., 2011; Poma et al., 2010; Sharma and Sharma, 2010). Additionally, nanoMIP may be conjugated to various nanomaterials (such as golden nanoparticles and nanotube) to enhance their

sensitivity to sensing receptors for biosensors applications (Wackerlig and Lieberzeit, 2015).

Common nanoMIP synthesis strategies include precipitation polymerisation, core-shell approaches, mini- and micro-emulsion polymerisation, and living radical polymerisation processes (Wackerlig and Lieberzeit, 2015; Madhuri et al., 2014; Li et al., 2014; Poma et al., 2010). Among them, micro-emulsion and precipitation polymerisation have been widely applyied in nanoMIP synthesis. In 2013, an elegant and successful automatic reactor based on solid phase precipitation polymerization synthesis has been developed by Poma and co-authors at Cranfield University (Poma *et al.*, 2013). This method, schematically reported in **Figure 1-20**, allows producing nanoMIP within few hours, with affinity and specificity toward targets and to produce nanoMIPs with the homogeneous binding site (Canfarotta *et al.*, 2016).

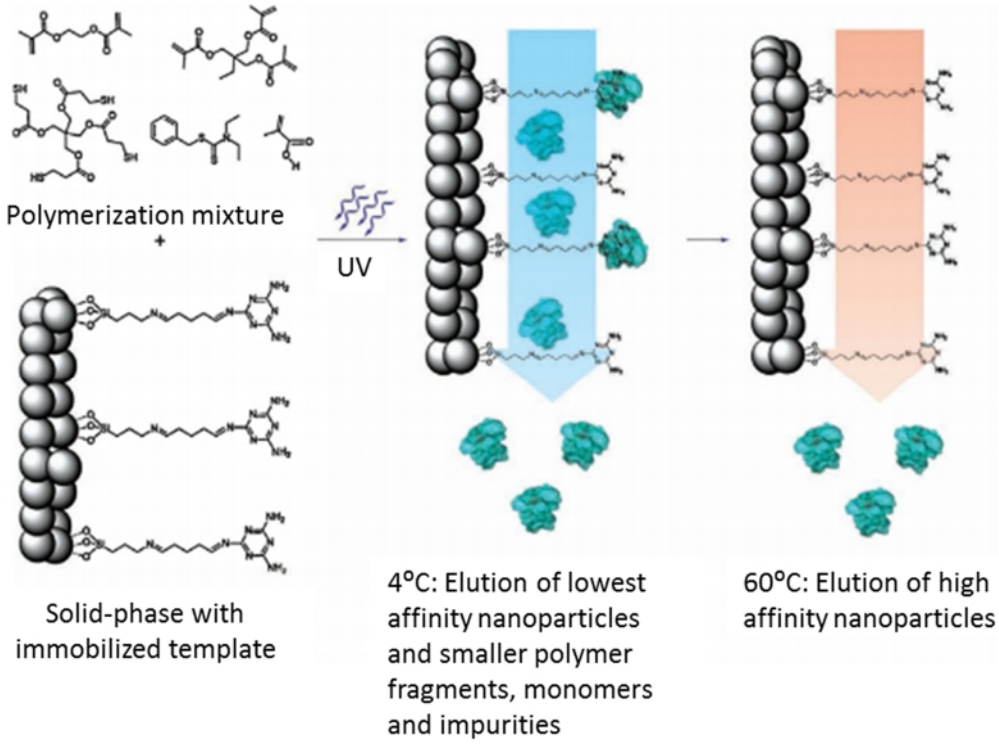

Figure 1-20: Solid phase precipitation polymerization method applied for nanoMIP production (Poma et al., 2013).

Interestingly, this method has been successfully applied to imprint both small molecules (< 500 Da) and macromolecules (>1500 Da) (Chianella *et al.*, 2013; Poma *et al.*, 2013; Korposh *et al.*, 2014; Abdin, Altintas and Tothill, 2015; Altintas, Guerreiro, *et al.*, 2015; Altintas, Pocock, *et al.*, 2015; Mazzotta *et al.*, 2016; Smolinska-Kempisty *et al.*, 2017). Furthermore, nanoMIP can be customised with various functional monomers to attach nanoMIP onto the sensor surface (Abdin, Altintas and Tothill, 2015), to introduce fluorescence properties (Wren *et al.*, 2014; Canfarotta *et al.*, 2016), thermoresponsive properties (Ambrosini *et al.*, 2013), electrochemical properties (Mazzotta *et al.*, 2016). Canfarotta and co-authors recently reviewed the solid phase nanoMIP protocols and gave details on both in water and in organic solvent synthesis processes (Canfarotta *et al.*, 2016).

1.12.2 MIPs for Drugs of Abuse Detection

MIP holds the ability to replace antibodies as sensing receptors for drugs of abuse detection. Overall, MIPs have been developed to detect several illicit drugs, such as cocaine, amphetamine, methamphetamine, THC, heroin and morphine. The most relevant studies are summarised in **Table 1-11**. Some of these studies specifically focused on researching the best MIP monomers composition via molecular modelling. Others aimed to develop biosensors. Although not all the studies reported some critical information (K_D, specificity assay), a wide range of syntheses methods and monomers composition are available in the literature.

Concerning the commercially available MIP designed to detect illicit drugs, MIPs against amphetamine, methamphetamine, phentermine, MDA, MDMA, MDEA are already on the market as stationary phase in solid phase extraction (SPE) cartridges, namely SupelMIP ® SPE cartridge (Sigma-Aldrich). According to the manufacturer, SupelMIP ® SPE cartridge offers an average recovery more than 80%.

Table 1-11: Summary of compositions of MIPs for drugs of abuse detection reported in the literature.

Template	form	functional monomers	Cross-linker	Initiator	Solvent	sensor (Y/N)	Ref.
Cocaine	nanoMIP	AA, DEAEM	TRIM, EGDMA	Iniferter	DMF	Y	(Smolinska-Kempisty *et al.*, 2017)
Cocaine	Hybrid Aptamer –MIP NPs	TBAm, AAc, Acrydite-aptamer	BIS	APS and TEMED	PBS	Y	(Poma *et al.*, 2015)
Cocaine	film	fluorophore, AA	EGDMA	AIBN	ACN	Y	(Wren *et al.*, 2014)
Cocaine	Particle	IA and MA	EGDMA	ACHN	DMF	N	(Piletska *et al.*, 2005)
Morphine	Particle	IA, MA	C	ACHN	ACN	N	(Piletska *et al.*, 2005)
Heroin	Film	TEOS, PTMOS, MTMOS, ethyl alcohol, HCl	-	-	water	Y	(Shang, Han and Song, 2014)
Δ^9-THC	Particle	MAA, 4-VPy, HEMA	EGDM	AIBN	Methanol	N	(Nestić *et al.*, 2013)
Δ^9-THC	n.a.	AA	-	-	Chloroform	N	(Fernandes *et al.*, 2015)
Catechin	Small Pills	PAVs and 4-Vpy	EGDM	AIBN	Triglyme	N	(Lendoiro *et al.*, 2014)
Catechin	Pills	AA	EGDMA	AIBN	Triglym, 7.5% PVAc	N	(Cela-Pérez *et al.*, 2016)
Methamphetamine	Particle	MA, IA, HEM	EGDMA	ACHN	DMF	N	(Piletska *et al.*, 2005)
Anabolic Steroids	Particle	MAA	EGDMA	AIBN	ACN	N	(Dong, Tong and Li, 2003)

Δ9-THC= (−)-trans-Δ^9-tetrahydrocannabinol Catechin= mimic template of Δ9-THC, MA = methacrylic acid, 4-VPy= 4- vinylpyridine, AA = acrylamide, AAc= acrilic acid, BIS = N,N′-methylenebisacrylamide; IA = itaconic acid, HEMA = 2-hydroxyethyl methacrylate, HEM = hydroxyethyl methacrylate, EGDMA=ethylene glycol dimethacrylate, AIBN = 2,2 -Azobis-isobutyronitrile, ACHN = 1,1 -azobis(cyclohexanecarbonitrile), DMF= dimethylformamide ,ACN = Acetonitrile PAVs= poly(vinylacetate), PTMOS = phenyltrimethoxysilane, MTMOS = methyltrime- thoxysilane, NIPAm = N -isopropylacrylamide, TBAm = N - tert –butylacrylamide, BIS = N,N′ -methylenebisacrylamide, APS= ammonium persulphate, TEMED = N,N,N′,N′ -tetra-methylethylenediamine, TEOS= tetraethylorthosilicate, TRIGLYME= triethylene glycol dimethyl ether,TRIM= trimethylolpropane trimethacrylate (TRIM).

1.13 Project Aim and Objectives

1.13.1 Aim

Limiting the drugs of abuse trafficking is a necessary action to improve collective security and safety. Despite illicit drugs regulations and penal repercussions, illicit drugs trafficking persists. Therefore, repressive policy, based on banning drugs use and trafficking, cannot be considered the only tool. Furthermore, repressive policy can be applied only if illicit trafficking is detected. Consequently, monitoring activities on illicit drugs trafficking is crucial in contrasting this criminal activity.

Currently, there are many methods available to detect illicit drugs, which can be grouped into presumptive and confirmatory tests. The major limitation of the former group is the high incidence of false-positive results, which may lead to unnecessary law enforcement systems workload. Therefore, all results gained by presumptive test must be confirmed by at least one confirmatory method, which provides accurate results, but at a high cost and with time-consuming and complex protocols. Also, false-negative results may occur, which may lead to inefficient control over illicit drugs trafficking. Biosensors and bio-inspired sensors are promising tools for screening and detecting drugs of abuse as they are easy to use, sensitive, specific and portable. Overall, by providing fast results, they are ideal tools to screen large quantity of seized suspected materials thus reducing time and cost of analysis. Although the promising performance, their application is only at the first stage. The few developed sensors aim to detect drugs in human body fluids, and mostly rely on antibodies and aptamer as sensing receptors.

This study aims to develop two kind of nanoMIPs based sensors for morphine and cocaine detection. The sensor platforms under investigation are the EIS and the QCM. Both the nanoMIP EIS and the QCM sensor platforms aims at the development of a fast, sensitive, specific accurate and on-site methods, able to detect morphine and cocaine at trace level. Due to their environmental stability, the use of nanoMIPs aims to provide high stability in the final devices.

1.13.2 Objectives

The specific objectives of this project are to:

1. Characterise the size of the cocaine and morphine nanoMIPs synthesised and dispatched by the University of Leicester (partner of the Nosy project).
2. Select and characterised the electrodes used to develop the EIS nanoMIP sensor for drugs of abuse detection. Specifically, the electrodes investigated in this study are the screen-printed electrodes (DPR C220AT, DropSens, Llanera, Spain) and two types of interdigitated electrodes, namely DPR IDEAu5 (DropSens, Llanera, Spain) and ED-IDE3Au (Micrux, Spain).
3. Develop nanoMIP sensor, based on EIS, to detect cocaine and morphine in salt form and in water based solution at traces level. This will be carried out on both round shaped working electrodes (SPE) and interdigitated electrodes (IDE):
4. Develop a nanoMIP sensor using a fully automated QCM instrumentation and able to detect AuNP conjugated morphine and cocaine in salt form and in water based solution
5. Evaluate and compare the nanoMIP EIS and QCM sensors performances.

1.14 Project Work Flow and Thesis Structures

The thesis structure is reported in **Figure 1-21** and reflects the project workflow. The project will be carried out following the workflow rule of PDCA (plan–do–check–adjust).

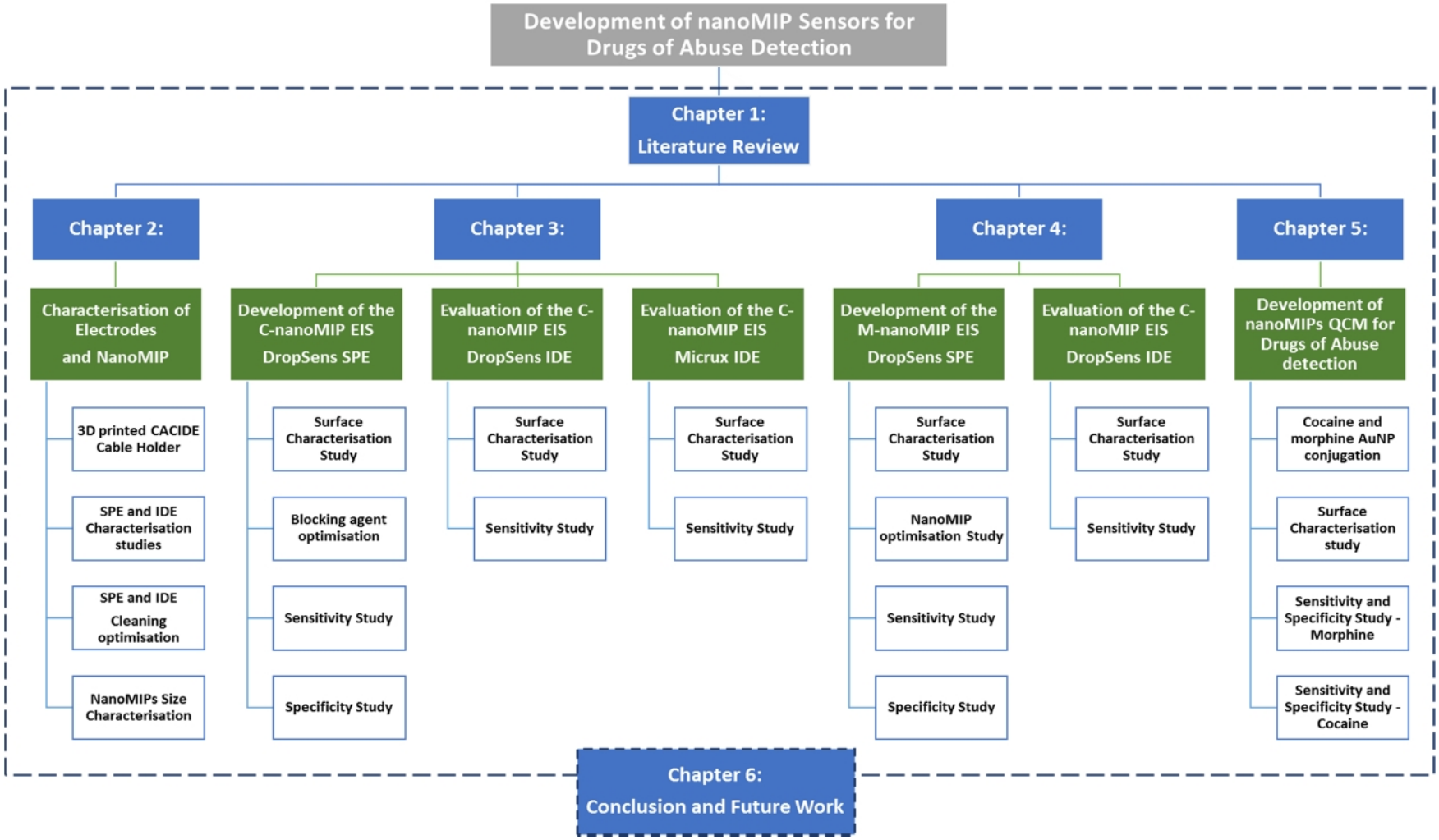

Figure 1-21: Thesis structure.

Chapter 2
Characterisation of Electrodes and MIP Nanoparticles

2.1 Introduction

The major components of a biosensor are the transducer, the interfacing receptor, and the signal processing system. In this work, the electrodes, both round shape and interdigitated, were used as the sensors, interfacing with nanoMIP as the receptor surface, while the electrochemical impedance spectroscopy (EIS) analyser was used as a sensor transducer.

In order to develop a biosensor, the electrode surface has to be clean from contaminating species, and all the reagents are filtered to minimise the contaminations. The cleanest the surface of the gold electrodes, the better the self-assembled monolayer (SAM) deposition and the resulting biosensor functionalisation process. To this aim, general instructions on electrodes cleaning procedures from the suppliers were followed and are reported in this chapter. Additionally, an optimisation study was carried out to explore the best procedure to clean the electrodes surface used in this work.

To develop an electrochemical affinity sensor, it is also imperative to choose a commercially available electrode which best suits the aims of the research. In this work both screen-printed round shape electrode (SPE) and sputtered interdigitated electrode (IDE) were considered. The former comes with a round shape working electrodes and with the conventional three electrodes configuration. The latter comes with interdigitated working electrodes and with two electrodes configuration. From a biosensor development and manufacturing point of view, both the electrodes and their respective connectors need to assure a good signal transmission. While the connectors are required to guarantee a good contact with the electrodes, the electrodes need to be manufactured with fewer imperfections as possible thus providing the best and consistent electrochemical signal and the lowest background/signal noise.

This chapter provides the results of the characterisation of the electrodes and the MIP nanoparticles used within this work. Furthermore, the setting used to carry out the EIS measurements and and the optimisation of the cleaning protocols used to clean the electrodes are reported and discussed.

2.2 Materials and Equipment

2.2.1 Materials

Potassium ferrocyanate ($K_4[Fe(CN)_6]$) and potassium ferricyanide ($K_3[Fe(CN)_6]$), 2-(N-morpholino) ethanesulfonic acid (MES, $C_6H_{13}NO_4S$), 3-(N-Morpholino) propanesulfonic acid (MOPS, $C_7H_{15}NO_4S$), ethanolamine, 11-mercaptoundecanoic acid (MUDA), and ethanol were purchased from Sigma-Aldrich Ltd (Dorset, UK). Several batches of cocaine and morphine molecularly imprinted polymer nanoparticles (nanoMIPs) and the non-imprinted particles (nanoNIPs) were provided by the Prof Piletsky's Group (University of Leicester - ULEIC University, Leicester, UK). All solutions were prepared with double distilled water (18 MΩ cm^{-2}) collected from the Barnstead™ Smart2Pure™ Water Purification System (Thermo Scientific™, Rugby, UK). N_2 tanks were supplied by BOC Gas & Gear (Northampton, UK) and connected to the related prime's pipeline. All the solutions used were filtered through filter system by means of nitrocellulose Whatman® filter 0.2 µm (Whatman International Ltd, Maidstone, UK) or by 0.2 µm Corning® syringe filter (Corning Inc., New York, US). All nanoMIPs solutions were filtered with 0.45 µm syringe filter (Corning®, Corning Inc., New York, US).

2.2.2 Electrodes and EIS Analyser

Three different electrodes were used in this work (**Figure 2-1**) and these include:

1. DropeSens Screen-printed electrodes (SPEs), DPR – C220AT (DropSens S.L., Llanera, Spain) and were purchased from Metrohm (Runcorn, UK). This electrode has high temperature curing, gold ink in a round-shape working electrode (WE, 12.56 mm^2), gold counter (or auxiliary) electrode (CE or AE), and a Ag/AgCl reference electrode (RE), on in ceramic substrate.
2. DropSense interdigitated electrodes (IDEs), DRP-G-IDEAU5 (DropSens S.L., Llanera, Spain) and were purchased from Metrohm (Runcorn, UK). This electrode has two gold interdigitated electrodes on a glass substrate. There are 250 digits per each interdigitated electrode. The length of each digit is 6760 µm, while the gap between the electrodes is 5 µm.

3. Micrux IDEs (ED-IDE3Au, Micrux Technologies S.L., Oviedo, Spain) and were purchased from Zimmer and Peacock Ltd S.L. (Roysto, UK). This electrode has a cell diameter of 3.5 mm. There are 180 pairs of 5 µm wide electrodes, while the gap between the electrodes is 5 µm.

The PalmSens3+ (PalmSens BV, Houten, The Netherlands) and, at a later stage, Palmsens4 (PalmSens BV, Houten, The Netherlands) were used as potentiostat/ Electrochemical Impedance Spectroscopy (EIS) analyser. Both instruments were purchased from Alvatek Ltd (UK) and used with the same conditions. Measurements were taken using VistaShield™ Faraday Cage (Gamry Instruments, Warminster, PA, US). Stainless steel and plastic tweezers were used to handle all the electrodes.

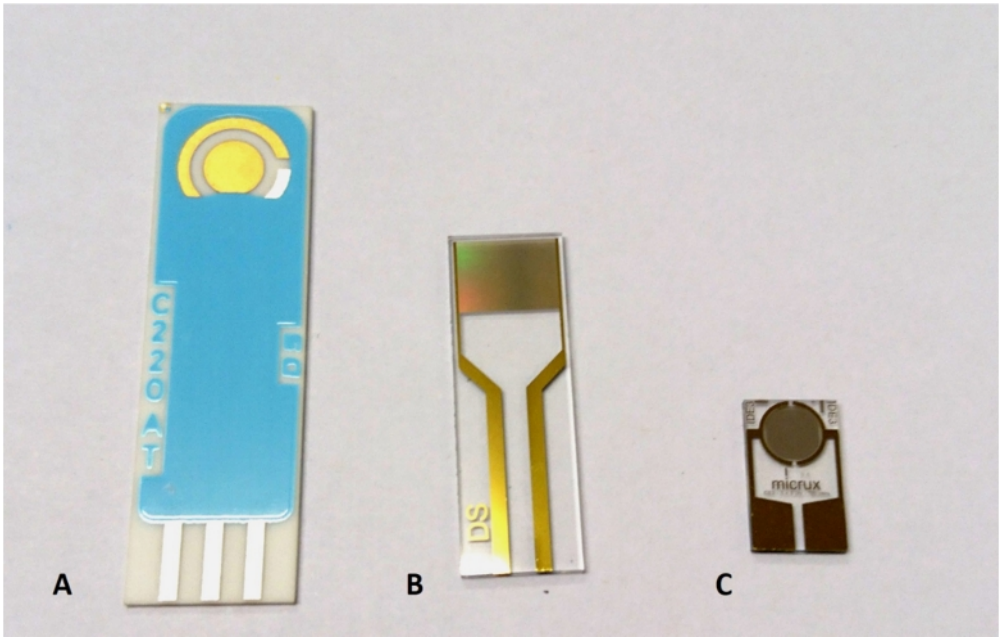

Figure 2-1: (A) DropSens SPE (DPR – C220AT), (B) DropSens IDE (DRP-G-IDEAU5 (C) Micrux IDE (ED-IDE3 Au).

2.2.3 Electrodes Connectors

As shown in **Figure 2-2**, DropSens IDE was connected to the instrument by a double shielded cable CACIDE (DropSens, Llanera, Spain), courtesy modified by PalmSens BV. Micrux IDE was connected via a dedicated Micrux connector (ED-DROP-CELL, Micrux

Technologies, Oviedo, Spain). The DropSens SPE was connected via universal sensor connector, which was coupled to the instrument by double-shielded cable with 2 mm banana connectors. A 3D printed and custom-made connector holder was build up to allocate the CACIDE connectors. The holder was designed and realised in collaboration with the Department Centre for Engineering Photonics (Cranfield University). Specifically, the holder and the cover were designed by the 3D modelling computer program (SketchUp®, Trimble Inc.) and realised using a 3D printer (Ultimaker 2+, Ultimaker B.V, Geldermalsen, The Netherlands). The holder was printed with a PLA Innofil 3D 2.85 mm (Innofil 3D BV, Emmen The Netherlands).

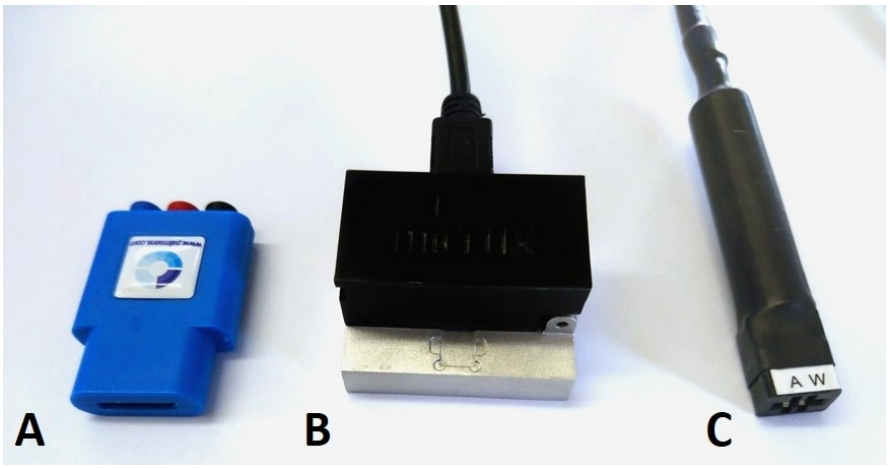

Figure 2-2: Electrodes connectors in use. (A) universal sensor connector (PalmSens®) for Dropsens SPE; (B) ED-DROP-CELL connector (Micrux) for Micrux IDE; (C) modified CACIDE connector (DropSens) for DropSens IDE.

2.2.4 EIS Set-Up and Software

The PalmSens EIS analyser was connected to a PC in which the dedicated PStrace 5 software (PalmSens BV, The Netherlands) was installed. For in-field application, the PalmSens EIS analyser can also be also connected to smartphone and tablet via Bluetooth technology and remotely controlled using PStouch app. The PalmSens EIS analyser was also connected to the appropriate electrode connector. The connectors were placed into VistaShield™ Faraday Cage (Gamry, US) during the recording of all EIS measurements to reduce the environmental, electrical noise. Typical instrumentation set-up with all type of electrodes and connectors is displayed in **Figure 2-3**.

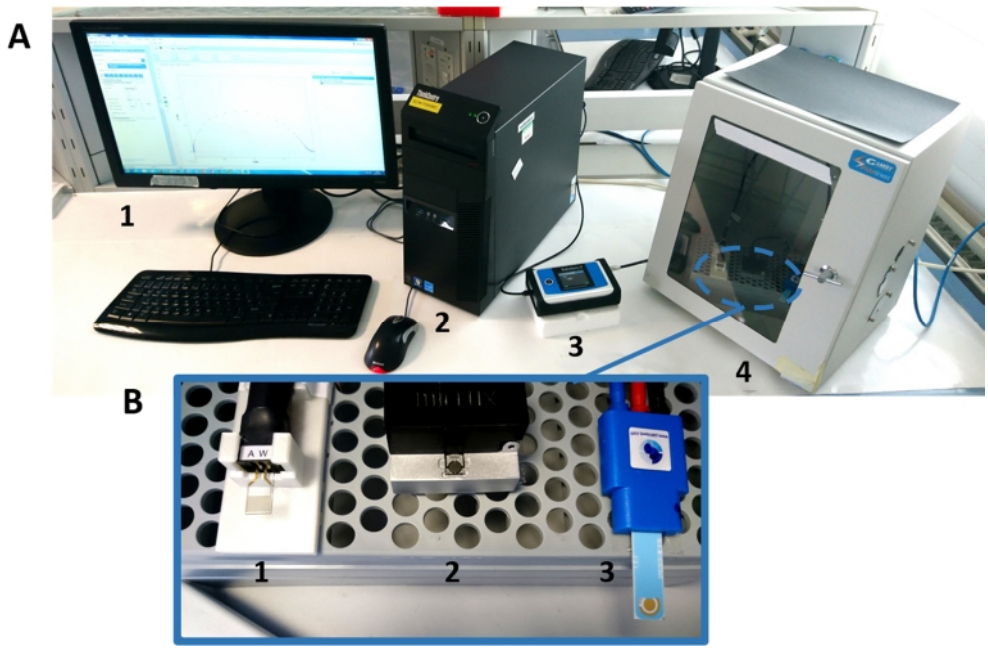

Figure 2-3: (A) EIS instrumentation set-up. (1) PC screen and (2) unit; (3) PalmSens 4 (4) Faraday cage. (B) Connectors and electrodes in use. (1) DRP IDEAu5 electrode and modified connector (CACIDE, DropSens) placed in a custom-made holder; (2) MicruX IDE3Au electrode and related connector (ED-DROP-CELL, Micrux); (3) DPR C220AT electrode and universal connector.

2.2.5 Other Equipment

Carbolite PF 300 DegC Fanned Convection Laboratory Oven was used to pre-treat the electrodes. Both Zetasizer Nano (Nano-S) from Malvern Instruments Ltd (Malvern, UK) and Transmission Electron Microscope (TEM) (Philips CM20, Philips Research, Cambridge, UK) were used to assess the nanoMIPs diameter sizes. When needed, NanoMIPs purification was carried out by a 10 mL syringe (Syringe 2-piece disposable sterile 10 mL, Fisher Scientific, Loughborough, UK) connected to 0.45 μm cellulose acetate sterile syringe filter (Corning®, Corning Inc., New York, US).

Sonication Bath Sonic 6MX (James Products Europe Ltd., Dorset, UK) Eppendorf Concentrator 5301 (Eppendorf AG, Hamburg, Germany), Clifton unstirred bath (Nickel-Electro Ltd., Weston-Super-Mare, UK), vortex (IKA® VORTEX Genius 3, Fisher Scientific, Loughborough, UK), incubator (IKA® KS 4000 I control, Fisher Scientific, Loughborough, UK), N_2 stream, pipettes and general consumable were also used to carry out the experiments.

2.3 Methods

2.3.1 EIS Measurement Parameters and Software

Faradaic EIS measurement relies on a redox reaction mediated by a redox probe that triggers an electrical signal at the electrode surface. The probe concentration, the composition and charge of the sensor surface, the layer thickness, the pH and temperature are all parameters able to influence the EIS measurement. The most used redox probe is the ferrocyanide-ferricyanide solution, which mediated the following redox reaction:

$$[Fe(CN)_6]^{4-} \rightleftharpoons [Fe(CN)_6]^{3-} + e^-$$

Several concentrations are suggested in the literature, generally ranging from 1 mM up to 20 mM (Li *et al.*, 2007; Hua *et al.*, 2010; Ebrahimi *et al.*, 2012; Sheng *et al.*, 2014; Bozokalfa *et al.*, 2016; Roushani and Shahdost-fard, 2016). Concerning the DropsSens electrodes (both SPE and IDE), the EIS measurements were performed in a frequency range from 50kHz to 0.1 Hz, having a DC equal to 0.12 V with a stimulus wave of 10 mV (**Figure 2-4**). The redox couple solution was composed by potassium hexacyanoferrate III ($K_3[Fe(CN)_6]$) and potassium hexacyanoferrate(II) trihydrate ($K_4[Fe(CN)_6]3H_2O$), at the 10 mM, and dissolved in MOPS (10 mM, pH 7.4). A 50 µL of 10 mM redox couple solution ($[Fe(CN)_6]^{3-/4-}$) solution (pH 7.4) was dropped onto the Dropsens SPE before starting the EIS measurement. The volume of the redox solution was increased to 60 µL for the DropsSens IDE.

A slightly different setting was applied to MicruX IDE3 AU and according to the manufacturer instructions. When the Micrux IDE was used, the EIS was carried out over the same frequency range, but having 0.23 V as DC potential and a modulation voltage of 10 mV (**Figure 2-4**). The EIS measurements were recorded by dropping 10 µL of redox couple solution onto the electrodes surface. Also, an optimisation study was performed to assess the best redox couple solution concentration to use for the Micrux electrode. This was done as the 10 mM concentration was burning the electrodes To this aim, the following $[Fe\ (CN)_6]^{3-/4-}$ concentrations were explored: 1 mM, 2.5 mM, and 5 mM. The optimised concentration of the redox couple solution was applied to carry out the experiments.

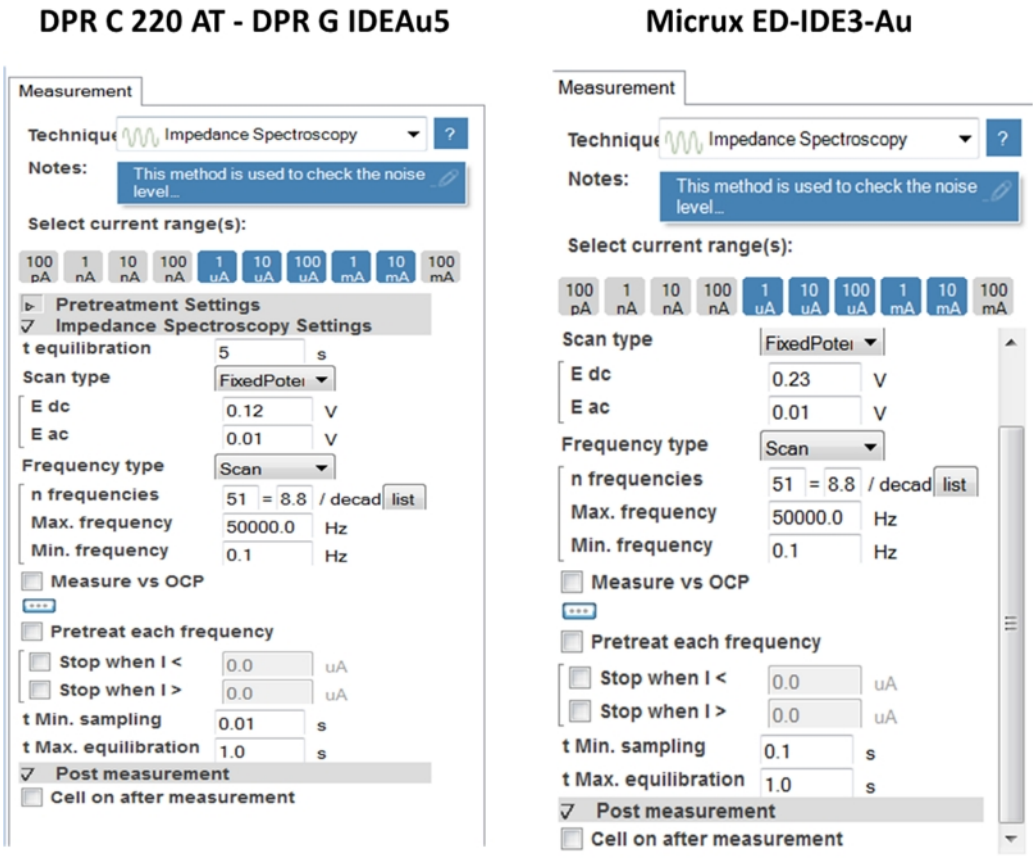

Figure 2-4: Screenshots of the measurement setting applied to each electrode and used to perform the EIS read out.

All electrodes were rinsed with double distilled water and dried with a gentle N_2 stream before and after EIS measurement was carried out. All EIS measurements were carried out at room temperature (23±1° C).

2.3.2 EIS Data Fitting and Analysis

The experimental data were fitted onto an appropriate equivalent circuit by EIS spectrum analyser® v1.0 (Bondarenko, Ragoisha and Pomerantsev, 2005). Briefly, Faradaic EIS spectrum of a sensor surface appears as a semicircle followed by a straight line in the Nyquist plot and, therefore is described by Randles equivalent circuit, as shown in **Figure 2-5**.

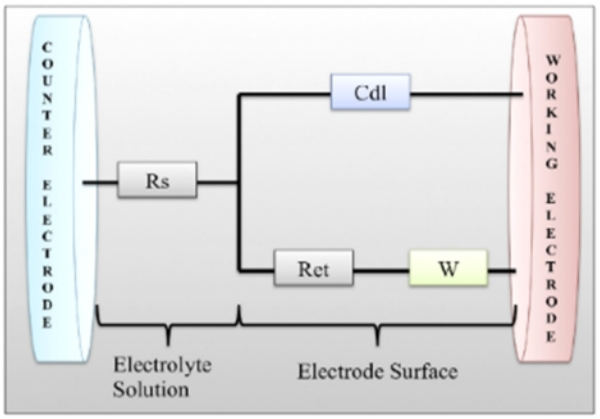

Figure 2-5: Randles circuit (Uygun and Ertuğrul Uygun, 2014).

When Warburg (W) electrical component does not appear, the simplified Randles equivalent circuit is used to describe the sensor response. The semicircle appears in the high frequency and gives information about both the charge transfer resistance (Rct) and the double layer capacitance (Cdl), while the line refers to the mass transfer resistance (Warburg component, W).

The accuracy of the fitting was evaluated by the average of the percentage Error (% Error) value. The fitted data were collected and analysed by Microsoft® Excel® and IBM® SPSS® Statistics 24.0 software. An example of the EIS experimental data fitted into Randles is shown in **Figure 2-6**.

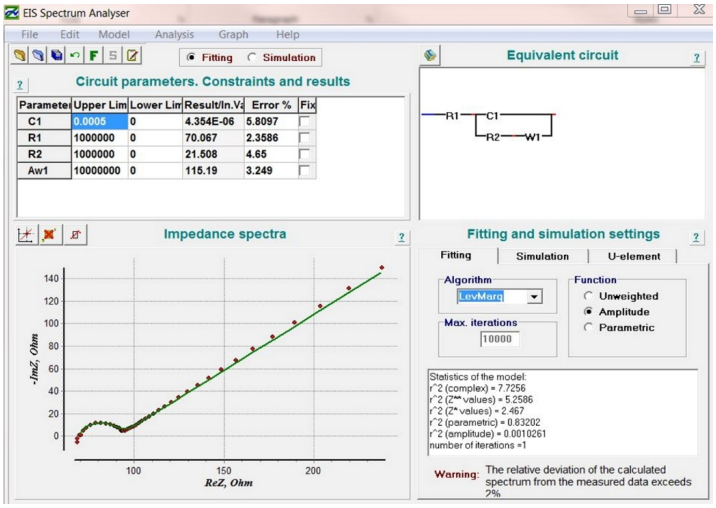

Figure 2-6: Screenshot of the EIS spectrum analyser® software showing the results of the experimental data fitting into Randles equivalent circuit. R1 = solution resistance; C1 = double layer capacitance; R2 = resistance charge transfer; W1 = Warburg diffusion element.

2.3.3 Electrodes Cleaning Optimisation

2.3.3.1 DropSens SPE (DPR C220AT)

Four different cleaning protocols were applied to clean the DropSens SPE as detailed below:

1. **Thermal treatment:** The SPE was heated at 120 °C for 30 minutes in the oven. The SPE was allowed to cool down, and then was thoroughly rinsed with double distilled water and dried under a gentle stream of N_2.
2. **Water rinsing/thermal treatment:** The SPE was rinsed with 1 mL of doubled distilled water and then was heated at 120 °C for 30 minutes in the oven. The SPE was allowed to cool down, and then was thoroughly rinsed with double distilled water and dried under a gentle stream of N_2.
3. **KOH/H_2O_2 cleaning:** The SPE was placed in a petri dish, containing KOH/H_2O_2 solution (50 mM KOH and 25% (v/v) of H_2O_2 in water). After 15 minutes, the KOH/H_2O_2 solution was discarded, and the SPE was thoroughly rinsed with double distilled water and dried under a gentle stream of N_2.
4. **Piranha cleaning:** The SPE upper part of the electrode (WE, CE and RE) was dipped into 4 mL of piranha solution (3:1 H_2SO_4 and H_2O_2) for 1 minute. Subsequently, the electrodes were thoroughly washed with ultrapure deionised water and dried under N_2 stream.

Each cleaning protocol was investigated on four replicates.

2.3.3.2 DropSens IDE (DPR IDEAu5)

The interdigitated electrode cleaning was performed according to the supplier instruction. The supplier indicated to clean the electrodes with ethanol and water only. The use of piranha solution and sonication was discouraged. Therefore, three type of cleaning procedures were investigated:

1. **Dipping:** For each IDE, three glass vials (5 mL Fisherbrand™, Thermo Scientific™, Rugby, UK) were first rinsed with deionised water and dried. Then, one of the vial

was filled with 2 mL of pure ethanol and the other two were filled with distilled water. The upper part of the IDE (two WEs) was vertically dipped for 15 minutes at room temperature in the ethanol vial first. Then it was removed and rinsed with ethanol and water. The same electrode was consecutively dipped in other two water vials. Finally, the electrode was rinsed again with double distilled water and dried under a gentle stream of N_2.

2. **Rinsing:** The IDE was rinsed twice with 0.5 mL of ethanol and, then, twice with 0.5 mL of double distilled water. Subsequently, the IDE was dried under a gentle stream of N_2.

Each cleaning protocol was investigated on four replicates.

2.3.3.3 Micrux interdigitated electrodes (ED-IDE3Au)

The following cleaning protocols were investigated for Micrux IDE:

1. **Rinsing:** The electrode was rinsed twice with 0.5 mL of ethanol and twice with 0.5 mL of double distilled water. Subsequently, the electrode was rised with water and dried under a gentle stream of N_2.
2. **Sonication:** The upper part of the electrode (two WEs) was vertically dipped into a vial, containing 0.25 mL of ethanol. The tube was placed into a sonication bath (set at 37 kHz and 240 W) and was sonicated for 10 minutes. Subsequently, the electrode was rised with water and dried under a gentle stream of N_2.

Each cleaning protocol was investigated on four replicates.

2.3.3.4 Cleaning protocols evaluation

The evaluation of the cleaning protocols were carried out for each electrode type, using cleaning protocol by recording the EIS spectra before and after the cleaning treatments. The obtained spectra were fitted into the Randles equivalent circuit, and the Rct (resistance charge transfer) was extrapolated and expressed as a percentage (%) of the bare electrode before the cleaning, set as 100%. The protocol that achieved the lowest %Rct was then chosen as the optimal cleaning procedure in this work. The attachment of

the MUDA (as described in Section 3.2.4) was also evaluated to indirectly assess the quality of the cleaning protocols developed for the DropSens SPE.

2.3.4 Electrodes Surface Characterisation

2.3.4.1 Atomic Force Microscopy (AFM)

The Atomic Force Microscopy (AFM) is a surface characterisation technique based on interatomic forces and has some advantages when compared to the Transmission Electron Microscopy (TEM) and the Scanning Electron Microscopy (SEM). Among them, the AFM produces 3D topography image of the sampled surface, while preserving the surface and achieving resolution of 0.1 nm (Jagtap Ambre, A. H., 2006; Zhou *et al.*, 2017). Furthermore, AFM enables the study of non-conductive polymer surface in environmental or liquid condition, and do not require sample preparation, which usually leads to artefacts (Kontomaris and Stylianou, 2017). Along with very informative 3D images topography of the working electrode gold surface, AFM can also provide useful information about the roughness of the surface. The roughness parameters (R) are the most significant in characterising the surface profile. Among them, the following three parameters are the most reported and are shown in **Figure 2-7** (De Oliveira *et al.*, 2012):

- Arithmetic Average Roughness (Ra). This value provides the arithmetical average of the absolute values of the height of the surface profile. Being just an arithmetical average, it often provides the same figures for two surfaces with different profiles.
- Geometric Average Roughness (Rq). Also known as the root mean square roughness (RMS), it is the average squared of the absolute values of the surface roughness profile. This parameter provides more information about the peaks and the valleys occurring onto the sample surface, and it is higher than the Ra value.
- The maximum height of the profile (Rmax). It is the measure of the highest peak from the baseline registered onto the sampled area.

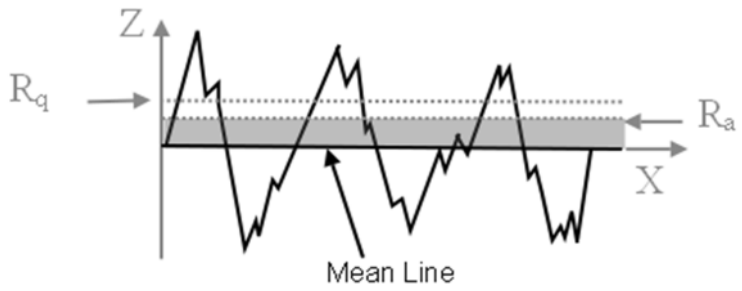

Figure 2-7: Schematic illustration of Ra and Rq parameters calculation along the sample profile (from www.rubert.co.uk). Z = investigated height.

The AFM analysis of the bare electrode surface will provide information about the roughness and the cleanness of the surface. Both this features are relevant to the self-assembly monolayer (SAM) deposition (Fischer *et al.*, 2009; Altintas *et al.*, 2012). The cleaned bare electrodes were investigated by Atomic Force Microscopy (Dimension 3100 AFM, Bruker). All AFM measurements were carried out in tapping (or intermittent) mode on dry electrodes on a 400 mm^2 scan area.

2.3.4.2 Scanning Electron Microscope (SEM)

Scanning Electron Microscopy relies on the use of electrons for imaging the surface of a solid sample. An electron beam is generated by the machine and is directed towards the sample surface, which needs to be conductive. The emitted electrons are then generated and detected by an electron detector. The image of the morphology of the sample surface is generated according to the intensity of the emitted electrons (Berbel Manaia *et al.*, 2017). For non-conductive materials, sample preparation is required and this includes the sputter-coating of the sample surface with an ultra-thin coating of conducting metal (such as gold). This process may induce artefacts or conceal some features of the sample and therefore a carefully interpretation of the results is required (Raab and Bachelet, 2017).

Scanning Electron Microscope (SEM- XL30 'S'FEG, Philips) was also used to investigate the manufacturing quality and the geometry of the DropSens and Micrux IDEs. Before all the analysis, the electrodes were rinsed with double distilled water and dried under a gentle stream of N_2. A thin layer of gold (10 nm) was deposited on the electrode via physical vapour deposition before performing the SEM analysis.

2.3.5 Cocaine NanoMIPs

The cocaine nanoMIPs were produced using solid-phase synthesis method as reported by Smolinska-Kempisty et al. (2017) at the University of Leicester. The synthesis was carried out in an organic solvent, dimethylformamide through UV irradiation. The monomers composition is reported in **Table 2-1**. Several batches of Cocaine nanoMIP were received as reported in

Table 2-2. All the nanoMIPs were provided with an external amine functional group, thus allowing the covalent attachment via amine coupling.

Table 2-1: Monomers mixture composition used to synthesise the cocaine nanoMIP (Smolinska-Kempisty *et al.*, 2017) .

Component	Substance	Amount (g)
Solvent	Dimethylformamide	25
Monomers	Acrylamide	2.38
	N-(3-aminopropyl)methacrylamide hydrochloride	0.112
Cross-Linker	ethylene glycol dimethacrylate	3.24
	trimethylolpropane trimethacrylate	3.24
Initiator	pentaerythritol tetrakis(3-mercaptopropionate)	0.18
	N, N-diethyldithiocarbamic acid benzyl ester	0.75

Table 2-2: Cocaine nanoMIP batches in acetonitrile received from ULEIC and related information.

Date	Batch	Concentration (mg mL^{-1})	Quantity
23/04/16	1	0.5	10 mL
08/09/16	2	0.76	10 mL
25/10/16	3	1.8	10 mL
23/11/16	4	1.8	10 mL
19/05/17	5	0.23	15 mL × 3
22/05/17	5	0.23	10 mL

2.3.6 Morphine NanoMIPs

Morphine nanoMIP were synthesised using the same protocol as the cocaine nanoMIP (section 2.3.5) at the University of Leicester (ULEIC). The monomers composition is as reported in **Table 2-3**. The morphine nanoMIPs were provided with an external amine functional group, thus allowing the covalent attachment onto the electrode surface. The details of morphine nanoMIP batches are listed in **Table 2-4**.

Table 2-3: Monomers mixture composition used to synthesise the morphine nanoMIP (provided by ULEIC).

Component	Substance	Amount (g)
Solvent	Acetonitrile	10.5
Monomers	Meta acrylamide	2.16
	Hydroxyethyl methacrylate	1.09
	N-(3-aminopropyl)methacrylamide hydrochloride	0.112
Cross-Linker	ethylene glycol dimethacrylate	3.24
	trimethylolpropane trimethacrylate	3.24
	pentaerythritol tetrakis(3-mercaptopropionate)	0.18
Initiator	N, N-diethyldithiocarbamic acid benzyl ester	0.75

Table 2-4: Morphine nanoMIP batches in a mixture of acetonitrile in water (3:1) received From ULEIC and related information.

Date	Batch	Concentration (mg mL^{-1})	Quantity
07/02/17	1	0.10	10 mL
03/04/17	2	0.24	50 mL
19/05/17	3	0.23	45 mL
12/07/17	4	0.14	10 mL

2.3.7 NanoMIPs Characterisation

2.3.7.1 Dynamic Light Scattering (DLS) analysis

The DLS has been applied to measure the NanoMIPs hydrodynamic diameter (d_H) within this work. DLS is a rapid, feasible and low-cost spectroscopic technique to assess the apparent hydrodynamic diameter of the nanoparticles. The principle of this technique relies on the Brownian motion of a particle. The smaller the particle, the faster their motion at given a solution and temperature (Lapresta-Fernández et al., 2014). This relationship is described by the Stokes-Einstein equation (2-2):

$$D_T = \frac{K_B T}{3\pi\mu d_H} \tag{2-1}$$

Where:

- K_B *is the Boltzmann constant (1.38064852 × 10^{-23} J/K);*
- T *is the absolute temperature (K);*
- μ *is the dynamic viscosity of the dispersion medium;*
- d_H *is the hydrodynamic diameter (equal to the diameter of a hypothetical sphere that diffuse with the same speed of the particle under investigation);*
- D_T *is the translational diffusion coefficient.*

When an incident laser light hits a nanoparticle in colloidal dispersion, the nanoparticle scattered the light at an intensity, which is correlated to the diffusion coefficient D_T and is detected by DLS instrument (Zhou, Su and Cai, 2017). To be reliable, the sample has to be ideally monodispersed solution, and the particle size should not be greater than 1/10th of the wavelength of the incident light (Bhattacharjee, 2016). However, the concentration, the solvation of the particle as well as the ionic strength of the dispersant may affect the estimation of the D_H due to the agglomeration/aggregation of the nanoparticle and to the formation of a corona around the solid nanoparticle. For these reasons, the resulting d_H value is often higher compared to the real one (Fischer and Schmidt, 2016). Another factor that may lead to erroneous size determination is the high polydispersity index of the samples. Indeed, in a heterogeneous sample, particles with

bigger size tend to cover the signal of the smaller one, thus resulting in an overestimation of the particle size (Calzolai et al., 2012).

To perform the DLS analysis, in this work the nanoMIP solvent was exchanged to double distilled water via Eppendorf concentrator 5301 (Eppendorf Ltd, UK) and was then filtered using an appropriate filter membrane (0.45 μm or above). DLS analysis was carried out using Zetasizer Nano (Nano-S, Malvern Instruments Ltd, UK). A 1 mL of diluted nanoMIP in water samples were analysed in 3 cm^3 disposable polystyrene cuvettes at 25°C, having polystyrene latex as the reference material. At least 10 measurements were recorded for each batch.

Although being widely used, relatively low cost, fast and easy to perform, a DLS measurement should be combined with another technique, such as Transmission Electron Microscopy (TEM) for particles size evaluation.

2.3.7.2 Transmission Electron Microscopy (TEM) analysis

TEM analysis was carried out to obtain the 2D image of the nanoMIP and, thus, to characterise further the diameter size. The TEM was also used to assess possible sample polydispersity and agglomeration/aggregations phenomena, which may have led to an overestimation of the diameter size by DLS technique. Although, TEM error in assessing the size may not be excluded and is expressed by the following equation (2-3):

$$\varepsilon = x_i - x \tag{2-2}$$

Where:

- ε *is the error;*
- x_i *is the measured size;*
- x *true (but unknown) size;*

Pixel resolution, the magnification calibration, spherical aberration particles/substrate holder boundary may contribute to the error (ε) in the nanoMIP size estimation (Pyrz and Buttrey, 2008). Artefact during sample preparation (drying) and polymer damages due to

the electron beam may also lead to inaccurate size/morphology description (Jagtap Ambre, A. H., 2006; Michen *et al.*, 2015).

The nanoMIP sample were prepared by filtering 1 mL of the nanoMIPs solution via a 0.45 syringe filter. Then, 10 µL of the nanoMIP solution was placed on a silicon chip attached to a TEM holder and left to dry overnight in a fume hood. Software-assisted image processing approach was used to evaluate the diameter size of both the cocaine and morphine nanoMIP. Specifically, the TEM images were analysed by ImageJ® software. Briefly, measurements were taken along the four-axis of the nanoparticles circumference for each numbered nanoMIP (i.e., vertical, horizontal and oblique diameters), as illustrated in **Figure 2-8**. The measurements were then averaged and expressed as the average diameter size (±SD). For the sake of convenience, only one batch was analysed using TEM and the results were used to optimise the DLS analysis protocol.

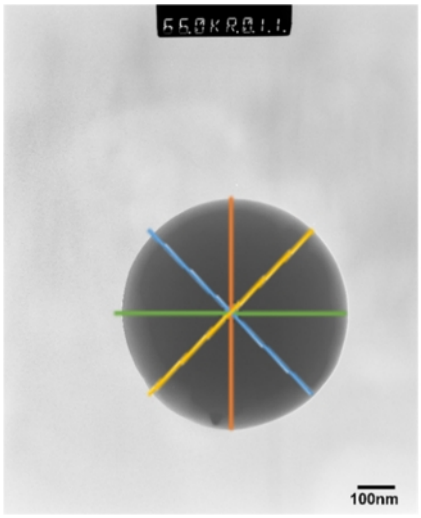

Figure 2-8: Schematic diameter measurements recorded for each nanoMIP captured by TEM analysis.

2.3.7.3 Statistical Analysis

Data were collected and analysed by Microsoft® Excel® and IBM® SPSS® Statistics 24.0. Other than the calculation of the average and standard deviation, also One-way ANOVA with Post Hoc study (Scheffé's method) was used. The significance (*p*-value) was set to be equal to 0.05.

2.4 Results and Discussion

2.4.1 Fabrication of the 3D Printed IDE Connector Holder

Overall, three issues occurred when working with the DropSens IDE. Firstly, a loose connection between the electrodes and the DropSens CACIDE connector was observed, which resulted in the loss of signal during the experiments. Secondly, the DropSens CACIDE cable easily turned around, thus making the electrodes bending laterally during the EIS measurements. Thirdly, the repeated insertion of the IDE to the connector resulted in electrodes contact pads scratch which damage the contact pad as shown in **Figure 2-9**.

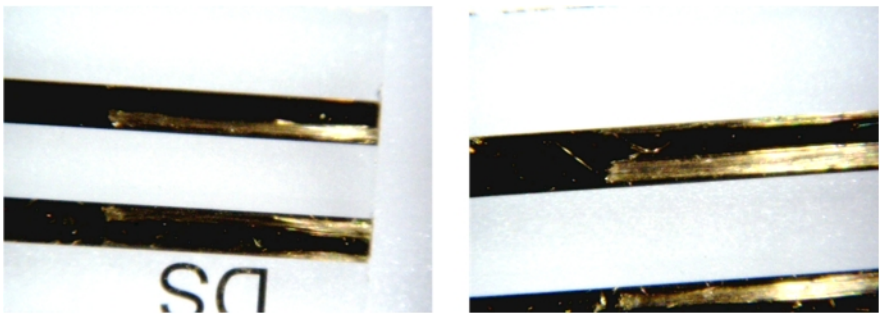

Figure 2-9: Image of the DPR IDEAu5 electrodes, showing the damages of the connections.

To overcome these problems, an in-house and custom-made CACIDE holder was designed and 3D printed using a 3D printer. The holder was designed to allocate the cable in, thus to avoid any rotation during the electrodes connection and handling. Since the electrode connector is designed to have a working space, the electrodes often appear to be loosely connected, resulting in an electrode bending. This lead to the loss of the signal. To overcome this issue, the holder was also designed to provide a support to the electrode, thus to minimise the electrodes bending while guarantying easy handling (**Figure 2-10**A). To minimise the scratches onto the IDE contact pads, it was decided to keep the electrode inserted into the cable connector as much as possible during the experiments. Therefore, also a cover holder (**Figure 2-10**B) was designed and 3D printed, thus to protect the electrode from environmental contamination during the handling outside the Faraday cage (such as during the washing step).

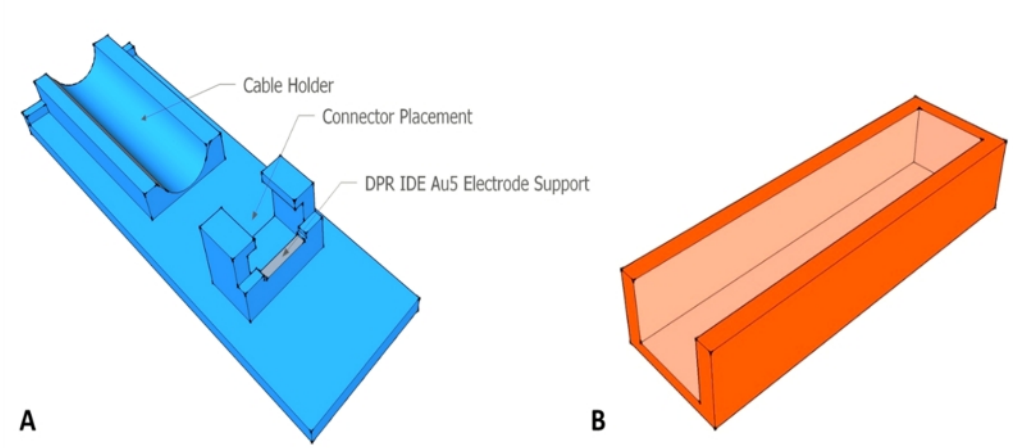

Figure 2-10: 3D model of the DPR IDEAu5 connector (A) holder and (B) cover realised by SketchUp® software.

The development of the final cable holder encompassed different designs. In the first attempt, the electrode support was design to allocate and support the front part of the electrodes, thus preventing any possible bending. However, the front electrode support (**Figure 2-11**) reduced the working space needed to handle the electrode with the tweezer. Also, it increased the likelihood to break the glass substrate of the IDE. Therefore, the support was reduced to few millimetre ahead of the connectors and designed only to minimise the bending of the electrodes. The fully developed cable holder connector and the cover are displayed in **Figure 2-12**. Tape was used to keep the cable connector fixed to the holder. The working setting inside the Faraday cage is displayed in **Figure 2-12**C.

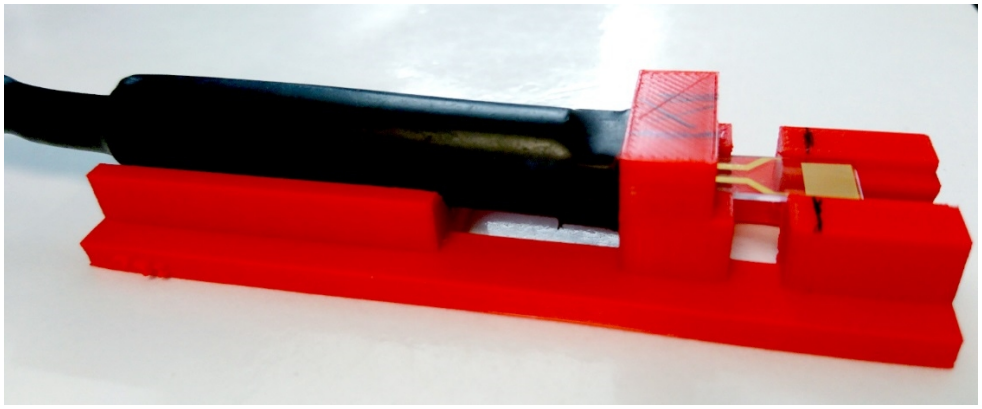

Figure 2-11: 3D print of the first concept of DPR IDEAu5 connector holder: DPR IDEAu5 electrode support.

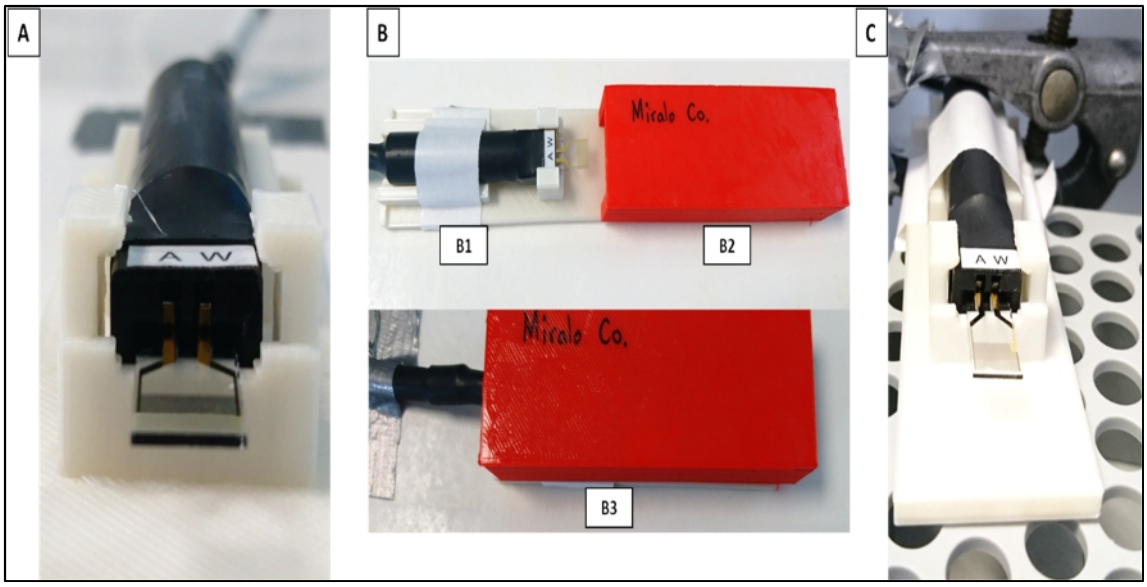

Figure 2-12: (A) Final 3D printed DPR IDEAu5 holder (front view). (B1) Final 3D printed DPR IDEAu5 holder and (B2) holder cover (top view). (B3) 3D printed DPR IDEAu5 holder entirely enclosed by the holder cover. (C) 3D printed DPR IDEAu5 holder placed inside the Faraday cage.

2.4.2 Redox Couple Optimisation Study for Micrux Electrodes

The EIS read-out conditions were adjusted as indicated by the electrode manufacturer. The EIS measurements were recorded in a frequency range between 0.1 Hz and 50000 Hz, having DC and AV equal to 0.23 V and 0.01 V, respectively.

Due to the small size of the Micrux IDE working electrodes (2.40 mm^2), the redox couple concentration needed to be optimised also. This was due to the burn out of the electrode surface when a 10 mM ferrocyanide-ferricyanide $[Fe(CN)_6]^{3-/4-}$ dissolved in 10 mM of MOPS (pH 7.4) was used. Therefore, an optimisation study was carried out to evaluate the best $[Fe(CN)_6]^{3-/4-}$ concentration to use, keeping the MOPS concentration and pH constant. The following concentrations were explored: 0.1 mM, 2.5 mM, and 5 mM redox couple concentration. The best signal was achieved by using the 2.5 mM redox solution concentration as the semicircle was fully occurring, while the 1 mm and 5 mM showed uncomplete semicircles. The IDEs were preserved at all the concentration explored (**Figure 2-13**). Therefore, 2.5 mM $[Fe(CN)_6]^{3-/4-}$ dissolved in MOPS (10 mM, pH 7.4) was used to carry out all the measurements on Micrux IDE.

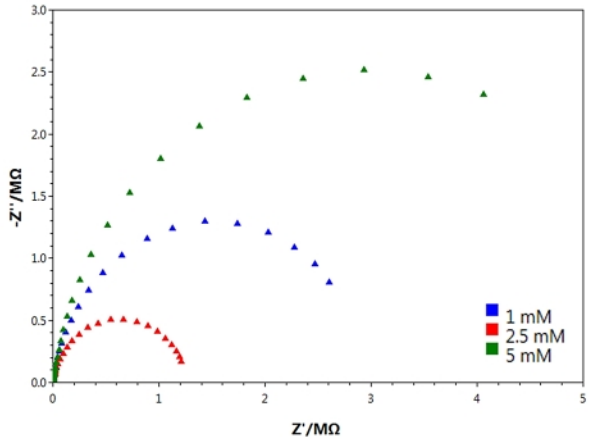

Figure 2-13: Nyquist plots achieved using different concentration $[Fe(CN)_6]^{3-/4-}$ redox couple solution (1 mM, 2.5 mM and 5 mM).

2.4.3 Electrodes Cleaning Procedures Optimisation

As the sensors used in this work were fabricated using different inks and substrates, a different cleaning procedure was required for each sensor to insure self-assembly monolayer (SAM) attachment without damaging the electrodes. The cleaner the surface the lower the value of the % Rct, expressed as a % of the bare (uncleaned) surface, which was set at 100%.

2.4.3.1 DropSens SPE (DPR C220AT)

According to the supplier (DropSens S.L., Llanera, Spain) suggested to clean the SPE (DPR C220AT) with an aqueous solution. On the other hand, the use of organic solvent was discouraged as they can remove the insulation layer, thus disrupting the SPE performances. Therefore, cleaning using organic solvent was not attempted.

A literature search was carried out and revealed that several protocols were developed to clean the electrodes surface (Fischer *et al.*, 2009; Bhalla *et al.*, 2010; Ahmed, J. V Rushworth, *et al.*, 2013) and these include using heating or chemical cleaning. Four cleaning methods were used for this electrodes (Section 2.3.3.1). Two chemical cleaning methods were carried out, namely piranha solution and KOH/H_2O_2. The former is

considered a very aggressive solution compared to KOH/H_2O_2. As shown in **Figure 2-14**, cleaning using piranha solution led to an increase of the Rct value and, also, damaged the silver reference electrode which was partially eroded. It is likely that the piranha also deposited dielectric material onto the electrodes surface as previously suggested by Ahmed et al. (2013). On the other hand, KOH/H_2O_2 cleaning induced a reduction of Rct, while apparently preserving the electrodes integrity. This result was in agreement with the study carried out by Fisher et al., (2009), which reported that the KOH/H_2O_2 cleaning method was the best among the other cleaning protocol attempted, such as ultraviolet ozone cleaning, DMAB (made by 800 mM KOH, 750 mM Na_2CO_3, and 50 mM dimethylamine borane), piranha solution, aqua ragia, hydrochloric acid potential cycling, sulfuric acid potential cycling. A thermal treatment cleaning methods were also investigated (Section 2.3.3.1). The results showed that the water rinsing and oven treatment gave the lowest % of Rct, when compared to oven treatment alone (**Figure 2-14**).

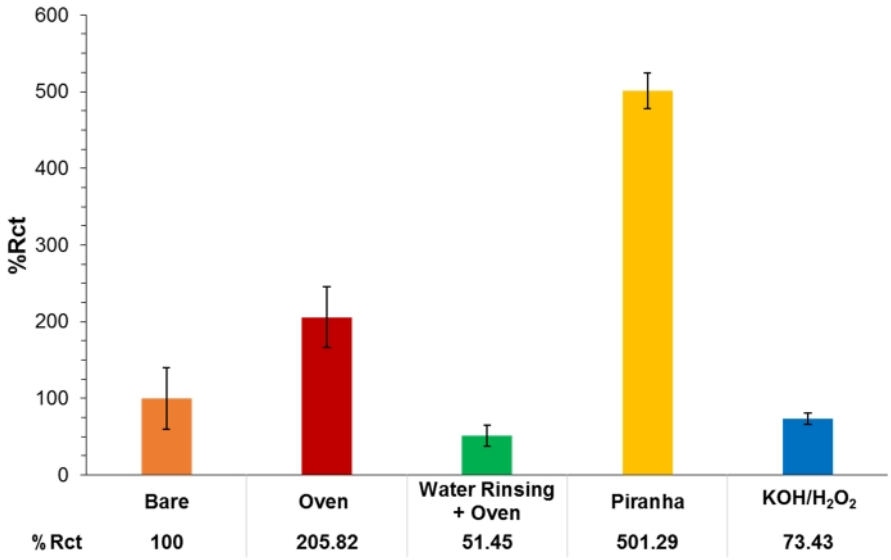

Figure 2-14: Comparison between the %Rct values related to the bare SPEs (100%) and the SPEs cleaned using the following methods: oven treatment (red), water rinsing followed by oven treatment (green), piranha (yellow) and KOH/H_2O_2 (blue) solution treatments. Error bars refer to the standard deviation (n=4).

As both the water rinsing followed by oven treatment and the KOH/H_2O_2 solution methods were effective in cleaning the surface, the amount of MUDA attached was used

to discriminate the best cleaning protocol. Therefore, MUDA attachment was performed onto two groups of electrodes (n=4). One group was cleaned according to water rinsing followed by oven treatment and the other group was cleaned according to the KOH/H_2O_2 solution protocols. The MUDA is a negatively charged and a hydrophobic substance (Altintas *et al.*, 2012), therefore an increase of the Rct (Ω) value is expected as a result of the MUDA attachment onto the gold electrode surface (Adnane, 2011; Thanh Ngo *et al.*, 2014). The results showed that although MUDA attachment was achieved after both the cleaning methods, a much higher average values (±SD) of the Rct (Ω) was recorded following the water and oven cleaning method (**Figure 2-15**). Therefore, this cleaning procedure was the best among the explored and was applied in further studies.

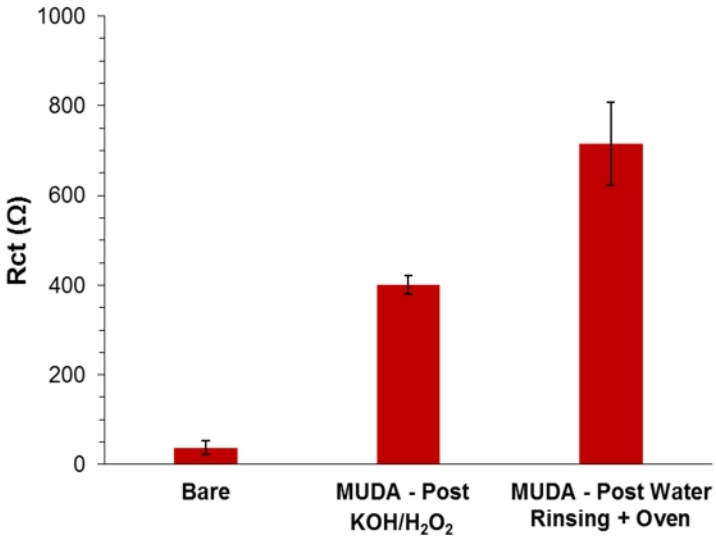

Figure 2-15: Average (±SD) of the Rct (Ω) values related to the bare SPEs, the MUDA coated SPEs cleaned according to the KOH/H_2O_2 protocol and water rinsing coupled with oven treatments. Error bars refer to the standard deviation (n=4).

2.4.3.2 DropSens IDE (DPR IDEAU5)

Various protocols to clean the gold IDEs have been reported in the literature. Piranha solution, alone or in combination with other chemicals, have been successfully used to clean in-house fabricated IDEs (de la Rica, Fernández-Sánchez and Baldi, 2006; Ohno *et al.*, 2013; Li *et al.*, 2017). Other protocols included the cyclic voltammetry using H_2SO_4 (Kaushik *et al.*, 2016), NaOH and HCl solution (Wen *et al.*, 2017), the plasma cleaning

(Singh *et al.*, 2011), sonication (Lian *et al.*, 2015) and organic solvent and water rinsing (Arya *et al.*, 2010).

The DropSens IDE used in this work, the supplier (DropSens S.L., Llanera, Spain) indicated that the cleaning of the IDEs (DPR IDEAu5) should be done using organic solvent and water rinsing, while sonication or aggressive chemical cleaning procedure should be avoided as it can lead to the removal of the thin gold layer. Therefore, the cleaning procedure was based on electrodes washing with ethanol and water (as reported in Section 2.3.3.2). One protocol was based on simply electrodes rinsing. The other protocol was carried out by sequentially dipping the electrodes into clean glass vials containing ethanol and into sterile containers filled with water. The results showed that the rinsing protocol provides a higher reduction of the %Rct with better reproducibility (**Figure 2-16**), and, therefore, was used as the DropSens IDE cleaning method within this work.

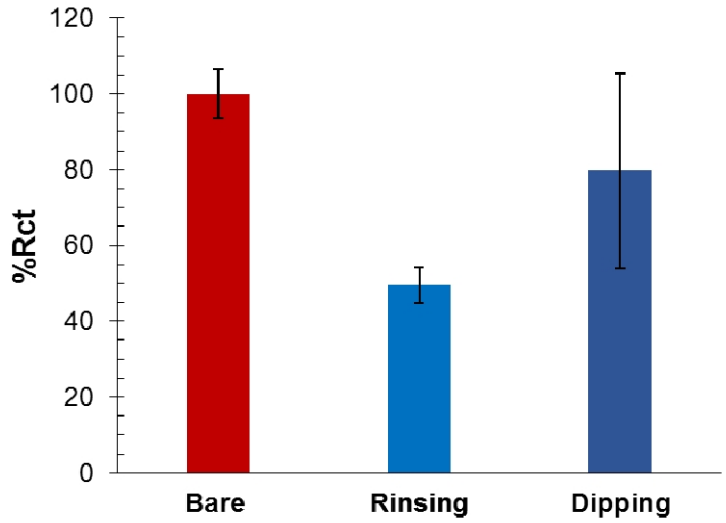

Figure 2-16: Comparison between the %Rct values related to the bare DropSens IDE (set as 100%) and the DropSens IDE cleaned using the following methods: rinsing (light blue) and dipping (dark blue) in ethanol and water. Error bars refer to the standard deviation (n=4).

2.4.3.3 Micrux IDE (ED-IDE3Au)

The supplier indicated that the conventional cleaning protocols of the Micrux IDEs are ethanol sonication or ethanol and water rinsing. Therefore this methods were investigated in this work (Section 2.3.3.3). The results showed that a better cleaning was achieved by rinsing the electrodes with ethanol and water (**Figure 2-17**). Although promising, the sonication was less reproducible and occasionally led to electrodes damage (i.e., no signal was detectable during EIS measurement). Therefore, the ethanol and water rinsing was selected to clean the Micrux IDE.

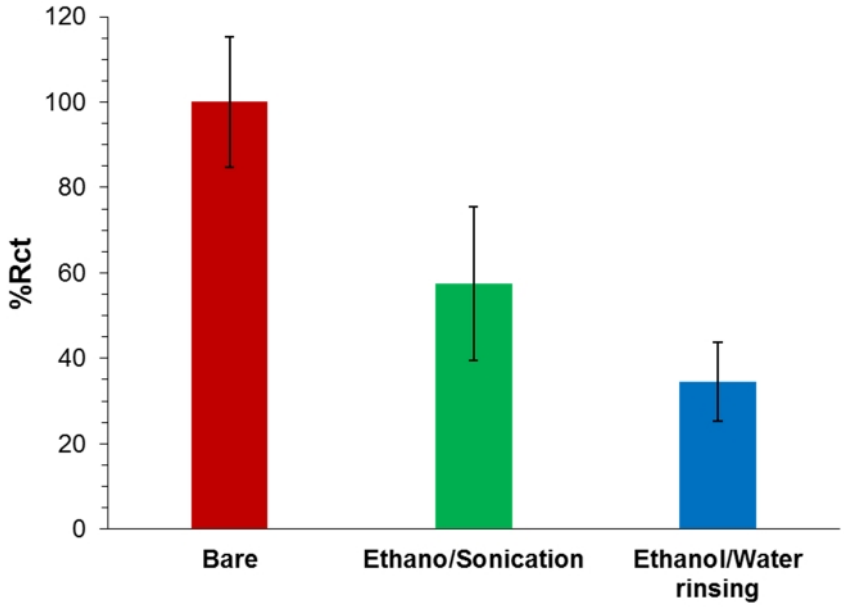

Figure 2-17: Comparison between the %Rct of the bare MicruX IDEAu5 (100%) and the %Rct obtained by cleaning the MicruX IDEAu5 by sonication and ethanol and water rinsing. Error bars refer to the standard deviation (n=4).

2.4.4 Electrodes Surface Characterisation

All three different electrodes were investigated to develop the EIS nanoMIP affinity sensor for drugs of abuse detection. Although specifications of each type of electrodes are provided in **Appendix A**., the electrodes were investigated using AFM (Dimension 3100, Bruker, US) and SEM techniques to obtain information about the surface roughness and topography as well as the geometry, as reported in Section 2.3.7.

2.4.4.1 AFM Characterisation

DropSens SPE (DPR C220AT)

The AFM study (**Figure 2-18**) has revealed that the surface of the screen-printed electrodes (SPE) is rough, although the gold deposition appeared regular. Concerning the roughness, peaks appeared on the 3D image topography of the WE surface with the Rmax value equal to 487 nm. The Ra (67.9) and Rq (85.4 nm) parameters also confirmed that the surface profile was not regular.

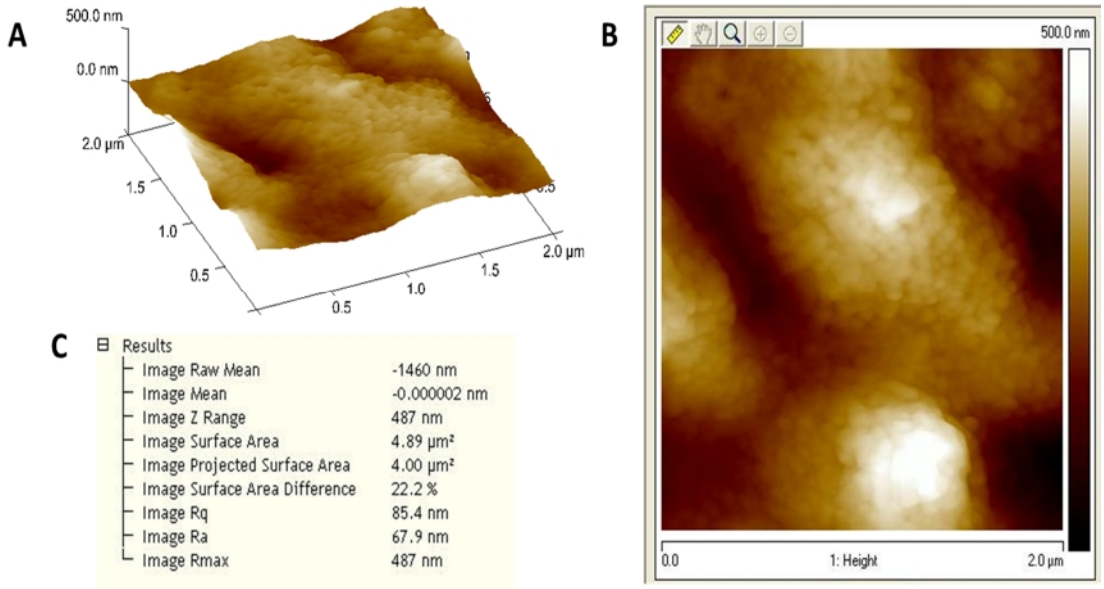

Figure 2-18: AFM characterisation of the bare SPE electrodes. (A) 3D and (B) 2D image of the SPE surface topography (scan area 4 μm^2; height 500 nm), and (C) the related roughness parameters values.

DropSens IDE (DPR IDEAu5)

The results of the AFM characterisation study performed on the DPR IDEAU5 electrode surface are presented in **Figure 2-19**. The 3D surface topography showed a flat and regular gold surface, although some irregularities can be seen at the edges of the IDEs. The roughness of the surface was carried out on a smaller area of one gold interdigitate

electrode (4 μm^2). The 3D and 2D image topography revealed the presence of very tiny peaks, with the Rmax value equal to 18.4 nm.

The roughness parameters (Ra and Rq) of the surface indicate that the average of the peaks is in the order of few nanometres. Concerning the geometry, the IDEs width and the interdigital space seem to reflect the manufacturer specification (both of them equal to 5 µm).

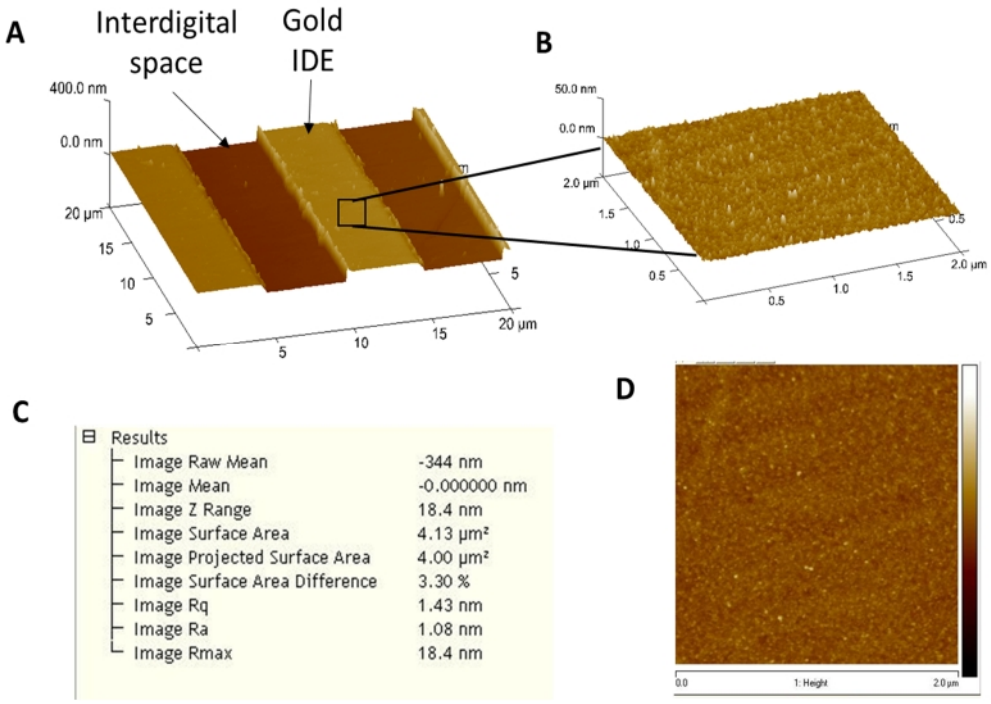

Figure 2-19: AFM characterisation of the bare DropSens IDE. The 3D images of the IDE surface topography are related to (A) 400 μm^2 scan area (height 400 nm) and (B) 4 μm^2 scan area (height 50 nm). (D) 2D image surface topography of the IDE (4 μm^2 scan area) and the (C) related roughness parameters values.

Micrux IDE (ED-IDE3Au)

The AFM characterisation study was also carried out on Micrux IDE. As shown from the 3D image topography, irregularities appeared both on the gold surface and at the edge of the IDEs (**Figure 2-20A**). The 3D image topography and the surface roughness analysis was carried out on a scan area of μm^2 of the working IDE and revealed that small peaks occurred on the IDE. These peaks looked similar to the peaks detected on the DropSens

IDE. The Ra and Rq were equal to 1.43 nm and 2.15 nm, respectively, while the Rmax was equal to 38.7 nm. However, it seems that the geometry of the Micrux IDE was slightly different compared to the manufacturer specification of 5 µm between the electrode.

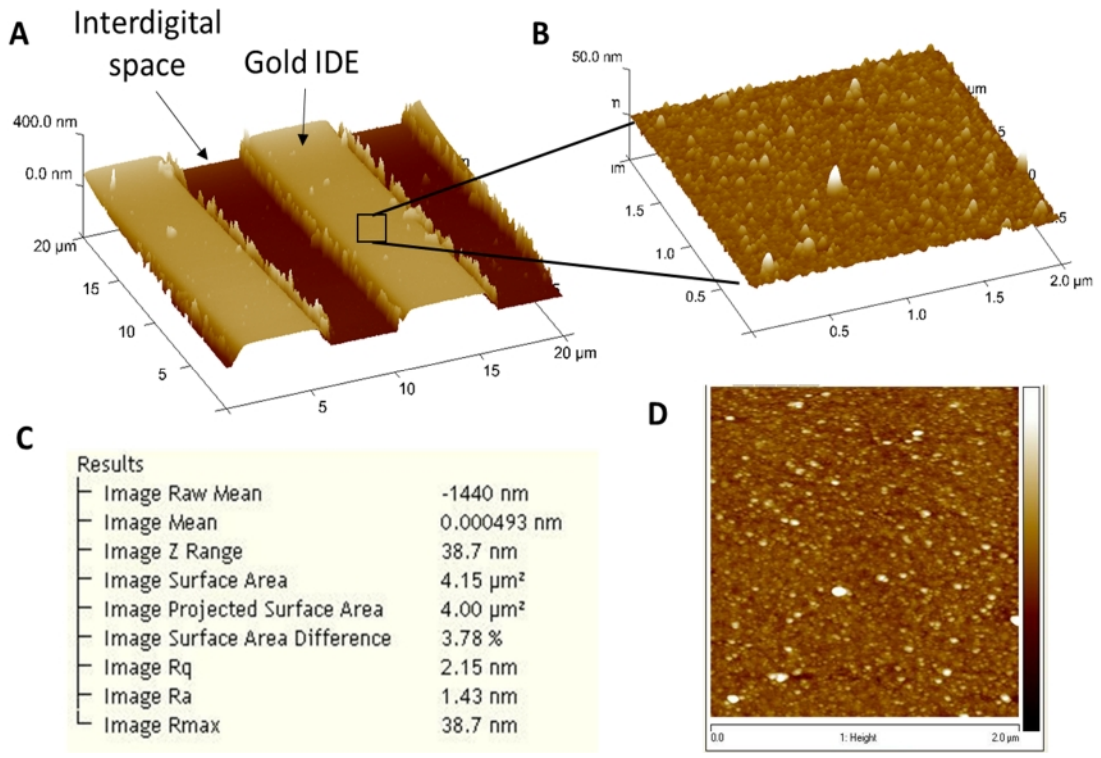

Figure 2-20: AFM characterisation of the bare Micrux IDE. The 3D images of the IDE surface topography are related to (A) 400 µm^2 scan area (height 400 nm) and (B) 4 µm^2 scan area (height 50 nm). (D) 2D image surface topography of the IDE (4 µm^2 scan area) and the (C) related roughness parameters values.

2.4.4.2 SEM Analysis

The scanning electron microscope (SEM) is among the few instruments able to investigate micro and nanostructures. Although a thin layer coating is required to perform the analysis of non-conductive surface, the SEM can provide an accurate 2D image of the surface structure and allows geometrical characterisation analysis. Within this study, the SEM analysis was carried out mainly to verify the geometry of the DropSens and Micrux IDEs, regarding the width of the IDE and the interdigitated gap, which is declared to be equal to 5 µm for both IDEs types.

DropSens IDE (DPR IDEAu5)

The analysis confirmed the presence of some irregularities at the edge of the DropSens IDE, which, at low magnification (1250x), induced a striped pattern on the surface (**Figure 2-21A**). At a higher magnification (10000x), the defects appeared as gold curling (**Figure 2-21B**). Concerning the geometry study (**Figure 2-22**), the average value (±SD) of the IDE width and interspace were of 4.79 µm (± 0.15 µm) and 5.20 µm (± 0.07 µm), respectively.

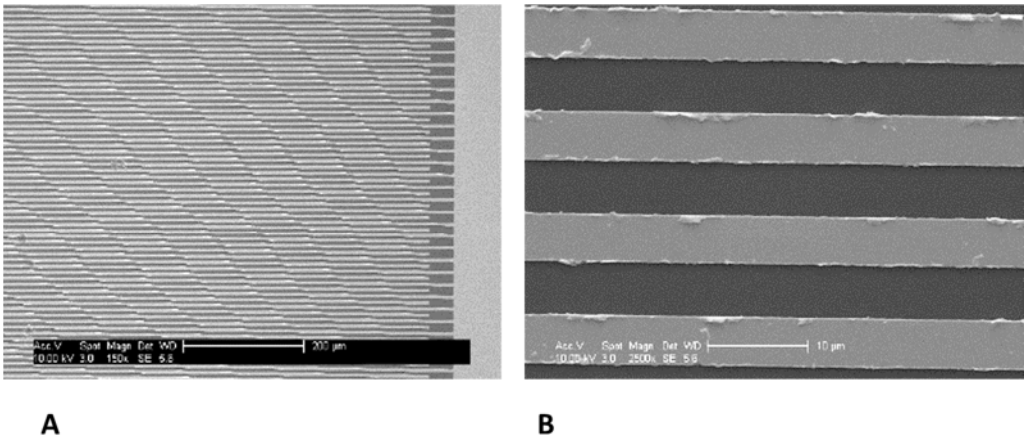

Figure 2-21: Quality and geometry characterisation of DPR IDEAU5. (A) At lower magnification (150x), a regular striated pattern appeared onto the IDEs. (B) At higher magnification (2500x), the defects appear as gold electrodes curling at the edge of the IDE.

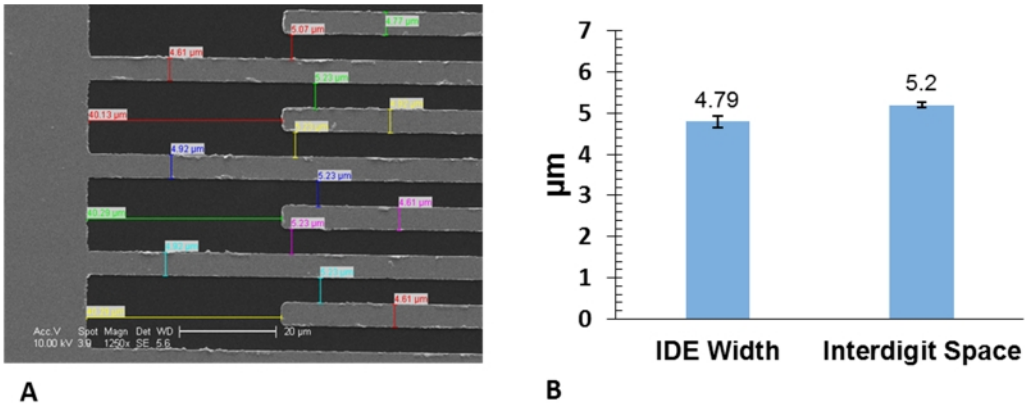

Figure 2-22: The width and interspace values (A) measured during the SEM analysis of the DropSens IDE (1250x) and (B) plotted into a bar chart (average value in the collaouts). Errror bars refer to the standard deviation of replicates (n=6).

Overall, the SEM study allowed to verifying the manufacturing quality of the IDE, which was considered acceptable. Furthermore, SEM study revealed that the IDE geometry was almost in agreement with the manufacturer specification.

Micrux IDE (ED-IDE3Au)

The same analysis has been carried out onto Micrux IDE (**Figure 2-23**). The SEM study revealed the presence of irregularities at the edges of IDE and roughness on the gold IDE surface. The roughness may be considered an artefact introduced by the sample preparation, as they were not detected during the AFM analysis. Concerning the geometry, the average IDE width (±SD) was equal to 5.80 µm (± 0.10 µm), whereas the average IDE interspace (±SD) was equal to 4.37 µm (± 0.09 µm). Overall, the SEM study revealed that the surface geometry differed from the manufacturer specification. However, limitation to this results are the few number of measuraments recorded (n=3) and the higher magnification used to record the measuraments (5000x) compared to the magnification (1250x) used during the Dropsens IDE analysis.

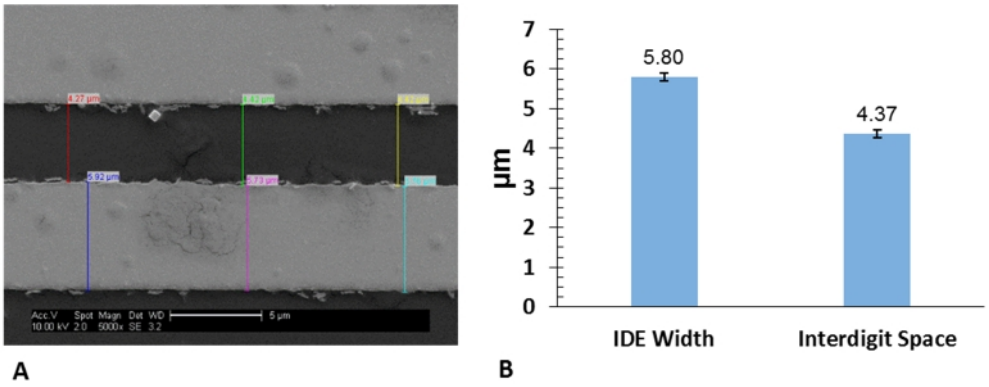

Figure 2-23: The width and interspace values (A) measured during the SEM analysis of the DropSens IDE (5000x) and (B) plotted into a bar chart (average value in the collaouts). Errror bars refer to the standard deviation of replicates (n=3).

2.4.5 NanoMIP Characterisation

Dynamic light scattering (DLS) and Transmission electron microscopy (TEM) are two common techniques in use to assess the size of nanoparticles. DLS and TEM were used

to characterise the diameter size and morphology of the morphine and cocaine nanoMIPs as described in Section 2.3.7.

2.4.5.1 Cocaine nanoMIP

Overall, five batches of cocaine nanoMIP dissolved in acetonitrile were received from the University of Leicester. In order to perform the DLS analysis, the acetonitrile was exchanged with double distilled water via Eppendorf concentrator 5301. Then, a study was carried out to assess the optimal nanoMIP concentration to perform the DLS analysis. Hence, one batch of nanoMIP (batch 2) were investigated at the following concentrations: 0.9 mg mL^{-1}, 0.45 mg mL^{-1}, 0.22 mg mL^{-1} and, 0.11 mg mL^{-1}. The results showed that although the samples were not filtered, the quality report of the DLS analysis was "very good" by the instrument for all the analysis and the PDI values were always less than 0.300. As shown in **Figure 2-24**, the d_H of the cocaine nanoMIP decreased as the concentration decreased, getting close to the same average value (312.89±10.33 nm and 302.31±39.91 nm) at the two highest dilutions (0.22 mg mL^{-1} and, 0.11 mg mL^{-1}, respectively).

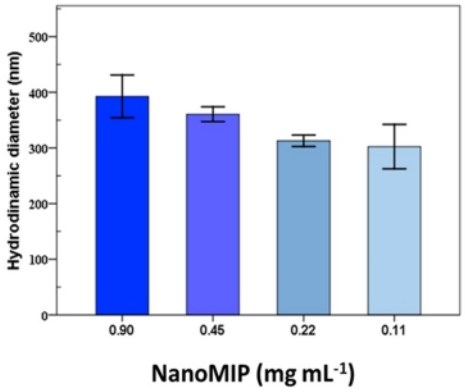

nanoMIP (mg mL^{-1})	d_H(nm)	SD (±)	PDI	SD (±)
0.11	302.31	39.91	0.300	0.063
0.22	312.89	10.33	0.233	0.017
0.45	360.60	13.30	0.166	0.030
0.90	392.65	38.40	0.127	0.053

Figure 2-24: DLS results of the cocaine nanoMIP (batch 2) without filtering and at different concentrations (specifically, 0.11 mg mL^{-1}, 0.22 mg mL^{-1}, 0.45 mg mL^{-1}, 0.90 mg mL^{-1}).

The TEM analysis, performed on the same batch (batch 2) analysed by the DLS, revealed that the nanoMIP size varied as well as that the nanoMIPs tend to agglomerate/aggregate (**Figure 2-25**). According to the TEM analysis, the cocaine nanoMIPs size ranged from

128.98 nm -193.09 nm, with an average (±SD) diameter size equal to 148.35 ± 24.69, which is smaller compared to the values achieved by DLS (>300 nm), but in agreement with the size reported in the literature (size range 90 – 130 nm) (Smolinska-Kempisty *et al.*, 2017).

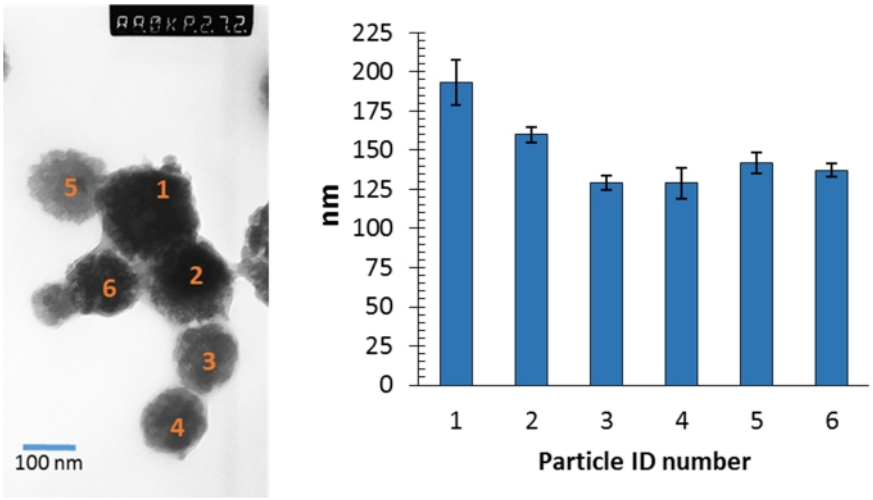

Figure 2-25: TEM image of cocaine nanoMIP batch 2 and bar chart of each measured nanoMIP diameter. Numbers are used to identifying different nanoMIP. Error bars refer to the SD (±) of measurement recorded along four nanoMIP axes (n=4).

Therefore, it was assumed that a certain degree of aggregation still occurred in the sample analysed by DLS. To remove the big aggregates, the batch 2 was adjusted at a concentration of 0.22 mg mL^{-1}, filtered by 0.45 µm syringe filter, and was analysed again by DLS. The DLS results showed that both the average value of the d_H (±SD) and of the PDI (±SD) decreased to 132.3 ± 7.06 nm and to 0.1600 ± 0.0206, respectively (**Table 2-5**). Therefore, it was concluded that filtration through 0.45 µm membrane and a concentration of 0.22 mg mL^{-1} were the optimal conditions to perform the DLS analysis and these were applied for all the other batches analysis (excluding batch 1 as it ran out). The DLS results are reported in **Table 2-5**, while the graphs related to the size distribution by intensity (%) are reported in Appendix C.1. The PDI values were < 0.400, thus highlighting the good quality of the measurements and the nanoMIPs per batch. The PDI values were slightly higher for both batch 1 and batch 5. The size of batch 1 was bigger as the sample was not properly diluted and filtered before taking the DLS measurement. Although the batch 5 was appropriately filtered and the concentration was adjusted at

0.22 mg mL^{-1}, the d_H size of batch 5 was bigger compared to the others. This was probably due to an inconsistent batch production or to aggregation still occurring in the sample.

Table 2-5: Average value (±SD) of hydrodynamic diameter and polydispersity index across the different cocaine nanoMIP batches obtained during DLS analysis.

Cocaine nanoMIP				
	d_H (nm)		PDI	
Batch	Mean	SD±	Mean	SD±
1*	398.86	9.89	0.3400	0.0405
2	132.33	7.06	0.1600	0.0206
3	102.33	8.62	0.1527	0.0743
4	180.73	14.98	0.3281	0.0399
5	259.80	8.96	0.1585	0.0180

*Batch 1 has not been assessed with the optimised DLS protocol.

Overall, the optimised DLS data analysis revealed that the average of the cocaine nanoMIP hydrodynamic diameter was equal to 168.80 ± 68.73 nm. However, the one-way ANOVA revealed that the differences of the d_H between the batches was significant (p-value <0.0001) (**Table 2-6**). These differences may be due to the variability occurring during the manual nanoMIP synthesis across the different batches.

Table 2-6: Results of the one-way ANOVA and Post Hoc Scheffé's test obtained by comparing the d_H of each cocaine nanoMIP batch.

ANOVA

d_H Mean(nm)	Sum of Squares	df	Mean Square	F	Sig.
Between Groups	551050.08	4	137762.52	1406.11	.000
Within Groups	7641.98	78	97.97		

	nanoMIP Batch	Subset for alpha = 0.05				
		1	2	3	4	5
Scheffe[a,b]	3	102.33				
	2		132.33			
	4			180.73		
	5				259.80	
	1					398.86
	Sig.	1.000	1.000	1.000	1.000	1.000

Means for groups in homogeneous subsets are displayed.

a. Uses Harmonic Mean Sample Size = 12.191.

b. The group sizes are unequal. The harmonic mean of the group sizes is used. Type I error levels are not guaranteed.

2.4.5.2 Morphine nanoMIP

The DLS analysis was carried out according to the optimised procedure applied to cocaine nanoMIP (Section 2.4.5.1), despite the morphine nanoMIP has a different composition compared to the cocaine nanoMIP. Overall, PDI values were very low and below 0.300 for all the DLS readings, thus confirming the purity of the nanoMIP samples. The results related to the size distribution by intensity (%) are reported in Appendix C.2. The average value (±SD) of the d_H (nm, SD±) and PDI (SD±) are reported in **Table 2-7**.

Table 2-7: Average value (±SD) of hydrodynamic diameter and polydispersity index across the different morphine nanoMIP batches obtained during DLS analysis

Morphine nanoMIP				
Batch	d_H (nm)		PDI	
	Average	SD±	Average	SD±
1	130.59	3.12	0.1283	0.0144
2	268.39	37.39	0.2287	0.0345
3	163.45	2.66	0.0867	0.0227
4	124.57	5.44	0.2659	0.0083

Overall, the DLS analysis indicated that the average of the morphine nanoMIP hydrodynamic diameter was equal to 170.09 ± 54.75 nm. As reported in **Table 2-8**, the one-way ANOVA statistical analysis revealed that d_H (nm) of batch 1 and batch 4 were not significantly different. However, there was a difference between batch 2 and 5 and of the d_H (nm) of batch 2 and 3.

The TEM analysis was performed only on batch 2. As shown in **Figure 2-26**, the morphine nanoMIPs diameter ranged from 213.75 nm to 295.08 nm, with an average size value (±SD) equal to 250.16 nm (± 24.30 nm). The TEM results and SD (±) were consistent with the d_H value of DLS result of batch 2 (268.39 ± 37.38 nm).

Table 2-8: Results of the One-way ANOVA and Post Hoc Scheffé's test obtained by comparing the d_H of each morphine nanoMIP batch.

ANOVA

d_H Mean(nm)	Sum of Squares	df	Mean Square	F	Sig.
Between Groups	133835.224	3	44611.741	157.014	0.000
Within Groups	13069.809	46	284.126		
Total	146905.033	49			

	NanoMIP Batch	Subset for alpha = 0.05		
		1	2	3
Scheffe[a,b]	4	124.57		
	1	130.59		
	3		163.46	
	2			268.39
	Sig.	0.866	1.000	1.000

Means for groups in homogeneous subsets are displayed.
a. Uses Harmonic Mean Sample Size = 11.429.
b. The group sizes are unequal. The harmonic mean of the group sizes is used. Type I error levels are not guaranteed.

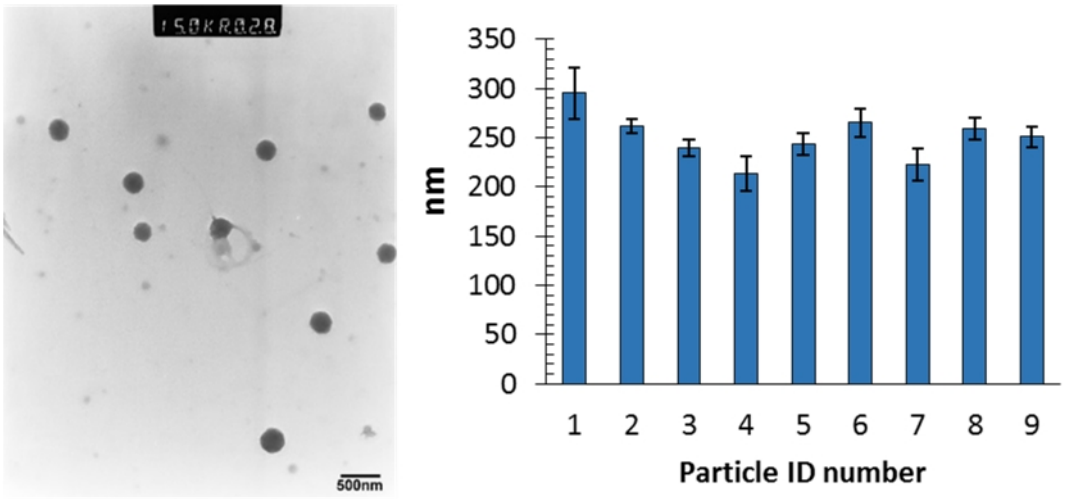

Figure 2-26: TEM image of morphine nanoMIP batch 2 and bar chart of each measured nanoMIP diameter. Error bars refer to the SD (±) of measurement recorded along different nanoMIP axes.

2.5 Conclusion

The characterisation studies of the components of the nanoMIP EIS sensor were reported in this chapter. Before the electrodes characterisation study, *ad-hoc* cleaning procedures was developed for each electrode under study. The SPEs and IDEs electrodes were successfully cleaned by means of double distilled water combined with ethanol rinsing, and water rinsing, respectively. Overall, the cleaning procedures, optimised for each type of electrodes (SPE, DropSens IDE, Micrux IDE), were able to reduce the Rct value by 50% compared to the Rct value recorded to the uncleaned electrodes.

Other than setting the optimal condition for the SAM deposition, the cleaning procedure reduces the likelihood of artefacts or inaccuracy during the AFM and SEM characterisation study. The AFM characterisation study revealed that the SPE working electrode has a rough surface, characterised by peaks with a Rmax value equal to 487 nm. On the other hand, gold working electrodes of both DropSens and Micrux IDEs have a smoother surface (Rmax values were 18.4 nm and 38.7 nm, respectively). As the connection between the DropSens IDE and the connector appeared to be loose, resulting in the electrodes bending and affecting the EIS signal, a custom-made IDE holder with related cover was successfully developed.

Finally, both the cocaine and morphine nanoMIPs provided by University of Leicester, were successfully characterised by TEM and DLS techniques. A summary of the obtained results are reported in **Table 2-9**. An explorative study was carried out to develop the DLS sample preparation. For both types of nanoMIPs, the DLS measurement were taken on nanoMIP at a concentration of 0.22 mL^{-1} and filtered by 0.45 syringe filter. Overall, the size of both cocaine and morphine nanoMIPs slightly varied across the batches, highlighting the need of further optimisation in the solid phase synthesis of the nanoMIPs. According to the results of the DLS analysis performed on all the batches, the average size of the cocaine and morphine nanoMIPs are 168.80 ± 68.73 nm and 170.09 ± 54.75 nm. Other studies reported a more consistent d_H values among different nanoMIP batches, which were produced by a fully optimised solid phase synthesis methods (Abdin, Altintas and Tothill, 2015; Altintas, Guerreiro, *et al.*, 2015). Whereas studies aimed to develop a nanoMIPs synthesis protocol reported only the d_H result of one optimised batch (Moczko

et al., 2013; Smolinska-Kempisty *et al.*, 2017). Concerning the TEM studies, an optimised protocol to prevent nanoMIP artefact during sample preparation has never been reported before. It is expected that a too concentrated sample will lead to nanoMIP aggregation/agglomeration thus reducing the quality of the images and affecting the size distribution study, which has to be carried out on at least 100 2D image of nanoMIPs.

Table 2-9: Summary of the nanoMIP size characterisation study performed by DLS and TEM analysis.

NanoMIPs	TEM (nm)	SD (±)	DLS (nm)	SD (±)
Cocaine (Batch 2)	148.35	24.69	132.3	7.06
Cocaine (all batches)			168.80	68.73
Morphine (batch 2)	250.16	24.30	268.39	37.38
Morphine (all batches)			170.09	54.75

Chapter 3
Cocaine NanoMIP EIS Sensor Development

3.1 Introduction

Cocaine is classified as central nervous system (CNS) stimulant and, when abused, induces an elevation in mood, euphoria, appetite suppression, energy, alertness and endurance, while its overdose may induce stupor, delirium, cardiac arrhythmias, seizures and coma (Caddy, 2003; WHO, 2004). Cocaine is known to be the most abused drugs in the world after cannabis. Furthermore, with over 655 tons detained yearly, cocaine is one of the most seised drugs of abuse worldwide (UNODC, 2016). It is also one of the major drugs of abuse illegally trafficked in European Countries, where there are more than 17.5 million of users (EMCDDA, 2016). Regulations set out worldwide punish the unauthorised use, possession, manufacture or trafficking of drugs of abuse (UNODC, 2015). Illicit drugs related crimes are of great concern due to the burden over LEA (Law Enforcement Agencies), and healthcare systems with associated social and economic problems. To control and manage drugs of abuse trafficking, LEA takes advantage of the powerful olfactory system of the "sniffer dogs". After an appropriate training, these dogs are able to "smell and detect" very low concentration (in the range of ppb) of illicit drugs concealed in various items/packages/containers (Leitch *et al.*, 2013; Jezierski *et al.*, 2014; Cerreta and Furton, 2015). However, the primary police dog limitations are the long and continuous training required, work fatigues constraint and related animal welfare commitments, visibility and their penchant to be deceived by handlers while searching for evidence (Lorenzo *et al.*, 2003; Leitch *et al.*, 2013).

Therefore, this work aims to develop a rapid, stable and reproducible sensor, able to detect cocaine in trace levels and be used in diverse scenarios. Ideally, the sensor should mimic the dog's olfactory receptor cell response system. Furthermore, the sensor aims at the detection of cocaine occurring in environmental samples, such as wastewater samples and powder samples collected from solid surfaces (e.g. glass, marble, wood, skin and nails) (Li et al., 2014a). Two of the most recent advanced products in nanotechnology manufacturing and electrochemical sensors, namely, nanoMIP and electrochemical impedance spectroscopy, are combined in this work for the first time. Specifically, the aim is to develop a biomimetic, yet highly sensitive and specific, nanoMIP EIS affinity sensor to detect cocaine at trace level, thus providing a cheap and portable analytical tool to use during drugs of abuse investigative activities.

3.2 Materials and Methods

3.2.1 Materials

The University of Leicester synthesised cocaine nanoMIPs and nanoNIP and dispatched them in acetonitrile solution. Cocaine hydrochloride, morphine hydrochloride (trihydrate), caffeine, levamisole and mannitol were purchased from Sigma-Aldrich Ltd (Dorset, UK). All the drugs of abuse were handled according to the Home Office (UK) guidelines, and the appropriate procedure for drugs of abuse handling was elaborated and set in place. Phosphate buffered saline tablet (PBS: 0.0027 M potassium chloride, 10 mM phosphate buffer and 0.137 M sodium chloride, pH 7.4) and 3-(N-Morpholino) propanesulfonic acid powder (MOPS) were purchased from Sigma-Aldrich Ltd (Dorset, UK) and used to make buffer solutions. 11-mercaptoundecanoic acid (11-MUDA) was purchased from Sigma-Aldrich Ltd (Dorset, UK) and was dissolved in 10 mL of ethanol (pure ethyl alcohol, anhydrous, ≥ 99.5%) at a concentration of 5 mM. N-hydroxysuccinimide (NHS) and 1-Ethyl-3-(3-dimethylaminopropyl) carbodiimide (EDC), were purchased from Thermo Scientific™ (Rugby, UK) and dissolved in water to obtain 0.1 M and 0.4 M solution, respectively. Ethanolamine, PVA (polyvinyl alcohol), Bovine Serum Albumin (BSA), milk proteins, and Tween 20 were purchased from Sigma-Aldrich Ltd (Dorset, UK) and used as blocking agents at the respective concentrations of 1 M, 0.1% (w/v), 10 % (v/v) and 1% (v/v).

The 10 mM redox couple solution ($[Fe\ (CN)_6]^{3-/4-}$) was prepared by dissolving potassium ferrocyanate ($K_4[Fe(CN)_6]$) and potassium ferricyanide ($K_3[Fe(CN)_6]$) in MOPS (10 mM, pH 6.0 or pH 7.4).

All the solutions used were filtered through filter system by means of a nitrocellulose Whatman® filter 0.2 μm (Whatman International Ltd, Maidstone, UK) or by 0.2 μm Corning® syringe filter (Corning Inc., New York, US). All nanoMIPs and non-imprinted polymers (nanoNIPs) solutions were filtered with 0.45 μm syringe filter (Corning®, Corning Inc., New York, US).

3.2.2 Faradaic EIS Setting and Measurement Parameters

The parameters of the EIS measurements were set as reported in Section 2.3.1, while the EIS data were analysed as described in Section 2.3.2, using EIS spectrum analyser® v1.0 (Bondarenko, Ragoisha and Pomerantsev, 2005). A summary of the relevant EIS measurements parameter and conditions applied in this Chapter is reported in **Table 3-1**.

Table 3-1: Summary of the relevant EIS condition applied to each investigated electrode used to develop the cocaine nanoMIP IES sensor.

			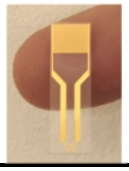	
		DPR C220AT	DPR IDEAu5	Micrux ED-IDE3 Au
DC (V)		0.12	0.12	0.23
AV (V)		0.01	0.01	0.01
Frequency range (Hz)		0.1 – 50,000		
N° frequency points		51		
Redox Couple Solution $[Fe(CN)_6]^{3-/4-}$	Concentration	10 mM		2.5 mM
	Buffer	10 mM MOPS		
	pH	6.0 or 7.4	7.4	7.4
	µL	50	60	10

3.2.3 Faradaic EIS Measurement

The Faradic EIS measurement was used in all the tests performed within this work. Briefly, the electrode was dried by a stream of N_2 to prevent atmospheric oxygen dissolving onto the electrode surface. Then, the electrode was inserted in the connector, and a drop of ferrocyanide-ferricyanide redox couple solution ($[Fe(CN)_6]^{3-/4-}$) (as in **Table 3-1**) was placed on the electrode surface. The EIS reading was performed, and soon after, the redox couple solution was discarded, and the electrode washed with 0.2 µm filtered deionised water and dried under a gentle stream of N_2. Specifically, 1.2 mL of water was used to wash both DropSens electrodes, while only 0.6 mL of water was used to rinse the Micrux IDE. For the cumulative assay, the washing step was carried out with

the buffer used as the analyte diluent. While not in use, the functionalised electrodes were stored under dark and humid condition.

3.2.4 Cocaine nanoMIP Sensor Assembly

A general and consistent protocol was applied to develop the cocaine nanoMIP sensor surface (Abdin et al., 2015; Altintas et al., 2015c; Masdor et al., 2017; Ashley et al., 2017).

The SPE gold electrodes were cleaned according to the optimised protocol already discussed in Section 2.4.3. Subsequently, they were incubated overnight in an ethanol solution containing 5 mM 11-MUDA to create a self-assembled monolayer (SAM). Excess of MUDA was removed by rinsing the electrode surface with 1.2 mL ethanol and then 1.2 mL water. The electrode surface was then dried with a gentle stream of N_2, and the EIS measurements were recorded. The electrode was washed as described above and 20 µL of a mixture of EDC/NHS solution (0.2 M of EDC and 0.05 M of NHS) in water was dropped only on the working electrodes. The electrode was left for 1 hour at room temperature in a petri dish and covered with aluminium foil. This step activates the SAM and allows the nanoMIP/nanoNIP attachment via amine coupling procedure. The electrode was washed with 0.2 µm filtered doubled distilled water and dried under a gentle stream of N_2. Afterwards, an EIS measurement was recorded.

As previously stated, cocaine nanoMIP were produced introducing amine groups onto the external surface during their synthesis. The amine groups allowed their attachment onto the gold working electrodes via amine coupling conjugation, according to a well-established protocol developed for other biosensor platforms, like QCM or SPR (Altintas *et al.*, 2012; Abdin, Altintas and Tothill, 2015; Altintas, Gittens, *et al.*, 2015). The nanoMIPs and nanoNIPs (non-imprinted polymer) solutions were evaporated via Eppendorf Concentrator 5301 (Eppendorf AG, Germany) until 5 mg mL^{-1} concentration was reached calculated by volume reduction. A drop of nanoMIP or nanoNIP was placed onto the activated MUDA surface and incubated at 37 °C for 1 hour. The electrode surface was washed with 0.2 µm filtered doubled distilled water and dried under a gentle stream of N_2. An EIS measurement was recorded. It is likely that some of the carboxyl group (COOH) were not involved in the MIP attachment, thus acting as a source of non-specific

bindings. Therefore, 1 M ethanolamine dissolved in MOPS (10 mM) and adjusted to 8.5 was placed on the surface and incubated for 1 hour at room temperature. The ethanolamine is a small molecule and can easily reach the unreacted carboxyl group (COOH), thus forming an amide bond and blocking the surface. The pH was adjusted at pH 8.5 to introduce more protonated amine groups, thus promoting the amide bond formation. The surface was once again washed with doubled distilled water as previously described and an EIS measurement was recorded.

The same sensor surface was replicated onto all the electrodes, including both type of IDEs (DPR IDEAu5 and ED-IDE3Au) by applying the protocol reported above. However, the volume of each reagent was adjusted to cover the whole electrode surface (**Table 3-2**), while the concentration was kept constant.

Table 3-2: Summary of the reagents and volumes used during the functionalisation of each type of electrodes.

Reagents	DPR C220AT	DPR IDEAu5	ED-IDE3Au
MUDA	1.2 mL	0.6 mL	0.3 mL
EDC/NHS	20 µL	50 µL	10 µL
NanoMIP	20 µL	50 µL	20 µL
Blocking agents	50 µL	50 µL	20 µL
Washing (water or ethanol)	1.2 mL	1.2 mL	0.6 mL

3.2.5 Cocaine nanoMIP Sensor Characterisation

Faradaic EIS measurements is a powerful method to investigate surface modification during sensors fabrication (Atta, Hassan and Galal, 2014; Bozokalfa *et al.*, 2016; Cheraghi, Taher and Karimi-Maleh, 2016), therefore, the EIS measurement was recorded after each step of the cocaine nanoMIP fabrication process as reported in Section 3.2.4. The experimental data were fitted in an appropriate equivalent circuit, and the data were processed as described in section 2.3.2, and the Rct was expressed as a percentage (%) of the average Rct of the MUDA coated electrodes (set as a 100%). Furthermore, to assess the quality of the cocaine nanoMIP attachment onto the gold electrodes surface, the bare,

MUDA coated, and nanoMIP electrode surface was investigated using AFM (Dimension 3100, Bruker, US) performed in tapping mode. Both 3D surface topography characterisation and roughness analysis (Ra and Rq) were carried out and compared. Similarly, the DropSens IDE surface was also characterised using SEM.

Before performing the AFM and SEM analysis, the bare electrode surface was cleaned according to the procedures optimised for each type of electrodes (DropSens SPE, DropSens IDE, and Micrux IDE) as described in Section 2.4.3. The MUDA fuctionalised sensor surface and the nanoMIP functionalised sensor surface were rinsed with doubled deionised water and dried well under a gentle stream of nitrogen before performing the AFM and SEM analysis. For the SEM analysis, a thin gold layer (15 nm) was also deposited onto the electrodes surface.

3.2.6 Development and Optimization Studies of the Cocaine NanoMIP EIS Sensor onto DropSens SPE

3.2.6.1 Cocaine Cumulative Assays on an Un-Optimised Sensor (in water)

The cocaine nanoMIP EIS sensor was fabricated as described in Section 3.2.4 and the sensor surface was blocked with ethanolamine dissolved in 10 mM MOPS (50 µL, 1 M, pH 8.5). The cocaine nanoMIP EIS sensor ability to detect the cocaine molecule was tested by performing cumulative assays. Cocaine hydrochloride was dissolved in water and increasing concentrations were prepared (100 pg mL^{-1}– 50 ng mL^{-1}). Water solution was used as a blank sample. A 20 µL of the blank solution was left in contact with the sensor surface for 30 minutes and then the EIS read out was recorded. This step was repeated at least three times on the same sensor and until a stable blank signal was achieved. Subsequently, 20 µL of each concentration of cocaine, from the lowest to the highest (100 pg mL^{-1}– 50 ng mL^{-1}), was incubated onto the sensor surface for 30 minutes. At the end of each incubation step, the electrode surface was washed with 1.2 mL of water solution and dried under a gentle stream of N_2. A drop of redox couple $[Fe(CN)_6]^{3-/4-}$ (50 µL, 10 mM, pH 6.0) was placed on the sensor surface and the EIS measurement was performed as reported in **Table 3-1**. All the incubations were carried out at room

temperature and in dark and humid conditions. To this aim, the electrodes were placed on a wet paper in a petri dish covered with aluminium foil.

To confirm that the analyte was binding to the cocaine nanoMIP, a cumulative assay was carried out onto another group of sensors. One group (n=3) was functionalised without the nanoMIP (control sensor) and other group (n=3) with cocaine nanoNIP (non-imprinted polymer nanoparticle, which were synthetized applying the same nanoMIP protocol, but in absence of the template). All the experiments were carried out on independent sensor surfaces and at least in triplicates. The list and conditions of the cocaine cumulative assay carried out are reported in **Table 3-3**.

Table 3-3: Cocaine cumulative assay conducted on an un-optimised sensor. All the assays were carried out within the same cocaine concentration range (100 pg mL^{-1}– 50 ng mL^{-1}).

Test ID	MIP/NIP	Sensor Blocking agent	Sample Diluent
1	Cocaine MIP	Ethanolamine 1M, pH 8.5	water
2	Cocaine NIP	Ethanolamine 1M, pH 8.5	water
3	Control (no MIP)	Ethanolamine 1M, pH 8.5	water

3.2.6.2 Specificity Assays on an Un-Optimised Sensor (in water)

The sensor specificity was evaluated versus two major street cocaine cutting agents, namely caffeine and mannitol. The sensors were fabricated with cocaine nanoMIP according to the protocol reported in section 3.2.4. Each analyte was dissolved either in water, and increasing concentrations (from 100 pg mL^{-1} to 50 ng mL^{-1}) were prepared, as reported in **Table 3-4**.

Table 3-4: List of the specificity assay carried out and related assay conditions.

Test ID	NanoMIP (Yes/No)	Substance	Blocking Agent	Diluent
2	YES	Caffeine	Ethanolamine	Water
3	YES	Mannitol	Ethanolamine	Water
4	NO	Caffeine	Ethanolamine	Water

The cumulative assay was carried out for each selected analyte, following the same incubation and washing procedure reported in Section 3.2.6.1. All the experiments were carried out on independent sensor surfaces and at least in triplicates. The EIS experimental data were processed as described in Section 3.2.6.5. To assess the specificity, the sensor response for caffeine and morphine was compared against the sensor response for cocaine.

3.2.6.3 Blocking Agent Optimisation Study

Due to the arising of non-specific binding and cross-reactivity, an optimisation study was carried out to overcome these events and caffeine was used as a model analyte. To assess if the sensor response recorded towards increasing concentration of caffeine was due to the non-specific binding or to the cross-reactivity, the caffeine cumulative assay was carried out on the control sensor (sensor functionalised without the nanoMIP). Then, several blocking agents were used in combination with ethanolamine, namely BSA (0.1%, w/v) and Tween 20 (1%, v/v), milk protein (10%,v/v), and PVA (1%, v/v), as shown in Table 3-5. All the new blocking agents solutions were prepared in MOPS (10 mM, pH7.4). Several groups of sensor were fabricated as described in Section 3.2.4 and the surface of each group of sensors was blocked by incubating the investigated blocking agents (50 μL) for 1 hour at room temperature. The sensor surface was then rinsed with deionised water and dried under a stream of N_2.

Each blocking strategy was tested by performing the caffeine cumulative assay following the same incubation and washing procedure reported in Section 3.2.6.1. For the cumulative assay, caffeine was dissolved in 10 mM MOPS at either pH 6.0 or 7.4, as detailed in **Table 3-5**. For each cumulative assay, the selected diluent was used as blank sample. The washing buffers used were as specified and reported in **Table 3-5**. The EIS experimental data were processed as described in Section 3.2.6.5. The sensor responses obtained in each assay were averaged (±SD), plotted and compared. The blocking agent with the Rct value closer to the zero (=blank signal) was chosen as the optimised blocking condition. This condition was used to carry out the cocaine cumulative assay to verify the sensor specificity for cocaine detection. When the blocking agents and the buffer pH used

were able to remove the caffeine cross-reactivity, while allowing the cocaine detection, the nanoMIP EIS sensor was considered optimised.

Table 3-5: List of the blocking agent assays tested and related assay conditions.

Assay ID	pH Diluent	Blocking Agent	Washing Buffer	pH buffer
1	6.0	Ethanolamine + BSA – T20	MOPS	6.0
2	6.0	Ethanolamine + BSA – T20	MOPS + T20	6.0
3	6.0	Ethanolamine + milk protein	MOPS	6.0
4	7.4	Ethanolamine + BSA – T20	MOPS	7.4
5	7.4	Ethanolamine + PVA	MOPS	7.4

BSA = 0.1% Bovine serum albumin in MOPS; T20 = 1% Tween 20 in MOPS; Milk protein= 10% milk protein in MOPS; PVA = 1% polyvinyl alcohol in MOPS.

3.2.6.4 Specificity Assays on Optimised Sensor

The optimised sensors were fabricated according to the protocol reported in section 3.2.4. The optimised blocking agents were used to block the sensor surface and these include the ethanolamine (50 µL, 1 M dissolved in MOPS, pH 8.5), followed by a 50 µL MOPS buffer solution (50 µL, 10 mM, pH 7.4) containing BSA (0.1%, w/v) and Tween 20 (1%, v/v). Then, the specificity of the optimised sensor was evaluated versus three major street cocaine cutting agents, namely levamisole, caffeine and mannitol. Cross-reactivity towards morphine was also evaluated.

Each analyte was dissolved in MOPS (10 mM, pH 7.4) and increasing concentrations (100 pg mL^{-1} - 50 ng mL^{-1}) were prepared. The MOPS (10 mM, pH 7.4) was also used as the washing buffer and as the blank sample. The cumulative assay was carried out for each selected analyte, following the same incubation and washing procedure reported in Section 3.2.6.1. All the experiments were carried out on independent sensor surfaces and at least in triplicates.

3.2.6.5 Cumulative Assay Data Analysis

The experimental data were fitted in an appropriate equivalent circuit, and the obtained Rct (Ω) value was expressed as a percentage of the blank signal, thus standardising the sensor response across the sensors and as reported in previous works (Ahmed, J. V. Rushworth, *et al.*, 2013). In detail, the experimental data were processed according to the following steps:

1. For each measurement, the experimental data were fitted into an appropriate equivalent circuit (such as Randles or simplified Randles circuit). An example is reported in Figure 2-6 (Section 2.3.2, Chapter 2).
2. For each measurement, the fitted data were exported as a report, and the data (Rct, Rsol and Cdl, and W values) were entered into a database for further analysis.
3. For each sensor, the average value (±SD) of the Rct values observed for the blanks EIS readings was calculated, thus obtaining the Rct_{blank} value.
4. The Rct value related to each concentration ($Rct_{concentration}$) was expressed as:

$$\Delta\,\%Rct = \frac{Rct_{concentration} - Rct_{blank}}{Rct_{blank}} \times 100 \qquad (3\text{-}1)$$

5. The Δ %Rct values related to each replicate and obtained at the same concentration were averaged and the SD (±) was calculated.
6. The average Δ %Rct values were plotted aginst the analyte concentration, thus obtaining the calibration curve. The average of the Δ %Rct values were plotted as -Δ %Rct, when negative values were obtained.

3.2.6.6 Sensitivity Study and LOD determination

The obtained Δ %Rct values were plotted against the analyte concentrations. The linearization was achieved by expressing the concentration as LOG10. To assess the sensor performances, the slope of the calibration curve, the coefficient of determination (R^2) of the linear regression, and the significance (p-value≤0.05) were considered. The following equation (3-2) was applied to calculate the LOD (Harris, 2010):

$$LOD = \frac{[(3 \times SD\ BLANKS) - b]}{m} \quad (3\text{-}2)$$

Where:

b *is the y-intercept of the linear calibration curve;*
m *is the slope of the linear calibration curve.*

3.2.6.7 Thermal Regeneration Explorative Test

The optimised sensors were fabricated according to the protocol reported in section 3.2.4. The optimised blocking agents were used to block the sensor surface and these include the ethanolamine (50 µL, 1 M dissolved in 10 mM MOPS, pH 8.5), followed by a 50 µL MOPS buffer solution (50 µL, 10 mM, pH 7.4) containing BSA (0.1%, w/v) and Tween 20 (1%, v/v). The sensors were used to carry out the cocaine cumulative assay (100 pg mL^{-1} - 100 ng mL^{-1}) applying the optimised assay conditions. Then, the nanoMIP EIS sensor was used to carry out a thermal regeneration experiment. Briefly, the thermal regeneration of the sensor surface was attempted by dipping the sensor into a glass vial containing 3 mL of ultrapure deionised water pre-heated at 60°C for 20 minutes. The electrode surface was washed as usual and allowed to cool down for 45 minutes. Later, a drop of redox couple (50 µL, 10 mM, pH 7.4) was placed on the sensor surface and the EIS measurement was performed as reported in Section 3.2.3. To assess the outcome of the thermal regeneration, the EIS spectra recorded after the incubation of the last cocaine concentration (100 ng mL^{-1}) and after the thermal regeneration were compared.

3.2.7 Evaluation Studies of Cocaine NanoMIP Sensor onto DropSens IDE

The ability of the cocaine nanoMIP EIS sensors fabricated using DropSens IDE were assessed using the un-optimised and optimised sensors. The un-optimised cocaine nanoMIP EIS sensors were fabricated as detailed in section 3.2.4 using DropSens IDE and blocking the surface with only ethanolamine (60 µL, 1 M dissolved in 10 mM MOPS, pH 8.5). The optimised cocaine nanoMIP EIS sensors were fabricated as detailed in section 3.2.4 using DropSens IDE and the optimised blocking agents, i.e. the

ethanolamine (60 µL, 1 M dissolved 10 mM MOPS, pH 8.5), followed by a 60 µL MOPS buffer solution (60 µL, 10 mM, pH 7.4) containing BSA (0.1%, w/v) and Tween 20 (1%, v/v).

The cocaine cumulative assay was replicated on each type of cocaine nanoMIP sensor (un-optimised and optimised) by dissolving cocaine hydrochloride in MOPS (10 mM, pH 7.4) and increasing concentrations were prepared (100 pg mL^{-1} - 50 ng mL^{-1}). The MOPS (10 mM, pH 7.4) was used as a washing buffer and as a blank solution. To assess the blank noise, 60 µL of the blank solution was incubated at least three times onto the sensor surface for 30 minutes, and the EIS readout was recorded. Subsequently, 60 µL of each concentration, from the lowest to the highest, was incubated onto the sensor surface for 30 minutes. At the end of each incubation step, the electrode surface was washed with 1.2 mL of 0.2 µm filtered diluent solution used during the experiment and dried under a gentle stream of N_2. Then, 60 µL of the redox couple solution $[Fe(CN)_6]^{3-/4-}$ (60 µL, 10 mM, pH 7.4) was placed on the sensor surface and the EIS measurement was performed with the setting parameters detailed in Section 3.2.2 and according to the procedure detailed in Section 3.2.3.

All the incubations were carried out at room temperature and in dark and humid condition. This was achieved by placing the electrode on a wet paper allocated in one well of the six multi-well plate (Nunc™ Cell-Culture Treated multi-well plates, Thermo Scientific™). The multi-well plate was covered with aluminium foil. All the experiments were carried out on independent sensor surfaces and at least in triplicates. The experimental data were processed as described in Section 3.2.6.5. The sensor sensitivity and the LOD were determined as described in Section 3.2.6.6.

3.2.8 Evaluation Studies of Cocaine NanoMIP Sensor onto Micrux IDE

The optimised cocaine nanoMIP EIS sensor on the Micrux IDE was fabricated as described in Section 3.2.4 and using the optimised blocking agents applied for the DropSens IDE and detailed in Section 3.2.7. The cocaine cumulative assay was replicated dissolving cocaine hydrochloride in MOPS (10 mM, pH 7.4) and preparing different concentrations (10 pg mL^{-1} - 50 ng mL^{-1}). The MOPS (10 mM, pH 7.4) was used as a

washing buffer and as a blank solution. To assess the blank noise, 10 µL of the blank solution was incubated at least three times onto the sensor surface for 30 minutes. After rinsing the electrodes with 600 µL of 10 mM MOPS pH 7.4 and drying it, the EIS readout was recorded by dropping 10 µL of the redox couple solution $[Fe(CN)_6]^{3-/4-}$ (2.5 mM, pH 7.4). Subsequently, 10 µL of each concentration, from the lowest to the highest, were incubated onto the sensor surface for 30 minutes. At the end of each incubation step, the electrode surface was washed with 600 µL of 10 mM MOPS and dried under a gentle stream of N_2. EIS measurement was performed with the setting parameters detailed in Section 3.2.2 and according to the procedure detailed in Section 3.2.3.

All the incubations were carried out at room temperature and in dark and humid condition, as described in Section 3.2.7. All the experiments were carried out on independent sensor surfaces and at least in triplicates. The experimental data were processed as described in Section 3.2.6.5. The sensor sensitivity and the LOD were determined as described in Section 3.2.6.6.

3.2.9 Data Processing and Statistical Analysis

All the data of each experiment were collected on an Excel® database spreadsheet and identified by a unique code. Statistical analyses were carried out with the aids of Microsoft® Excel® and IBM® SPSS® Statistics 24.0 software. Descriptive statistic and related plots were used to present the results. The significance level (*p-value*) was set at 0.05. Both parametric and non- parametric statistics were applied as appropriate. In detail, the one-way ANOVA test and *post-hoc* analysis have been applied to assess any difference between two or more experiments and related contrasts, respectively. When the number of records was considered not enough to run parametric tests ($n<30$), non-parametric tests were applied. Specifically, Mann–Whitney U test was applied to compare two groups of data, and when the number of the available experimental data were not enough to run the *t*-test data within the same group. The Kruskal–Wallis test was used when two or more independent groups of data were compared, and the number of the available experimental data were not enough to run the one-way ANOVA test.

3.3 Result and Discussion

This section will report and discuss the results of the characterisation and performances of the Cocaine nanoMIP EIS sensor developed on three types of electrodes. Briefly, the characterisation study was performed during the sensor fabrication using EIS, AFM and, when needed, SEM. The performance studies focused on the sensitivity and specificity evaluation, with an exploration of the thermal regeneration assay of the sensor surface. The sensitivity of the sensor was assessed by means of the cumulative assay, during which the sensor response was assessed against increasing concentration of cocaine. The related calibration curve and LOD were the parameters used to evaluate the sensitivity of the sensors.

Concerning the specificity assay, the non-specific binding and the cross-reactivity towards the cutting agents and drugs were assessed, namely levamisole, caffeine, mannitol and morphine. As reported in the majority of the recent study, levamisole and caffeine are among the most abundant cocaine cutting agents, while mannitol is mostly used as a diluent (Botelho *et al.*, 2014; Broséus *et al.*, 2015; Lapachinske *et al.*, 2015). The cocaine cumulative and specificity assays were performed onto SPE (namely, DPR C220AT). The SPE was also used to optimise the sensor surface. Once an optimised sensor was achieved, only the cumulative assay has been replicated onto both IDEs sensors, thus comparing the feasibility onto electrodes that hold a different geometry.

3.3.1 Cocaine NanoMIP EIS Sensor Development onto SPE

3.3.1.1 EIS Characterisation Study

DropSens screen-printed electrodes (SPEs, DPR C220AT) were cleaned as reported in 2.4.3.1 and functionalised by directly attaching the Cocaine nanoMIP onto the working electrodes via amine coupling, as detailed in Section 3.2.4. A schematic diagram of the SPE functionalisation is shown in **Figure 3-1**. The resulting EIS spectra are shown in **Figure 3-2A** and are consistent with previously published work.

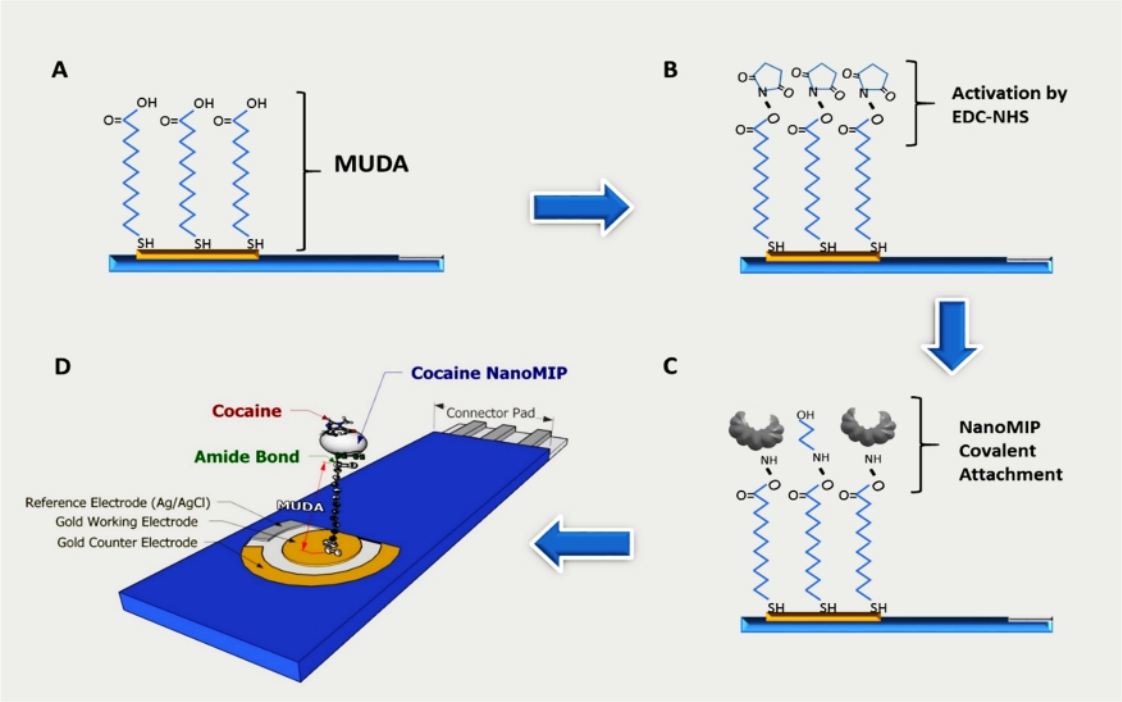

Figure 3-1: Steps to achieve the nanoMIP attachment onto gold working electrode surface (SPE DPR C220AT, DropSens). (A) SAM formation; (B) Carboxylic group activation by EDC/NHS; (C) nanoMIP covalent attachment via amine coupling. (D) 3D scheme of the final nanoMIP sensor for cocaine detection.

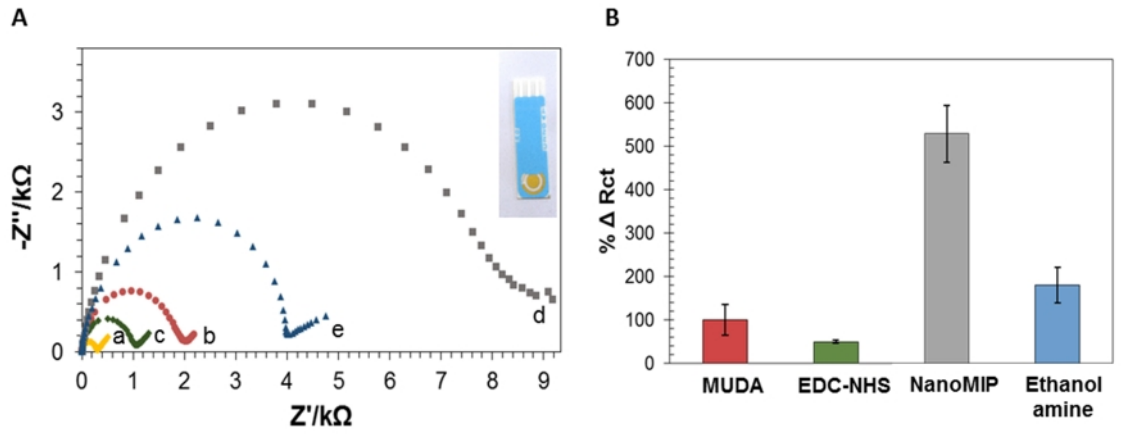

Figure 3-2: (A) Nyquist plots obtained during Cocaine nanoMIP EIS sensor fabrication using SPE electrode (inset sensor image): Bare electrode (a), after MUDA (b), EDC/ENS activation (c), nano-MIP attachment (d), ethanolamine blocking (e). (B) Average of %Rct values (±SD) at each functionalization points obtained by EIS. Error bars refer to the standard deviation of the replicates (n=5).

From **Figure 3-2A (a)**, the cleaned bare electrode gave low Rct value as expected after cleaning with heat treatment and water rinsing. The MUDA attachment to the gold surface is due to thermodynamically favourable chemisorption of the thiol groups (Mendes et al., 2004). In addition, at a basic pH, deprotonation of the MUDA interfacial carboxylic acid groups occurred. Consequently, the electrostatic repulsion between the negatively charged interface and the anionic redox probe induced an increase in Rct value compared to the bare electrode signal (Zhao et al., 1999; Sanders et al., 2008). As our result indicated in **Figure 3-2A (b)**, an increase in Rct value was observed after the MUDA attachment when compared to the bare electrode. In the third step, the carboxylic groups were activated by EDC-NHS (Hermanson, 2013), which decreased the negative charges of the SAM and, hence, induced a drop of the Rct value, as observed in the EIS spectrum in **Figure 3-2A(c)** (Hushegyi et al., 2015). The activated carboxylic groups reacted with the amine groups of the cocaine nanoMIP thus enabling their covalent attachment. Hence, the Rct value increased due to the nanoMIP (**Figure 3-2A, d**). Finally, the ethanolamine was used to block any unreacted carboxylic groups, thus minimising the unspecific binding occurrence. The ethanolamine decreased the negative charge of the surface and introduced hydrophilic groups onto the sensor surface, thus leading to a drop of Rct value (**Figure 3-2A, e**). Overall the EIS revealed that nanoMIPs were successfully attached to the electrode surface.

The experimental data were fitted in the Randles equivalent circuit. However, the simplified Randles equivalent circuit was used to fit the data, when the diffusion effect was not visible. The goodness of the fit revealed that the average % error of the Rct values was 2.50 % (± 0.76). The Rct values were expressed as % of the MUDA Rct value, which was set at 100%. The results were plotted in a bar chart and is shown in **Figure 3-2B**. Although nanoMIP adsorption onto the surface events cannot be completely excluded, the nanoMIP attachment was found to be reproducible.

3.3.1.2 AFM Characterisation Study

AFM in a tapping mode has been applied to characterise the SPE surface functionalisation. Although AFM is a powerful technique, it is essential to take into

account the following consideration:

1. The surface of the SPE electrodes is rough, and this may affect the AFM baseline, thus affecting Ra and Rq values obtained at each functionalisation point (namely, bare, MUDA and MIP attachment). Furthermore, since it is not possible to sample precisely the same area at each functionalisation point, it is likely that Ra, Rq and Rmax values will not be able to differentiate between the functionalisation points.
2. NanoMIPs deposition results in a heterogeneous layer deposition. Noticeably, this will affect the Ra and Rq and Rmax values, which will not reflect the actual height and coverage of the nanoMIP deposition onto the sensor surface.
3. The sensor was fabricated manually and without microfluidic condition. This may introduce artefacts and imperfections due to nanoMIPs agglomeration or human errors (which refers to the operator's *intra*-variability in carrying out sensor assembly).

A 400 μm^2 area scan was performed onto bare, MUDA coated and nanoMIP functionalised SPE electrodes (as reported in Section 3.2.4). To assess the MUDA layer deposition also a 4 μm^2 area scan was performed. The surface roughness analysis was also carried out and results are shown in Figure 3-6. Concerning the MUDA deposition, the same sensor was assessed before and after the MUDA layer deposition. In the 400 μm^2 area scan (height 3 μm), results showed a rough surface both onto the bare and the MUDA functionalised surface (**Figure 3-3A** and **Figure 3-3B**, respectively). A slight difference was visible at 4 μm^2 area scan (**Figure 3-3C** and **Figure 3-3D**).

The cocaine nanoMIPs were then attached onto the MUDA activated surface and blocked with ethanolamine. The sensor was then analysed using the AFM. Although the roughness of the bare working electrode, Cocaine nanoMIP were visible onto nanoMIP functionalised surface as more elevated and larger peaks were observed (**Figure 3-4B**). The roughness study was carried out onto three independent electrodes per each functionalisation step on 400 and 4 μm^2 area, and the Ra, Rq and Rmax values were recorded and these are reported in **Table 3-6**. The independent sample Kruskal-Wallis test revealed that the difference was not significant ($p>0.05$). Overall, the 3D AFM images of the sensor surface topography were the more informative than the roughness analysis.

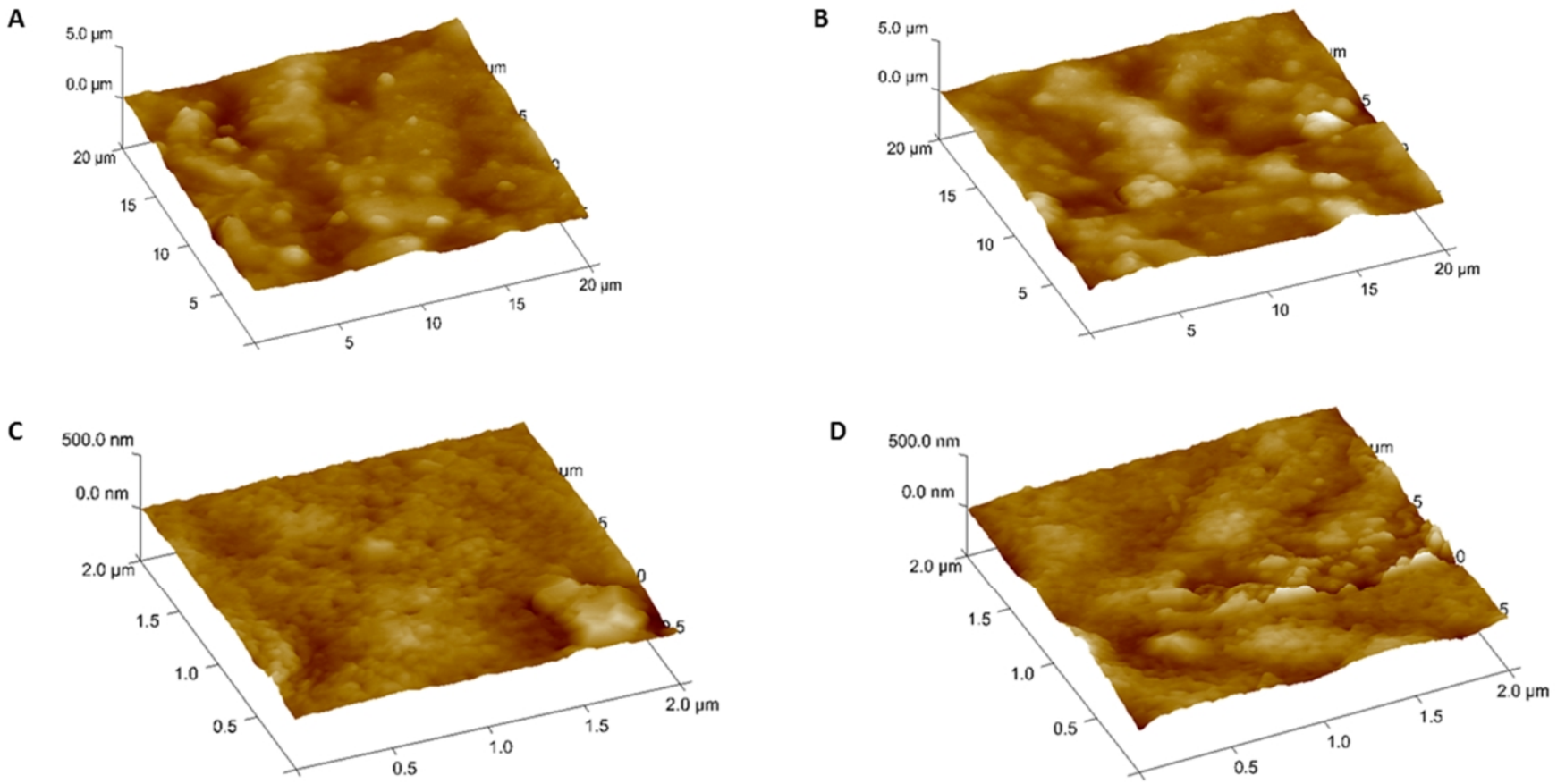

Figure 3-3: AFM 3D images of the SPE surface topography before and after MUDA deposition. 3D surface topography of the (A) bare surface (400 µm^2 area scan, height 3 µm), (B) MUDA functionalised surface (400 µm^2 area scan, height 3 µm), (C) Bare surface (4 µm^2 area scan, height 500 nm), (D) MUDA functionalised surface (4 µm^2 area scan, height 500 nm).

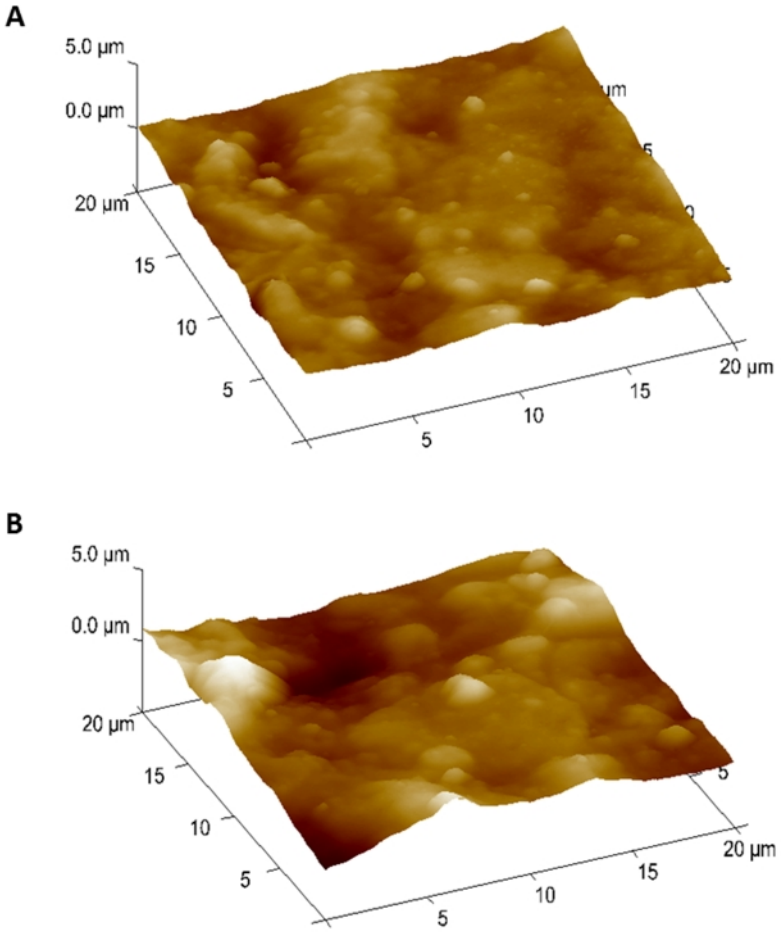

Figure 3-4: AFM study of SPE surface before and after cocaine nanoMIP deposition. 3D surface topography of the (A) bare surface (400 µm^2 area scan, height 3 µm). (B) NanoMIP functionalised surface (400 µm^2 area scan, height 5 µm).

Table 3-6: Roughness parameters obtained by AFM study performed onto the SPE surface and related to each deposition points.

Functionalisation point / scan area	Rq (nm)	SD(±)	Ra (nm)	SD(±)	Rmax (nm)	SD(±)
Bare (4 µm^2)	44	5	33	0.6	373	30
MUDA (4 µm^2)	46	16	39	13	378	106
Bare (400 µm^2)	278	32	222	25	1895	324
MUDA (400 µm^2)	315	119	254	99	2157	784
Cocaine nanoMIP (400 µm^2)	454	40	362	47	3134	220

3.3.1.3 Sensor Sensitivity in Water Samples

To assess the ability of the EIS nanoMIP sensor to detect cocaine, a cumulative assay was carried out using cocaine HCl dissolved in water and by preparing several dilutions (100 pg mL^{-1} to 50 ng mL^{-1}). Each sample was incubated for 30 minutes at room temperature. After each incubation, the surface was rinsed with water, dried under a gentle nitrogen stream and the EIS measurements were conducted using a redox solution (10 mM $[Fe(CN)_6]^{3-/4-}$) in MOPS (pH 6.0) as reported in Section 3.2.6.2. The results of the assay are shown **Figure 3-5A** and these were fitted in Randles equivalent circuit.

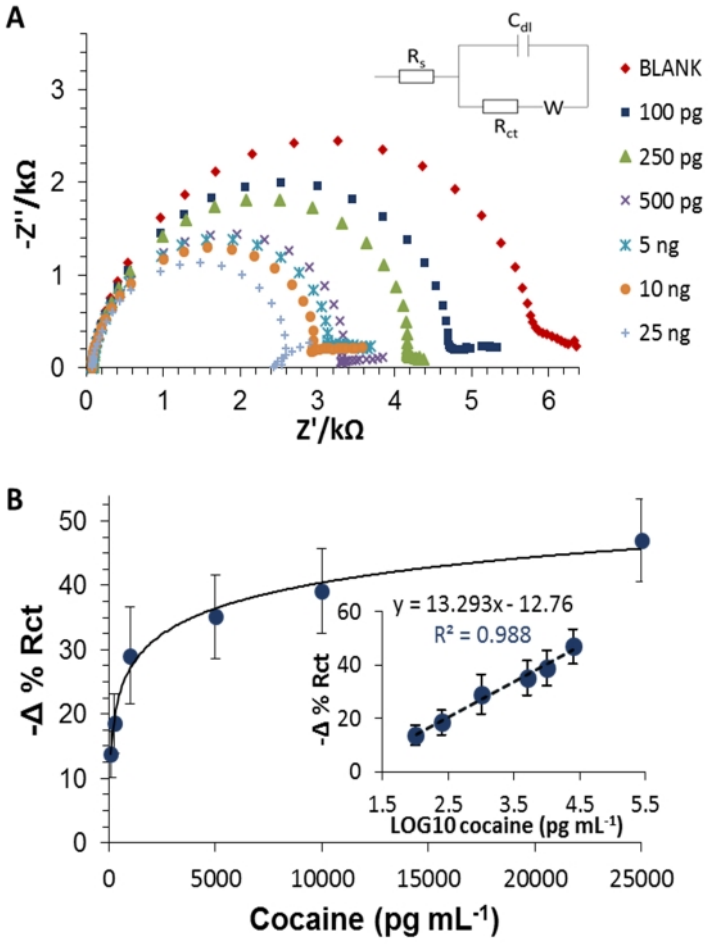

Figure 3-5: (A) EIS spectra of the blank signal and the increasing concentration of cocaine dissolved in double distilled water (18.2 MΩ cm^{-2}). Inserted picture displays the Randles equivalent circuit used to fit the data. (B) The non-linear and linear (insert graph) curves obtained by plotting the - Δ %Rct values against the cocaine concentration, expressed as concentration (pg mL^{-1}) and the LOG10 of the concentration (pg mL^{-1}), respectively. Error bars refer to the standard deviation of replicates (n=5).

The Rct values were expressed as Δ %Rct with respect to the blank signal (distilled water). **Figure 3-5B** shows that the sensor response increased as the increasing concentrations of cocaine were tested on the sensor surface. The inset graph shows the linear regression of the assay (R^2= 0.988, p-value< 0.0001). The limit of detection (LOD) was calculated as 3 times the standard deviation of the blank signal, interpolated into the linear equation and was as low as 0.52 ng mL^{-1}. To prove that the cocaine was binding to the nanoMIP, the cocaine cumulative assay was repeated onto sensors functionalised in the same way, but without the cocaine nanoMIP (control sensor). As shown in **Figure 3-6**, the increasing concentration of cocaine induced an Rct increase of only few ohms. This can be ignored as the Rct values usually decreased in the order of KΩ, when the sensor is functionalised with cocaine nanoMIP.

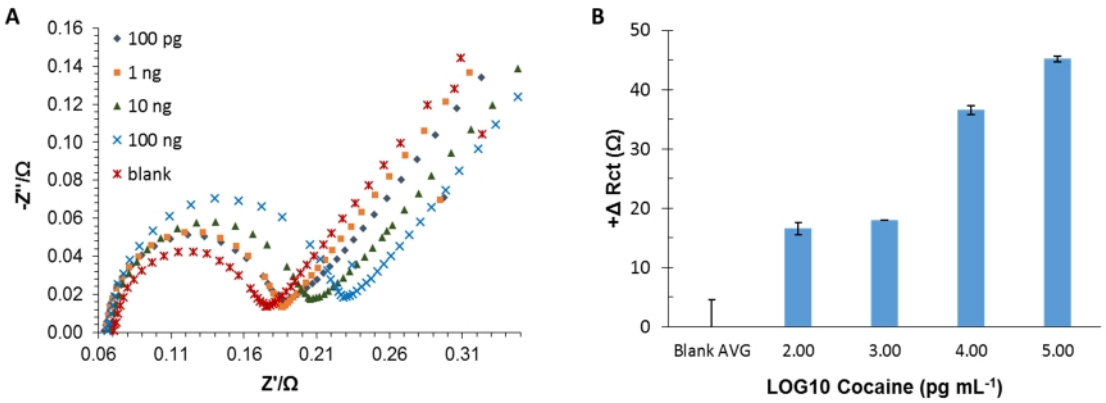

Figure 3-6: (A) Nyquist plots and (B) average (±SD) of the Rct value related to the cocaine cumulative assay performed on the control sensor (DPR 220AT without the cocaine nanoMIP). Error bars refer to the standard deviation of replicates (n=3).

However, the binding between cocaine and the nanoMIP may be due to non-specific binding occurring between the cocaine and the functional groups other than the one present at the specific nanoMIP binding site. Therefore, the cocaine cumulative assay was replicated onto the sensor functionalised with the cocaine nanoNIP (non-molecularly imprinted polymer). The nanoNIPs are synthesised in the same way, but in the absence of the template, thus resulting in a structure similar to the MIP but without the specific binding sites (Chianella *et al.*, 2002; Poma *et al.*, 2013; Canfarotta *et al.*, 2016). Results of both nanoNIP and nanoMIP cumulative assays are shown and compared in **Figure 3-7**.

As shown by the results achieved with the sensor functionalised with the nanoNIPs, a high standard deviation was observed between the three sensors tested and no correlation was detected. Overall, the nanoMIP and nanoNIP sensors response were different, thus suggesting that the cocaine is binding specifically to the nanoMIP binding site created during the solid phase synthesis. This has proven the specificity of the cocaine nanoMIP sensor towards its analyte.

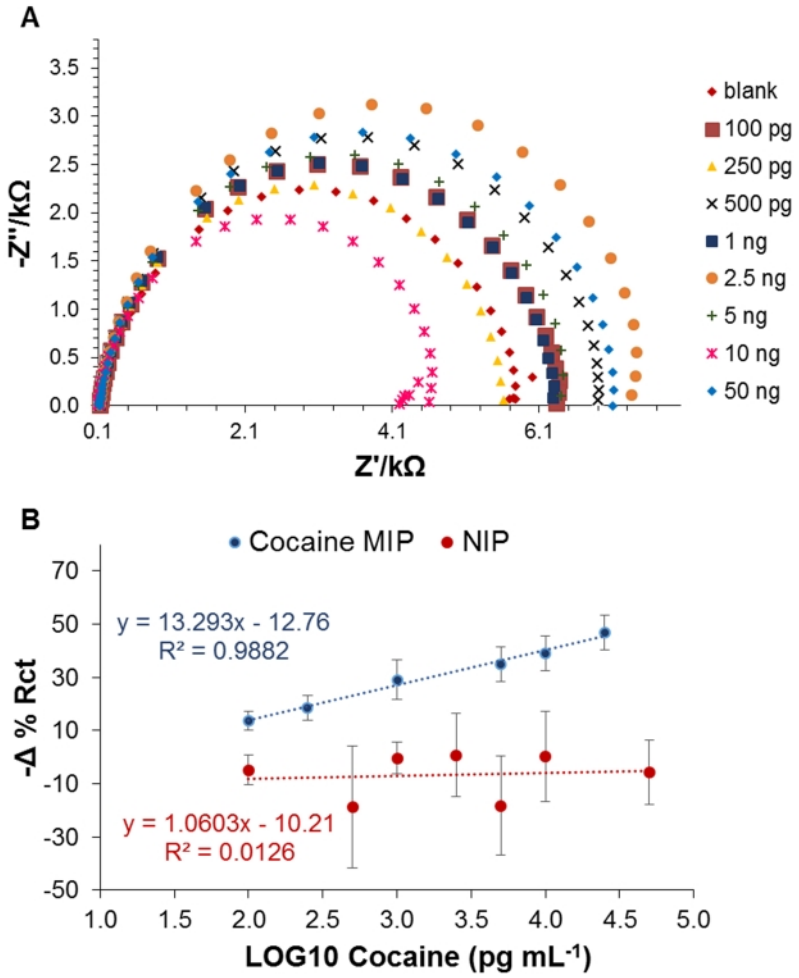

Figure 3-7: (A) Nyquist plots obtained during the cocaine cumulative assay functionalised with cocaine nanoNIP. (B) Comparison between the cocaine linear calibration curves performed onto cocaine nanoMIP (blue) and onto nanoNIP (red) EIS sensors. The linear calibration curves were obtained by plotting the respective - Δ %Rct values against the cocaine concentration, expressed as LOG10 of the concentration (pg mL^{-1}). Error bars refer to the standard deviation of replicates (n=3).

3.3.1.4 Sensor Specificity in water samples

Other than detecting cocaine-HCl, the EIS nanoMIP sensor is required to be able to discriminate the cocaine from its major cutting agents, such as caffeine, levamisole and mannitol. According to the European Monitoring Centre for Drugs and Drug Addiction (EMCDDA) statistics, the average of the purity of cocaine seized in Europe has been estimated to be 45% (±13.23%) in 2015 (EMCDDA, 2012). As reported in the majority of the recent literature, levamisole and caffeine are among the most abundant cocaine cutting agents, while mannitol is mostly used as a diluent (Botelho *et al.*, 2014; Broséus *et al.*, 2015; Lapachinske *et al.*, 2015). Therefore, the nanoMIP specific binding sites should specifically allow the binding towards cocaine, thus avoiding cross-reactivity events against other drugs and cutting agents. In addition, it should avoid the non-specific binding between these substances and the reactive groups present on the sensor surface (non-specific binding events). The results of this work showed that the sensor responded linearly towards the increasing concentration of caffeine and mannitol diluted in water (**Figure 3-8**). These indicate that in its present format the sensor is prone to false positive results as caffeine and mannitol showed linear responses similar to cocaine. Therefore further optimisation studies are required to eliminate the cross-reactivity/non-specific binding of caffeine and mannitol.

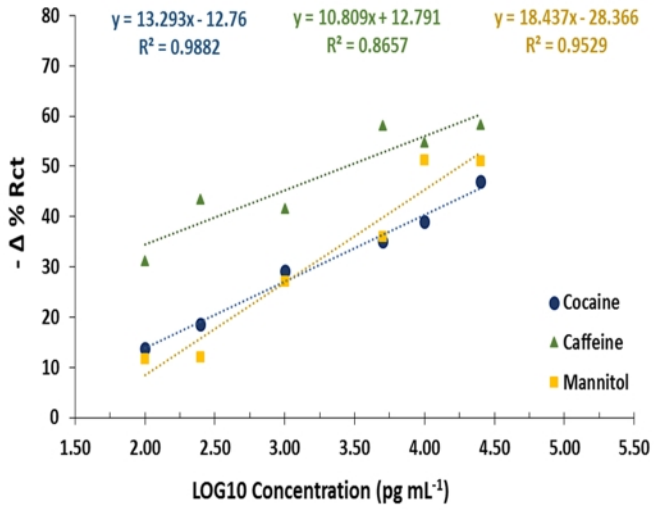

Figure 3-8: Comparison between the cocaine linear calibration curve (blue) and caffeine (green) and mannitol (yellow) calibration curves. Cocaine, caffeine and mannitol were diluted in double distilled water in a concentration range from 100 pg mL^{-1} to 50 ng mL^{-1}.

3.3.1.5 Surface blocking optimisation study

Since the sensor showed non-specific response towards some of the chemicals, surface blocking optimisation study was required to minimise any possible non-specific binding or cross-reactivity events. Although the sensor responded linearly towards the increasing concentration of caffeine and mannitol diluted in water**,** only caffeine was used as a model analyte to carry out the blocking optimisation studies. Firstly, the control sensor surface was fabricated without attaching the cocaine nanoMIP or the nanoNIP using the method described in Section 3.2.4. This was then followed by a caffeine cumulative assay (100 pg mL^{-1} - 100 ng mL^{-1}), to assess whether caffeine was binding to the nanoMIP or to the control sensor surface. The results showed that the response of the control sensor was negligible to increasing caffeine concentrations (**Figure 3-9**).

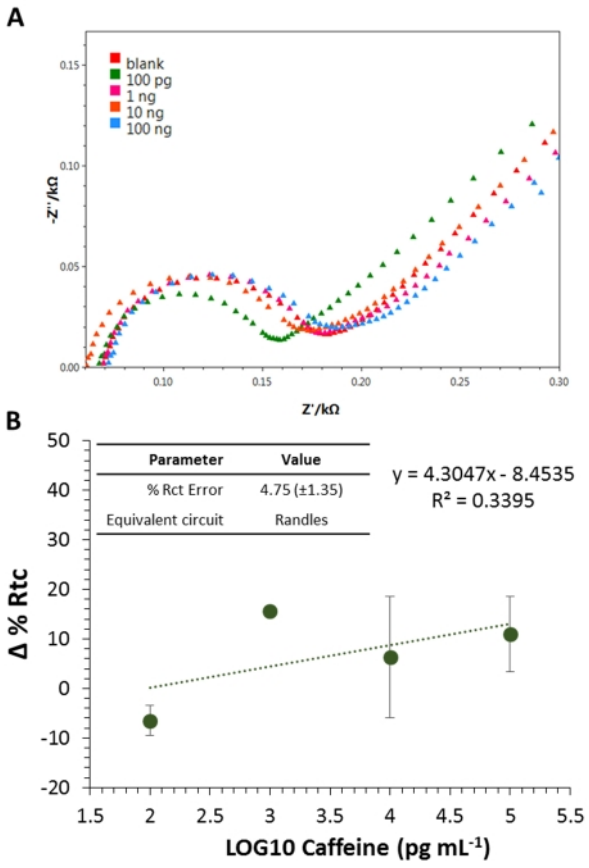

Figure 3-9: (A) Nyquist plot of the caffeine cumulative assay performed on assay on the sensor surface functionalised without the nanoMIP. (B) Caffeine non-specific binding assay on the sensor surface functionalised without the nanoMIP. Sensor surface was blocked with ethanolamine 1 M pH 8.5. Error bars refer to the standard deviation of replicates (n=3).

Overall, the sensor response was around 10 Δ %Rct as the caffeine concentration (LOG10) increased. Hence, it was concluded that the caffeine was mainly cross-reacting with the MIP surface, which may lead to sensor false positive results thus affecting the overall sensor performance.

Changing the working pH as well as optimising the blocking agents are usually effective strategies in encompassing these cross-reactivity/non-specific binding events (Parker and Tothill, 2009; Atta, Hassan and Galal, 2014; Riquelme *et al.*, 2016). Thus, the assay condition was adjusted to pH 6.0 and two different blocking agents were explored. Specifically, the caffeine dilutions were prepared using 10 mM MOPS adjusted at pH 6.0. The redox couple solution (10 mM $[Fe(CN)_6]^{3-/4-}$) in MOPS (pH 6.0) was used to perform the EIS measurement. The two types of blocking agents were milk proteins based blocking agents (BSA and milk protein mixtures) as reported in Section 3.2.6.2, as they are commonly used in bioassay development. The MOPS buffer solution (50 µL, 10 mM, pH 6.0) containing BSA (0.1%, w/v) and Tween 20 (1%, v/v) was also used, as this mixture introduces more hydrophilic groups onto the surface (Riquelme *et al.*, 2016) and has been reported to be a successful blocker in previous nanoMIPs based assay development (Chianella *et al.*, 2013). When used as a blocking agent, Tween 20 was also added to the washing solution. Therefore, the specificity assay was also investigated by spiking the washing solution (10 mM MOPS pH 6.0) with 1% (v/v) Tween 20. The – Δ %Rct values obtained during the cumulative assays were grouped in a box plot, thus highlighting the – Δ %Rct mean value and the range of – Δ %Rct values variation within each performed assay.

As shown in **Figure 3-10**, when caffeine was dissolved in and washed by MOPS pH 6.0 and the sensor surface was blocked with BSA and Tween 20, the achieved – Δ %Rct values were closer to 0 (which is set as the blank value). Therefore, this condition successfully removed the cross-reactivity between cocaine nanoMIP and the caffeine. On the other hand, when the washing buffer was spiked with Tween 20, the – Δ %Rct were higher probably due to the background signal introduced by this washing buffer. When the sensor was blocked with the milk proteins, the - Δ %Rct varied not linearly with the increasing concentration of caffeine. This was probably due to the mixed composition of the milk proteins blocking agent, which makes the sensors surface less consistently

blocked. Therefore, using MOPS pH 6.0 and blocking the sensor surface with ethanolamine (1M, pH 8.5), followed by MOPS buffer solution (50 µL, 10 mM, pH 6.0) containing BSA (0.1%, w/v) and Tween 20 (1%, v/v), were the best assay conditions for the development of the cocaine nanoMIP EIS sensor.

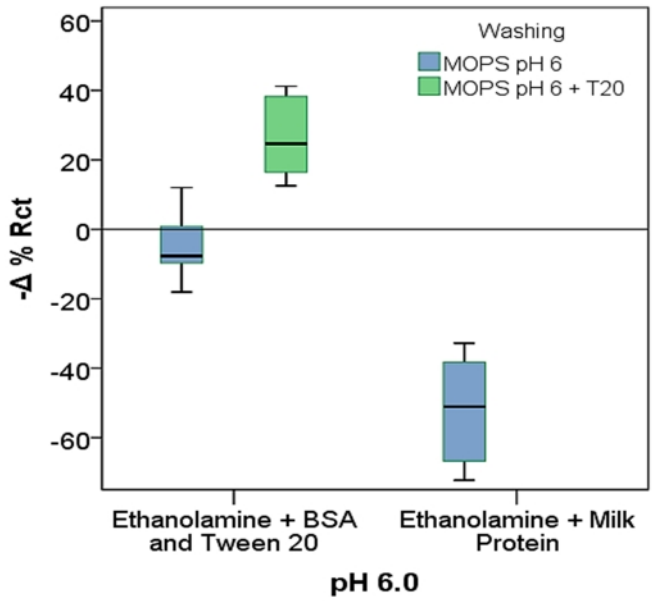

Figure 3-10: Box plot of caffeine cumulative assay performed at pH 6 and having different blocking agents and washing buffer combinations.

To verify that the optimised sensor condition allowed the cocaine detection, the cocaine cumulative assay was repeated using the new blocking and pH condition. Cocaine was diluted in 10 mM MOPS (pH 6.0) and the sensor surface was blocked with 1 M ethanolamine (50 µL, 1 M, pH 8.5), followed by MOPS buffer solution (50 µL, 10 mM, pH 6.0) containing BSA (0.1%, w/v) and Tween 20 (1%, v/v). MOPS (1.2 mL, 10 mM, pH 6.0) was used as the washing buffer and the redox couple solution (10 mM $[Fe(CN)_6]^{3-/4-}$) in MOPS (pH 6.0) was used to perform the EIS measurement.

Using the above condition, the results (**Figure 3-11A**) showed that the cocaine binding did occur and gave a significant calibration curve (R^2=0.978, p-value = 0.001). Although, the -% Δ Rct values were fluctuating between a positive and a negative signal (**Figure 3-11B**). The use of this pH seems to have an effect on the overall charge occurring at the sensor surface, thus affecting the EIS read out signal through the assay.

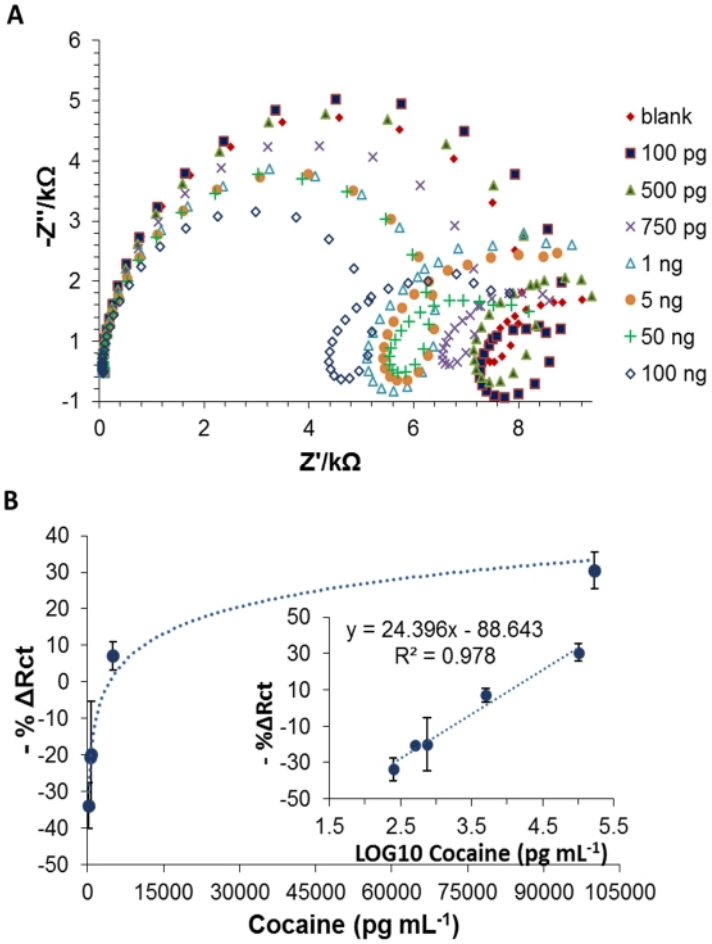

Figure 3-11: Non-linear (A) and linear (B) calibration curve of cocaine cumulative assay (100 pg mL^{-1}- 50 ng mL^{-1}) performed onto Cocaine nanoMIP EIS sensor (DPR C220AT), using MOPS (10mM) at pH 6.0. Error bars refer to the standard deviation of replicates (n=3).

Furthermore, the cocaine hydrochloride is a strong base (pKa = 8.85), therefore at pH 6.0 it is highly ionised and positively charged. However, at pH 6.0, the lowest concentration of cocaine induced an increase of the resistance (+Δ %Rct), which then decreased as the cocaine concentration increased. Also, the blank signal was not stable at pH 6.0 and the SD value of the blank signals was as high as 9%, which indicated that the background noise affected the sensor response. Overall, these observations indicated that the sensor is not able to differentiate the cocaine from the blank signal (set as 0%) with this assay condition. Therefore, the pH of the redox couple and of the cocaine diluent was adjusted to pH 7.4 value. A polymeric blocking agent was also tested at this pH condition. Specifically, new caffeine cumulative assays were performed on two group of cocaine

nanoMIP EIS sensors. One group of sensor was fabricated as detailed in Section 3.2.4 and the sensor surface was blocked with ethanolamine (1 M, pH 8.5), followed by PVA (1%) as detailed in Section 3.2.6.3. Another group of sensor was fabricated as detailed in Section 3.2.4 and the sensor surface was blocked with ethanolamine (1 M, pH 8.5), followed by BSA (0.1%, w/v) and Tween 20 (1%, v/v). The redox couple solution was prepared in 10 mM MOPS (pH 7.4). The caffeine cumulative assay (prepared in 10 mM MOPS, pH 7.4) was then performed on the different group of sensors fabricated with the cocaine nanoMIPs and blocked using different blocking strategies and according to the procedure described in Section 3.2.6.1. The – Δ %Rct values obtained during the cumulative assays were grouped in a box plot, thus highlighting the – Δ %Rct mean value and the range of – Δ %Rct values variation of each performed assay. Comparing the results achieved from the caffeine cumulative assay performed on the two group of cocaine nanoMIP sensors (**Figure 3-12**), the ethanolamine (1 M, pH 8.5) combined with the BSA (0.1%, w/v) and Tween 20 (1%, v/v) MOPS (10 mM, pH 7.4) buffer solution gave the optimal blocking condition and therefore, was chosen as the best strategy to minimise non-specific binding.

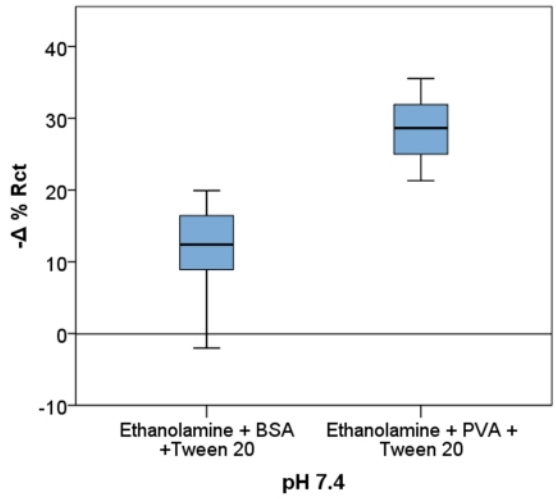

Figure 3-12: Box-plot obtained by plotting the average – Δ %Rct values, obtained by sensors blocked with Ethanolamine, BSA and Tween 20, sensors blocked with ethanolamine and milk proteins, sensors blocked with Ethanolamine, PVA and Tween 20. All assay were conducted at pH 7.4.

To verify that this conditions are also suitable for the cocaine detection, the cocaine cumulative assay was repeated under this new optimised assay condition. Therefore, a

new group of cocaine nanoMIP EIS sensors were prepared as described in Section 3.2.4 and were blocked with ethanolamine (50 µL, 1 M, pH 8.5), followed by MOPS buffer solution (50 µL, 10 mM, pH 7.4) containing BSA (0.1%, w/v) and Tween 20 (1%, v/v). Cocaine hydrocloride was dissolved in 10 mM MOPS (pH 7.4) and increasing concentrations were prepared (100 pg mL^{-1} - 100 ng mL^{-1}). MOPS (1.2 mL, 10 mM, pH 7.4) was used as the washing buffer and the redox couple solution (10 mM $[Fe(CN)_6]^{3-/4-}$) in MOPS (pH 7.4) was used to perform the EIS measurement. The assay was performed as described in Section 3.2.6.1. The Nyquist plots (**Figure 3-13**) obtained during the cocaine cumulative assay showed a decrease in the Rct (Ω) values as the cocaine concentrations increased.

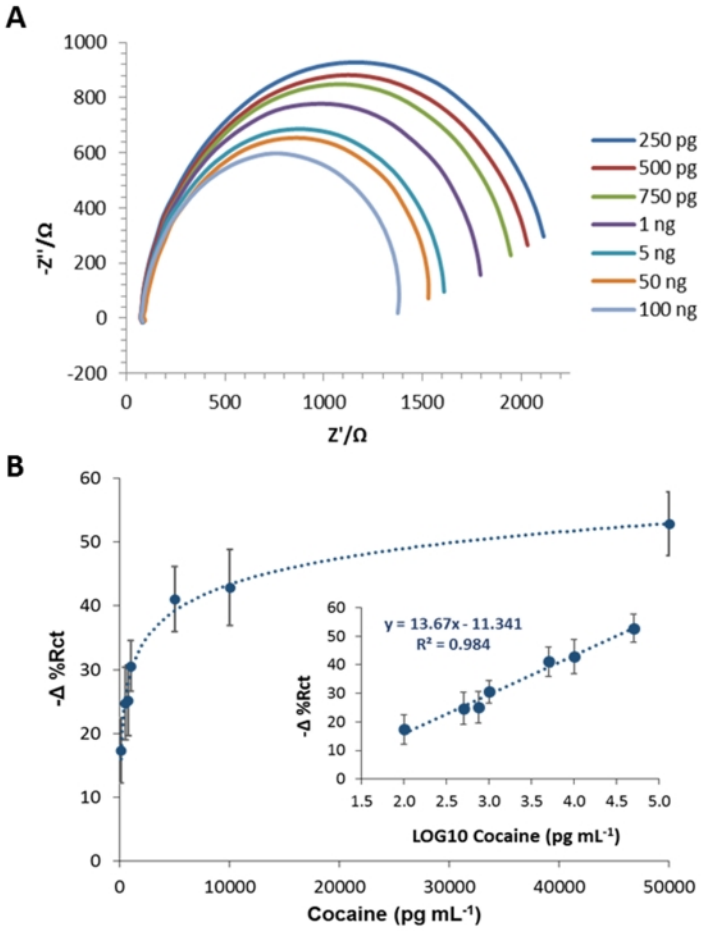

Figure 3-13: (A) Nyquist plot of the data obtained during the cocaine cumulative assay (100 pg mL^{-1}- 100 ng mL^{-1}) using the optimised assay condition and fitted by using the simplified Randles equivalent circuit. (B) Non-linear and linear (insert graph) calibration curve of the cocaine cumulative assay performed using the optimised cocaine nanoMIP EIS sensor (DPR C220AT). Error bars refer to the standard deviation of replicates (n=5). All assays were conducted at pH 7.4.

The results of the assay were fitted into simplified Randle equivalent circuit and the Rct values were extrapolated with an average value (±SD) of the % Error of Rct fitting equal to 2.44% (± 1.55%). The Rct values were then expressed as a –Δ %Rct as described in Section 3.2.6.5 and these values were used to plot the calibration curve. As shown in **Figure 3-13**, the cocaine nanoMIP EIS sensor was able to detect cocaine using these optimised assay conditions, without a signal fluctuation between the positive and negative Δ %Rct value. The linear calibration curve (**Figure 3-13B**) showed that the sensor response (–Δ %Rct) increased as cocaine concentration, expressed as LOG10, increased. The R^2 of the linear calibration curve was equal to 0.984 (*p*-value< 0.0001). The limit of detection (LOD) was calculated as 3 times the standard deviation of the blank signal, interpolated into the linear equation and was as low as 0.24 ng mL^{-1} (0.70 pM), which was lower than the LOD achieved using the un-optimised nanoMIP EIS sensor (LOD= 0.52 ng mL^{-1}). Therefore, the cocaine nanoMIP EIS sensor, which showed optimal performance, was tested in further assays.

3.3.1.6 Specificity of the Optimised Sensor

The new optimised cocaine EIS nanoMIP was tested for specificity towards three major cutting agents (levamisole, caffeine, and mannitol) and towards one drug of abuse (morphine). A new group of cocaine nanoMIP EIS sensors were prepared as described in Section 3.2.4 and were blocked with 1 M ethanolamine (50 µL, 1 M, pH 8.5), followed by MOPS buffer solution (50 µL, 10 mM, pH 7.4) containing BSA (0.1%, w/v) and Tween 20 (1%, v/v). Each analyte was dissolved in 10 mM MOPS (pH 7.4) and increasing concentration were prepared (100 pg mL^{-1} - 100 ng mL^{-1}). MOPS (1.2 mL, 10 mM, pH 7.4) was used as the washing buffer and the redox couple solution (10 mM $[Fe(CN)_6]^{3-/4-}$) in MOPS (pH 7.4) was used to perform the EIS measurement. The blank solution and the increasing concentrations of each analyte (100 pg mL^{-1} to 50 ng mL^{-1}) were incubated onto the sensor surface and the EIS spectra were recorded as described in Section 3.2.6.. The data were processed as described in Section 3.2.6.5 and the plots of each analyte concentrations (expressed as LOG10) versus Δ %Rct were thus achieved. The results are shown in **Figure 3-14 - 3-17**. The average (±SD) % error of Rct values and other statistics of each specificity assay are reported in **Table 3-7**. The results showed that the sensor

was not responding towards increasing concentration of caffeine, levamisole and, morphine. The sensor was still showing a response towards mannitol, although the signal achieved for cocaine was overall higher (**Figure 3-17**).

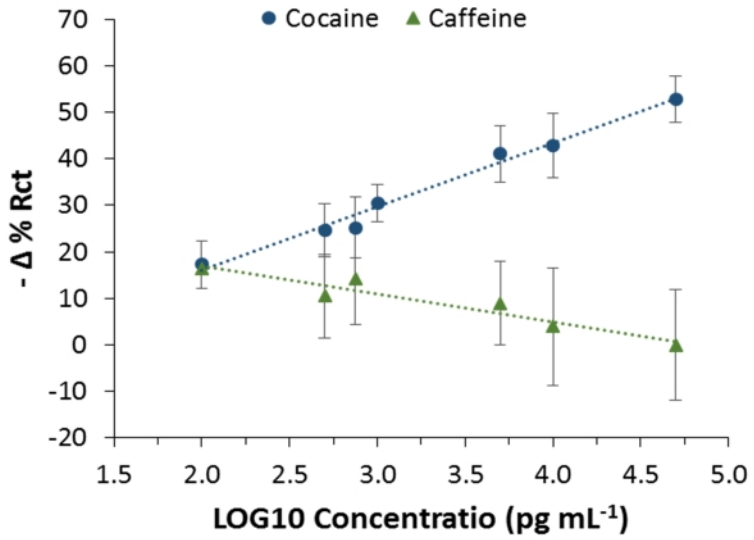

Figure 3-14: Comparison between the cocaine and caffeine linear calibration curves obtained using the optimised cocaine nanoMIP sensors.

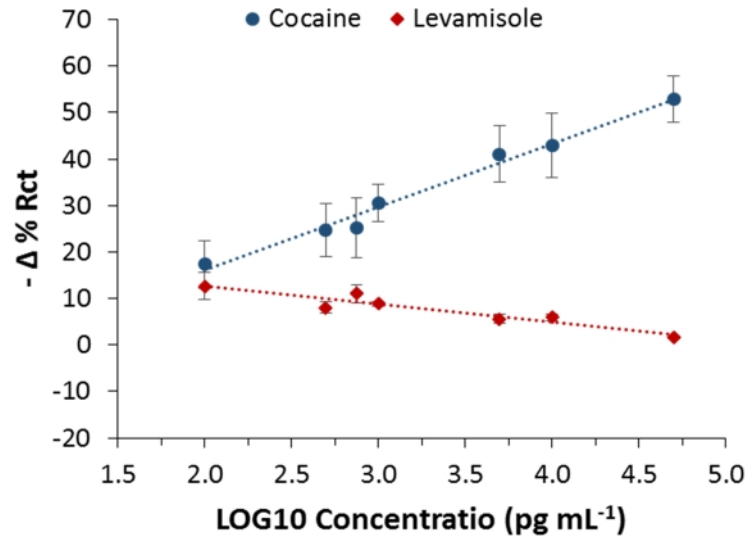

Figure 3-15: Comparison between the cocaine and levamisole linear calibration curves obtained using the optimised cocaine nanoMIP sensors.

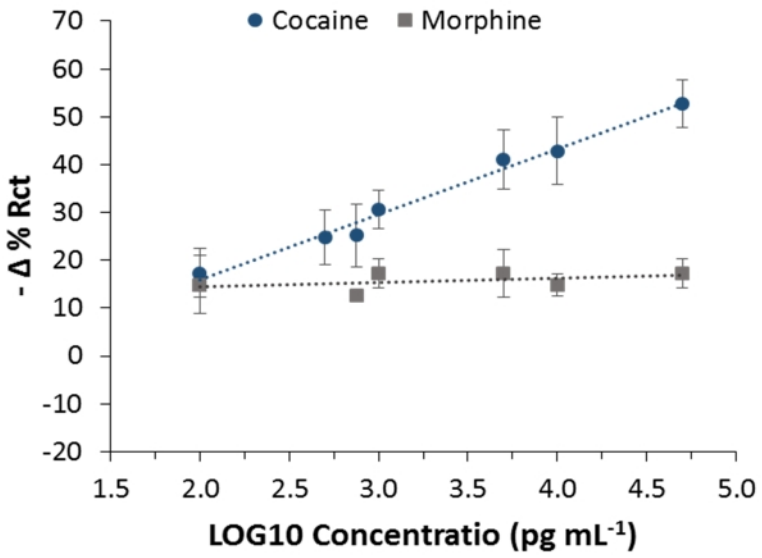

Figure 3-16: Comparison between the cocaine and morphine linear calibration curves obtained using the optimised cocaine nanoMIP sensors.

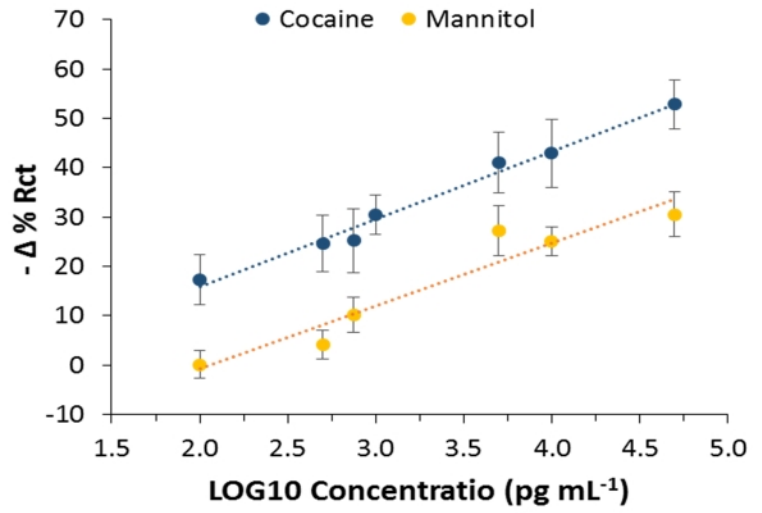

Figure 3-17: Comparison between the cocaine and mannitol linear calibration curves obtained using the optimised cocaine nanoMIP sensors.

Table 3-7: Statistics and the linear calibration curve related to the listed cumulative assay.

Analyte	NanoMIP (Yes/No)	Error %Rct (±SD[1])	Linear equation	R^2	*p*-value
Cocaine	Yes	2.44 (± 1.55)	$y = 13.67x - 11.341$	0.984	0.00001
Caffeine	Yes	3.52 (± 1.60)	$y = -6.0073x + 28.998$	0.906	0.003
Morphine	Yes	3.31 (± 1.76)	$y = 0.8783x + 12.742$	0.193	0.353
Levamisole	Yes	1.47 (± 1.33)	$y = -3.8668x + 20.375$	0.879	0.001
Mannitol	Yes	2.00 (± 1.74)	$y = 12.691x - 26.019$	0.921	0.002
Mannitol	No	2.55 (± 0.91)	$y = 4.5503x + 2.776$	0.87	0.002

[1] SD = Standard Deviation; Diluent = MOPS pH 7.4

Therefore, mannitol cross-reactivity towards the sensor surface was futher investigated. The control sensor was once again fabricated without attaching the cocaine nanoMIP to the surface and blocking the surface with the optimised blocking agents, i.e. ethanolamine (50 µL, 1 M, pH 8.5), followed by MOPS buffer solution (50 µL, 10 mM, pH 7.4) containing BSA (0.1%, w/v) and Tween 20 (1%, v/v). The mannitol cumulative assay was replicated and, as shown in **Figure 3-18**, a similar calibration curve was achieved (R^2=0.872, p-value=0.002) (**Table 3-7**).

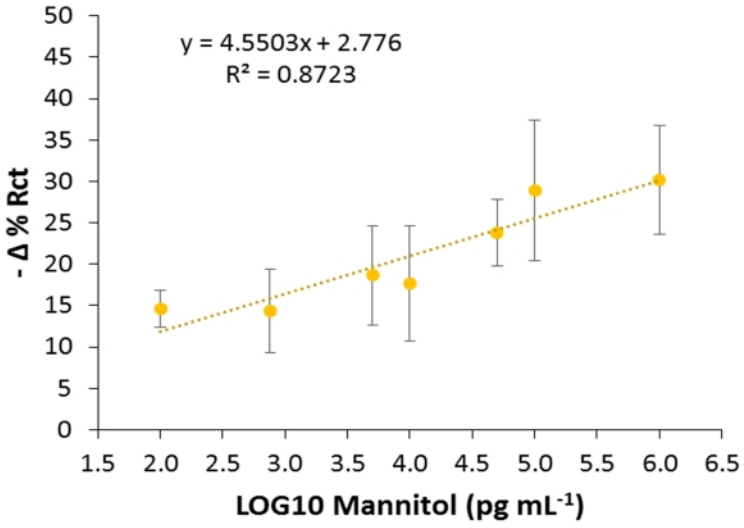

Figure 3-18: Mannitol cumulative assay performed on the optimised cocaine nanoMIP EIS sensor fabricated without the cocaine nanoMIP.

Results showed that the response (–Δ %Rct) of the sensor functionalised without the nanoMIP was higher compared to the response of the sensor fabricated with the nanoMIP, thus suggesting that the mannitol was more likely non-specifically binding to the sensor surface. The results indicated that the mannitol signal was due to the small sugar molecule non-specific adsorption onto the sensor surface alone, but not toward the cocaine nanoMIPs. Further, optimisation will be required to minimise the mannitol adsorption effect by exploring other blocking strategies or, if this proofed to be a challenge, by introducing a selective absorbent as a sample preparation step to remove the mannitol from the sample. Therefore, the cocaine nanoMIP EIS sensor and the assay condition were considered optimised and will be used in further investigations.

3.3.1.7 Thermal Regeneration Explorative Test

The regeneration of the sensor surface is a technique that allows to remove the bound analyte, while preserving the sensor surface performances. The regeneration of the sensor surface is highly desirable as it allows reusing the same sensor to carry out multiple assays, thus lowering the overall cost of the assays. Several sensor regeneration methods are reported in the literature (Goode, Rushworth and Millner, 2015), among which the chemical and thermal regenerations. Both of them can be used to overcome the non-covalent binding occurring between the nanoMIP and its selected analyte. While the chemical regeneration protocol were previously optimised in nanoMIP based sensor (Abdin, Altintas and Tothill, 2015), the thermal regeneration was less explored in previous studies. A thermal regeneration assay was attempted on the cocaine nanoMIP sensor (DPR – C220AT), after the cumulative assay was conducted. The nanoMIP sensor (DPR – C220AT) was heated at 60 °C for 20 minutes as described in Section 0, thus reproducing the same principle used to elute the high-affinity cocaine nanoMIP during their synthesis. The EIS measuraments was recorded after the sensor cooled down. The Nyquist plots of the blank sample and of the last cocaine concentration tested (100 ng mL^{-1}) were compared with the Nyquist plot obtain after the thermal regeneration.

The results (**Figure 3-19**) showed that the Nyquist plot achieved after the thermal treatment were almost overlapping the Nyquist plot of the blank signal, thus indicating

the success of the thermal reeneration. This result, although preliminary, suggests that it is possible to regenerate the nanoMIP sensor surface by means of thermal treatment.

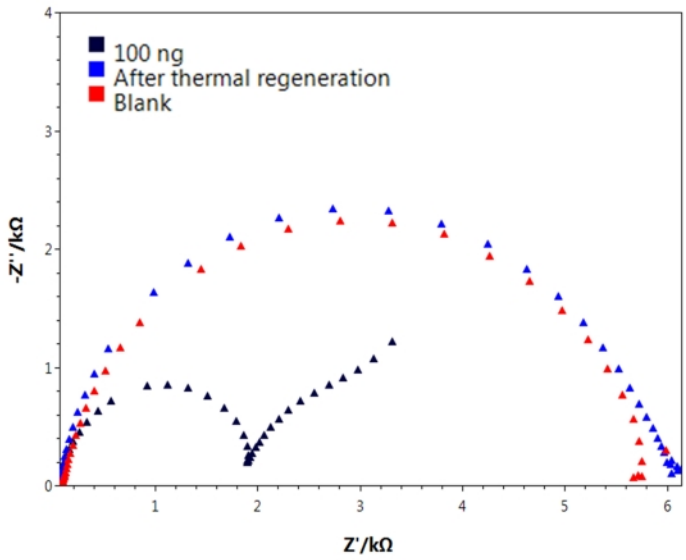

Figure 3-19: Nyquist plots related to the regeneration assay on NanoMIP sensor (DPR C220AT).The spectra in red (▲) is blank signal and was recorded before performing the cumulative assay. The spectra in black (▲) was recorded after 100 ng of cocaine was incubated on the cocaine nanoMIP EIS sensor surface. The spectra in blue (▲) was recorded after thermal regeneration and overlapped the spectra of the blank signal.

3.3.2 Evaluation Studies of the Cocaine NanoMIP EIS Sensor onto IDEs

The cocaine nanoMIP sensor, fabricated using two type of IDEs, were investigated in this work. The IDE were investigated because was required by the NOSy project and because IDEs are regarded to be more sensitive although less investigated than the conventional screen-printed electrodes (such as DPR 220AT electrode) (Arya *et al.*, 2010). The major advantages of the IDEs are: 1) the increased sensitivity due to the favourable electrodes geometry and larger electrode surface area; 2) the enhanced speed of the oxidation and reduction cycle due to the proximity of the anodic and cathodic electrodes, which is equal to 5 µm for the IDEs investigated within this work; 3) the faster attainment of the steady state with improved signal-to-noise ratio; 4) no need for a reference electrode when faradic EIS mode is applied (Ohno *et al.*, 2013; Arya *et al.*, 2018).

The IDEs investigated in this work are the DropSens DPR IDEAu5 electrodes and the Micrux ED-IDE3-Au. Both IDEs were produced onto a glass substrate with 5 μm width gold interdigitated electrodes separated by 5 μm inter-digits gap. However, the electrode surface area of the DropSens IDE (16.9 mm^2) was larger than in the Micrux IDE (2.40 mm^2). During the evaluation study of the DropSens IDE and Micrux IDE, a large number of IDEs were found to be faulty. An average of one out of two IDE electrodes (50%) were not giving any change in %Rct value during the fabrication process, although the AFM revealed that the functionalisation of the sensor surface occurred. For the DropSens IDE, this issue was probably due to the loose connection between the IDE and the CACIDE connector, thus revealing issues with the IDE and IDE connector manufacturing. At this stage the connection was stabilised by placing plastic support underneath the CACIDE connector, while a three finger clamp was used to avoid the cable twisting. For the Micrux IDE, the issue was probably due to the small dimensions of the electrodes which hinder the handling of the electrodes and makes them prone to scratches.

3.3.2.1 Characterisation Study

3.3.2.1.1 DropSens IDE (DPR IDEAu5)

Although the total IDEs surface area is slightly bigger than SPE working electrode (16.9 mm^2 versus 12.56 mm^2), the cocaine nanoMIP IES sensor was reproduced onto DropSens IDE and all the reagents were kept at the same concentration. The fabrication was reproduced onto 10 independent IDEs. The EIS technique was performed according to the procedure described in Section 3.2.2 and 3.2.3 and was applied to characterise the sensor surface modification at each step of the fabrication process as described in Section 3.2.5. The resulting Nyquist plots, presented in **Figure 3-20A,** showed that the changes of the Rct values were consistent to the changes of the Rct values previously observed on the SPE and discussed in section 3.3.1.1.

The experimental data were fitted in the simplified Randles equivalent. The goodness of the fit assessment revealed that the average % Error of the Rct values was as low as 3.21 % (±2.77). The Rct values were expressed as % of the MUDA Rct value, which was set at 100%. The results were plotted in a bar chart as shown in **Figure 3-20B**. Although the

cocaine nanoMIP adsorption onto the surface events cannot be completely excluded, the nanoMIP covalent attachment was found to be reproducible.

The AFM (applied in tapping mode) and SEM analysis were carried out on the IDE sensor after the surface was cleaned according to the optimised procedure (as described in Section 2.4.3.2, Chapter 2), after the surface was functionalised with the MUDA layer and after the surface was fuctionalised with the cocaine nanoMIPs (as described in Section 3.2.4). The results of the AFM 3D image performed on 400 nm^2 scan area are presented in **Figure 3-21**.

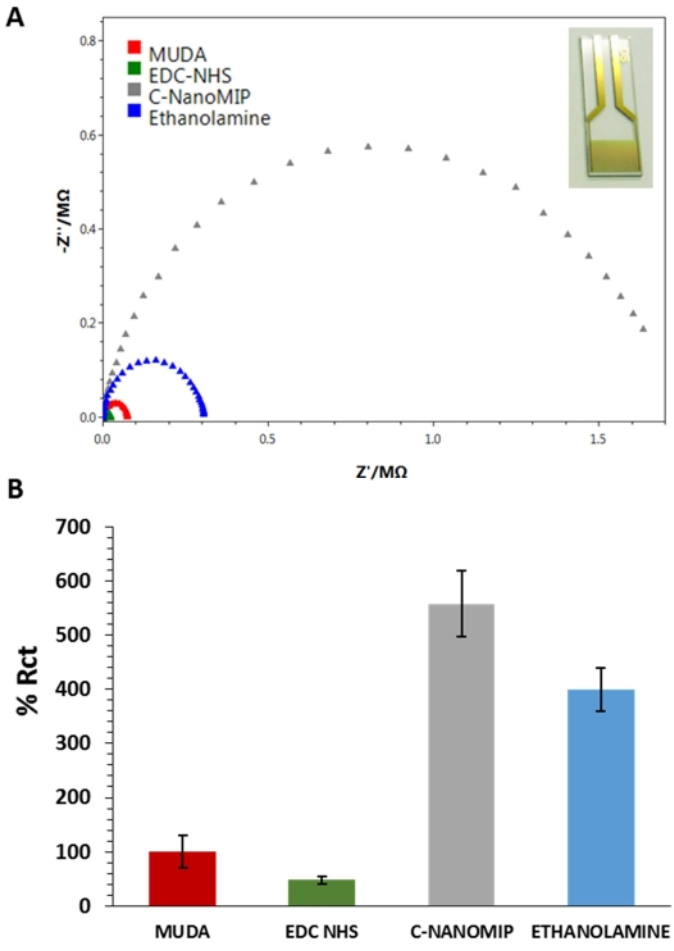

Figure 3-20: (A) Nyquist plots obtained during cocaine nanoMIP EIS sensor fabrication using DropSens IDE (inset image): the electrode coated with MUDA (red), EDC/ENS activation (green), nano-MIP attachment (grey), ethanolamine blocking (blue). (B) Average of %Rct values (±SD) at each fabrication points obtained by EIS. Error bars refer to the standard deviation of the replicates (n=6).

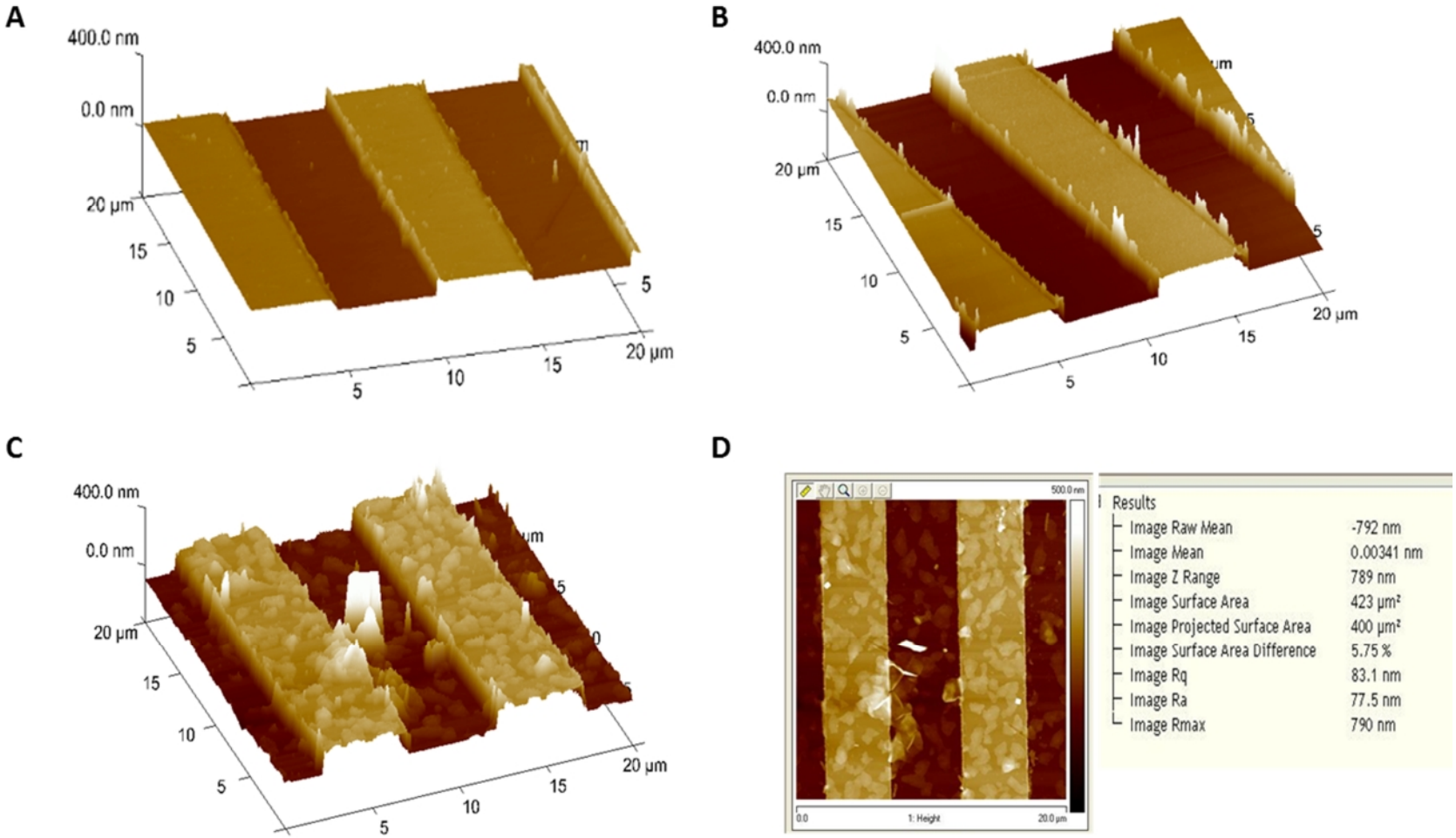

Figure 3-21: AFM 3D images of the (A) bare, (B) MUDA and (C) nanoMIP functionalised electrodes surfaces (400 µm^2 scan area, height 400 nm). (D) 2D image and roughness study of the nanoMIP functionalised electrode.

The AFM 3D topography images showed a clear difference between the MUDA (**Figure 3-21**A) and the cocaine nanoMIP functionalised electrodes surfaces (**Figure 3-21**C), as the nanoMIP were deposited on both the gold IDEs and at the inter digits gap of the investigated 400 nm^2 scan area. The AFM analysis also included the analysis of the roughness of the surface and the results are displayed in **Figure 3-22**. The electrodes surface is made of interdigitated electrodes, which have an estimated height of 10/15 nm. Therefore, the interdigitated electrodes counted as valleys and peaks of the sensor surface, thus affecting the Ra, Rq and Rmax values. Moreover, the AFM study is affected by the annotation discussed at point 3 in Section 3.3.1.1.

The Kruskal Wallis test was used to assess the statistical differences of the Ra, Rq and Rmax values among the bare, MUDA coated and nanoMIP functionalised sensor surfaces. Overall, the differences between the Ra and Rq values of the bare and MUDA coated sensor surface were not significant (*p*-values equal to 1.50 and 0.78, respectively). On the other hand, a significant difference (*p*-values= 0.32) was found between Rmax values of the MUDA coated and Rmax the nanoMIP functionalised sensor surface, as shown in **Figure 3-22B**. Furthermore, the electrode surface was investigated by SEM, which confirmed the success in the cocaine nanoMIP EIS fabrication. In details, the SEM provided evidence of a homogeneous MUDA coating onto the sensor surface as shown in **Figure 3-23B**.

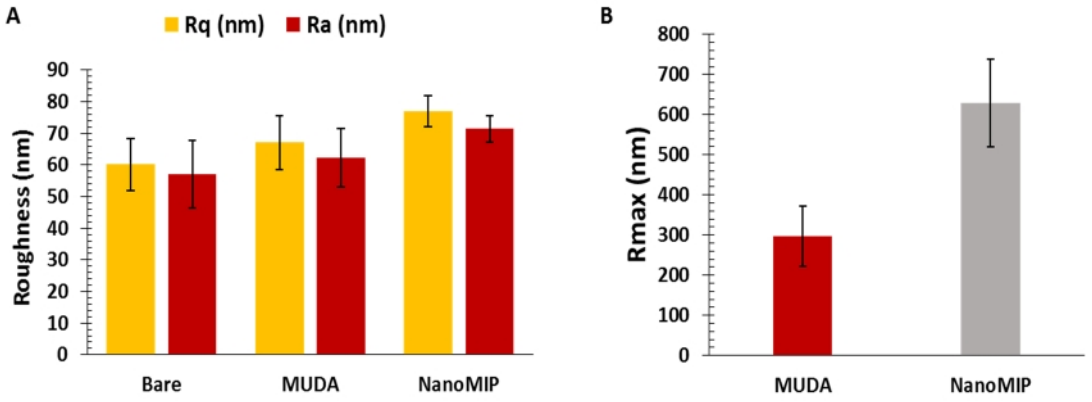

Figure 3-22: (A) Rq and Ra average values (nm) obtained by AFM roughness analysis on bare, MUDA and nanoMIP functionalised DropSens IDE. (B) Average highest peak values (Rmax, nm) recorded onto MUDA and nanoMIP functionalised electrode. Error bars refer to the SD (±nm) of replicates (n=4).

The deposition of the nanoMIP occurred both onto the gold IDE and at the interdigitated gap space which is made by a glass surface. The latter can be attributed to a cocaine nanoMIPs adsorption onto the glass substrate (**Figure 3-23**C and **Figure 3-23**D). This did not affect the sensor response and performances, although the deposition might be optimised in a future study by treating the glass surface (i.e., silanisation) to minimise the nanoMIP adsorption.

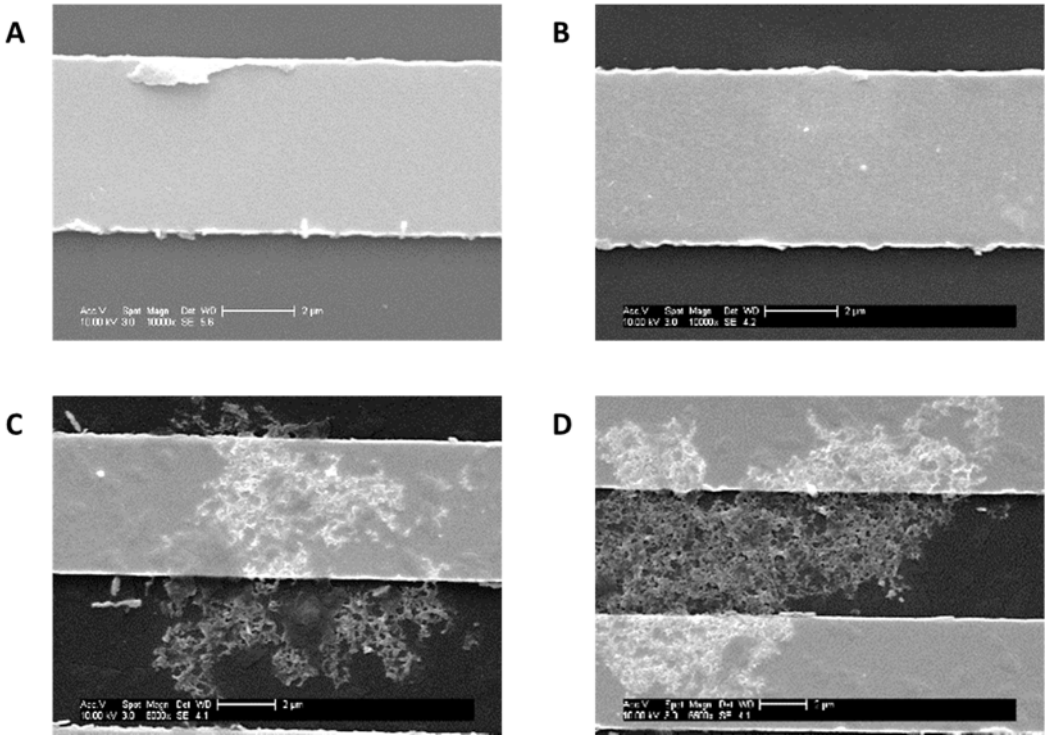

Figure 3-23: SEM image related to the (A) bare (10000x), (B) MUDA (12000x) and (C and D) nanoMIP (6000x and 6600x, respectively) functionalised DPR - IDEAu5 electrodes.

3.3.2.1.2 Micrux IDE (ED-IDE3-Au)

The Micrux IDE was also used to reproduce the cocaine nanoMIP EIS sensor, using the same reagents and concentrations. The faradic EIS technique was carried out using 2.5 mM $[Fe(CN)_6]^{3-/4-}$ dissolved in 10 mM MOPS at pH 7.4 and according to the optimised procedure discussed in Section 2.4.2. The EIS was applied to characterise the cocaine nanoMIP as detailed in Section 3.2.5. Overall, the EIS Nyquist spectra (**Figure 3-24**) showed that the changes of the Rct values were consistent to the changes of the Rct values

previously observed on the DropSens SPE and IDE, as discussed in Section 3.3.1.1. The Micrux IDE was also investigated by AFM (performed as reported in Section 3.2.5), which confirmed that the cocaine nanoMIPs EIS sensor fabrication was successfully achieved. The 3D topography images of the nanoMIP functionalised IDE showed more height peaks compare to the peaks observed onto the bare electrode (**Figure 3-25**). As the development of the cocaine nanoMIP EIS sensor onto Micrux IDE was abandoned (as it will be discussed in Section 3.3.2.3), no further AFM investigation were carried out.

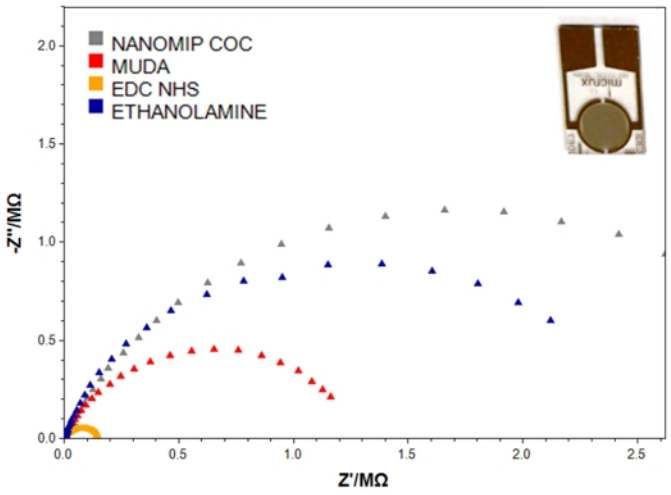

Figure 3-24: Nyquist plots achieved during cocaine nanoMIP EIS sensor fabrication using Micrux IDE (inset image): Nyquist plots obtained during: the electrode coated with MUDA (red), EDC/ENS activation (green), nano-MIP attachment (grey), ethanolamine blocking (blue).

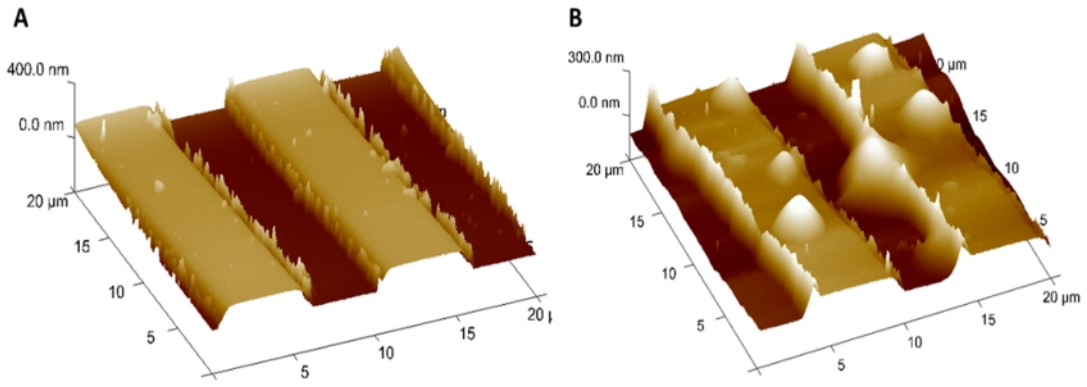

Figure 3-25: AFM 3D image related to the (A) bare (400 µm^2 scan area, height 400) and (B) nanoMIP (400 µm^2 scan area, height 300 nm) functionalised Micrux IDE electrode surfaces.

3.3.2.2 Sensitivity Study and LOD determination - DropSens IDE

The sensitivity study was performed on the un-optimised and optimised cocaine nanoMIP EIS sensor fabricated using the DropSens IDE (DPR IDEAu5) according to the procedure described in Section 3.2.4. Therefore, two different cocaine cumulative assays were carried out. The first cumulative assay was performed by preparing increasing cocaine concentrations in deionised water. Since a better sensitivity was expected, the tested concentrations ranged from 10 pg mL^{-1} - 50 ng mL^{-1}. Each sample was incubated for 30 minutes at room temperature. After each incubation, the surface was rinsed with water, dried under gentle nitrogen stream and the EIS measurements were conducted using a redox couple solution (10 mM $[Fe(CN)_6]^{3-/4-}$) in MOPS (pH 6.0). The resulting Nyquist plots (**Figure 3-26**) showed a decrease of Rct values (Ω) as the cocaine concentration increased.

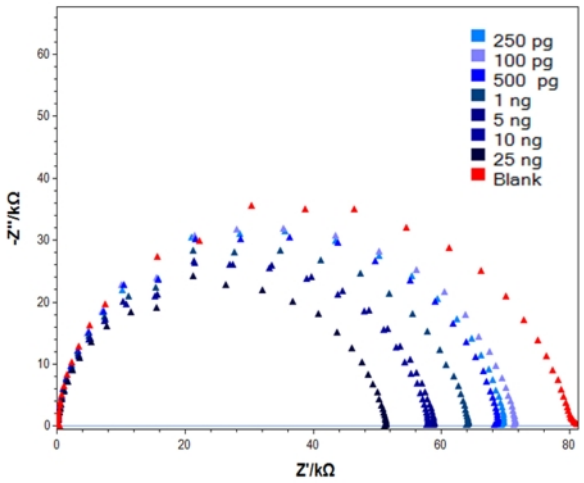

Figure 3-26: Nyquist plots gathered during the cumulative assay over cocaine nanoMIP EIS sensor (DPR IDEAu5). Tested cocaine concentrations rage from 100 pg mL^{-1} to 50 ng mL^{-1}.

The results of the assay were fitted in the simplified Randles equivalent circuit and the average (±SD) %Rct error was as low as 1.41 (±0.69), thus highlighting the goodness of the data fitting into the selected equivalent circuit. The Rct values were expressed as -Δ %Rct with respect to the blank signal (distilled water), according to the calculations described in Section 3.2.6.5, and these values were used to plot the non-linear and linear calibration curves (**Figure 3-27**).

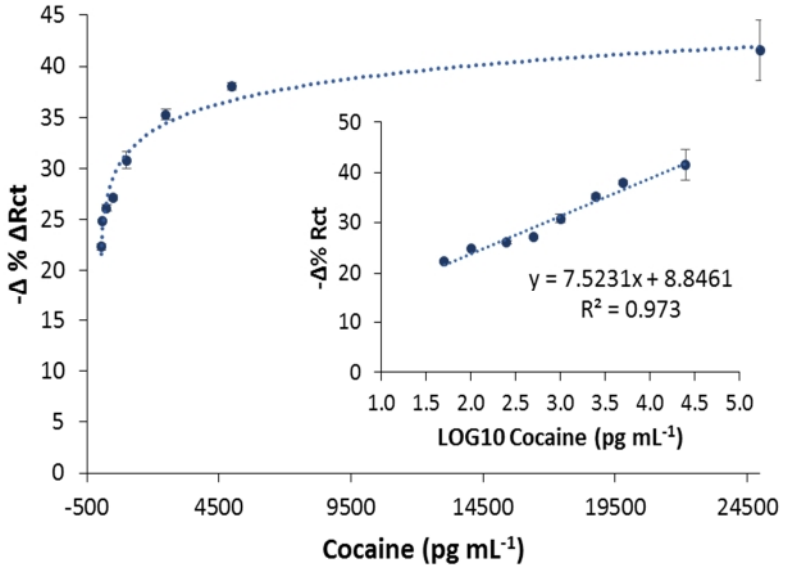

Figure 3-27: Non-linear (A) and linear (B) calibration curve of cocaine cumulative assay (10 pg mL^{-1}- 50 ng mL^{-1}) performed onto cocaine nanoMIP EIS sensor (DPR IDEAu5). Cocaine HCl has been diluted in water (18.2 MΩ cm^{-1}). Sensor surface has been blocked with ethanolamine. Error bars refer to the standard deviation of the replicates (n=3)

As shown in **Figure 3-27**, the sensor was able to detect the cocaine since the linear calibration curve (inset graph) showed that the sensor response (-Δ %Rct) increased as the cocaine concentrations, expressed as LOG10, increased. The R^2 of the linear calibration curve was equal to 0.973 (*p*-value= 0.00001). The limit of detection (LOD) was calculated as described in Section 3.2.6.6 and was as low as 0.46 ng mL^{-1}.

This results were consistent with the results of the un-optimised cocaine nanoMIP sensor fabricated on SPE, but the sensitivity did not improved as expected. Also, as the un-optimised sensor was cross-reacting against caffeine and mannitol, the sensitivity of the optimised cocaine nanoMIP sensor was investigated using DropSens IDE.

Therefore, the optimised cocaine nanoMIP EIS sensor was fabricated onto DropSens IDE according to the procedure described in Section 3.2.4 and the sensor surface was blocked with ethanolamine (50 µL, 1 M, pH 8.5), followed by MOPS buffer solution (50 µL, 10 mM, pH 7.4) containing BSA (0.1%, w/v) and Tween 20 (1%, v/v). Cocaine hydrocloride was dissolved in 10 mM MOPS (pH 7.4) and increasing concentrations were prepared from 10 pg mL^{-1} - 100 ng mL^{-1}, as a better sensitivity was expected. The MOPS (10 mM,

pH 7.4) was used as the washing buffer (1.2 mL) and blank sample (60 µL). The EIS measurements were conducted using a 10 mM redox solution ($[Fe(CN)_6]^{3-/4-}$) dissolved in MOPS pH 7.4 and the cocaine cumulative assay was performed as described in Section 3.2.7.

The EIS results were collected and processed as described in Section 3.2.6.5. The average (±SD) of the %Rct Error values was equal to 3.53 (±0.21). The non-linear and linear calibration curve were plotted (**Figure 3-28**) and the R^2 of the linear calibration curve was found to be 0.982 (p-value= 0.001). Results showed that the slope of the calibration curve increased (*m*=12.256, *p*-value= 0.001) compared to the slope of the calibration curve obtained with the un-optimised sensor (*m*=7.523, *p*-value= 0.00001). The LOD value was equal to 2.54 ng mL^{-1} and the sensor was able to detect the cocaine at higher concentrations (2.5 ng mL^{-1}-50 ng mL^{-1}) compare to the SPE, but still at trace level (sub-ppm). Therefore, the LOD is considered acceptable for investigative purposes. However, it is likely that the performances of the cocaine nanoMIP sensor developed onto DropSens IDE may improve working under a microfluidic condition, changing the cocaine nanoMIP concentration and blocking the glass substrate surface.

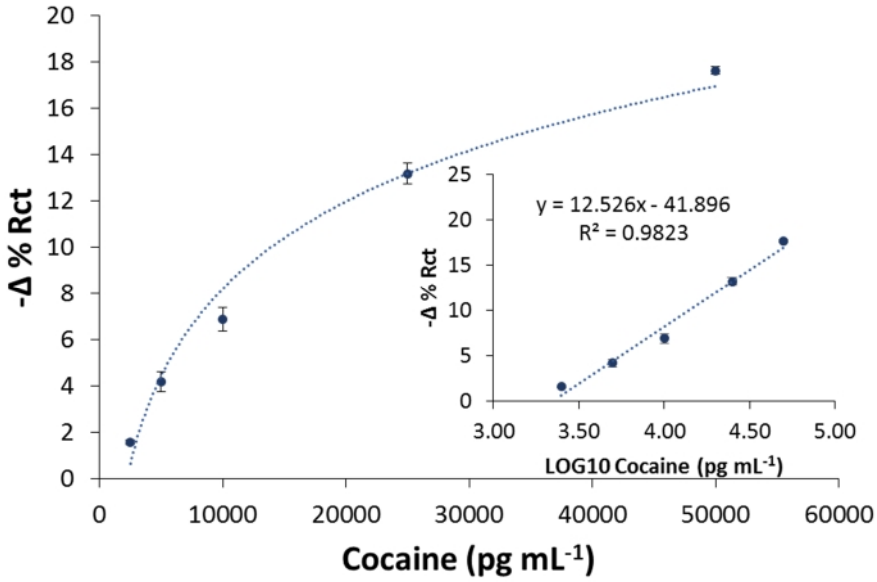

Figure 3-28: Non-linear (A) and linear (B) calibration curve of the cocaine cumulative assay (10 pg mL^{-1}- 100 ng mL^{-1}) performed on optimised cocaine nanoMIP EIS sensor (DPR IDEAu5).

3.3.2.3 Sensitivity Study and LOD determination - Micrux IDE

The Micrux IDE (ED-IDE3-Au) were evaluated only by reproducing the optimised cocaine nanoMIP EIS sensor. Therefore, the sensor was fabricated using Micrux IDE according to the procedure described in Section 3.2.4 and the sensor surface was blocked with ethanolamine (20 µL, 1 M, pH 8.5), followed by MOPS buffer solution (20 µL, 10 mM, pH 7.4) containing BSA (0.1%, w/v) and Tween 20 (1%, v/v). Cocaine hydrocloride was dissolved in 10 mM MOPS (pH 7.4) and increasing concentrations were prepared from 10 pg mL^{-1} - 50 ng mL^{-1}, as a better sensitivity was expected. The MOPS (10 mM, pH 7.4) was used as the washing buffer (0.6 mL) and blank sample (10 µL).

The EIS measurements were conducted using a 10 mM redox solution ($[Fe(CN)_6]^{3-/4-}$) dissolved in MOPS pH 7.4 and the cocaine cumulative assay was performed as described in Section 3.2.8. The data were collected and processed as indicated in section 3.2.6.5. The average (±SD) of the %Rct Error values was equal to 4.51 (±2.29). The non-linear and linear calibration curves were plotted as shown in **Figure 3-29**.

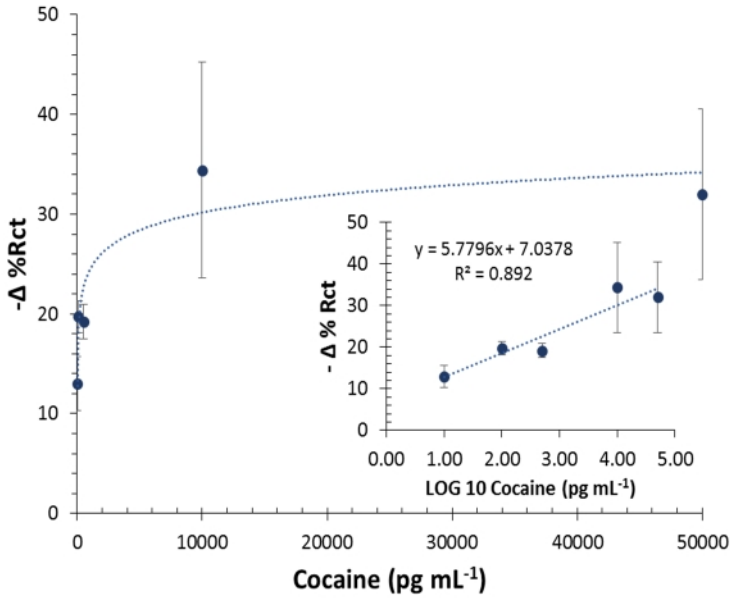

Figure 3-29: Non-linear (A) and linear (B) calibration curve of cocaine cumulative assay (10 pg mL^{-1}- 100 ng mL^{-1}) performed onto cocaine nanoMIP EIS sensor (ED-IDE3 Au, MicruX). Error bars refer to the standard deviation of replicates (n=3).

Although the coefficient of determination of the regression line was significant, the (R^2=0.892, *p*-value= 0.016), the data points were less closed to the regression line, whereas the SD (±) was too wide at the higher cocaine concentration, at which the saturation of the sensor surface also occurred. Furthermore, the slope (*m*) of the calibration curve was as low as 5.779 (*p*-value= 0.016). Therefore, the sensor was considered overall less sensitive compared to the DropSens IDE and further analysis were not carried out. The less sensitivity observed may be due to the smaller surface area of the Micrux IDE (2.40 mm^2) compared to both DropSens SPE (12.56 mm^2) and IDE (16.9 mm^2) electrodes. Therefore, it is likely that the sensor requires lower concentration of cocaine nanoMIP on the surface to detect the cocaine. Furthermore, a similar number of faulty IDEs electrodes was observed for the MicruX ED-IDE3-Au as for the DropSens IDE. Therefore, it was concluded that major optimisation studies were required to develop a cocaine nanoMIP sensor using Micrux IDE. Due to these reasons Micrux electrodes were not investigated further within this work, and it was concluded that even though more expensive, DPR GIDEAu5 were, overall, more suitable for the cocaine EIS affinity sensor development.

3.3.3 Comparison of the Developed Cocaine NanoMIP EIS Sensors

As highlighted in **Table 3-8** the three sensors varied in terms of sensitivity, electrodes format/configuration, and of the surface area of the working electrodes.

Table 3-8: Summary of the format, configuration, the surface area, LOD and linear range of each the investigated electrodes.

Electrodes	Format	WE Surface Area (mm^2)	LOD (ng mL^{-1})	Linear Range
DropSens – C220AT	SPE - three electrodes	12.56	0.24	0.1 – 100
DropSens – IDEAu5	IDE - two electrodes	16.9	2.54	2.5 - 50
Micrux ED-IDE3 Au	IDE - two electrodes	2.40	-	

Overall, all the cocaine nanoMIP sensors developed onto the DropSens electrodes (both, SPE and IDE) were responsive to increasing concentration of cocaine at trace level (LOD < ppm). However, the best sensitivity was achieved by developing the optimised cocaine nanoMIP sensor onto the DropSens SPE, which achieved a detection limit as low as 240 pg mL^{-1} and worked in a broad linear range (100 pg mL^{-1} – 100 ng mL^{-1}).

Concerning the performance of the cocaine nanoMIP sensor developed onto the DropSens IDE, the LOD (2.54 ng mL^{-1}) achieved by the optimised sensor was higher compared to the LOD (0.46 ng mL^{-1}) achieved by the un-optimised sensor. Furthermore, the linear range of the un-optimised sensor was a lower cocaine concentrations (50 pg mL^{-1} to 25 ng mL^{-1}) compared to the linear range of the optimised sensor (2.5 ng mL^{-1} – 50 ng mL^{-1}). The worsening of the sensor performances might be due to the loose IDE insertion into the CACIDE connector, which may have affected the EIS measurements. Overall, due to the promising results achieved by the un-optimised sensor, it is likely that the sensitivity of the optimised cocaine sensor fabricated onto DropSens IDE can be improved with further optimisation studies. Furthermore, the EIS measurements can be more reliable by increasing the stability at the electrode connector interface and working under microfluidic conditions.

The optimised cocaine nanoMIP EIS sensor replicated using the Micrux IDE showed a far less sensitivity compared to the optimised cocaine nanoMIP EIS sensor fabricated using both DropSens electrodes. Therefore, it was concluded that major optimisations were needed to increase the Micrux IDE performances. Since the cocaine nanoMIP sensor developed onto DropSens IDE performed better than the Micrux IDE, the development of the nanoMIP EIS sensor using Micrux IDE was not investigated further.

One of the major factors that may have negatively affected the performances of the cocaine nanoMIP sensor developed onto DPR IDEAu5 electrodes is related to the difference between the SPE and IDE configuration. Indeed, The SPE electrodes are built upon ceramic substrate, with a three electrodes configuration. During the sensor fabrication, only the working electrode was functionalised with the nanoMIPs. During the EIS experiment, a small voltage perturbation is introduced at the working electrode (WE), which triggered a system response. The analyte binding occurring at the WE generated a change in the current response, which can be accurately measured by

comparison to the current generated at the counter electrode. At the same time, the reference electrode (RE) guaranteed continuous control of the applied voltage over the experiment.

In the two electrodes configuration, there are only the working and the counter electrodes fabricated on a glass substrate, while the reference is not required (Arya *et al.*, 2018). Thus, the applied voltage cannot be controlled over the whole EIS measurements. Furthermore, both the counter and the working electrodes were functionalised with the nanoMIP during the sensor fabrication and, therefore, the binding event occurs at both WE and CE. This means that, using the IDE, the signal is purely driven by the analyte binding occurring at the whole sensor surface, which introduced a change of the ionic current between the CE and the WE, while no RE are in place to control the applied voltage. This may affect the EIS nanoMIP sensor signal, yielding to a less sensitive sensor.

3.4 Discussion and Conclusion

This work demonstrated that MIP nanoparticles coupled with an EIS sensor platform can be used to detect cocaine at trace levels. To the best of our knowledge, a sensor platform based on the nanoMIP-EIS system has not been previously reported. The opportunity to develop the cocaine nanoMIP sensor onto gold working electrodes with different format and configuration (namely, IDE and SPE) was explored. The results showed that the cocaine nanoMIP can be attached to the gold electrode surface with good reproducibility and can be used as a biomimetic receptor to develop an EIS based platform for the detection of cocaine at sub-ppb level. The LOD of the cocaine nanoMIP EIS fabricated using the SPE (0.24 ng mL^{-1} or 0.70 pM) was one order of magnitude lower than the LOD achieved on the same sensor fabricated using the IDE (2.54 ng mL^{-1}). This highlights that the EIS nanoMIP sensor can be developed using both the electrode formats (SPE and IDE). Overall, the applied protocol is more suitable for the SPE, but if further optimised, it may improve the performances of the nanoMIP sensor fabricated using IDE. The lack of stability of the DropSens IDE cable connector may also have affected the results of this work. The developed sensor demonstrated high sensitivity and specificity, being able to discriminate cocaine from morphine and from the most common cutting agents, namely levamisole and caffeine. For mannitol, this sugar still showed some non-specific adsorption to the sensor surface, which will require further optimisation studies to minimise or remove the non-specific binding. Finally, the thermal regeneration study performed at 60 °C showed promising results, although it should be investigated further.

Overall, the developed cocaine EIS nanoMIP sensor fabricated using DropSens SPE promises to be a valuable alternative to the current on-site screening methods in use, being cheaper, portable, highly sensitive and specific. The achieved LOD is higher than the estimated LOD of dog's olfactory system (0.03 ng mL^{-1}), but still below the ppb range. However, it has to be noted that the ability of the dog to detect illicit drugs varies according to the breed, training and environmental interference, while the event of cocaine incorrect indication has been reported to be as high as 26% (Jezierski *et al.*, 2014). Compared to the available presumptive analytical tools (**Table 3-9**), the sensor developed within this work has a lower LOD and, therefore, it is more sensitive. Although mass spectrometry can achieve a very low limit of detection, the cocaine nanoMIP EIS sensor

can provide faster results compared to Raman and mass spectroscopy analysis, which requires long and tedious sample preparation procedures.

Table 3-9: Current tools and biosensor platforms available to detect cocaine in biological and environmental samples and their LOD.

Detection tools Description	Sample	LOD	Reference
Dogs Olfactory system	Illicit cocaine vapour	0.03 ng mL^{-1} – 88.3 pM	Waggoner et al., 1997
Transportable Raman spectrometer	Mixture of street sample seized materials	5 mg mL^{-1} 14.71 mM	(Weyermann *et al.*, 2011)
Immune-based kit	Biological and environmental samples	10- 50 ng mL^{-1} 29.43 – 147.14 ng mL^{-1}	(Wille *et al.*, 2010; Musshoff *et al.*, 2014)
Paper spray Ion Trap Mass Spectrometry	Surface sample, bulk powder	2 ng cm^{-2}	(Ma *et al.*, 2015)
Paper spray Ion Mobility Spectroscopy (IMS)	Surface samples	5 ng per surface area samples	(M. Li *et al.*, 2014)
	Liquid sample	2 µg mL^{-1} 5.88 µM	
Various Hyphenated MS Methods	Indoor and outdoor air	In the range of 0.001 to 29.4 ng m^{-3}	(Cecinato, Balducci and Perilli, 2016)
EIS aptasensor	Wastewater	0.1 µM - 34 ng mL^{-1}	(Z. Yang *et al.*, 2016)
EIS aptasensor	Spiked serum	200 pM (68 ng mL^{-1})	(Roushani and Shahdost-fard, 2016)
Voltammetric aptasensor	Spiked serum	1-8 nM 0.33 – 2.7 ng mL^{-1}	(Roushani and Shahdost-fard, 2016)
Amperometric immunosensor	Serum, saliva, urine	14.4 ng mL^{-1} - 42.38 nM (urine) 3.6 ng mL^{-1} - 10.6 nM (saliva) 25.2 ng mL^{-1} - 74.16 nM (serum)	(Vidal *et al.*, 2016)
Potentiometric sensor MIP	Blood serum	3.3 µM - 1.12 µg mL^{-1}	(Smolinska-Kempisty *et al.*, 2017)
SPR –MIP film	Diluted cocaine	From 0 to 400 µM (linear range) 0 – 135.92 µg mL^{-1}	(Nguyen, Sun and Grattan, 2016)
Optical fibre MIP	Diluted cocaine	From 500 to 1000 µM (linear range) 169.91 – 339.81 µg mL^{-1}	(Wren *et al.*, 2014)
Electromagnetic piezoelectric acoustic sensor (EMPAS) aptasensor	Diluted cocaine	0.9 µM (305.83 ng mL^{-1})	(Neves *et al.*, 2015)

The developed sensor can also compete with the extensively used IMS. While the commercially available IMS has a LOD in the sub ng range (IONSCAN 500DT®, Smiths Group plc, UK), it is still prone to false positive results due to the competitive ionisation of cutting agents or other environmental compounds (Verkouteren and Staymates, 2011). The sensor developed within this work is based on a direct assay format, which decreases the likelihood of false positive results often linked to the use of the competitive inhibition immunoassay screening kits (ELISA kit or lateral flow device) (Kerrigan *et al.*, 2011; Harper, Powell and Pijl, 2017).

Although confirmatory methods, such as mass spectrometry hyphenated methods, can achieve a very low limit of detection, the cocaine nanoMIP EIS sensor can provide faster results compared to Raman and mass spectroscopy analysis, which requires a long and tedious sample preparation procedures.

Biosensor platform for drugs of abuse detection have been explored previously, and these have shown a low limit of detection, while being faster and cheaper compared to the commercially available analytical tool (Gandhi *et al.*, 2015). As shown in **Table 3-9** most of the developed biosensor can detect cocaine in traces (in the range of ng mL^{-1}) and in a wide range of sample matrices (mostly biological ones).

The synthetic receptor (nanoMIP) used in this sensor guarantees a higher stability against environmental factors that usually affect bio-derived receptors (antibodies, aptamers), such as high or low temperatures and enzymatic degradation. It also has to be noted that the sensor response is due to the detection of the binding between the nanoMIP and the cocaine at the electrodes interface. On the other hand, aptamers based sensors mostly rely upon the folding of the aptamers, which occurs when the aptamer binds the target (Z. Yang *et al.*, 2016), although non-specific aptamer folding cannot be excluded. Compared to the MIP film based biosensor developed by Wren et al. (Wren *et al.*, 2014) and Nguyen et al. (2016), the cocaine concentration range achieved in this work is far lower and the EIS nanoMIP sensor specificity has been demonstrated against the most common cutting agents (levamisole, caffeine and mannitol) and morphine. Compared to the optical and piezoelectric platforms, the EIS analyser used in this work is cheaper and portable. Furthermore, the faradic EIS technique enables the sensitivity in a sub-ppb range, making

the developed sensor a promising platform to detect traces of cocaine in both environmental and biological sample with high sensitivity and specificity.

This is the first work to demonstrate the detection of traces of cocaine based on MIP nanoparticles coupled with an EIS sensor platform (0.24 ng mL^{-1} or 0.70 pM), while being also highly specific (no cross-reactivity towards levamisole, caffeine and morphine). The cocaine EIS nanoMIP sensor developed onto the DPR IDEAu5 electrode also has a LOD (2.54 ng mL^{-1}) lower or comparable to the other biosensors platform currently reported in the literature. Additionally, the convenient two electrodes format makes it more amenable for miniaturisation and integration onto a portable devices (Sarkar *et al.*, 2014).

Chapter 4

Morphine NanoMIP EIS Sensor Development

4.1 Introduction

Morphine is an anaesthetic drug legally used in the treatment of acute and chronic severe pain. However, morphine and its derivative heroin are also abused and misused as a recreational and doping drugs, often leading to addiction and accidental death due to overdoses (UNODC, 2017b; WADA, 2017). The United Nations Office on Drugs and Crime (UNODC) has recently warned on a possible increase in illicit morphine and heroin trafficking due to the massive increase in poppy plants cultivation and forecasted illicit morphine price drop (UNODC, 2017a).

A wide range of analytical tools is currently in use to detect illicit morphine in both environmental and biological samples, while the police dogs remain the preferred tools for the investigative activities. However, the major limitations of the analytical tools are related to the high rate of false positive or false negative results (presumptive tests), to the high cost (confirmatory tests), and to the time-consuming procedure and low portability of the analytical devices (both presumptive and confirmatory tests).Therefore, a rapid, portable and cost-effective analytical tool is highly demanded. This necessity has recently prompted the development of nano-biosensors platforms (Yang *et al.*, 2014; Rezaei, Foroughi-Dehnavi and Ensafi, 2015; Vergara *et al.*, 2016; Farka *et al.*, 2017; Harper, Powell and Pijl, 2017; Liu *et al.*, 2017). As the EIS and the nanoMIPs are at the forefront of the nano-sensor development, this Chapter reports the development of the nanoMIPs EIS sensor for both pharmaceutical and illicit morphine detection at trace levels and in a water-based solution. Overall, the nanoMIPs EIS sensor developed in this work aims to replace police dogs and the presumptive methods employed during the investigative activities of illicit drugs crimes (i.e., misuse, possession, manufacturing and trafficking).

4.2 Materials and Methods

4.2.1 Materials

Morphine nanoMIPs in acetonitrile and water (3:1) solution were synthetised by Prof Piletsky's Group (University of Leicester - ULEIC University, Leicester, UK). Morphine hydrochloride (trihydrate), cocaine hydrochloride, paracetamol, and caffeine, were purchased from Sigma-Aldrich Ltd (Dorset, UK). All the drugs of abuse were handled according to the Home Office (UK) guidelines, and a correct drugs of abuse handling procedure was elaborated and set in place. Phosphate buffered saline tablet (PBS: 0.0027 M potassium chloride, 10 mM phosphate buffer and 0.137 M sodium chloride, pH 7.4) and 3-(N-Morpholino)propanesulfonic acid powder (MOPS) were purchased from Sigma-Aldrich Ltd (Dorset, UK) and used to make the buffer solutions. 11-mercaptoundecanoic acid (11-MUDA) was purchased from Sigma-Aldrich Ltd (Dorset, UK) and was dissolved in 10 mL of ethanol (pure ethyl alcohol, anhydrous, ≥ 99.5%) at a concentration of 5 mM. N-hydroxysuccinimide (NHS) and 1-Ethyl-3-(3-dimethylaminopropyl) carbodiimide (EDC), were purchased from Thermo Scientific™ (Rugby, UK) and dissolved in water to obtain 0.1 M and 0.4 M solution, respectively. Ethanolamine, Bovine Serum Albumin (BSA) and Tween 20 were purchased from Sigma-Aldrich Ltd (Dorset, UK) and used as blocking agents at the respective concentrations of 1 M (pH 8.5), 0.1% (w/v), and 1% (v/v) in MOPS (10 mM, pH 7.4).

The 10 mM redox couple solution ($[Fe(CN)_6]^{3-/4-}$) was prepared by dissolving potassium ferrocyanate ($K_4[Fe(CN)_6]$) and potassium ferricyanide ($K_3[Fe(CN)_6]$) in MOPS in MOPS (10 mM, pH 6.0 or pH 7.4) or PBS (pH 9). When the PBS (pH 9.0) was used to perform the cumulative assay, the redox couple solution was prepared by dissolving 10 mM of $Fe(CN_6)^{3-/4-}$ in PBS (pH 9.0). All the solutions were filtered through filter system by means of a nitrocellulose Whatman® filter 0.2 µm (Whatman International Ltd, Maidstone, UK) or by 0.2 µm Corning® syringe filter (Corning Inc., New York, US). All nanoMIPs solutions were filtered with 0.45 µm syringe filter (Corning®, Corning Inc., New York, US).

4.2.2 Faradic EIS Setting and Measurement

The IES instrumentation and software were set-up as described in Section 2.2.4. The custom-made CACIDE holder (Section 2.4.1, Chapter 2) was applied to carry out the EIS measurements using DropSens IDE (DPR IDEAu5). The parameters of the EIS measurements were set as reported in Section 2.3.1, while the measurements were performed as reported in Section 3.2.3. The EIS data were analysed as described in section 2.3.2, using PStrace v5.2 equivalent circuit-fitting tool (first release June 2017 by BV, The Netherlands). A summary of the relevant EIS measurements parameter and conditions applied in this Chapter are reported in **Table 4-1**.

Table 4-1: Summary of the relevant EIS condition applied to each investigated electrode used to develop the cocaine nanoMIP IES sensor.

				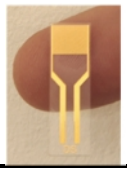
		DPR C220AT		DPR IDEAu5
DC (V)		0.12		0.12
AV (V)		0.01		0.01
Frequency range (Hz)		0.1 – 50,000		
N^0 frequency points		51		
Redox Couple Solution $[Fe(CN)_6]^{3-/4-}$	Concentration	10 mM		10 mM
	Buffer	10 mM MOPS	PBS	10 mM MOPS
	pH	6.0 or 7.4	9.0	7.4
	µL	50		60

4.2.3 Morphine nanoMIP Sensor Assembly

Morphine nanoMIP EIS sensor was fabricated using morphine nanoMIP (1.2 mg mL^{-1} or 2.4 mg mL^{-1}) and applying the procedure described in section 3.2.4. The sensor surface was blocked using 1 M ethanolamine dissolved in MOPS (10 mM) and adjusted at pH 8.5, followed by a mixture of 0.1% (w/v) of BSA and 1% (v/v) of Tween 20, as reported in Section 3.2.6.3.

4.2.4 Morphine nanoMIP Sensor Characterisation

The surface of the morphine nanoMIPs EIS sensors, fabricated according to the procedure indicated in Section 4.2.3, were characterised using EIS and AFM techniques according to the procedures reported in Section 3.2.5. The EIS measurement was performed as reported in Section 4.2.2 and the redox couple solution (10 mM $[Fe(CN_6)]^{3-/4-}$) was dissolved in MOPS buffer (10mM, pH 7.4). The obtained EIS data were fitted in the appropriate equivalent circuit, the data were analyse as described in Section 2.3.2, and the Rct was expressed as a percentage (%) of the average Rct value of the MUDA coated electrodes (set as a 100%). The AFM analysis was carried out according to the procedure outlined in Section 3.2.5 and only on the fully functionalised morphine nanoMIPs EIS sensors on a scan areas of 400 μm^2 and 4 μm^2. The obtained results were compared with the AFM results of the bare and MUDA functionalised electrodes previously performed and reported in Section 3.3.1.2 (DropSens SPE) and 3.3.2.1.1 (DropSens IDE).

4.2.5 Development and Optimization Studies of the Morphine NanoMIP EIS Sensor onto DropSens SPE

4.2.5.1 pH Optimisation Study of the Morphine Cumulative Assays

Morphine cumulative concentrations assay was used to assess the ability of the morphine nanoMIP EIS sensor to detect morphine tetrahydrate hydrochloride dissolved in buffer (i.e. 10 mM MOPS or PBS) and at three different pH (6.0, 7.4, 9.0). The morphine was dissolved in PBS buffer when the pH was adjusted to 9.0, as this pH value is out of the working pH range of MOPS buffer. The pH 6.0 was the pH value obtained by dissolving MOPS (10 mM) in the deionised water. Morphine concentrations, in the range of 100 pg mL^{-1} -50 ng mL^{-1}, were prepared according to the investigated buffers and pH conditions, i.e.10 mM MOPS pH 6.0, 10 mM MOPS pH 7.4 and PBS pH 9.0. Several morphine nanoMIP EIS sensors were fabricated as described in Section 4.2.3 and used for the assay (each sensor for each pH tested). To confirm that the analyte was binding to the morphine nanoMIP, a cumulative assay was carried out on another group of sensors (n=3)

functionalised without the nanoMIP (control sensor) and using the optimised buffer and pH condition.

The morphine cumulative assay was carried out on each group of morphine nanoMIP EIS sensors and control sensors according to the procedure described in Section 3.2.6.1. The investigated buffers (i.e.10 mM MOPS pH 6.0, 10 mM MOPS pH 7.4 and PBS pH 9.0) were used as washing buffer (1.2 mL) and as the blank sample (50 µL). The EIS measurement was performed as reported in Section 4.2.2 and the redox couple solution (10 mM $[Fe(CN_6)]^{3-/4-}$) was dissolved in the buffer with a pH adjusted to the pH used in the cumulative assay. The EIS experimental data were analysed as described in Section 3.2.6.5. All the experiments were carried out on independent sensor surfaces and at least in triplicates. The list and the conditions of the cumulative assays carried out in this work are reported in **Table 4-2**.

Table 4-2: List of the morphine cumulative assays carried out and related assays conditions.

Test ID	nanoMIP	nanoMIP Concentration (mg mL^{-1})	diluent	pH
1	Morphine nanoMIP	2.4	MOPS	6.0
2	Morphine nanoMIP	2.4	PBS	9.0
3	Morphine nanoMIP	2.4	MOPS	7.4
4	Without nanoMIP	-	MOPS	7.4

4.2.5.2 Concentration Optimisation Study of the Morphine Cumulative Assays

To optimise the nanoMIP concentration to use for the morphine nanoMIP EIS sensor assambly, one group of sensors (n=6) was fabricated using 1.2 mg mL^{-1} of morphine nanoMIP (suspended in a mixture of 3:1 acetonitrile and water) and according to the procedure described in Section 4.2.3. The EIS technique was used to characterise the surfaces of the sensors fabricated using 1.2 mg mL^{-1} and 2.4 mg mL^{-1} of morphine nanoMIP according to the procedure reported in Section 4.2.4. The % Rct values were then obtained and were compared.

The morphine cumulative assay, using the optimised buffer and pH condition, was

replicated on the sensor fabricated using 1.2 mg mL^{-1} of morphine nanoMIP. Morphine (1 mg) was dissolved in 1 mL of MOPS (10 mM, pH 7.4) and a concentrations range of 100 pg mL^{-1} -50 ng mL^{-1}, were prepared using the sample buffer The morphine cumulative assay was performed according the incubation and washing procedure reported in Section 3.2.6.1. The MOPS (10 mM, pH 7.4) was used as the washing buffer and as the blank sample. The EIS measurements were performed as reported in Section 4.2.2 and the redox couple solution (10 mM $[Fe(CN_6)]^{3-/4-}$) was dissolved in MOPS (10 mM, pH 7.4). The EIS experimental data were analysed as described in Section 3.2.6.5. The results of this cumulative assays were compared to the results of the optimised sensor functionalised using 2.4 mg mL^{-1} of morphine nanoMIPs, thus assessing the optimal concentration to be used to fabricate the morphine nanoMIP EIS sensor.

4.2.5.3 Specificity Assays

The optimised sensor was fabricated using morphine nanoMIP, at a concentration of 2.4 mg mL^{-1} and suspended in mixture of acetonitrile and water (3:1), and according to the procedure detailed in Section 4.2.3. The sensor specificity was evaluated versus one of the common cutting agents (i.e., paracetamol). The cross-reactivity towards one drug of abuse (i.e., cocaine) was also investigated. Each analyte was dissolved in MOPS (10 mM, pH 7.4) and increasing concentrations (100 pg mL^{-1} - 50 ng mL^{-1}) were prepared. The MOPS (10 mM, pH 7.4) was also used as the washing buffer and as the blank sample. The cumulative assay was carried out for each selected analyte, following the incubation and washing procedure reported in section 3.2.6.1. To assess the specificity, the optimised sensor response towards morphine was compared to the optimised sensor response towards paracetamol and cocaine. All the experiments were carried out on independent sensor surfaces and at least in triplicates.

4.2.5.4 Sensitivity Study and LOD determination

The sensitivity study and the LOD of the cumulative assays were determined as described in section 3.2.6.6.

4.2.6 Evaluation Studies of Morphine nanoMIP Sensor onto DropSens IDE

The fully developed 3D printed CACIDE cable holder (as described in Section 2.4.1) was used in this work. The ability of the optimised nanoMIP EIS sensors to detect morphine was assessed by performing the optimised morphine cumulative assay. Therefore, a group (n=6) optimised nanoMIP EIS sensors were fabricated using DropSens IDE according to the procedure reported in Section 4.2.3. The EIS measurement was performed as reported in Section 4.2.2, using the redox couple solution (10 mM $[Fe(CN_6)]^{3-/4-}$) dissolved in MOPS buffer (10mM, pH 7.4). The nanoMIP EIS sensors were characterised as detailed in Section 4.2.4. The optimised morphine cumulative assay was performed by dissolving morphine in 10 mM MOPS pH 7.4 and preparing several concentrations in the range of 10 pg mL^{-1} - 50 ng mL^{-1}. The cumulative assay was performed according to the incubation and washing procedure reported in section 3.2.6.1, while the LOD was calculated applying the equation (3-2).

4.2.7 Data Processing and Statistical Analysis

All the data of each experiment were collected on an Excel® database spreadsheet and identified by a unique code. Statistical analyses were carried out by Microsoft® Excel® and IBM® SPSS® Statistics 24.0 software. Descriptive statistic and related plots were used to present the results.

Both parametric and non-parametric statistics were applied as appropriate and the significance level (*p-value*) was set at 0.05.

4.3 Results and Discussion

4.3.1 Morphine NanoMIP EIS Sensor Development onto DropSens SPE

4.3.1.1 EIS Characterisation Studies

DropSens screen-printed electrodes (SPEs, DPR C220AT) were cleaned according to the optimised procedure (Section 2.4.3.1) and functionalised by covalently attaching the morphine nanoMIP (2.4 mg mL^{-1}, suspended in a mixture 3:1 acetonitrile/water) onto the working electrodes via amine coupling, as detailed in Section 4.2.3. As a technique used to assess modifications occurring at the surface boundaries, the EIS analysis was used to characterise the sensor fabrication at each fabrication step of the morphine nanoMIP EIS sensor according to the procedure described in Section 4.2.4. The resulting EIS spectra are shown in **Figure 4-1** and are consistent with the results observed in the characterisation study of the cocaine nanoMIP EIS sensors (Section 3.3.1.1).

As shown in **Figure 4-1A,** the ethanolamine (1 M, pH 8.5) induced a drop of Δ %Rct value by around 85%. This indicated that the ethanolamine blocked the activated carboxyl group occurring at the MUDA layer, thus decreasing the negative charges and introducing hydrophilic groups at the surface solution interface. On the other hand, the second blocking agent (0.1% BSA – 1% Tween 20) introduced an increase of the %Rct due to the protein (BSA) attachment on the sensor surface.

The EIS data were fitted in the Randles or in the simplified Randles equivalent circuit with a % error of the Rct fitting of 4.01 % (±1.51) and the χ^2 of the equivalent circuit data fitting of 0.025 (±0.019), thus indicating a minimal discrepancy between the observed data and the selected equivalent circuit model. The Rct values were expressed as % of the MUDA Rct value, which was set at 100%. The results were plotted in a bar chart and is shown in **Figure 4-1B** and indicated that the nanoMIP attachment was reproducible, although nanoMIP adsorption onto the surface events cannot be completely excluded.

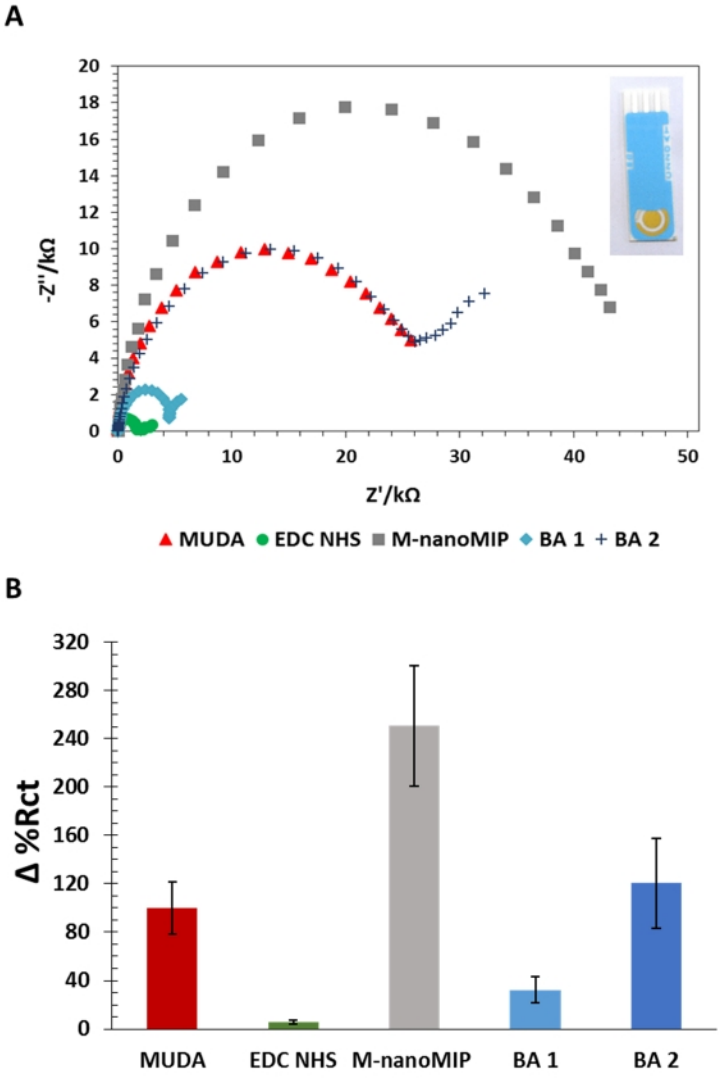

Figure 4-1: (A) Nyquist plots obtained during morphine nanoMIP EIS sensor fabrication using DropSens SPE (inset): the electrode coated with MUDA (red), EDC/ENS activation (green), nano-MIP attachment (grey), ethanolamine blocking (blue). Morphine nanoMIP = 2.4 mg mL-1; BA 1 = Ethanolamine pH 8.5; BA 2 = 0.1% BSA – 1% Tween 20. (B) Average of Δ %Rct values (±SD) obtained at each sensor fabrication point performing EIS analysis.

4.3.1.2 AFM Characterisation Study

The AFM analysis was performed in the tapping mode to characterise the sensor surface fabricated using SPE, according to the procedure indicated in Section 4.2.4. Therefore, the optimised morphine nanoMIP IES was fabricated on the SPE according to the procedure described in Section 4.2.3 and using the morphine nanoMIP at the concentration of 2.4 mg mL^{-1}. The sensor was rinsed with deionised water and a 400 nm^2

area was scan by AFM. Overall, the AFM study were affected by the same considerations discussed in Section 3.3.1.2.

The resulting 3D AFM image of the sensor surface topography is shown in **Figure 4-2**B and is compared with the sensor surface topography functionalised with the MUDA (**Figure 4-2**A). Although the roughness of the SPE is visible, the morphine nanoMIP were seen as more elevated and larger peaks on the working electrode surface.

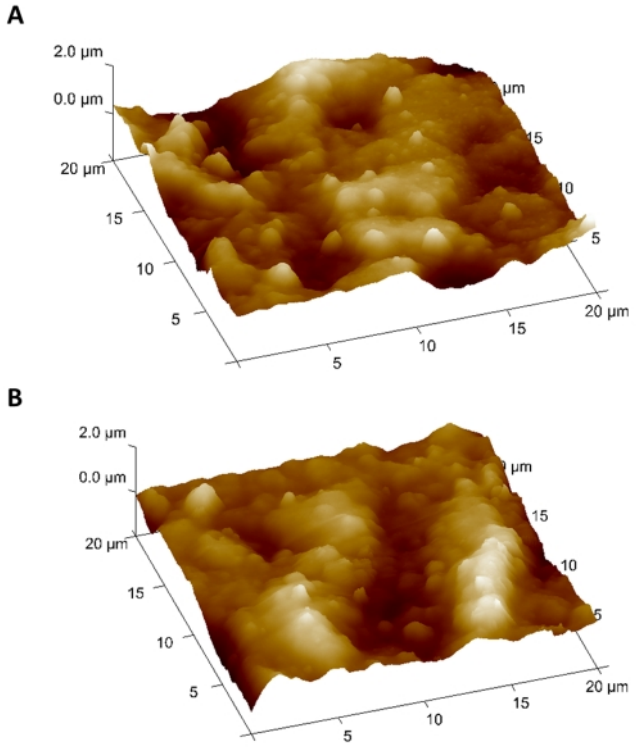

Figure 4-2: AFM 3D images of the DropSens SPE surface topography before and after the morphine nanoMIP deposition. 3D surface topography of the (A) MUDA functionalised surface (400 µm^2 scan area, height 2 µm). (B) Morphine nanoMIPs functionalised surface (400 µm^2 scan area, height 2 µm).

The roughness analysis was performed on both 400 µm^2 and 4 µm^2 areas of the electrode surface and the results are reported in **Table 4-3**. The statistical analysis was carried out to assess the difference between the MUDA and the nanoMIP functionalised sensor surface. However, the results indicated that no significant differences (p-value>0.05) occurred between the Ra, Rq and Rmax values of the MUDA functionalised sensor and of the morphine nanoMIP functionalised sensor.

Table 4-3: Results of the AFM roughness analysis performed onto the SPE surface and related to each sensor fabrication point. The AFM roughness analysis was performed onto both 4 µm2 and 400 µm2 scan areas.

Functionalisation point / scan area	Rq (nm)	SD(±)	Ra (nm)	SD(±)	Rmax (nm)	SD(±)
Bare (4 μm^2)	44	5	33	0.6	373	30
MUDA (4 μm^2)	46	16	39	13	378	106
Morphine nanoMIP (4 μm^2)	**40**	**0.2**	**28**	**3**	**334**	**14**
Bare (400 μm^2)	278	32	222	25	1895	324
MUDA (400 μm^2)	315	119	254	99	2157	784
Morphine nanoMIP (400 μm^2)	**298**	**96**	**233**	**67**	**2092**	**501**

4.3.1.3 Cumulative Assay Optimisation Study and Sensitivity Assessment

4.3.1.3.1 pH Optimisation Study

As shown in **Figure 4-3**, morphine is a small molecule (375.84 g mol^{-1}) and acts as a zwitterion, having three negative charge functional groups and one positive charge functional group. The pH can affect the ionisation of these functional groups, thus changing the overall charges distribution of morphine as the pH approaches the pk_a (6.13) or the pk_b (9.85) values (PubChem).

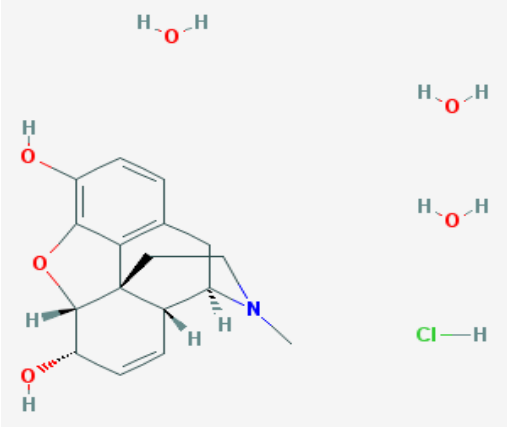

Figure 4-3: 2D chemical structure of the morphine hydrochloride trihydrate (PubChem, 2018).

At the same time, the Rct values of the EIS sensor response is affected by the variations of the charges distribution onto the sensor surface and by other factors, such as the hydrophobicity of the surface. The pH value also plays a role in the binding between the nanoMIP receptor and the analyte.

Therefore, a pH scouting is needed to determine the appropriate working pH condition, which will enhance the sensor signal due to the binding between the morphine and the morphine nanoMIP, while avoiding false positive response due to cross-reactivity or non-specific binding events. Therefore, the morphine cumulative assay was carried out at a neutral pH value (pH= 7.4), a slightly acidic pH (pH= 6.0) and a slightly basic pH (pH= 9.0) values, thus to assess the effect of the pH on the sensitivity of the of the morphine nanoMIP sensor. Several groups of sensor were fabricated using 2.4 mg mL^{-1} morphine nanoMIPs and according to the procedure outlined in Section 4.2.3. The cumulative assays and the EIS measurements were performed according to the procedure described in Section 4.2.5.1. The results of the of the morphine cumulative assay performed at pH 6.0 are shown in **Figure 4-4**.

The EIS data of the cumulative assay (**Figure 4-4**A) indicated that the Rct (Ω) did not varied as the increasing concentrations of morphine (50 µL, 100 pg mL^{-1} – 1 mg mL^{-1}) dissolved in MOPS (10 mM, pH 6.0) were tested on the sensor surface. The EIS data were then fitted in Randles equivalent circuit as described in Section 2.3.2. The average value (±SD) of the % error of the Rct fitting was equal to 6.01% (± 1.83%), which indicated a slightly discrepancy between the observed data and the data predicted under the model. The Rct values were expressed as -Δ %Rct with respect to the blank signal as described in Section 3.2.6.5. The linear calibration curve (**Figure 4-4**B) was obtained plotting the -Δ %Rct against the morphine concentration expressed in LOG10.

The results showed that there was no correlation between the -Δ %Rct values and the increasing concentration of morphine when the assay was performed at pH 6.0 ($r=0.429$; $n=9$; *p*-value= 0.250), thus confirming that the morphine nanoMIP EIS sensor was not responsive towards increasing concentrations of morphine tested during the cumulative assay performed at pH of 6.0.

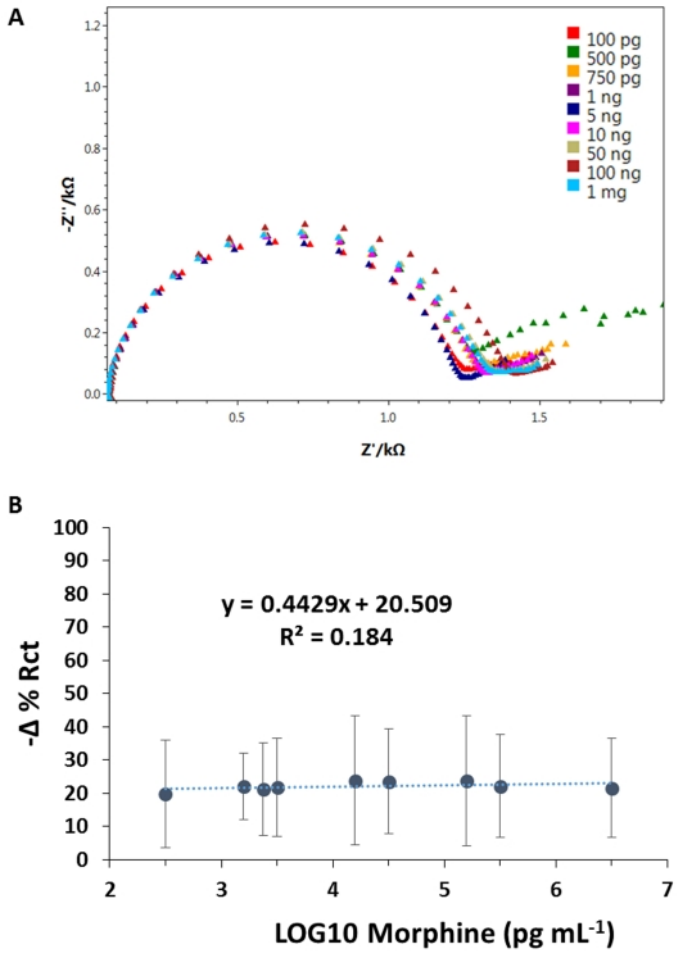

Figure 4-4: (A) Nyquist plots of the data obtained during the morphine cumulative assay performed at pH 6.0 (100 pg mL^{-1} – 1 mg mL^{-1}) and (B) calibration curve obtained by plotting the -Δ %Rct against the increasing concentration of morphine expressed in LOG10 scale. Morphine nanoMIP EIS sensors were fabricated on DropSens SPE and using morphine nanoMIP at the concentration equal to 2.4 mg mL^{-1}. Error bars refer to the standard deviation of replicates (n=3).

The results of the of the morphine cumulative assay performed at pH 9.0 are shown in **Figure 4-5**. The EIS data of the cumulative assay (**Figure 4-5**A) showed that the Rct (Ω) did not varied as the increasing concentrations of morphine (50µL, 100 pg mL^{-1} – 100 ng mL^{-1}) dissolved in PBS (10mM, pH 6.0) were tested on the sensor surface. The EIS data were then fitted in Randles equivalent circuit as described in Section 2.3.2. The average value (±SD) of the % error of the Rct fitting was equal to 5.12% (± 2.17%), which indicated that the data predicted under the model were in agreement with the observed data. The Rct values were expressed as -Δ %Rct with respect to the blank signal as

outlined in Section 3.2.6.5. The linear calibration curve (**Figure 4-5**B) was obtained plotting the -Δ %Rct against the morphine concentration expressed in LOG10 and no significant correlation between them (r= 0.95; n=8; *p*-value= 0.823) was observed.

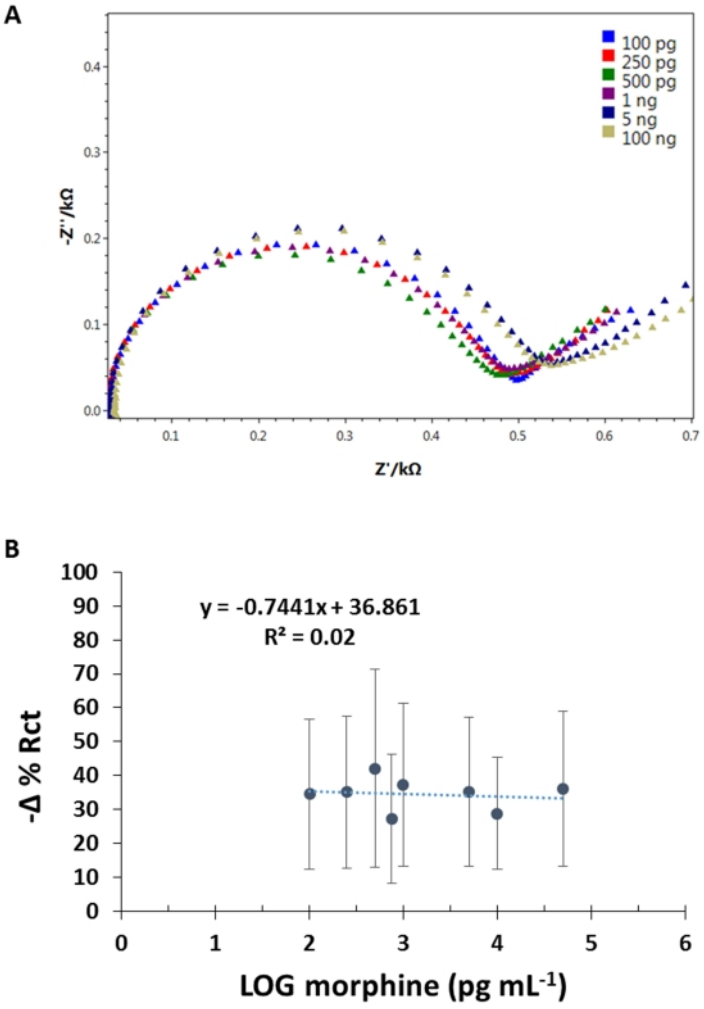

Figure 4-5: (A) Nyquist plots of the data obtained during the morphine cumulative assay performed at pH 9.0 (100 pg mL^{-1} - 100 ng mL^{-1}) and (B) calibration curve obtained by plotting the Δ %Rct against the increasing concentration of morphine expressed in LOG10 scale. Morphine nanoMIP EIS sensors were fabricated on DropSens SPE and using morphine nanoMIP at the concentration equal to 2.4 mg mL^{-1}. Error bars refer to the standard deviation of replicates (n=3).

Therefore the results indicated that the morphine nanoMIP EIS sensor was not responsive towards increasing concentrations of morphine tested during the cumulative assay performed at pH of 9.0.

The results the morphine cumulative assay at pH 7.4 are shown **Figure 4-6**. The in Nyquist plots indicated that a decrease of the Rct value (Ω) was visible at each increasing morphine concentration.

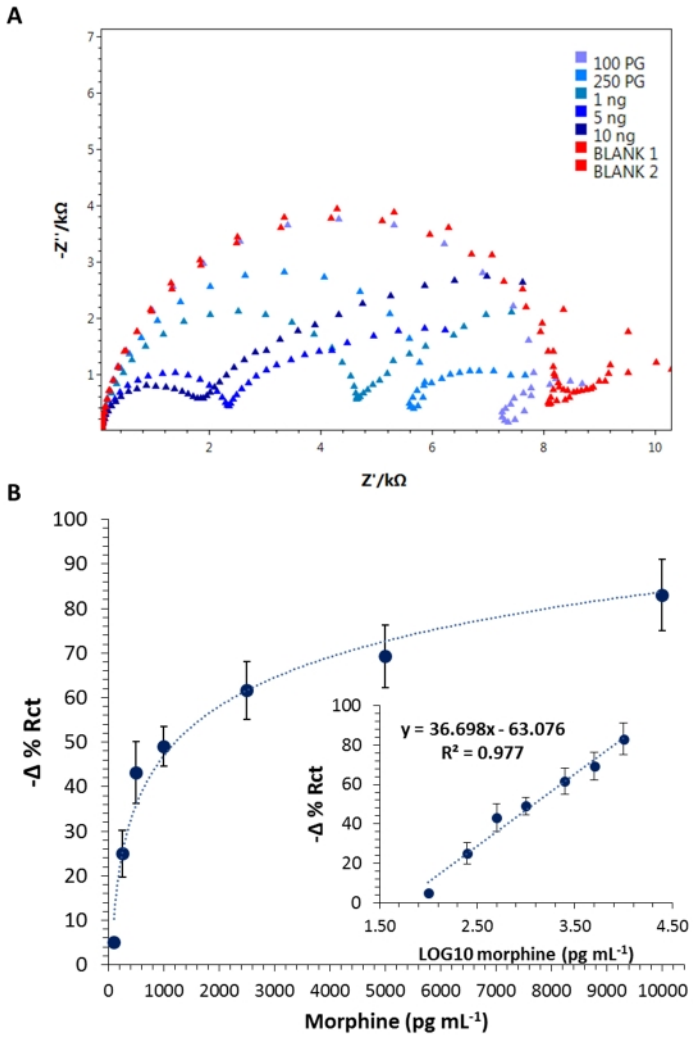

Figure 4-6: (A) Nyquist plots of the data obtained during the morphine cumulative assay performed at pH 7.4 (100 pg mL^{-1} - 50 ng mL^{-1}). (B) The non-linear and linear (inset graph) calibration curves related to the morphine cumulative assay performed at pH 7.4 (100 pg mL^{-1} - 50 ng mL^{-1}) performed onto the morphine nanoMIP EIS sensor (fabricated using SPE DPR C220AT). The sensors were fabricated using morphine nanoMIP at the concentration equal to 2.4 mg mL^{-1}. Error bars refer to the standard deviation of replicates (n=6).

The EIS data were fitted into a Randles equivalent circuit and the Rct value were extrapolated with an average (±SD) of the % Rct error of the fitting equal to 2.94% (±0.58%) and a χ^2 as low as 0.012 (± 0.005), thus highlighting a good agreement between

the data observed and predicted under the selected model. The Rct values were expressed as -Δ %Rct with respect to the blank signal as outlined in Section 3.2.6.5 and these values were used to plot the non-linear and the linear calibration curve. The statistical analysis revealed that there was a positive correlation between these two values (r=0.986, n=7, *p*-value<0.0005). The R^2 of the calibration curves was equal to 0.977 (*p*-value<0.0005), whereas the LOD was calculated using the equation (3-2) and was equal to 108.63 pg mL^{-1}. Therefore, it was concluded that the sensor was responsive to the increasing concentration of morphine (100 pg mL^{-1} – 100 mg mL^{-1}) when the assay was carried out at the working pH of 7.4. Consequently, these conditions (buffer composition and pH) were considered optimal and were applied in further investigations.

To prove that the morphine was binding to the nanoMIP, the optimised morphine cumulative assay was replicated using control sensors (i.e., the sensor fabricated without the morphine nanoMIP) manufactured as outlined in Section 4.2.3. As shown in **Figure 4-7**, the increasing concentration of morphine (expressed in LOG10) induced the fluctuation of the sensor response between 5 and 25 -Δ %Rct and was not correlated to the increasing morphine concentration (r= 0.600; n=5; *p*-value= 0.250).

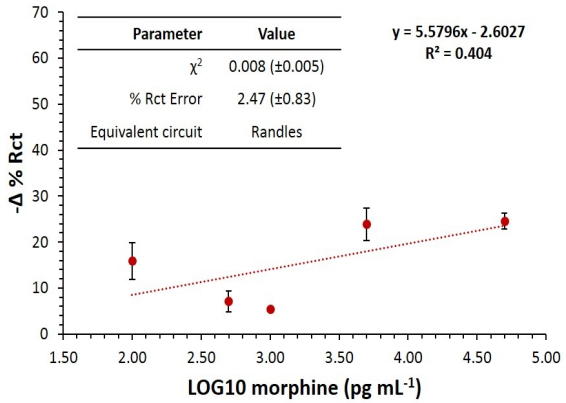

Figure 4-7: Linear calibration curve of the non-specific binding assay performed using morphine control sensor (fabricated onto SPE DPR C220AT). Error bars refer to the standard deviation of replicates (n=3).

Therefore, the result of this assay confirmed that the sensor surface functionalised with the morphine nanoMIP (2.4 mg mL^{-1}) was able to detect morphine under the optimised assay conditions.

4.3.1.3.2 Concentration Optimisation Study

To optimise the nanoMIP concentration, the attachment of the morphine nanoMIP was investigated using a lower concentrations, i.e. 1.2 mg mL^{-1} (suspended in 3:1 acetonitrile-water solution), thus assessing whether a lower concentration could be used for the morphine nanoMIP EIS sensor fabrication. Therefore, six sensor were fabricated using 1.2 mg mL^{-1} morphine nanoMIPs and according to the procedure outlined in Section 4.2.3 and the EIS measurements were used to characterise the manufacturing of the sensor, according to the procedure reported in Section 4.2.4.

The EIS data were fitted in the Randles equivalent circuit, achieving an average (±SD) % error of the Rct fitting of 4.04 % (±1.60) and a χ^2 of the equivalent circuit data fitting equal to 0.025 (±0.016). The Rct values were expressed as % of the MUDA Rct value, which was set at 100%. The resulting %Rct values were plotted in a bar chart and are shown in **Figure 4-8**.

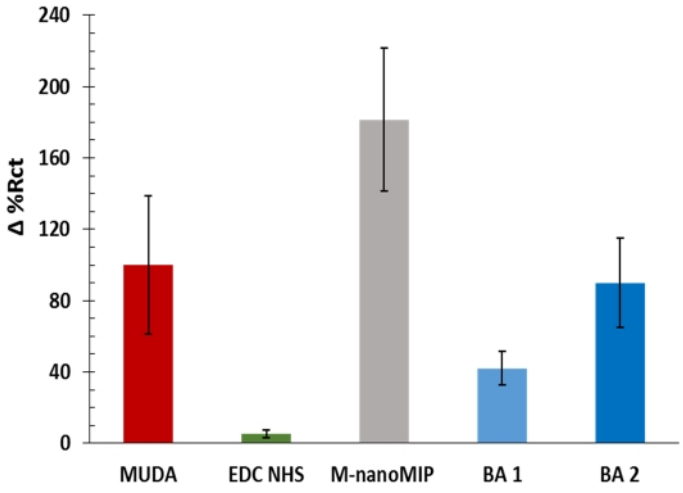

Figure 4-8: Average of Δ %Rct values (±SD) obtained at each morphine nanoMIP EIS sensor fabrication point using M- nanoMIPs at the concentration equal to 1.2 mg mL^{-1}. Error bars refer to the SD of the replicates (n=6). BA 1 = Ethanolamine pH 8.5; BA 2 = 0.1% BSA – 1% Tween 20.

The results revealed that the changes of the Δ %Rct values during the sensor fabrication were consistent with the results obtained in the EIS caracterisation study of the sensor fabricated using morphine nanoMIP at a concentration of with 2.4 mg mL^{-1} (Section

4.3.1.1). As the EIS attachment study revealed that a good sensor functionalisation was achieved using morphine nanoMIP at a concentration equal to 1.2 mg mL^{-1}, these group of sensors were used to perform the morphine cumulative according to the procedure described in Section 4.2.5.2 and under the optimised assay conditions (i.e., using 10 mM MOPS, pH 7.4). The aim of this experiment was to assess which concentration (i.e., 1.2 mg mL^{-1} and 2.4 mg mL^{-1}) allowed a better sensor sensitivity. The EIS measurements were performed according to the procedure described in Section 4.2.2. The morphine concentrations (50 µL, 100 pg mL^{-1} – 50 ng mL^{-1}) and the redox couple solution were all prepared in 10 mM MOPS at pH 7.4. This buffer solution was also used as the blank solutions (50µL) and the washing buffer (1.2 mL).

The EIS data (**Figure 4-9**) indicated that the Rct decrease as increasing concentration of morphine were tested. The fitting of the EIS data using Randles equivalent circuit yield to a χ^2 equal to 0.011 (± 0.006) and a %Rct error equal to 3.70% (± 1.74%), thus confirming the good fitting of the data into the selected model. The statistical analysis was carried out and revealed a positive correlation between the -Δ %Rct values and the morphine concentrations expressed as LOG10 (r=0.990; n=7; *p*-value < 0.0005). The R^2 of the linear calibration curve was equal to 0.979 (*p*-value < 0.0005) and the LOD, calculated using equation (3-2) was equal to 323.44 pg mL^{-1}. Therefore, the results showed that the sensor was able to detect morphine.

Overall, both the concentrations allowed a reproducible morphine nanoMIPs fabrication onto the gold working electrodes. However, a higher amount of the morphine nanoMIPs were immobilised onto the sensor surface when the 2.4 mg mL^{-1} nanoMIP concentration was used. Overall, a lower morphine nanoMIP concentration can still yield to the fabrication of an efficient sensor, but with less sensitivity and a higher LOD (323.44 pg mL^{-1}) compared to the morphine nanoMIP EIS sensor fabricated using a concentration of 2.4 mg mL^{-1} (LOD= 108.63 pg mL^{-1}). Therefore, in this study 2.4 mg mL^{-1} was considered the optimal morphine nanoMIP concentration for the sensor fabrication and was used in further studies.

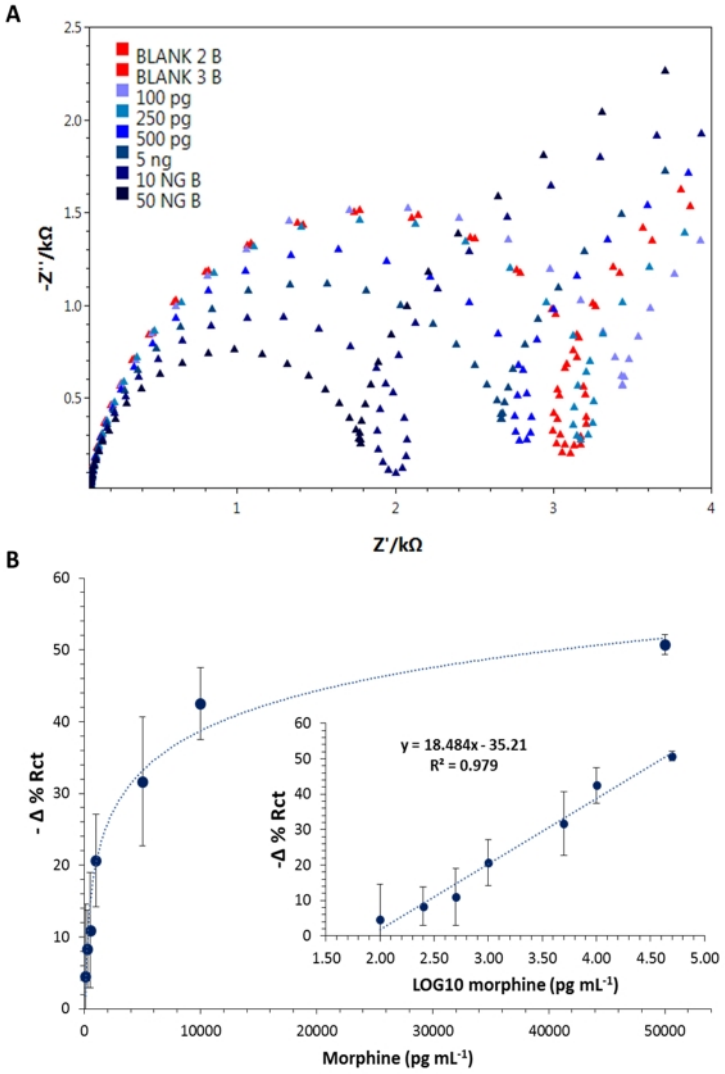

Figure 4-9: (A) Nyquist plot obtained during the morphine cumulative assay performed at pH 7.4 (100 pg mL^{-1} - 50 ng mL^{-1}) onto morphine nanoMIP EIS sensors. (B) The non-linear and linear (inset graph) calibration curves related to the morphine cumulative assay performed onto the morphine nanoMIP EIS sensor (fabricated on SPE DPR220AT). The sensors were fabricated using morphine nanoMIP at the concentration equal to 1.2 mg mL^{-1}. Error bars refer to the standard deviation of replicates (n=6).

4.3.1.4 Specificity Study

As highlighted by the World Drug Report released in 2017 (UNODC, 2017b), the cocaine and morphine are among the major abused and trafficked controlled drugs. Although they both belong to Schedule 2 drug class, it is important to discriminate between the two, as the penalties may vary according to the detected quantity. Therefore, the ability of the

optimised morphine nanoMIP EIS sensor to discriminate morphine from cocaine was investigated. Therefore, a new group of optimised sensor (n=6) were fabricated as outlined in Section 4.2.3. The cocaine was suspended in MOPS (pH 7.4) and concentrations in the range of 100 pg mL^{-1} - 100 ng mL^{-1} were prepared. The morphine nanoMIP EIS sensor response was thus investigated by performing a cocaine cumulative assay according to the optimised condition. The EIS data were fitted using Randles equivalent circuit. The data were fitted under the model achieving a low values of the % Rct error (0.005% ± 0.002%) and of the χ^2 (1.83 ± 0.45). The -Δ %Rct was obtained by processing the experimental data as described in Section 3.2.6.5.

The results indicated that the sensor response (-Δ %Rct) did not increase while increasing concentration of cocaine. To highlight the difference, the morphine nanoMIP EIS sensor response against cocaine and morphine were plotted together and are displayed in **Figure 4-10**.

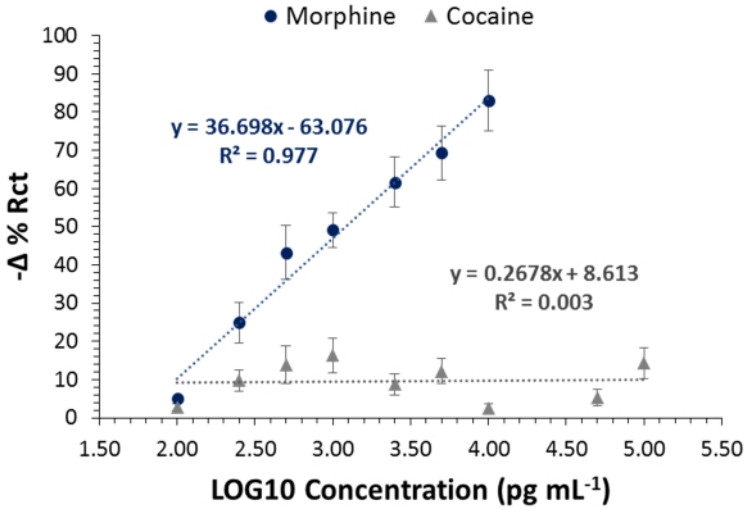

Figure 4-10: Comparison between the cocaine and the morphine linear calibration curves and related R^2 values.

The specificity of the optimised morphine nanoMIP EIS sensor was also assessed against one of the most abundant cutting agent occurring in the morphine and heroin street samples, i.e. paracetamol (Broséus *et al.*, 2015). Therefore, paracetamol cumulative assay was carried out at the optimised pH value (7.4) and at the concentration range used for

the cocaine cumulative assay (100 pg mL^{-1} - 50 ng mL^{-1}). The simplified Randles circuit was used to fit the experimental data and the data were analysed as described in Section 3.2.6.5. The low χ^2 (0.014 ±0.006) and of the %Rct Error (3.22% ±0.81) confirmed the goodness of the data fitting. The –Δ %Rct data were plotted against the paracetamol concentration (expressed as LOG10) and along with the sensor response obtained from the optimised morphine nanoMIP EIS sensor (**Figure 4-11**). The results of the linear regression analysis showed that the sensor response did not correlate with the increasing concentration of paracetamol (r= -0.048, n= 8, *p*-value- 0.911).

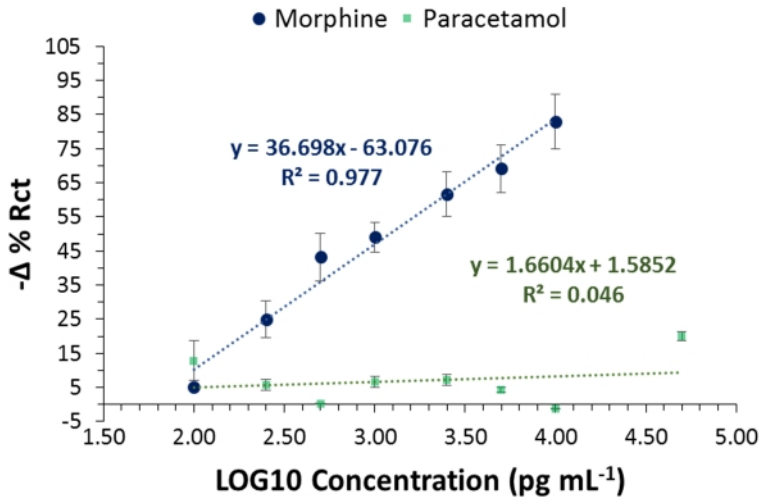

Figure 4-11: Comparison between the paracetamol and the morphine linear calibration curves and related R^2 values.

Overall, the results indicated that the optimised morphine nanoMIP EIS sensor is able to specifically detect morphine without cross-reacting with cocaine and paracetamol.

4.3.2 Evaluation Studies of Morphine NanoMIP Sensor onto DropSens IDE

The 3D printed CACIDE cable holder was available in the final design (as described in Section 2.4.1) and was used to perform the EIS measurements in all the DropSens experiments reported in this Chapter. Notably, the use of the cable holder successfully stabilised the connector electrode interface, thus allowing to perform the EIS measurement on all the investigated IDE electrodes without any loss of signal.

4.3.2.1 EIS Surface Characterisation Study

The optimised morphine nanoMIP sensor was fabricated according to the procedure outilined in Section 4.2.3 using DropSens interdigitated electrodes (IDEs, DPR IDEAu5), cleaned aacording to the optimised procedure (Section 2.4.3.2). Therefore, morphine nanoMIP, at a concentration of 2.4 mg mL^{-1} and suspended in a mixture 3:1 acetonitrile/water), were covalently immobilised onto the gold electrodes surface by amine coupling. The EIS analysis was performed at each fabrication step of the sensor assembly as described in Section 4.2.4. The redox couple solution (10 mM $[Fe(CN_6)]^{3-/4-}$) was prepared using 10 mM MOPS buffer at pH 7.4. The resulting EIS spectra are shown in **Figure 4-12** and are consistent with the results of the EIS characterisation studies performed on morphine nanoMIP sensor fabricated using DropSens SPE (Section 4.3.1.1).

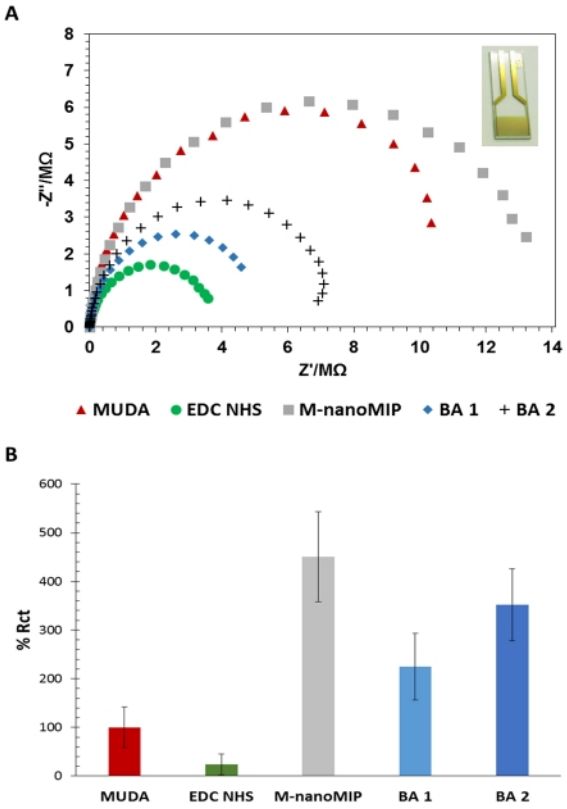

Figure 4-12: (A) Nyquist plots obtained during the steps of the morphine nanoMIP EIS sensor fabrication onto DropSens IDE. Morphine nanoMIP= 2.4 mg mL^{-1}; BA 2 = Ethanolamine pH 8.5; BA 1 = 0.1% BSA – 1% T20. (B) Bar charts of the Δ %Rct values and SD (±) obtained during the morphine nanoMIP EIS sensor fabrication onto SPE, using 2.4 mg mL^{-1} morphine nanoMIPs. BA 1 = Ethanolamine pH 8.5; BA 2 = 0.1% BSA – 1% T20. Error bars refer to the SD (±nm) of replicates (n=6).

The simplified Randles equivalent circuit was used to fit the experimental data as no diffusion process was evident in the EIS spectra. The % error value (±SD) of the Rct data fitting was equal to 4.69 % (±1.40), while the χ^2 of the equivalent circuit fitting was equal to 0.024 (±0.012). The obtained Rct value were expressed as % of the MUDA Rct value, set at 100%. The average value (±SD) of the %Rct obtained at each functionalisation point were plotted in a bar chat and are displayed in **Figure 4-12**.

Overall, the average value (±SD) of the %Rct related to morphine nanoMIP attachment step was lower compared to the average value (±SD) of the %Rct of the cocaine nanoMIP attachment step achieved during the fabrication of the cocaine nanoMIP EIS sensor onto DropSens IDE (section 3.3.2). These difference may be due to the lower nanoMIP concentration (2.4 mg mL^{-2}) used in the fabrication of the morphine nanoMIP EIS sensor and to the different composition between the two type of nanoMIPs (cocaine and morphine), as reported in Section 2.3.5 and 2.3.6.

4.3.2.2 AFM Surface Characterisation Study

The AFM surface characterisation study was carried out in tapping mode on the sensor surface fabricated using DropSens IDE. Three sensors were investigated on 400 μm^2 area and then a scan on 67.7 and 4 μm^2 were recorded. These were compared with the result of the AFM characterisation of the bare and MUDA functionalised IDE, discussed in section 3.3.2.1.1. The AFM 3D images (**Figure 4-13**) revealed a successful morphine nanoMIP immobilisation onto the electrodes surface. Morphine nanoMIP appeared as peaks onto the IDE, although the surface was not fully saturated.

The roughness analysis was carried out and the average values (±SD) of the roughness parameters (Rq and Ra) at different functionalisation steps (bare, MUDA, and nanoMIPs functionalised electrode) are provided in **Figure 4-14**.

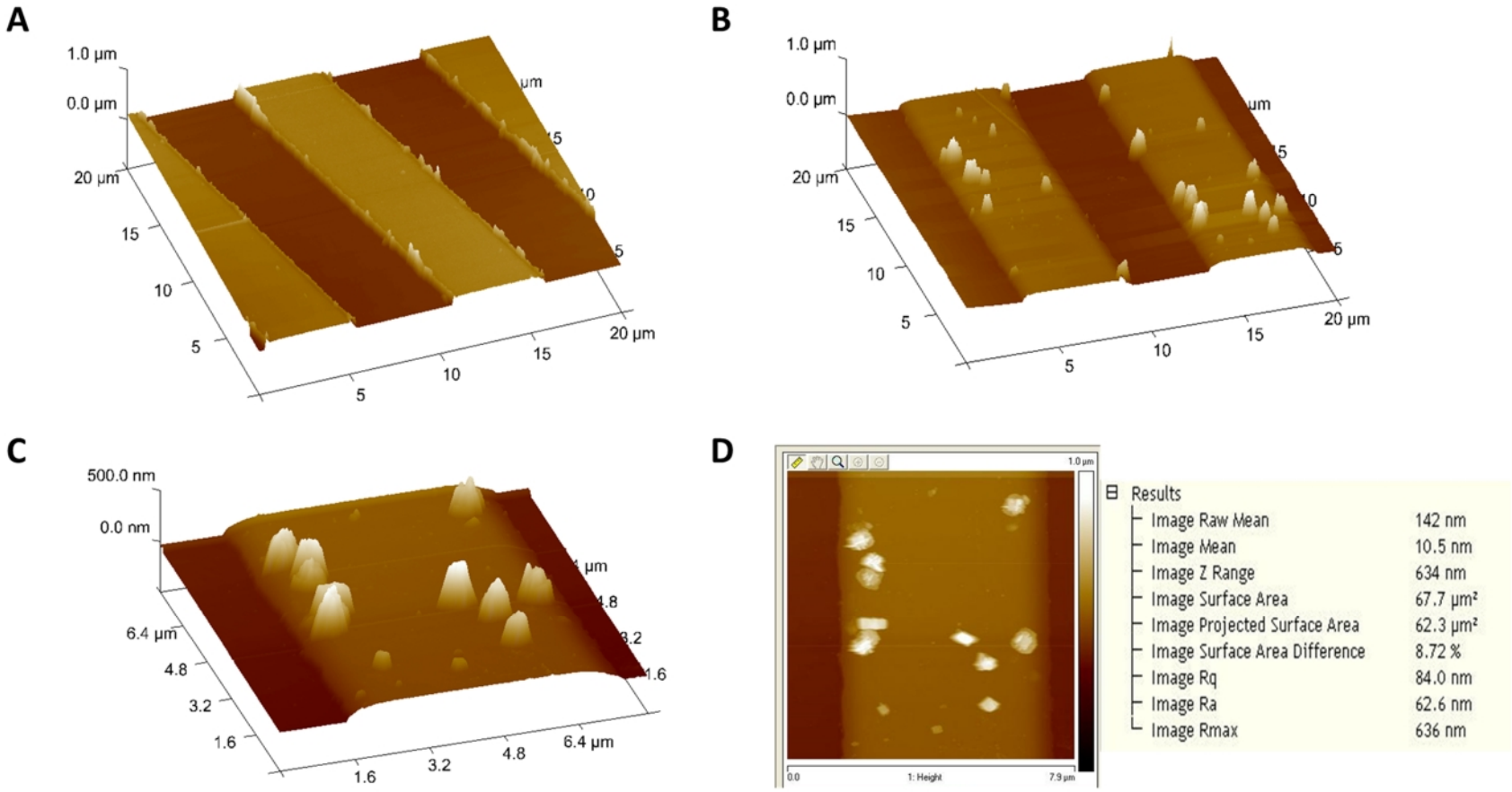

Figure 4-13: AFM 3D images of the surface topography of the (A) MUDA (400 µm^2 scan area, height 1 µm) and (B) morphine nanoMIP functionalised electrodes surfaces (400 µm^2 scan area, height 1 µm). (C) Morphine nanoMIP functionalised electrodes surfaces (67.7 µm^2 scan area, height 1 µm) and related (D) 2D image and roughness study.

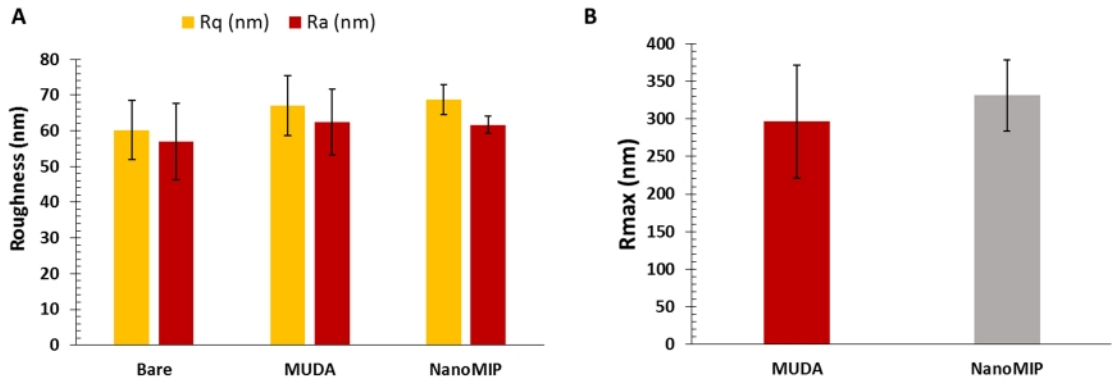

Figure 4-14: Bar charts of (A) Rq and Ra average values (±SD) obtained by AFM roughness analysis on bare, MUDA and morphine nanoMIP functionalised DropSens IDE; and (B) the average highest peak values (Rmax, nm) recorded onto the MUDA and the nanoMIP functionalised electrode. Error bars refer to the SD (±nm) of replicates (n=6).

Although visible on the 3D images of the sensor surface topography, significant differences in the Ra and Rq related to bare, MUDA and morphine nanoMIP functionalised sensor surface were not detected (p-value >0.05). Also, the difference in the highest peaks (Rmax) recorded onto the MUDA and the morphine nanoMIP functionalised sensor surface was not significant. The roughness analysis was affected by the limitations discussed in section 3.3.1.1 and 3.3.2.1 and proved to be less informative than the AFM 3D images of the sensor surface topography and of the results of the EIS characterisation study performed at the different functionalisation points.

4.3.2.3 Sensitivity Study and LOD Determination

The sensitivity of the optimised morphine sensor fabricated using IDE was evaluated by performing the morphine cumulative assay as optimised in Section 4.2.5.1. Therefore, a group (n=4) of optimised morphine nanoMIP EIS sensors were fabricated on the IDE using morphine nanoMIP at a concentration of 2.4 mg mL^{-1} and suspended in a solution of acetonitrile and water (3:1). As the IDE are considered more sensitive than SPE (Arya *et al.*, 2018), the investigated morphine (dissolved in 10 mM MOPS, pH 7.4) concentrations ranged from 10 pg mL^{-1} to 50 ng mL^{-1}. The EIS analysis was performed at each fabrication step of the sensor assembly as described in Section 4.2.4, using the

redox couple solution (10 mM [Fe (CN_6)]$^{3-/4-}$) prepared in MOPS buffr (10 mM, pH 7.4). The resulting EIS data (**Figure 4-15**) were fitted using the simplified Randles equivalent circuit.

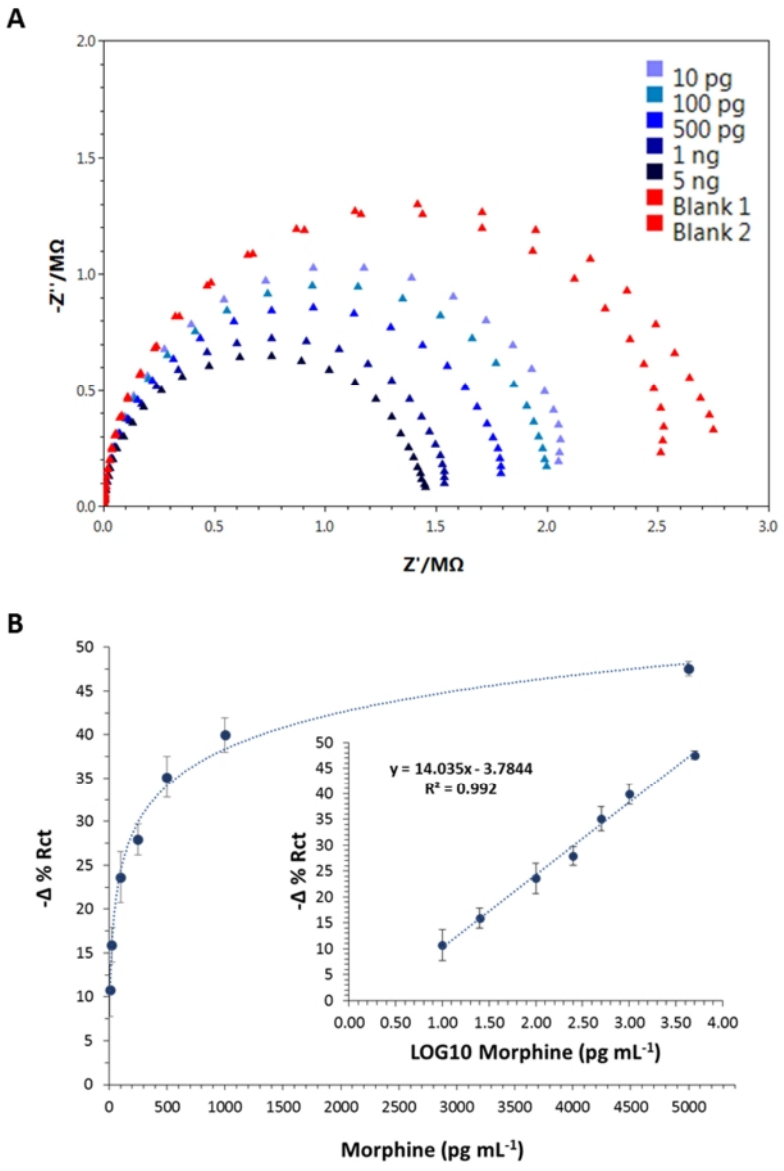

Figure 4-15: (A) Nyquist plots data obtained during the morphine cumulative assay performed at pH 7.4 (100 pg mL^{-1} - 50 ng mL^{-1}) using morphine nanoMIP EIS sensors (fabricated on IDE). (B) The non-linear and linear (insert graph) calibration curves related to the morphine cumulative assay performed onto the morphine nanoMIP EIS sensor (fabricated on DropSens IDE). The sensors were fabricated using morphine nanoMIP at the concentration equal to 2.4 mg mL^{-1}. Error bars refer to the standard deviation of replicates (n=4).

The achieved χ^2 and %Rct Error values (±SD) were equal to 0.0052 (± 0.0013) and 2.03% (±0.46), respectively, thus confirming the good fit of the selected model with the measured EIS data. The -Δ %Rct values were obtained according to the methods outlined in Section 2.3.2 and these values were plotted against the morphine concentrations, expressed as pg mL^{-1}. The results showed a positive correlation (r= 0.996; n= 7; *p*-value< 0.0005) between the sensor response (-Δ %Rct) and the morphine concentrations in the linear range of 10 pg mL^{-1} - 5 ng mL^{-1}. The saturation was observed at concentration above the 5 ng mL^{-1}. The non-linear and linear calibration curves were plotted and the R^2 of the calibration curve was equal to 0.992 (*p*-value< 0.0001). The LOD was calculated as described in Section 4.2.5.4 and was found to be as low as 114.01 pg mL^{-1}.

Therefore, both the morphine nanoMIP sensor developed on the IDE and the SPE achieved a similar LOD and were able to detect morphine at trace level.

4.3.3 Comparison of the Morphine NanoMIP EIS Sensors

All the optimised morphine nanoMIP EIS sensors fabricated onto the two different type of electrodes (SPE and IDE) were able to detect morphine at a very low concentration (< ng mL^{-1}). A summary of all the morphine nanoMIP EIS sensors performances achieved in this work is provided in **Table 4-4**.

Table 4-4: Summary of the features and performances of the morphine nanoMIP sensors investigated in this work.

Electrode	Format and configuration	Morphine nanoMIP (mg mL^{-1})	LOD (ng mL^{-1})	Linear range (ng mL^{-1})
DropSens – C220AT	SPE - three electrodes format	1.2	0.323 (860.57 pM)	0.1 - 50
	SPE - three electrodes format	2.4	0.109 (289.03 pM)	0.1 - 10
DropSens – IDEAu5	IDE - two electrodes format	2.4	0.114 (303.35 pM)	0.01 - 5

The LODs achieved using SPE (0.109 ng mL^{-1}) and IDE (0.114 ng mL^{-1}) were almost equal. However, the lowest detectable concentration achieved by the morphine nanoMIP sensor fabricated onto IDE was as low as 10 pg mL^{-1}, which highlights the possibility to improve the sensitivity of the sensor. Therefore, it is possible that that both the sensitivity and the linear range of the sensor developed onto IDE can be improved by increasing the concentration of the morphine nanoMIPs attached onto the sensor surface.

4.4 Discussion and Conclusion

The development of a highly sensitive nanoMIP EIS based sensor was presented in this chapter. The work considered the application of two type of electrodes, having a different geometry (interdigitated and round shaped working electrodes). Both of them achieved an outstanding LOD, which was slightly above 100 pg mL^{-1}. Results showed that the morphine nanoMIP EIS sensor fabricated on DropSens SPE can also be fabricated with a lower amount of nanoMIP (1.2 mg mL^{-1}). Even if the use nanoMIP concentration slightly increases the LOD to 323.44 pg mL^{-1}, the morphine nanoMIP EIS sensor can still be considered competitive with the current available on-site analytical tool, while reducing of the half the amount of the synthetic receptor needed to fabricate the sensor. Furthermore, the sensor surface showed a high specificity towards morphine, with minimal morphine non-specific bindings and negligible cross-reactivity against cocaine and paracetamol. More importantly, this work provides the further evidence that the MIP nanoparticles can successfully be combined to the EIS sensor platform, thus broadening the collection of nano-sensor solutions to detect morphine.

Several publications in the literature reported the development of bio-nano-sensor platforms to replace the presumptive and confirmatory methods currently in use to detect morphine. Most of the developed biosensors (**Table 4-5**) aimed to detect morphine in a biological sample (such as urine and plasma). Among them, the EIS immune-based sensor developed by Yang et al. (2014) achieved an outstanding LOD (0.27 pg L^{-1}), when morphine was suspended in a water-based solution. However, the sensor specificity was not assessed and the calibration curve was not shown. Compared to the LOD of morphine nanoMIP EIS sensor, Fei et al (2013) and Shcherbakova et al. (2017) achieved a lower value of LOD (67 pg mL^{-1}), but the specificity of the sensor was not tested in this study.

Other electrochemical sensors were based on voltammetry techniques that relied on the electroactive property of the morphine due to the oxidation of the phenolic group. The signal was enhanced by the use of a nanostructured sensor surface. However, the reported LODs were all above the LODs achieved in this work. Furthermore, The LODs of the morphine nanoMIP EIS sensors were greater than the LOD of the capacitive EIS sensor based on MIP film, recently developed by Vergara et al. (2016).

Table 4-5: Current biosensor platforms available to detect morphine in biological and environmental samples, the LOD and the linear range.

Detection tools Description	Sample	LOD (ng mL^{-1})	Linear range (ng mL^{-1})	Specificity test	Reference
Electrochemilumi nescent immunoassay CdS quantum dots and gold nanoparticles	Blood sample	0.067 (0.17 nM)	0.2 – 180 (0.53 – 475.1 nM)	N	(Fei *et al.*, 2013)
Capacitive –MIP Films	Aqueous based solution	2240 (5.91 µM)	7520 – 15030 (19.85 – 39.67 µM)	Y (Nicotine, cholesterol	(Vergara *et al.*, 2016)
Differential Pulse Voltammetry aptamer	Aqueous based solution	3.76 (9.92 nM)	18.8 - 187920 (49.62 nM – 496 µM)	N	(Talemi and Mashhadizadeh, 2015)
Cyclic Voltammetry (CV) CdO NPs	Aqueous based solution	37.58 (99.19 nM)	187.92 – 300672 (496 nM – 794 µM)	Y (paracetam ol)	(Cheraghi, Taher and Karimi-Maleh, 2016)
Square Wave Voltammetry (SWV) MIP- Au - MWCNTs	Aqueous based solution, human urine and plasma	0.71 (1.87 nM)	3 – 2000 (7.92 nM – 5.28 µM)	Y (various plasma interferenc es)	(Rezaei, Foroughi-Dehnavi and Ensafi, 2015)
Differential Pulse Voltammetry (DPV) Chitosan Fe_3O_4 NPs	Urine	1.13 (2.98 nM)	3.76 - 751.68 (9.92 nM - 1.98 µM)	Y (blood interferenc es)	(Dehdashtian *et al.*, 2016)
EIS immunosensor	Spiked serum	$2.7x10^{-7}$ (0.7 fM)		N	(Yang *et al.*, 2014)
Chemosensor (fluorescence)	Human urine	0.07 (0.18 nM)		N	(Shcherbakova *et al.*, 2017)
nanoMIP EIS sensor	Aqueous based solution	0.109 (0.29 nM) (SPE) 0.114 (0.30 nM) (IDE)	0.1 - 10 (0.26 – 26.39 nM) (SPE)0.01 - 5 (0.03 – 13.2 nM) (IDE)	Y (cocaine, paracetam ol)	This work
SPR MIP film	Morphine in DMF/ACN (1:99)	0.001 (2.64 pM)	0.3 – 300 (0.79 nM – 791.85 nM)	Y (codeine)	(Hao *et al.*, 2014)

The specificity study carried out on morphine nanoMIP EIS sensor developed onto SPE demonstrated the sensor ability to discriminate morphine from cocaine and paracetamol. The ability of the sensor in discriminating the morphine from cocaine when the two drugs occurred in the same samples is a valuable feature as it overcomes the false negative results associated with the use of other screening analytical tools, such as the IMS (Verkouteren and Staymates, 2011). The ability to discriminate morphine from

paracetamol is desired in both counteracting doping and illicit drugs trafficking activities. For instance, paracetamol is not considered a doping substance, but it is often detected as an opioids adulterants.

In a recent work, Cheraghi et al. (2016) developed an electrochemical nano-sensor based on cyclic voltammetry technique able to concurrently detect paracetamol and morphine. However, the achieved LOD for morphine (37.58 ng mL^{-1} or 0.1 µM) was higher than the LODs of the morphine nanoMIP sensors developed in this work. Furthermore, and the specificity against other drugs of abuse was not tested in the work of Cheraghi et al. (2016). Hao et al. (2014) fabricated an SPR sensor based on MIP film and able to detect morphine at a concentration as low as 0.001 ng mL^{-1}. However, the calibration curve was shown without the standard deviation. Furthermore, the MIP SPR was able to detect morphine free-base dissolved in organic solvent (1:99 DMF and acetonitrile). Since the morphine is mostly trafficked and consumed in the morphine hydrochloride (which is the salt form and soluble in water), the application of the MIP SPR biosensor still require a sample preparation step, thus increasing the analysis time.

As a final remark, the developed morphine nanoMIP sensor promises to detect morphine with the same or greater sensitivity and specificity compared to the presumptive and confirmatory methods currently in use to test real sample and reported in **Table 4-6**.

Table 4-6: Conventional analytical tools available to detect morphine in biological and environmental samples, the LOD and the linear range.

Detection tools Description	Sample	LOD (ng mL^{-1})	Linear range (ng mL^{-1})	Specificity test	Reference
IMS-MS	Urine	0.1 (0.26 nM)	0.44-22 (1.16 – 58 nM)	-	(Rudnicka and Mochalski, 2010)
Immune-based device	spiked urine samples	5 (13.2 nM)		N	(Gandhi *et al.*, 2018)
RP-HPLC	Urine	50	150 – 2000	-	(Ruzilawati *et al.*, 2013)
LC MS-MS	Oral fluid	0.5 (1.32 nM))	1-100 (2.64 - 264 nM)	-	(Liu *et al.*, 2015)
GC-MS	Urine	50 (132 nM)	50 – 50000 (132 nM – 132 µM)	-	(Rana, Garg and Singla, 2014)

Chapter 5
Development of NanoMIPs QCM Sensors for Drugs of Abuse Detection

5.1 Introduction

This chapter will report and discuss the results related to the development of the cocaine and morphine nanoMIP sensor by means of quartz crystal microbalance (QCM) biosensor platform. Gold nanoparticle (AuNP) were used as signal enhanced technique and the nanoMIPs were applied as sensor receptor. The final aim of this work was to confirm the results achieved for the EIS sensor through the use of a sensor platform with a fully automated microfluidic system, such as the QCM instrument used in this work. This type of sensor platform can also be used for a lab-based test for drugs of abuse detection

The QCM signal arises from a resonant frequency shift due to the mass changes at the sensor interface, such as due to the receptor-analyte binding. The viscosity and density variations induce the change in the oscillation frequency of the quartz wafer embedded between two electrodes. While the QCM based biosensor usually works well in detecting analyte with high molecular weight (such as microorganism, proteins or DNA sequences), it often requires signal enhanced techniques to detect small molecules, such as small peptides, drugs, toxins and other small molecular weight molecules (Thies *et al.*, 2017). With this respect, nowadays a wide range of nanomaterials can be used to enhance the QCM sensitivity (Skládal, 2016). One of the most explored is the labelling with gold nanoparticle (AuNPs), which also has biocompatibility properties (Fenzl, Hirsch and Baeumner, 2016; Masdor, Altintas and Tothill, 2016). Due to the small molecular weight of both cocaine hydrochloride (339.81 g mol^{-1}) and morphine hydrochloride monohydrate (378.86 g mol^{-1}), the labelling with AuNPs was applied to enhance the QCM sensor response.

Furthermore, nanoMIP receptors were used in this work as they hold several advantages compared to other two widely used receptors in the affinity sensors development, such as antibody and aptamer. NanoMIPs are not affected by enzymatic degradation, being made by synthetic materials. Furthermore, NanoMIP has higher thermal and environmental stability, long lasting shelf-life, reduced production cost compared to both antibody and aptamer. Furthermore, they do not require animals for their production and benefit of nanomaterial properties.

Whereas the evaluation of the cocaine and morphine nanoMIP QCM sensors will be

discussed separately for each drug, the combination of the two sensors use paves the way to multiplexing, yet sensitive and specific, nanoMIP QCM sensor for drugs of abuse detection.

The final QCM sensor will be developed in a competitive assay format, thus allowing the detection of the un-labelled drugs occurring in the sample. As shown in **Figure 5-1**, the nanoMIPs (such as morphine nanoMIP) will be immobilised onto the gold QCM sensor chip and then surface will be exposed to an optimised mixture of unknown samples and AuNPs conjugated drug (morphine). The un-labelled morphine occurring in sample (if any) will compete with the AuNPs conjugated morphine at the morphine nanoMIP sensor surface, thus decreasing the sensor response compared to the negative control response (nanoMIP exposed to only AuNPs conjugated morphine). Furthermore, the level of sensor signal suppression will be used to quantify the un-labelled drugs occurring in the sample.

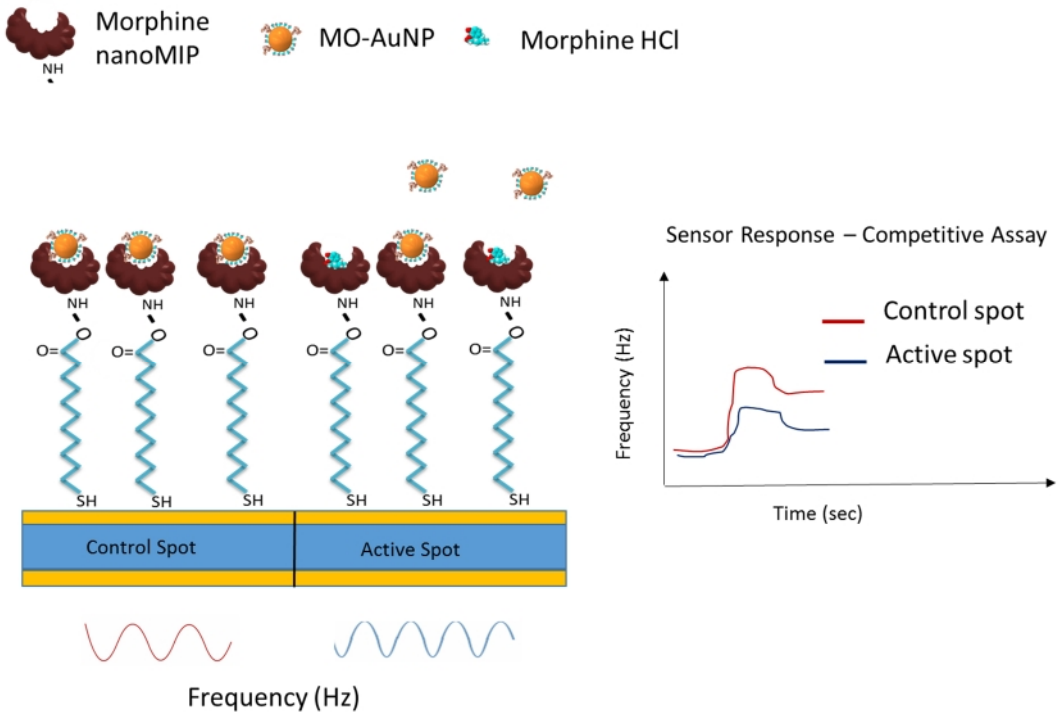

Figure 5-1: Schematic of the competitive assay for morphine detection for the development of the morphine nanoMIP QCM sensor.

5.2 Materials and Methods

5.2.1 Materials

All chemicals used in this Chapter were purchased as reported in Section 4.2.1 (Chapter 4), including the supply of cocaine and morphine nanoMIP. Tris Buffer, Sodium Chloride (NaCl), were purchased from Sigma-Aldrich Ltd (Dorset, UK). A 40 nm gold colloidal (AuNPs, ~7.2^{10} particles/mL, OD =1), suspended in 0.1 mM PBS. All the solutions were filtered with 0.2 µm syringe filter prior their use. All the buffers prepared for QCM experiments were degassed before use. All the solutions used were filtered through filter system by means of Whatman® nitrocellulose filter 0.2 µm (Whatman International Ltd, Maidstone, UK) or by 0.2 µm Corning® syringe filter (Corning Inc., New York, US). All nanoMIPs solutions were filtered with 0.45 µm Corning® syringe filter (Corning Inc., New York, US).

5.2.2 Equipment and Software

QCMA-1 affinity sensors chip and the biosensor instrument used in this work were purchased from Sierra Sensors GmbH (Hamburg, Germany) and are illustrated in **Figure 5-2**.

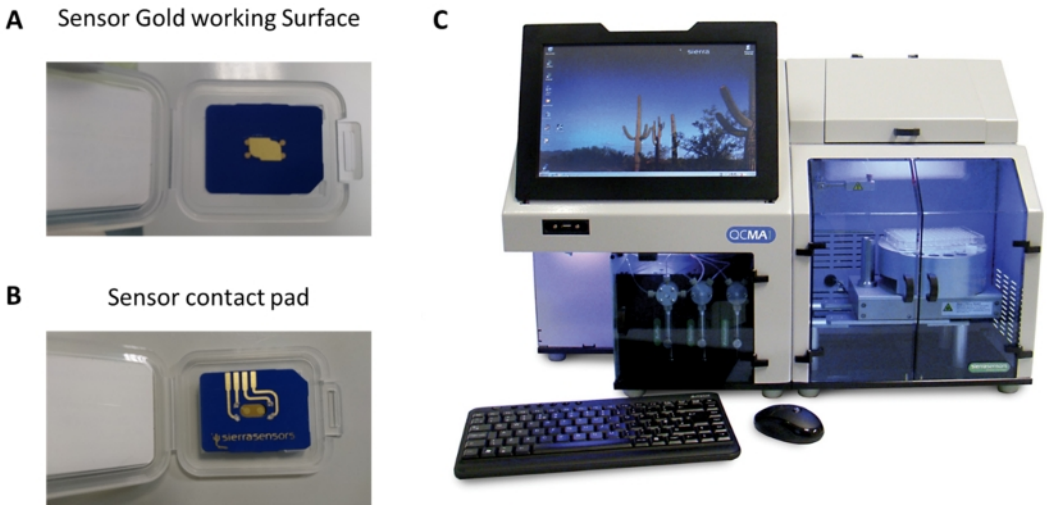

Figure 5-2: QCMA-1 affinity sensors: A) Top view of the gold working surface; B) Top view of the sensor contact pad and the two sensor array spots. C) The QCM biosensor platform.

The dedicated software Sierra Analyser v.3.1.10.0 (Sierra Sensors GmbH, Germany) was used to process the data. Surface characterisation studies were performed by AFM (Dimension 3100, Bruker, US), while Dynamic Light Scattering (DLS - Zetasizer Nano-S, Malvern Instruments Ltd, UK) was used to carry out all the DLS studies. Statistical analysis was performed by means of Excel (Microsoft®) and/or IBM SPSS statistics 24.0.0.1 (IBM Copr. ®).

5.2.3 Drugs of Abuse AuNPs Conjugation

Cocaine hydrochloride and morphine hydrochloride trihydrate were conjugated to 40 nm gold nanoparticles (AuNPs) according to a protocol developed at Cranfield Health (Uludag and Tothill, 2012; Salam, Uludag and Tothill, 2013; Altintas *et al.*, 2016; Masdor, Altintas and Tothill, 2016).

A 1 mL of gold AuNPs suspension was placed into an Eppendorf tube and the surface was activated by adding 5 µl of 0.2 M NaOH. The solution was gently mixed for 1 minute. Afterwards, 40 µL cocaine hydrochloride or morphine hydrochloride trihydrate (1 mg mL^{-1}) dissolved in PBS (pH 7.4) was added to the AuNPs activated solution. The tube was covered with aluminium foil to prevent photodegradation event. The mix was then incubated at room temperature for 60 minutes, under gentle shaking (30 rpm). Subsequently, the mixture was centrifuged at 10,000 rpm for 30 minutes, setting the temperature at 4°C. The supernatant was discarded and 33 µL of BSA 1 mg mL^{-1} were added to block the surface for 10 minutes. The tube was again centrifuged for 10 minutes at 10,000 rpm. Finally, the supernatant was discarded and 1 mL of double distilled water was used to suspend the cocaine conjugated AuNPs (cocaine AuNPs) or the morphine-conjugated AuNPs (morphine AuNPs). Since the bare gold nanoparticles tend to agglomerate in a salt solution, the success of the conjugation was assess by adding 5 µL of each conjugated AuNPs in 100 µL tris buffer in an Eppendorf and then adding 20 µl of 2.5 M NaCl. The absence of any flocculation or colour changes proved the success of the conjugation step.

The same procedure was applied to produce blank AuNPs, without adding the drugs of abuse into the activated AuNPs suspension. The blank AuNPs solution was used as

negative conjugation control as well as a blank solution for the cocaine and morphine cumulative assays. The PBS (pH 7.4) was used to suspend the morphine AuNPs, cocaine AuNPs, and the blank AuNPs, when they were used to perform the cumulative assay. A schematic of the bare, blank and conjugated AuNPs are reported in **Figure 5-3**.

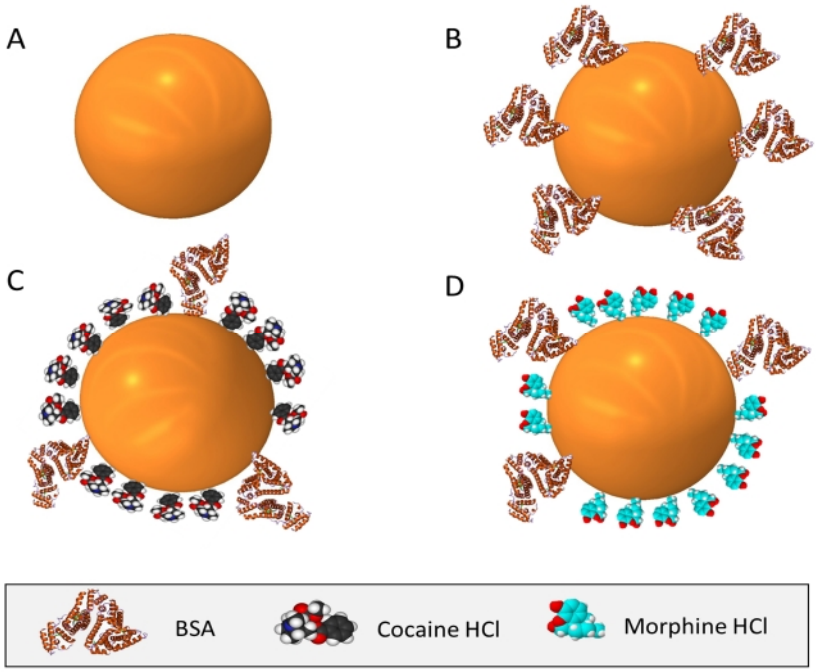

Figure 5-3: (A) Bare gold nanoparticle; (B) Blank gold nanoparticle (Blank AuNP), blocked with BSA (Bovine Serum Albumin); (C) Cocaine conjugated gold nanoparticles (cocaine AuNP); (D) Morphine conjugate gold nanoparticle (morphine-AuNP).

5.2.3.1 DLS Characterisation Study

DLS analysis was used to assess the success of the conjugation. Concisely, the bare AuNPs, blank AuNPs, cocaine AuNPs and morphine AuNPs were all suspended in doubled distilled water and analysed by means of DLS. All measurements were performed having gold nanoparticles as reference materials and water as eluent. At least ten measurements were recorded per each sample. Notably, each measurement given by the instrument was the average of 20 measurements. The data were collected and statistically analysed to reveal differences in the d_H (nm) size between across the investigated samples. With this respect, one-way ANOVA test with Sheffe's post hoc test was applied.

5.2.4 QCM Gold Chip Cleaning

The surface of the gold QCM chip was cleaned by means of the piranha solution. Briefly, the gold surface of used or new QCM chip was covered with few mL of the freshly made piranha solution (3:1 H_2SO_4:H_2O_2). After 15 minutes, the piranha solution was carefully discarded and the surface washed with a large amount of double filtered deionised water until the neutralisation was reached. The gold surface was then rinsed with ethanol and dried under a gentle stream of nitrogen.

5.2.5 Drugs of Abuse NanoMIPs QCM Sensor Assembly

The cleaned QCM gold chip was incubated into 50 mL solution of 50 mM 11-MUDA dissolved in pure ethanol overnight and in dark conditions. Subsequently, the chip was rinsed with ethanol, dried with nitrogen and docked into the QCMA-1 instrument. The functionalisation of the QCM sensor surface was performed having PBS (pH 7.4) as a running buffer (degassed and filtered), while the flow rate was kept fixed at 25 µL min^{-1} for the whole procedure. To perform the nanoMIP functionalization, a protocol previously developed at Cranfield Health was used (Salam, Uludag and Tothill, 2013; Abdin, Altintas and Tothill, 2015; Masdor, Altintas and Tothill, 2016). Briefly, the MUDA carboxylic groups were activated by injecting 100 µL of a freshly mixed EDC/NHS solution (0.4 M EDC and 0.1 M NHS dissolved in water) for four minutes at a flow rate of 25 µL min^{-1}. Then, 100 µL of morphine nanoMIPs (1.2 mg mL^{-1}) suspended in PBS (pH 7.4) was injected for other four minutes onto spot 1 (at a flow rate of 25 µL min^{-1}), thus allowing the attachment via amine coupling. Soon after, 100 µL of cocaine nanoMIPs (1.8 mg mL^{-1}) was injected onto spot 2, thus obtaining the nanoMIPs QCM sensor. The non-reacted carboxyl groups were capped by injecting 75 µL of ethanolamine (1 M, pH 8.5) in PBS for three minutes (at a flow rate of 25 µL min^{-1}).

The fabricated nanoMIPs-QCM sensor was used to test the morphine (morphine sensing mode), when the spot functionalised with morphine nanoMIP was set as the active spot and the spot functionalised with cocaine nanoMIP acted as control spot. When the spots setting was inverted (cocaine nanoMIP = active spot; morphine nanoMIP = control), the nanoMIPs- QCM was used to test cocaine (cocaine sensing mode). A schematic of the nanoMIPs-QCM sensor is presented in **Figure 5-4.**

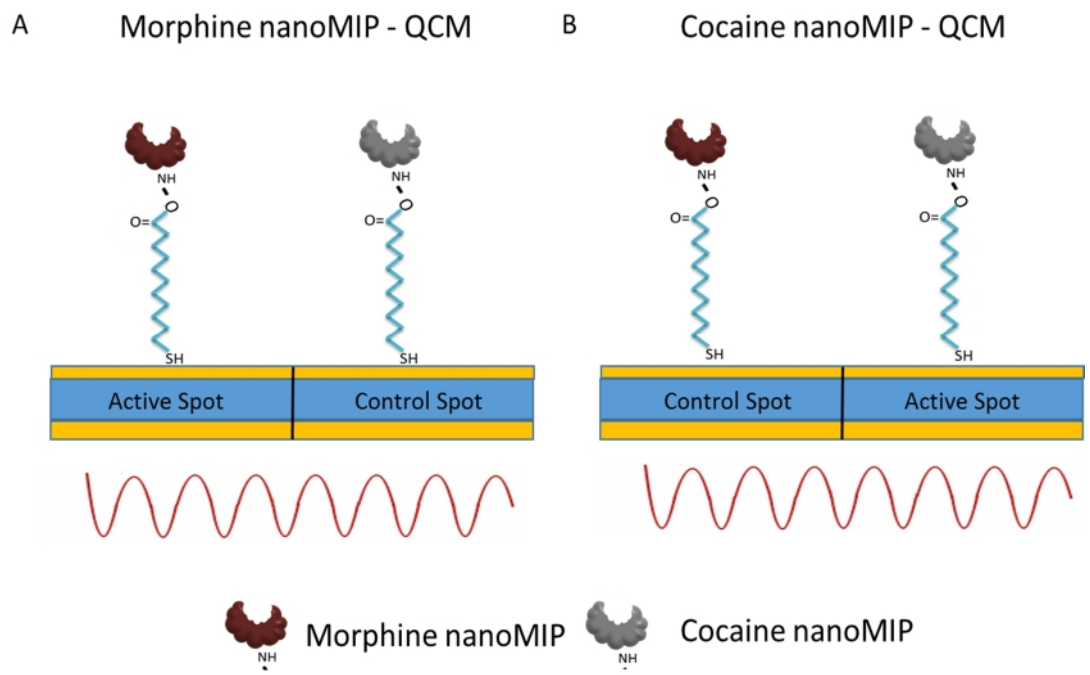

Figure 5-4: Schematic of the nanoMIPs QCM sensor in the format of (A) morphine and (B) cocaine sensing mode. (A) Morphine nanoMIP immobilised on the spot 1 (active spot) and the cocaine nanoMIP immobilised on the spot 2 (control spot). (B) Cocaine nanoMIP immobilised onto the spot 1 (active spot) and the morphine nanoMIP immobilised on the spot 2 (control spot).

5.2.5.1 Optimisation Study of the NanoMIPs Concentration

The optimal concentration of the nanoMIPs were achieved when the spot was considered saturated, i.e. the QCM frequency (Hz) response achieved a steady-state upon nanoMIPs injection. However, as the compositions of the two type of nanoMIP were different, it is unlikely that the same concentration can be used to saturate the spot. Therefore, different concentration were used to perform the experiments.

5.2.5.2 AFM Characterisation Study

The surface of the drugs of abuse nanoMIPs QCM sensor was characterised using AFM analysis. Specifically, The QCM chip was functionalised with MUDA and was analysed by AFM. Then, the same QCM chip was functionalised with morphine nanoMIP onto spot 1 and with cocaine nanoMIP on spot 2. The thus fabricated nanoMIPs QCM sensor was investigated by AFM. Results of the AFM analysis were compared to assess the goodness of the fabrication process. Prior to the analysis, the QCM chip surface was

thoroughly rinsed with deionised water filtered 0.2 µm syringe filter and dried under a gentle stream of nitrogen.

5.2.6 Sensitivity Studies of the Morphine NanoMIP QCM Sensor

To assess the sensitivity, the morphine AuNPs cumulative assay was performed on nanoMIPs QCM sensor, operating in morphine sensing mode. Briefly, morphine nanoMIPs were immobilised onto spot 1 (active) and cocaine nanoMIPs were immobilised onto spot 2 (control). The temperature was set at 25°C and the flow rate was kept as 25 µL min^{-1} throughout the assay duration. The assay was performed having PBS (pH 7.4) as the running buffer.

The nanoMIPs QCM sensor chip was docked into the QCM instrument and was primed several times with the selected running buffer until a stable sensor baseline was reached. Serial dilutions of morphine conjugated AuNPs (250 ng mL^{-1} - 50 µg mL^{-1}) were prepared using PBS (pH 7.4) as diluent. At least three injections of the blank solution were performed and until a stable blank signal was achieved. The blank solution was composed of bank AuNPs suspended in PBS (pH 7.4), produced as described in Section 5.2.3. Then, 100 µL of increasing concentrations of morphine conjugated AuNPs were injected onto both spots 1 and 2 for four minutes at the flow rate of 25 µL min^{-1}. The QCM sensor response, in terms of frequency (Hz), was recorded in a time solved mode. The data were collected and analysed using the dedicated software, Sierra Analyser v.3.1.10.0. The sensor response was subtracted from the control and blank signals and expressed in frequency (Hz). Then, the value of frequency recorded at the end of each injection was subtracted from the frequency value recorded before the injection, thus achieving the actual change of the sensor response, ΔF (Hz). The ΔF values were plotted versus the increasing concentrations of morphine, thus obtaining the non-linear calibration curve. By transforming the concentrations values to LOG10, the linear regression curve was achieved. The ΔF was then expressed as % of the highest ΔF (Hz) value obtained during the assay.

$$\% \, \Delta F = \frac{\Delta F_x}{\Delta F_{max}} \times 100 \tag{5-1}$$

The average (±SD) of the % ΔF values was then plotted against the increasing concentration of morphine, thus obtaining the standardised non-linear calibration curve. The concentration transformed to LOG10 was used to achieve the standardised linear calibration curve. A schematic of the morphine cumulative concentration assay is displayed in **Figure 5-5**.

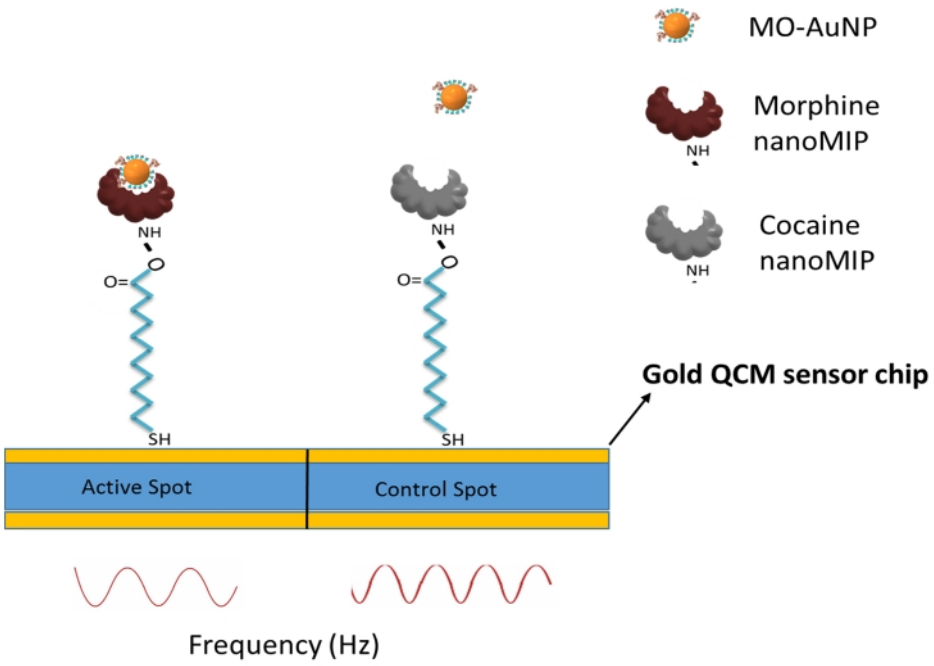

Figure 5-5: Schematic of the morphine AuNPs cumulative assay performed on the nanoMIPs QCM sensor operating in morphine sensing mode. A change in resonance frequency (Hz) is expected upon the binding between morphine conjugate AuNP (MO-AuNP) and the morphine nanoMIP.

5.2.7 Sensitivity Studies of the Cocaine NanoMIP QCM Sensor

The sensitivity study of the cocaine nanoMIPs QCM sensor was tested by performing the cocaine AuNPs cumulative assay. The morphine and cocaine nanoMIP were immobilised as discussed in Section 5.2.6, where the morphine nanoMIPs were immobilised onto spot 1, which was set as control spot. Cocaine nanoMIPs were immobilised onto spot 2, which was set as active spot. The instrument setting and the operating procedure of the cocaine AuNP cumulative assay were as described in section 5.2.6. The cocaine AuNPs

cumulative assay was performed using increasing concentrations of cocaine AuNPs prepared in PBS (pH 7.4) and ranging from 250 ng mL^{-1} - 50 µg mL^{-1}.

The data were collected and analysed using the dedicated software, Sierra Analyser v.3.1.10.0 and were processed as discussed in section 5.2.6. A schematic of the morphine cumulative concentration assay is displayed in **Figure 5-6**.

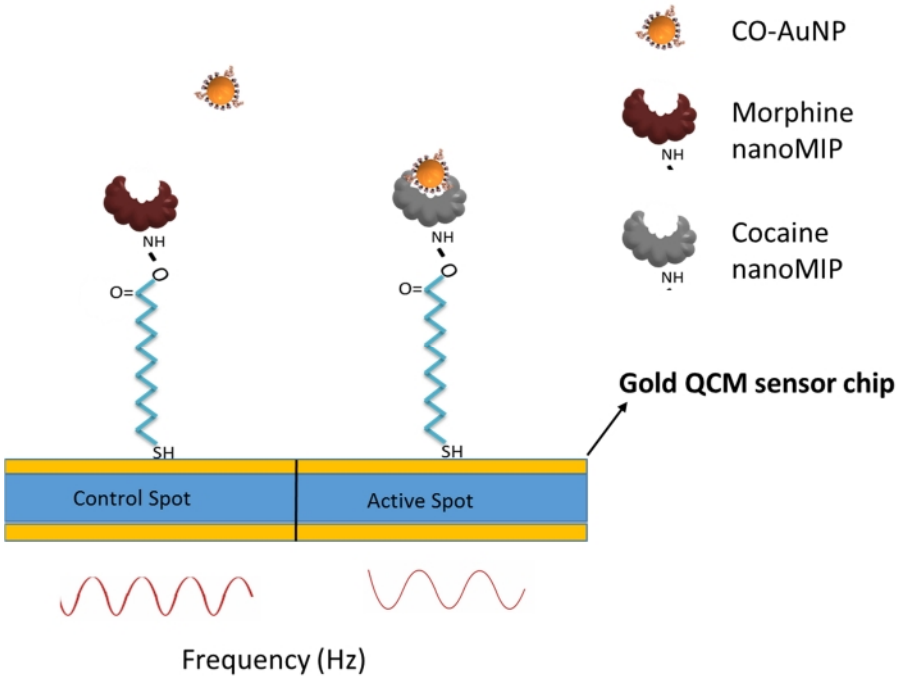

Figure 5-6: Schematic of the cocaine AuNPs cumulative assay performed onto the nanoMIPs QCM sensor operating in cocaine sensing mode. A change in resonance frequency (Hz) is expected upon the binding between cocaine conjugate AuNP (CO-AuNP) and the cocaine nanoMIP.

5.2.8 LOD and Kinetic Studies

The LOD was calculated as three times the standard deviation of the blank signal and by interpolating this value using the calibration curve, according to equation (3-2). The affinity between the nanoMIPs and the analyte was also assessed by performing a binding kinetic study with the aid of Sierra Analyser 3.1.10.0 and applying the Langmuir 1:1 model.

5.2.9 Morphine NanoMIP QCM Sensor Regeneration Study

The regeneration study of the morphine sensor surface was investigated by means of several regeneration buffer. It has been reported that both acid or basic solutions can be useful to remove the attraction forces between the analyte and the receptor, thus regenerating, while preserving, the sensor surface (Goode, Rushworth and Millner, 2015). Therefore, several combinations of regeneration solutions were tested as reported in **Table 5-1** and injected at a flow rate of 25 µL min^{-1}. The regeneration experiments were performed having PBS (pH 7.4) as a running buffer (degassed and filtered), while the flow rate was kept fixed at 25 µL min^{-1}.

Table 5-1: List of regenerations buffer and condition usd during the regeneration study of the morphine nanoMIP QCM sensor surface.

ID	Solutions	Concentration (mM)	Injection (µL)
2	HCl	100	25
3	Glycine hydrochloride	100	25
4	NaOH	10	25
5	HCl	500	25
	NaOH	10	25
7	NaOH	10	50
	60^0C doubled distilled water	-	100
8	NaOH	10	75
	PBS pH 7.4	10	100
9	NaOH	10	50
	HCl	500	50

5.2.10 Data Collection Statistical Analysis

Data of each experiment were collected, recorded on an Excel® database spreadsheet and identified by a unique code. Statistical analyses were carried out with the aids of by Microsoft® Excel® and IBM® SPSS® Statistics 24.0 software. Descriptive statistic and related plots were used to present the results. The significance level (*p-value*) was set at 0.05. Both parametric and non- parametric statistics were applied as appropriate. Specifically, the one-way ANOVA test and *post-hoc* analysis have been applied to assess any difference between two or more datasets and related contrasts.

5.3 Result and Discussion

5.3.1 Druga of Abuse AuNPs Conjugation

The QCM biosensor platform is not sensitive for the detection of small molecule, such as drugs (Thies *et al.*, 2017). In order to increase the molecular mass of the drugs and enhance the biosensor signal, the drugs were conjugated to gold nanoparticles (AuNPs) (Altintas, Guerreiro, *et al.*, 2015; Masdor, Altintas and Tothill, 2016). The full procedure is reported in Section 5.2.3. The success of the AuNP conjugation were investigated by DLS analysis. Briefly, at least ten DLS measurements of the bare AuNPs, the blank, the cocaine and morphine conjugated AuNPs were recorded. The one-way ANOVA test with Sheffe's *post hoc* test was applied to highlight the difference and contrast of the d_H among the samples. As shown by the results reported in **Figure 5-7** and **5-8**, the average of the hydrodynamic diameter size differed among the samples.

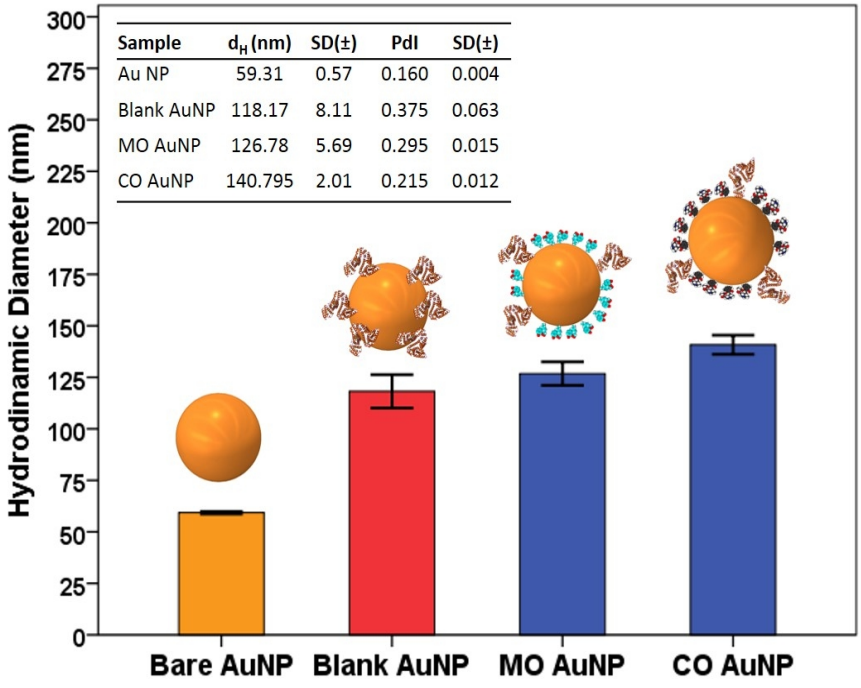

Sample	d_H (nm)	SD(±)	PdI	SD(±)
Au NP	59.31	0.57	0.160	0.004
Blank AuNP	118.17	8.11	0.375	0.063
MO AuNP	126.78	5.69	0.295	0.015
CO AuNP	140.795	2.01	0.215	0.012

Figure 5-7: Average of d_H values observed for bare AuNP, Blank AuNP and morphine conjugated AuNP (MO AuNP) and cocaine conjugated AuNP (CO AuNP) obtained by DLS analysis. Error bars refer to the standard of replicates (n=10). Inset table reports the average (±SD) of the d_H and related PDI values.

Specifically, the d_H of the blank AuNPs (118.17 ± 8.11 nm) was bigger than the bare AuNPs (59.31 ± 0.57 nm) and slightly smaller than the morphine conjugated AuNPs (126.78 ± 5.69 nm). Notably, the bare AuNPs average d_H size was slightly bigger than the 40 nm declared by the manufacturer due to possible spontaneous aggregation occurring in water solution. As reported in **Figure 5-8**, the one-way ANOVA test confirmed that the differences between the bare, blank and morphine conjugated AuNP samples were significant ($F(2,38)=535.071$; p-value< 0.00001). Furthermore, the Sheffe's *post hoc* test revealed that, on average, morphine AuNPs were 67.47 nm and 8.60 nm bigger than the AuNPs and blank AuNPs, respectively.

A

ANOVA

d_H (d.nm)

	Sum of Squares	df	Mean Square	F	Sig.
Between Groups	34082.804	2	17041.402	535.071	0.000
Within Groups	1210.257	38	31.849		
Total	35293.061	40			

B

Multiple Comparisons

Dependent Variable: d_H

	I Sample	J Sample	Mean Difference (I-J)	Std. Error	Sig.	95% Confidence Interval Lower Bound	95% Confidence Interval Upper Bound
Scheffe	AuNPs	Blank AuNPs	-58.86	2.47	0.00	-65.15	-52.58
		MO AuNPs	-67.47*	2.12	0.00	-72.87	-62.07
	Blank AuNPs	AuNPs	58.86*	2.47	0.00	52.58	65.15
		MO AuNPs	-8.60*	2.19	0.00	-14.17	-3.04
	MO AuNPs	AuNPs	67.47*	2.12	0.00	62.07	72.87
		Blank AuNPs	8.60*	2.19	0.00	3.04	14.17

*. The mean difference is significant at the 0.05 level.

C

d_H (nm)

Scheffe's *post hoc* test[a]

Sample ID	Subset for alpha = 0.05 AuNP	Blank AuNP	Mo AuNP
AuNP	59.3064		
Blank AuNP		118.1700	
Mo AuNP			126.7750
Sig.	1.000	1.000	1.000

Means for groups in homogeneous subsets are displayed.
a. Uses Harmonic Mean Sample Size = 12.453.

Figure 5-8: (A) Results of One-way ANOVA performed on bare, blank and morphine conjugated AuNPs. (B) Sheffe's *post hoc* multiple comparisons performed between the samples groups. (C) Grouped results obtained of the Sheffe's *post-hoc* test.

Analogously, the average (±SD) values of the d_H of the bare, blank and cocaine conjugated AuNP (140.80 ± 2.51 nm) were statistically different according to the one-way ANOVA ($F(2,47)$= 1731.997, p-value<0.00001). The Sheffle's *post hoc* test revealed that the d_H (nm) size of cocaine AuNPs was 22.26 nm bigger than the blank AuNPs (p-value<0.00001) and 81.46 nm bigger than the bare AuNPs (p-value<0.00001), as reported in **Figure 5-9**.

A

ANOVA

d_H (d.nm)

	Sum of Squares	df	Mean Square	F	Sig.
Between Groups	44522.171	2	22261.086	1731.997	0.000
Within Groups	604.084	47	12.853		
Total	45126.255	49			

B

Multiple Comparisons

Dependent Variable: d_H

	I Sample	J Sample	Mean Difference (I-J)	Std. Error	Sig.	95% Confidence Interval Lower Bound	95% Confidence Interval Upper Bound
Scheffe	AuNPs	Blank AuNPs	-59.20	1.39	0.000	-62.71	-55.69
		CO AuNPs	-81.46*	1.39	0.000	-84.97	-77.95
	Blank AuNPs	AuNPs	59.20*	1.39	0.000	55.69	62.71
		CO AuNPs	-22.26*	1.13	0.000	-25.13	-19.39
	CO AuNPs	AuNPs	81.46*	1.39	0.000	77.95	84.97
		Blank AuNPs	22.26*	1.13	0.000	19.39	25.13

*. The mean difference is significant at the 0.05 level.

C

d_H (nm)

Scheffe's *post hoc* test[a]

Sample ID	Subset for alpha = 0.05 AuNP	Blank AuNP	co AuNP
AuNP	59.3064		
Blank AuNP		118.1700	
CO AuNP			140.7950
Sig.	1.000	1.000	1.000

Means for groups in homogeneous subsets are displayed.

a. Uses Harmonic Mean Sample Size = 12.453.

Figure 5-9: (A) Results of One-way ANOVA performed on bare, blank and cocaine conjugated AuNPs. (B) Sheffe's *post hoc* multiple comparisons performed between the samples groups. (C) Grouped results obtained by using Sheffe's *post hoc* test.

5.3.2 Drugs of Abuse NanoMIPs QCM Sensor Fabrication

This work explored the assembly of the drugs of abuse nanoMIPs QCM chip. In order to achieve a good receptor immobilisation step, it is important to have a cleaned sensor surface. Therefore, the gold surface of the QCMA-1 chip was subject to piranha cleaning procedure. Subsequently, a self-assembly monolayer was created by submerging the cleaned chip onto 50 mL of mM 11-MUDA in ethanol solution for 12 hour and at room temperature. While the thiol group rapidly attached to the gold surface, the overnight incubation guaranteed the ordered arrangement of the carbon chain of the 11-undecanoic acid. Typically, this results in a layer of carbon chains with an inclination of 30° respect to the orthogonal line to the sensor chip surface (Altintas *et al.*, 2012).

After rinsing the sensor with ethanol and water, the QCM sensor chip was docked in the QCM biosensor instrument (QCMA-1, Sierra Sensors GmbH, Hamburg, Germany) to perform the nanoMIPs covalent attachment via amine coupling. Concisely, 100 µL of freshly mixed EDC-NHS solution was injected at a flow rate of 25 µL min^{-1} to activate the carboxylic group and, soon after, 100 µL of morphine nanoMIP (1.2 mg mL^{-1}) were injected on spot 1 at the same flow rate. As shown in **Figure 5-10**, this induced covalent attachment of the nanoMIPs onto the sensor chip. The used concentration was considered high enough to achieve the nanoMIPs immobilisation, without affecting the microfluidic of the instrument.

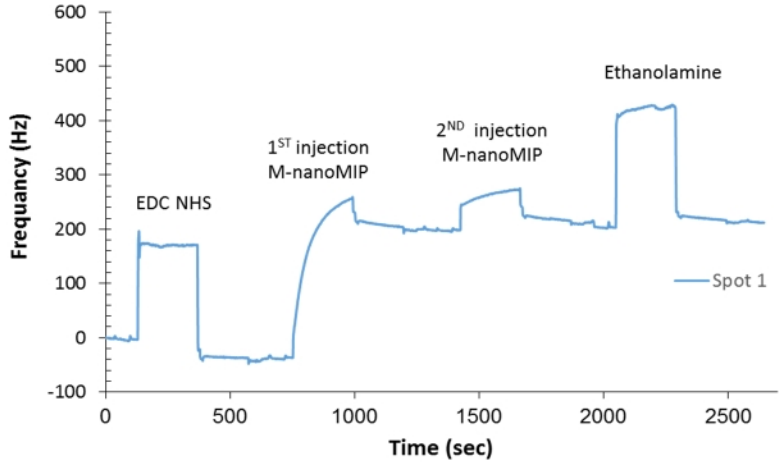

Figure 5-10: Sensorgram of morphine nanoMIP attachment onto spot 1 performed by two consecutive nanoMIP injections at a concentration of 1.2 mg mL^{-1}. No significant attachment was achieved after the first injection.

To assess whether the QCM spot surface was completely saturated with one injection of morphine nanoMIPs, a second injection was performed using the same concentration (1.2 mg mL^{-1}) and injection conditions (100 µL, flow rate = 25 µL min^{-1}). The result showed that the surface was saturated by the first injection. Therefore this concentration (1.2 mg mL^{-1}) was used for further investigation. The ethanolamine (1 M, pH 8.5) was used to cap the unreacted group and to prevent any non-specific binding events.

Similarly, the attachment of the cocaine nanoMIPs on spot 2 of the QCM chip was investigated as described in Section 5.2.5.1. A slightly higher concentration was needed to saturate the QCM surface spot. As shown by the sensorgram in **Figure 5-11**, no further cocaine nanoMIPs attachment was achieved after the first injection of the cocaine nanoMIP at a concentration of 1.8 mg mL^{-1}.

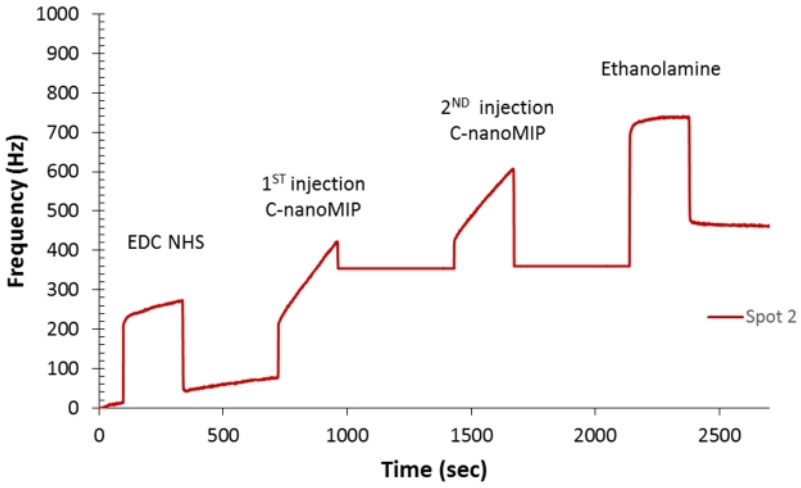

Figure 5-11: Sensorgram of cocaine nanoMIP attachment onto spot 1 performed by two consecutive nanoMIP injections at a concentration of 1.8 mg mL^{-1}. No significant attachment was achieved after the first injection.

Both the morphine nanoMIP and cocaine nanoMIP attachments were replicated and proved to be reproducible, as shown in the bar chart presented in **Figure 5-12**. The difference in the frequency response between the morphine nanoMIP (251.81 ± 6.49 Hz) and the cocaine nanoMIP (358.60 ± 6.55 Hz) can be ascribed to the difference in the concentration used and to the possible difference in the molecular weight of the two nanoMIPs. The two optimised nanoMIPs concentration were used to fabricate the

nanoMIPs QCM sensor chip for the drugs of abuse detection. A typical sensorgram of both cocaine and morphine nanoMIP attachment is reported in **Figure 5-13**.

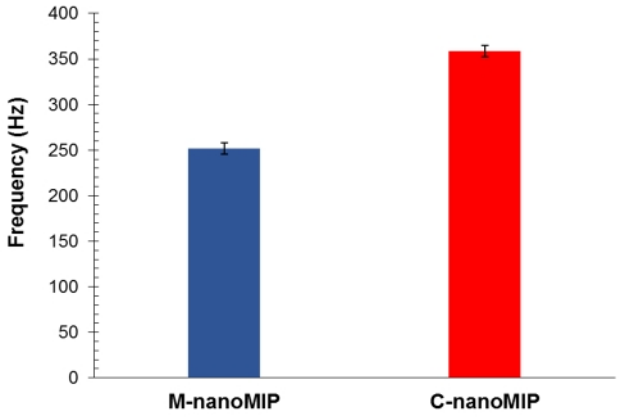

Figure 5-12: The results of the reproducibility study of morphine and cocaine nanoMIP attachment onto the QCM sensor surface. Error bars refer to the standard deviation of replicates (n=5).

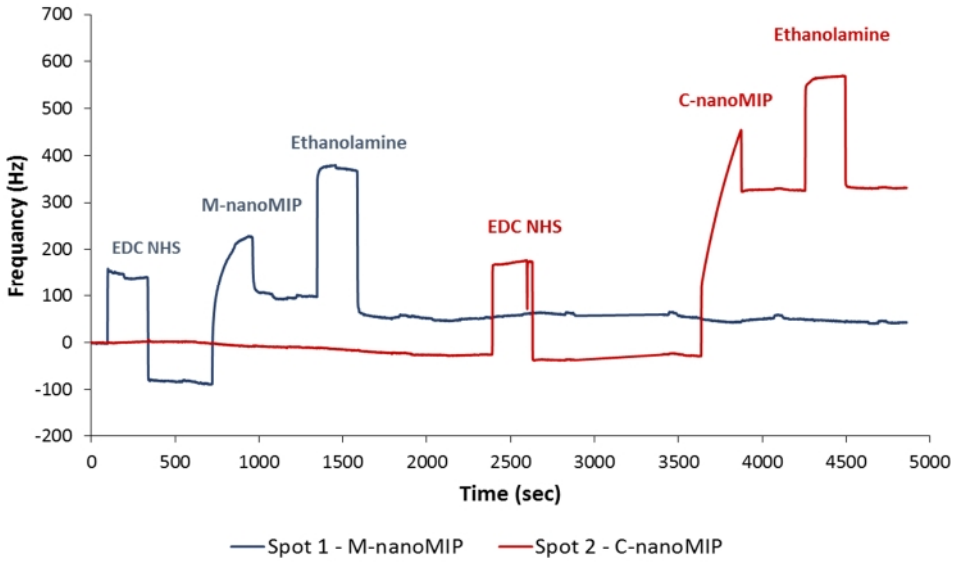

Figure 5-13: Full sensorgram obtained during morphine nanoMIP QCM sensor functionalisation, where each spot were functionalised separately.

5.3.2.1 AFM Characterisation Study of the NanoMIP QCM Sensor

The AFM surface characterisation studies was used to further probe the nanoMIPs attachments onto the QCM and was carried out according to the procedure reported in Section 5.2.5.2. The AFM was performed in tapping mode and the 3D images of the surface was recorded on a scan area of 400 μm^2. The roughness analysis was also performed. The AFM results of the morphine nanoMIP and the cocaine nanoMIP functionalised spots surface were compared to the AFM results of the MUDA coated surface. The obtained 3D images of the surface topography and the results of the roughness analysis are displayed in **Figure 5-14** and **Figure 5-15**, respectively.

The 3D AFM images of the surface topography highlighted the difference between the nanoMIP functionalised spot surface and the MADA coated QCM spot surface. Indeed, a uniform and well-distributed peaks characterised the QCM surfaces functionalised with morphine or cocaine nanoMIPs. This may be due to the use of the microfluidic system for the nanoMIP attachment, which guaranteed a uniform surface functionalisation. Interestingly, similar results were achieved by immobilising other type of sensing receptors onto the QCM sensor chip (Ohno *et al.*, 2013; Masdor, Altintas and Tothill, 2016). The peaks, detected on the QCM sensor spots, refer to the nanoMIPs, while the difference in peaks height and size can be due to the heterogeneous size of the nanoMIPs or to the possible nanoMIPs aggregations.

Furthermore, the roughness analysis confirms that the surface roughness of the QCM sensor surface increased due to the nanoMIP covalent immobilisation. Overall, the AFM analysis of the two QCM sensor surfaces (functionalised with cocaine and morphine nanoMIPs) showed a similar amount of nanoMIPs attachment. Therefore, the two spots were functionalised with a comparable amount of nanoMIPs, despite the difference in the QCM frequency response. The few tiny white peaks occurring onto the MUDA coated QCM chip can be ascribed to artefacts. Furthermore, the Ra and Rq values were similar in the two investigated MUDA coated QCM surface spots, thus indicating that the MUDA was homogeneously deposited onto the gold surface.

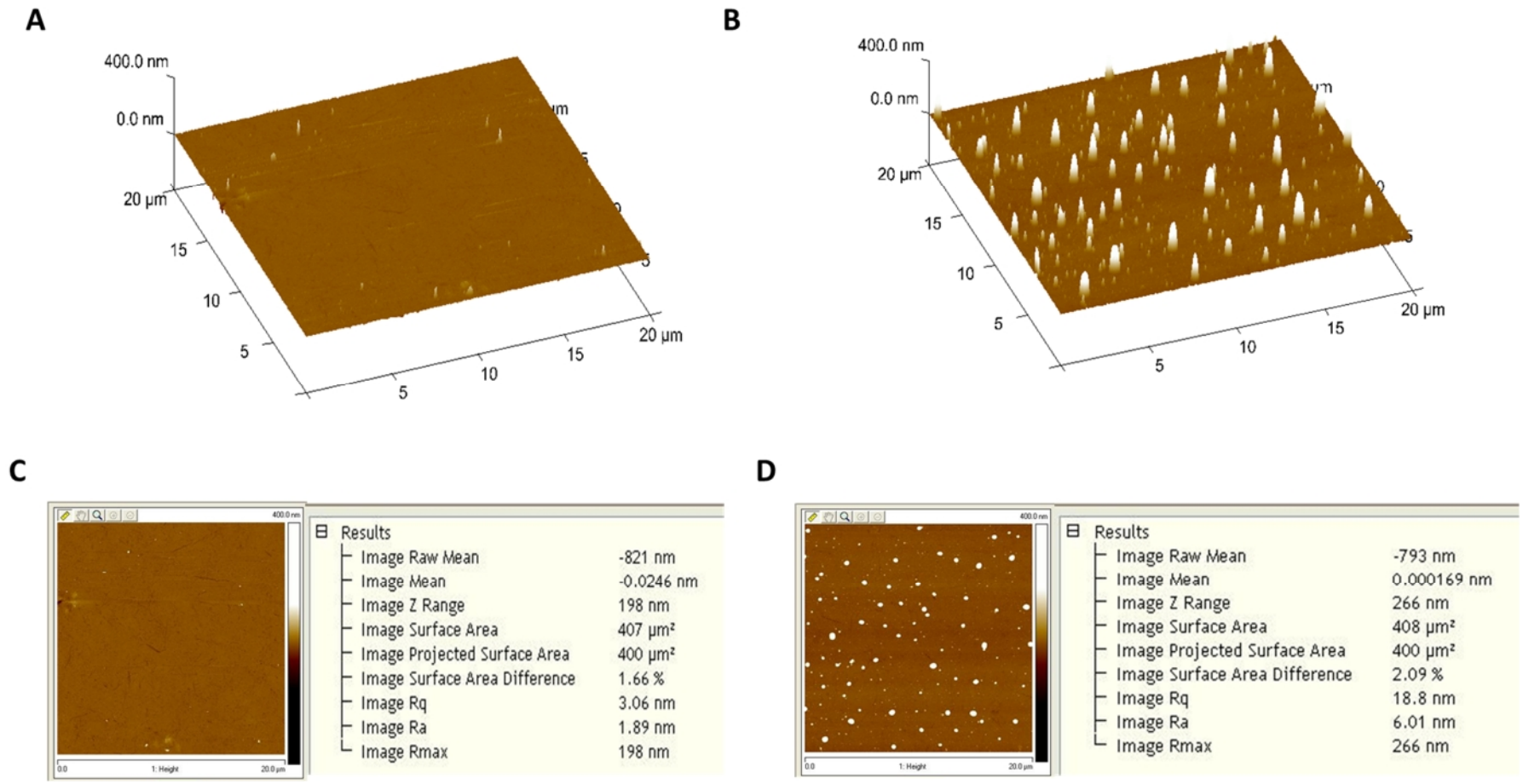

Figure 5-14: AFM 3D topography image related to (A) MUDA and (B) morphine nanoMIPs functionalised spots of the gold QCM sensor surface (scan area = 400µm^2; height = 400nm). White peaks s refer to the attached nanoMIPs. Results of the AFM roughness analysis related to the (C) MUDA and (D) morphine nanoMIP functionalised spots of the gold QCM sensor surfaces.

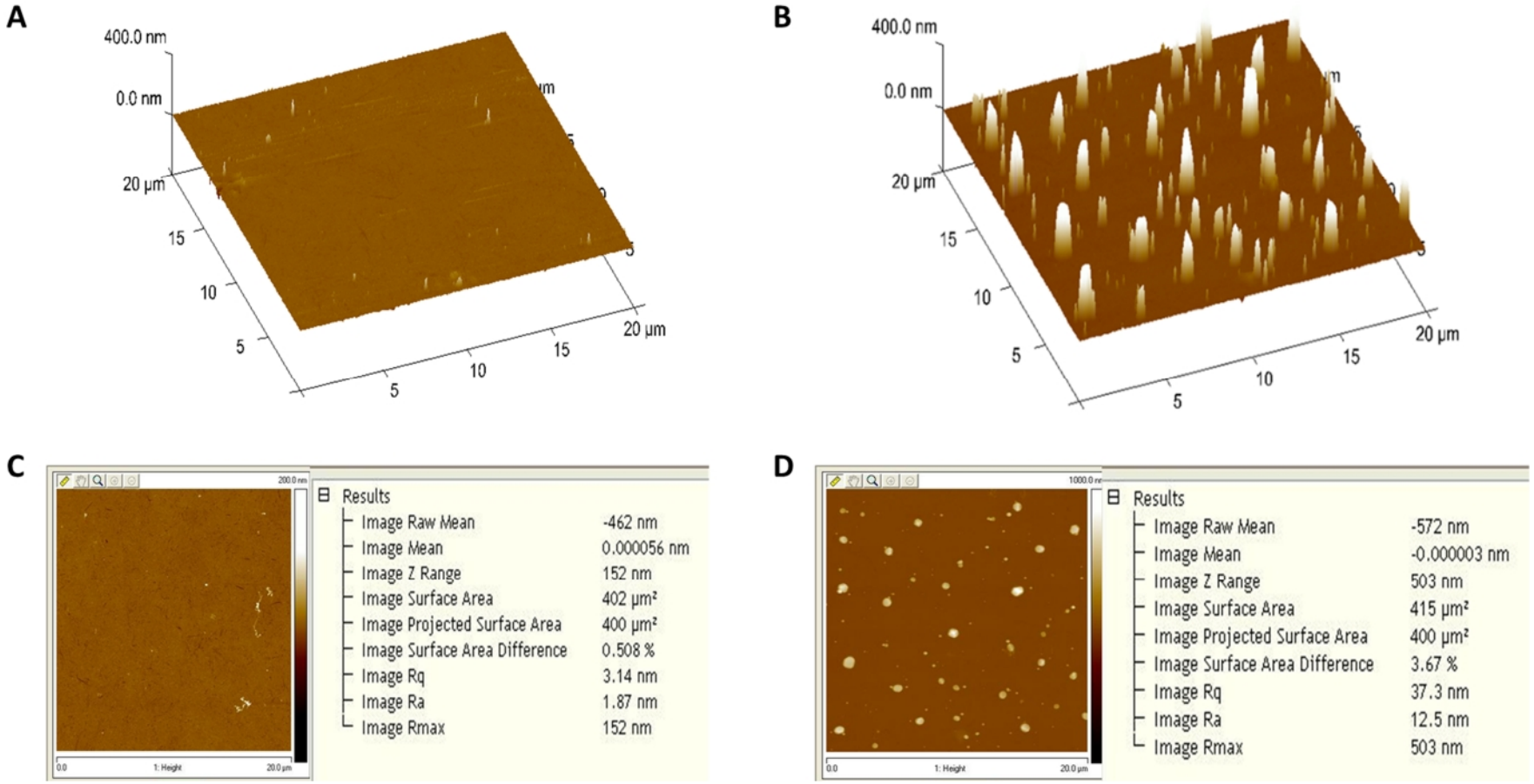

Figure 5-15: AFM 3D topography image related to (A) MUDA and (B) cocaine nanoMIPs functionalised spots of the gold QCM sensor surface (scan area = 400µm^2; height = 400nm). White peaks refer to the attached nanoMIPs. Results of the AFM roughness analysis related to the (C) MUDA and (D) cocaine nanoMIP functionalised spots of the gold QCM sensor surfaces.

5.3.3 Evaluation of Drugs of Abuse NanoMIPs QCM Sensor

The QCM sensing platform used in this work comes with an integrated and automated microfluidic system, which can operate with minimal environmental and human interferences. The system allowed programmable injections onto the docked nanoMIPs QCM sensor surface, thus allowing a real-time and quick response related to different samples injected onto the sensor surface during the cumulative assays. All the cumulative assays were performed on freshly fabricated nanoMIPs QCM sensor chip and in a direct assay format.

5.3.3.1 Morphine Cumulative Assay onto NanoMIPs QCM Sensor

The gold QCM chip was cleaned as described in section 5.2.4 and the nanoMIPs QCM sensor was fabricated as detailed in section 5.2.5. PBS (pH 7.4) was used as the running buffer, the flow rate was adjusted to 25 µL min^{-1}, and the temperature was set at 25°C. The surface was primed at least three times with the PBS to condition the sensor surface.

Afterwards, the QCM chip was set on morphine operating mode (Spot 1 = active; Spot 2 = control). The morphine AuNPs were suspended in PBS (pH 7.4) and concentrations ranging from 250 ng mL^{-1} to 50 µg mL^{-1} were prepared, having PBS (pH7.4) as diluent. The blank solution was prepared by suspending the blank AuNP in the same buffer (PBS, p H7.4). Each dilution and the blank solution were placed in a 1.5 mL labelled Eppendorf tubes and inserted in the automated samples carousel. The QCM automated sampler was programmed to inject 100 µL of the blank solution on both spot 1 and 2 for four minutes at a flow rate of 25 µL min^{-1}. This operation was repeated until a stable blank signal was achieved on both spot 1 and 2, as shown in **Figure 5-16**. This provided the blank signal baseline and the evidence that no false response occurred due to the interaction between the blank AuNPs and the nanoMIPs sensor surface.

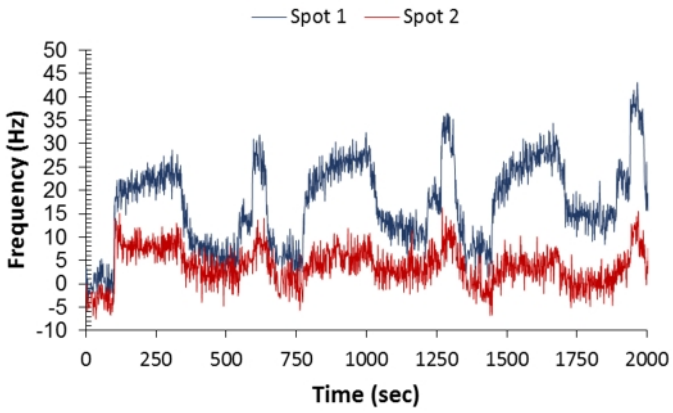

Figure 5-16: Typical sensorgram of stable blank signals onto both spot 1 and 2 for four minutes at a flow rate of 25 µL min^{-1}.

Then, the machine was programmed to inject 100 µL of each morphine AuNPs concentration, from the lowest to the higher, on both spot 1 and 2 for four minutes at a flow rate of 25 µL min^{-1}, and the cumulative assay was started. The results (**Figure 5-17**) showed that the active spot 1 of the nanoMIPs QCM sensor was proportionally responsive to the increasing concentration of the morphine AuNPs, while no apparent response was detectable onto spot 2.

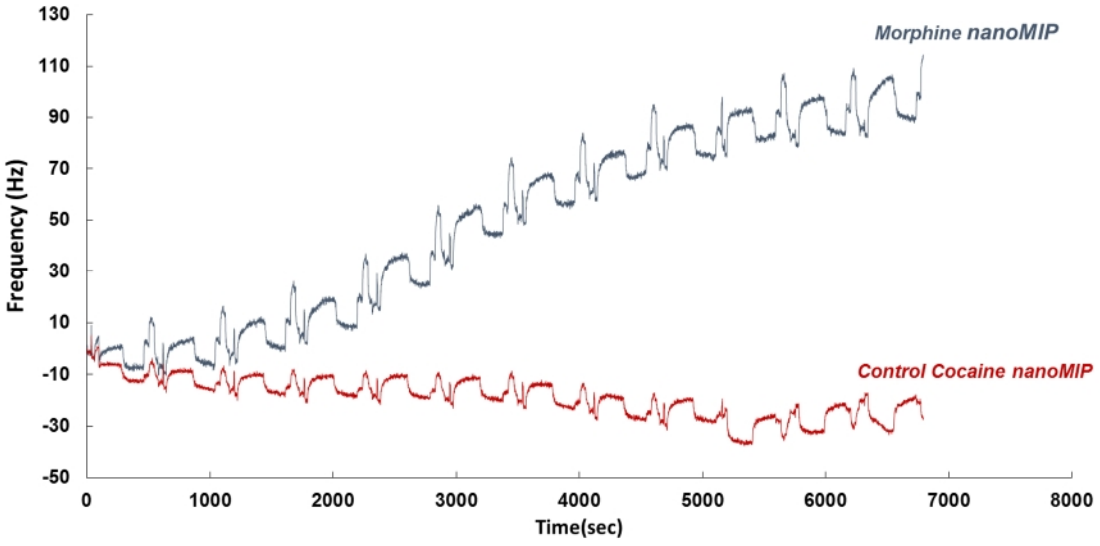

Figure 5-17: Sensorgram obtained during the morphine cumulative assay. The nanoMIPs QCM was operating in morphine sensing mode. The increase sensor response to morphine AuNPs is visible on spot 1 (=active spot).

The data were collected and analysed using the dedicated software, Sierra Analyser v.3.1.10.0. Therefore, the sensor response was subtracted from the blank and control signals. The ΔF (Hz) values were calculated as detailed in section 5.2.6 and were plotted versus the concentrations of the morphine, thus obtaining a non-linear calibration curve. To obtain the semi LOG linear calibration curve, the morphine concentrations were transformed to LOG10. The LOD was calculated according to procedure reported in Section 5.2.8 and was found to be 0.58 µg mL^{-1}. Furthermore, the binding kinetic study revealed that the K_D was equal to 0.886 µM (**Figure 5-18**), thus confirming the high affinity between the developed sensor surface and the morphine analyte.

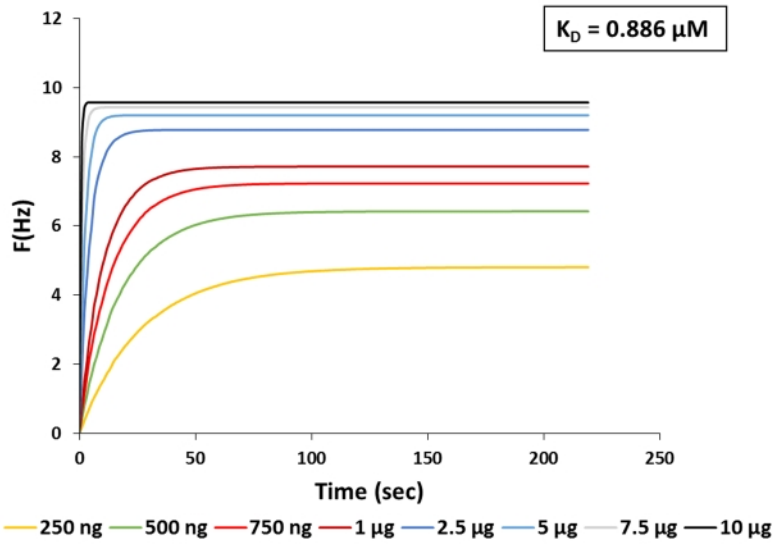

Figure 5-18: Kinetic fitting curves grouped by concentration and the related K_D value of the QCM based morphine nanoMIP sensor.

The assay has been replicated (n=3) and a similar results were obtained. The data of the sensors response were expressed in % ΔF as described in section 5.2.6. The average (±SD) of the % ΔF values were plotted against the morphine AuNPs concentrations, thus obtaining a standardised non-linear and linear calibration curve (R^2= 0.994; p-value < 0.0001), as shown in **Figure 5-19**. The LOD was found to be as low as 0.19 µg mL^{-1}. The average (±SD) of the K_D was equal to 6.47 x 10^{-8} ± 3.40 x 10^{-8}.

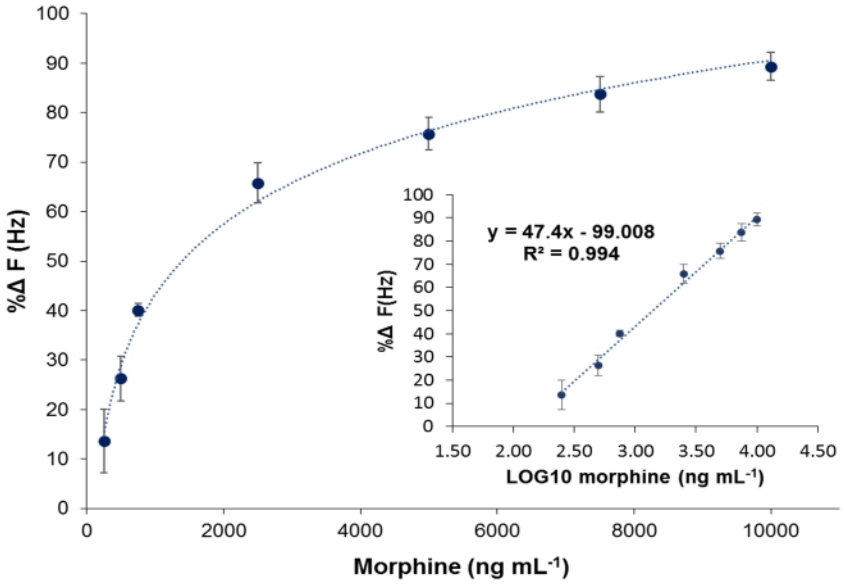

Figure 5-19: Standardised (A) Non-linear and (B) linear calibration (inset) curves related to the morphine cumulative assay. Error bars refer to the standard deviation of replicates (n=3).

5.3.3.2 Cocaine Cumulative Assay onto NanoMIP QCM Sensor

The ability of the nanoMIPs QCM sensor to detect cocaine was investigated performing the cocaine AuNPs cumulative assay. As the final aim is to inject an unknown conjugated AuNPs sample, the assay working conditions were kept consistent with the morphine cumulative assay. Briefly, the running buffer, the temperature and the flow rate were set as described in Section 5.3.3.1. A new nanoMIPs QCM sensor was cleaned and freshly fabricated as detailed in Section 5.2.4 and 5.2.5, respectively. Cocaine AuNPs dilutions were prepared using PBS (pH 7.4). Then, the setting were switched to the cocaine sensing mode (spot 1 = control; spot 2= active), the sensor surface was primed as described in Section 5.3.3.1,. As a general practice, 100 µL of the blank AuNPs solution was injected at least three times, thus providing the blank signal baseline and the evidence that no false response occurred due to the interaction between the nanoMIPs sensor surface and the blank AuNPs.

Then, the cumulative assay was carried out by injecting 100 µL of each concentration of cocaine AuNPs (250 ng mL^{-1} up to 10 µg mL^{-1}) onto both sensor spots for four minutes at a flow rate of 25 µL min^{-1}.The sensor response was recorded and the data processed as

described in section 5.3.3.1. The sensor was responsive to the cocaine AuNPs injection on spot 2 (active), whereas no response was observed on spot 1 (control). A correlation (r= 0.998; *p*-value<0.0001) between the ΔF (Hz) values and the increasing cocaine AuNPs concentrations was detected on spot 2. The results (**Figure 5-20**) were plotted according to the procedure outlined in Section 5.2.6, thus achieving the non-linear and linear calibration curves.

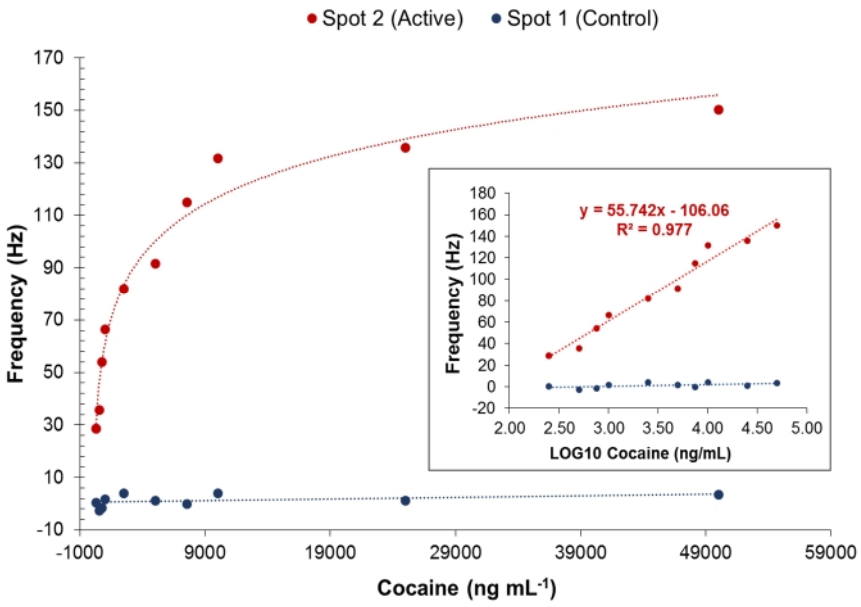

Figure 5-20: Linear calibration curve (blank and control subtracted - red line) obtained by injecting increasing concentration of cocaine AuNPs (250 ng mL^{-1} to 10 µg mL^{-1}) onto spot 2 (active). The blue line is the sensor response obtained onto the control spot (Spot 1 - functionalised with morphine nanoMIPs).

The coefficient of determination of the linear regression (R^2) was equal to 0.977. The LOD was found to be close to the previous one (0.23 µg mL^{-1}). The kinetic study (**Figure 5-21**) confirmed the good affinity between the receptor and the analyte (K_D= 0.364 µM). The assay was replicated (n=3) and the data of sensor response were standardised as described in section 5.2.6.

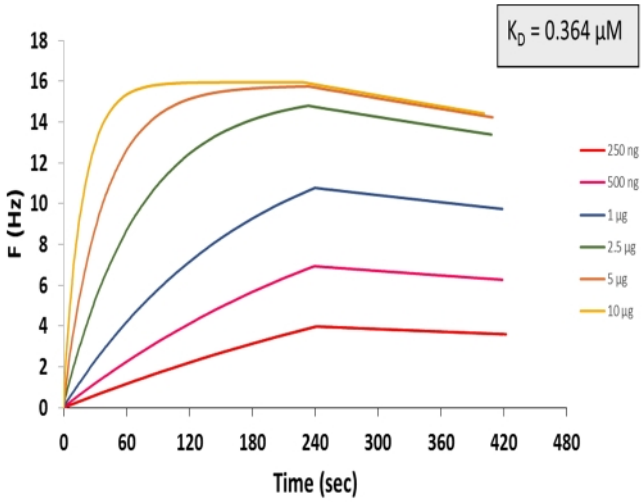

Figure 5-21: Kinetic binding study related to the cocaine nanoMIP QCM sensor.

The results are presensted in **Figure 5-22**. The standardised sensors response (%F (Hz)) of the replicates were averaged and plotted against the cocaine AuNPs concentrations, thus achieving the non-linear calibration curve. The cocaine concentration were then expressed as LOG10, and the standardised linear calibration curve was obtained with a R^2 equal to 0.978 (*p*-value <0.0001). The LOD was recalculated and was equal to 0.36 µg mL^{-1}. The average (±SD) of the K_D values was found to be 2.25 x 10^{-7} ± 1.9 x 10^{-7}.

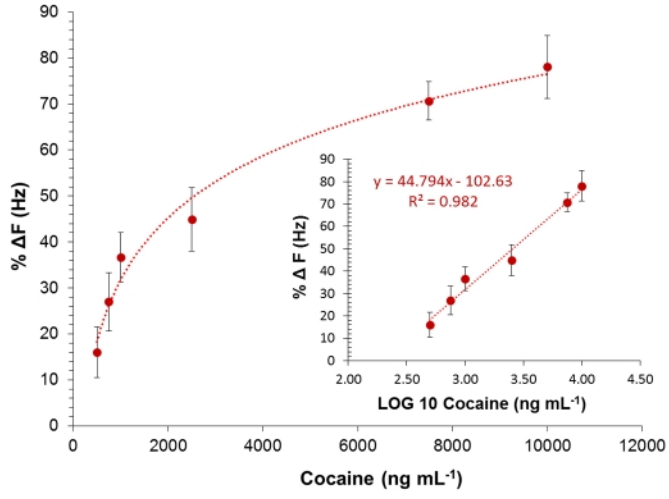

Figure 5-22: Standardised (A) non-linear and (B) linear calibration (inset) curves related to the cocaine cumulative assay performed onto the nanoMIPs QCM sensors. Error bars refer to the standard deviation of replicates (n=3).

5.3.4 Regeneration Study of the Morphine NanoMIP QCM Sensor

The possibility to regenerate the sensor surface is often desired and convenient feature, as it allows the sensor reuse and makes the sensor cheaper. The regeneration aims to overcome the binding forces between the analyte and the related receptor, leaving the sensor surface in the working condition for the next assay. Usually, the regeneration is achieved by chemical strategies, i.e. by injecting onto the used sensor surface a strong acid or basic solution or by combining them. Although, other strategies have also been explored, such as the use of detergent, electrochemical and thermal regeneration (Goode, Rushworth and Millner, 2015).

In this work, both chemical and thermal regenerations were attempted. Specifically, at the end of the cumulative concentration assays, several protocols were applied to regenerate the sensor surface. NaOH solution was previously applied to regenerate morphine immunosensor surface (Yang *et al.*, 2014), while acid solution have been successfully applied to regenerate nanoMIP based SPR sensor surface (Abdin, Altintas and Tothill, 2015; Altintas *et al.*, 2016) and AuNPs immunobased QCM sensor surface (Masdor, Altintas and Tothill, 2016). Moreover, the combination of acid/basic solution has been proved to be successful to regenerate the surface of both nanoMIPs and AuNPs - immunobased sensor surface (Altintas, Gittens, *et al.*, 2015; Pawula, Altintas and Ibtisam E. Tothill, 2016). Therefore, these solutions were explored. All the assays were performed having the flow rate of the running buffer and of all the injection set at 25 µL min^{-1}, while the temperature was kept at 25°C. When the regeneration of the sensor surface was achieved, an injection of 100 µL of morphine AuNPs (50 µg mL^{-1}) was performed to assess the integrity of the sensor after the regeneration.

To quantify the sensor regeneration, the sensor signal achieved at the end of the investigated regeneration protocol was expressed as a percentage of the sensor signal achieved before the regeneration, thus achieving the % of the surface regeneration. The results were plotted and are presented in **Figure 5-23**.

As a first attempt, acid regeneration buffers were tested. Specifically, 25 µL of HCl 0.1 M was injected for 1 minute onto the sensor surface and the sensor signal was reduced by 28.22%, but, upon morphine AuNPs injection (5 µg mL^{-1}), no rebinding occurred. In

another attempt, the injection of 25 µL of 100 mM of glycine hydrochloride in 0.1 M HCl was tested, but failed to regenerate the surface as the signal dropped only by 3.58%.

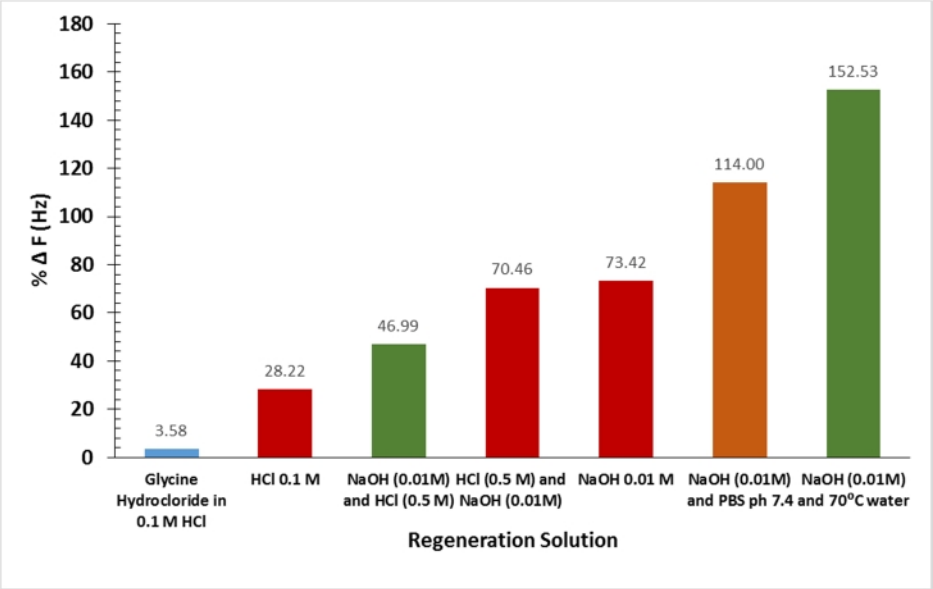

Figure 5-23: Bar chart of the % of the surface regeneration achieved applying the different regeneration strategies. Green bars indicate that the regeneration allowed the analyte rebinding. Red bars indicate that no rebinding occurred after the regeneration solution. Orange bar indicates that reduced rebinding occurred after the regeneration of the surface. Blue bar indicate that the rebinding was not assessed.

Therefore, basic regeneration solutions were attempted. As a first trial, the 25 µL of NaOH 0.01 M was injected for one minute onto the sensor surface. This solution reduced the signal by 73.42%. However, the sensor was not able to rebind the morphine AuNPs, thus indicating a modification of the sensor surface.

To overcome the rebinding issue, a combination of basic and acid solution was used in order to neutralising the pH at the sensor surface. The first attempt was carried out by injecting for 1 minute 25 µL of HCl 0.5 M, followed by one minute injection of 50 µL NaOH 0.01 M. This allowed to reduce the signal by 70.46%, but no rebinding occurred when 100 µL of morphine AuNPs (50 µg mL^{-1}) was injected. Therefore, it was assumed that the NaOH needs to be neutralised, thus reactivating the sensor surface. Therefore, the protocol was replicated by inverting the injection of the regeneration solution. Thus, 50

µL NaOH 0.01 M were injected onto the sensor surface for two minutes. Secondly, 50 µL of HCl 0.5 M was injected for other 2 minutes. Although the signal was reduced only by 46.99%, the surface was able to fully rebind the morphine AuNPs, thus indicating that a sensor surface neutralisation of the NaOH was needed. Other strategies were also explored, such as the combination of NaOH 0.01 M with a flush of 50 µL PBS 7.4 to neutralise and diluted further the basic solution. This protocol succeeded in regenerating the surface, although the rebinding with the morphine AuNPs injection gave only a small sensor response. Finally, the NaOH 0.01 M solution was explored in combination with the thermal regeneration. To achieve this, the injection of 50 µL of NaOH 0.01 M solution was followed by a flush of 100 µL of doubled distilled water pre-heated at 70°C. This induced a reduction of the signal equal to 152.53%, suggesting that the regeneration protocol partially removed the functionalised sensing layer. However, when the morphine AuNPs were injected again, the rebinding occurred, thus indicating that the sensor was still in a working condition.

To conclude, the regeneration protocol was investigated and, according to the results, both the NaOH (0.01M) combined with HCl (0.5 M) and the NaOH (0.01M) combined with 70°C water were able to regenerate the surface. However, further studies are needed to optimise the volume, injection time and the concentrations of the regeneration solutions.

5.4 Discussion and Conclusion

The development of nanoMIPs QCM sensor for a specific detection of cocaine and morphine was developed in this work. The attachment protocols of both cocaine and morphine were found to be reproducible and the AFM analysis proofed the uniformity of the deposition. Due to the QCM limits in detecting small analyte, the drugs were conjugated to AuNPs. This has been achieved by applying a consistent AuNP adsorption protocol previously developed and was verified by DLS analysis. The proof of concept was demonstrated by switching the QCM setting from morphine sensing mode to cocaine sensing mode and testing one illicit drug at a time.

Overall the nanoMIPs QCM sensor was able to specifically detect the two drugs at sub ppm range and with no visible cross-reaction or non-specific binding events. Although an enhanced signal strategy was required, the assay has been developed in a direct format for both cocaine and morphine detection. A summary of the performances of both the sensor are provided in **Table 5-2**.

Table 5-2: Summary of the performances of the nanoMIPs QCM sensor for drugs of abuse detection developed in this work.

QCM Sensor	Linear Range	LOD ($\mu g\ mL^{-1}$)	K_D ±SD (M)
Morphine	250 ng mL^{-1} to 10 µg mL^{-1}	0.191	$6.47 \times 10^{-8} \pm 3.40 \times 10^{-8}$
Cocaine	500 ng mL^{-1} to 10 µg mL^{-1}	0.360	$2.25 \times 10^{-7} \pm 1.9 \times 10^{-7}$

Since the conjugation step is easy and straightforward to execute, the developed nanoMIP QCM sensor can provide a fast and specific detection of cocaine and morphine in sample where a high concentration is expected, while the platform can be considered cheaper and more stable at different operational condition compare to other available analytical tools. The nanoMIPs QCM sensor developed in this work was able to detect morphine and cocaine conjugated to AuNPs in a concentration below the 0.5 µg mL^{-1} with a high level of discrimination between the two analyte. Due to integrated microfluidic system, the nanoMIPs QCM sensor operated in an automated mode and provided a real-time signal

of the binding occurring between the nanoMIP and the specific analyte. The linear range, the LOD and the K_D for each analyte are reported in **Table 5-2**.

The BIOSENS 600 (Biosensor Applications Sweden AB, Upplands Väsby, Sweden) is piezoelectric immunosensor based on surface acoustic wave technology and already available on the market. The BIOSENS 600 is able to simultaneously detect twelve analyte (drugs of abuse and explosive) at trace level (sub ppm). However, the automated samples injection and microfluidic system to allow programmable samples processing is not available with the BIOSENS600. Furthermore, the detection method is based on competitive immunoassay and therefore encounters the drawbacks highlighted in Section 1.6.1.

Compared to other sensors and biosensor platform available for cocaine and morphine detection (listed in **Table 3-9** and **Table 4-5**, respectively), the developed nanoMIPs sensor has the advantage to detect and discriminate between the two analytes. Also, the use of nanoMIP as receptor overcome the disadvantages hold by other frequently used biological receptors, such as antibodies and aptamers. The antibodies are expensive to produce, prone to conformational changes and enzyme degradation and the often are produced by the animal-aided process. On the other hand, the aptamer is produced by expensive protocol and are prone to conformational change and degradation by environmental DNAse.

Although further development are needed, the nanoMIPs QCM for drugs of abuse developed in this work can be applied as a fast screening tool when tons of seized suspected materials has to be quickly analysed, such as suspected materials seised at port or at warehousing terminal. In these samples, the drugs occur at high concentration and with a high level of purity. Therefore, the analytical tool has to quickly process a large number of samples with a high specificity rather than sensitivity. The on-site analytical tools applied in these scenario include the colourimetric and the immune-based kit. Both of them are only qualitative/ semi-qualitative tests, but are prone to possible false positive, false negative results. The ELISA is used as in-lab screening methods, although the results are produced within hours, the method is based on a competitive assay format, the test has a moderate discrimination ability, the expensive reagents and trained personnel are needed to carry out the analysis (Harper, Powell and Pijl, 2017). On the other hand, IMS

is a sensitive and specific analytical tool used both on-site and in-lab. However, the overloading of the instrument with bulk materials often results in the saturation of the instrument. Furthermore, the IMS is not able to discriminate cocaine from opiates as the cocaine signal often cover the opiates signal when both the drugs occurred in the same sample (Verkouteren and Staymates, 2011).

Therefore, the nanoMIPs QCM sensor for the cocaine and morphine detection offers a valid lab-based analytical tool due to the real-time, automated and easy-to-use sensor platform, the cheap reagents needed and the discrimination ability of the sensor. Furthermore, the direct assay format and the use of the low-cost and environmental stable nanoMIP boost the advantages of the nanoMIPs QCM sensor developed in this work.

Chapter 6

Final Conclusion and Future Work

6.1 Introduction

Presently, the use, manufacturing, trafficking of drugs of abuse are among the major societal challenges. Cocaine and morphine (which is the heroin precursor) are both plant-derived drugs and are trafficked as salt (hydrochloride) or as free-base form. Both drugs were among the most seized compounds worldwide in 2015, with 864 tons and 8.6 tons, respectively. The multibillion dollars profits related to the manufacturing and trafficking of cocaine and opioids (among which morphine) are financing the organised crime groups worldwide (UNODC, 2017b). On the other hand, the abuse illicit drugs, among which cocaine and heroin, can lead to addiction, increase the risk of acquiring life-threating infectious diseases (such as hepatitis C and HIV through the use of contaminated needles) and to death by overdoses. Therefore, heavy burdens are posed worldwide on law enforcement agencies (LEAs) in fighting illicit drugs related crimes and on healthcare in treating drugs of abuse disorders.

Due to their efficiency in detecting target substances, police dogs are currently considered vital in detecting illicit drugs and are employed during LEA patrol both at borders and street level. However, the police dogs require extensive and expensive training and are prone to olfactory fatigues (Leitch *et al.*, 2013). On-site illicit drugs methods offer an alternative or a support to the use of police dogs. Examples are Ion mobility spectroscopy (IMS) (Cumeras *et al.*, 2015), competitive inhibition immunoassay (Musshoff *et al.*, 2014), and colourimetric tests (Harper, Powell and Pijl, 2017). The reported cut-off of most used immune-based devices is in the range of 10 to 50 ng mL^{-1} (Musshoff *et al.*, 2014). Whereas, the IMS (IONSCAN 500DT, Smiths Detection Group Ltd, UK) has a limit of detection in the sub-ng range. Nevertheless, these methods provide only qualitative or semi-quantitative results, are prone to false positive and negative results and require trained personnel to conduct the assay. Confirmatory analysis is currently performed in an accredited ISO 17025 laboratories through several complex procedures and expensive analytical tools such as GC-MS and LC-MS (Cecinato, Balducci and Perilli, 2016). These methods are able to detect the cocaine in sub-ng range with high specificity and provide unequivocal evidence of criminal activities related to drugs of abuse, which may be used in court cases. Although, these methods are usually complex and time-consuming due to the long sample preparation procedures (extraction and

derivatization); highly expensive, due to the equipment needed and the consumables required to carry out the analytical methods; poor versatile since only experienced and qualified staff can perform the analytical methods; not suitable for fast on-site application (Harper, Powell and Pijl, 2017). Therefore, biosensors have been explored as a quick, cheap, portable, yet sensitive and specific analytical tool to detect illicit drugs trafficking and abuse.

This work covers the development of several nanoMIPs based affinity sensors aiming at the detection of illicit drugs at trace level or in bulky form, thus offering tools to directly tackle illicit drugs trafficking both at borders and at street level. Specifically, the cocaine nanoMIP EIS and the morphine nanoMIP EIS sensors aim at detecting traces of cocaine and morphine, thus promising to be a valid methods to replace police dogs. On the other hand, the nanoMIPs QCM sensor offers a lab-based screening methods to quickly detect high purity samples of morphine and cocaine derived from seizures of large quantity of suspected substances, such as seizures performed in port or at borders. Both types of nanoMIP sensors are designed to detect cocaine and morphine in salt form and dissolved in a water-based buffer, as cocaine and morphine are frequently trafficked in this forms in Europe (EMCDDA, 2016).

6.2 NanoMIP EIS Sensors for Drugs of Abuse Detection

The Faradic EIS sensor is a sensitive electrochemical sensor able to detect changes in resistance charge transfer (Rct) at the electrode interface. Due to the high sensitivity, the EIS sensor is suitable for traces analysis and therefore was used to develop nanoMIP EIS sensors for the detection of drugs of abuse at trace level. EIS FRA/potentiostat instrumentation used in this work (PalmSens 5, PalmSens BV, The Netherlands) can be controlled by a smartphone app (PStouch) through Bluetooth tethering and, therefore, can be considered a portable and flexible platform, amenable to “point of care” use and to be interfaced with a wide range of different electrodes (such as, screen-printed and interdigitated electrodes). While the consecutive EIS reading is allowed, the simultaneous EIS measurements of two or more electrodes is an option not yet available within the PalmSens platform, thus slowing down the outcome of this work. The work was also

affected by the need to modify the CACIDE cable thus allowing the connection to the PalmSens instrument. Furthermore, a custom-made 3D printed CACIDE cable holder had to be designed to stabilise the connector electrode interface. The 3D printed CACIDE cable holder was available for the development of the morphine nanoMIP EIS sensor. During the development of the cocaine nanoMIP EIS sensor, a plastic support was placed underneath the CACIDE connector, while a three finger clamp was used to avoid the cable twisting. Extensive time was also needed to fit the raw data (expressed as imaginary, Z'', and real impedance, Z') into the equivalent circuit, thus obtaining the actual sensor response unit of measurement (Rct). Furthermore, a real-time signal was not doable due to the lack of the microfluidic system within the EIS equipment. Even though microfluidic system are available in the market, the use has to be controlled externally by a peristaltic pump and in a non-automated way.

This work investigated the development of the EIS nanoMIP affinity sensor to detect cocaine and is based on the combination of EIS biosensor platform and nanoMIP artificial receptors. The whole concept attempts to mimic the dog's olfactory system and to offer a proof of concept for the replacement of the police dog with a biosensor platform able to tackle drugs of abuse use, manufacturing and trafficking. Currently, biotechnologists are not yet able to reproduce the complexity of the olfactory system. The olfactory receptor cells have on their surface chemoreceptors that are stimulated by molecules dissolved in mucus. Once olfactory receptor cells are stimulated by the odorants, electrical signals arise and are driven by olfactory nerve's axons to the olfactory bulbs. Here the signals are processed and, later are recognised by the olfactory cortex.

Analogously, the developed cocaine sensor has biomimetic receptors, namely nanoscale molecular imprinting polymers (nanoMIPs), which can be produced to detect a wide range of analyte dissolved in a physiological solvent. Most of the biosensors for cocaine detection have been developed having antibodies as molecular receptor and aim to screen the cocaine occurrence mainly in biological samples (Munoz *et al.*, 2011; Vidal *et al.*, 2016). Recently, other molecular receptors have been explored for detecting cocaine, such as aptamers, which are mainly composed by deoxyribonucleic acids and combined with EIS sensor platform (Cai *et al.*, 2011; Roushani and Shahdost-fard, 2016; Z. Yang *et al.*, 2016). Compared to antibodies, aptamers are more stable (Tothill, 2011; Altintas,

Guerreiro, *et al.*, 2015; Mokhtarzadeh *et al.*, 2015). Furthermore, the production step is more reproducible, faster and do not involve the use of animals. Though, compared to MIP, their production is more expensive, since an *in vitro* selection process, named SELEX (systematic evolution of ligands by exponential enrichment) technique, is required (Du *et al.*, 2015). Furthermore, their stability may be compromised by denaturation agents, such as nucleases or ribonucleases and which may occur both in the environmental and biological samples (Justino *et al.*, 2015). On the other hand, aptamers based sensors mostly rely upon the folding of the aptamers, which occurs when the aptamer binds the target (Z. Yang *et al.*, 2016). However, non-specific aptamer folding cannot be excluded and the use of a negative controls (such as, testing the sensor response using aptamer produced for other analyte or against analyte other than the selected illicit drugs) are not always reported in the studies (Hilton *et al.*, 2011; Bozokalfa *et al.*, 2016; Roushani and Shahdost-fard, 2016).

Therefore, NanoMIP has been reported to be a valid candidate to replace antibody and aptamer due to higher thermal and environmental stability, long lasting shelf-life, reduced production cost (Poma *et al.*, 2014). Furthermore, they do not require animal use in their production and benefit of nanomaterial properties (Canfarotta *et al.*, 2016). At the same time, electrochemical biosensors offer a similar way to transform the analyte-receptor binding into an electrical signal, thus mimicking the electrical signal occurring at the olfactory nerve. Among them, electrochemical impedance spectroscopy (EIS) based biosensor was selected due to the outstanding performance in detecting target molecules at very low concentrations in a direct assay format. Most of the EIS biosensors for cocaine detection have been developed using the three electrodes configuration (WE, CE, RE) and applying faradaic EIS format (Randviir and Banks, 2013; Rushworth *et al.*, 2013). However, interdigitated electrodes (IDE) popularity is increasing due to their claimed better sensitivity (Lisdat and Schäfer, 2008; Ohno *et al.*, 2013; Arya *et al.*, 2018). Therefore, both types of electrodes were explored as sensor transducer for the development of the EIS nanoMIP affinity sensor, which operated in faradaic EIS mode.

Both cocaine nanoMIPs and morphine nanoMIPs were synthesized via solid-phase synthesis approach at the University of Leicester, which was a partner of the NOSY EU project (funding this PhD project). However, a size characterisation studies by means of

DLS and TEM were carried out on the dispatched nanoMIPs batches. The study revealed that the d_H value slightly differs between the batches. Overall, the average (±SD) d_H values of the cocaine nanoMIPs and morphine nanoMIPs were similar and equal to 168.80 nm (±68.73) and 170.09 nm (±54.75), respectively.

An extensive EIS and AFM characterisation studies were carried out and compared on the surface of SPE and IDE at different fabrication step (bare, MUDA and nanoMIP functionalised). Overall, the EIS characterisation results showed that the covalent attachment of nanoMIPs onto both type of gold electrodes (SPE and IDE) was achieved with good reproducibility. The success of the nanoMIP attachment was demonstrated by 3D AFM images of the electrode surface topography and proved to be consistent with previous work related to the nanoMIP or antibodies attachment onto gold sensor surface (Ohno *et al.*, 2013; Ashley *et al.*, 2018). However, the roughness analysis was less informative due to the geometrical conformation of the IDE and to the irregularities on the WE of the SPE, which introduced a bias on the values of the roughness surface parameters (Ra, Rq and Rmax). Overall, the EIS successfully differentiated each sensor fabrication step. Therefore, EIS can be proposed as a powerful surface characterisation and monitoring analytical technique to routinely monitor the compliance of the sensors surface fabrication steps.

To be competitive against the police dog and the other lab-based screening tools currently in use to detect drugs of abuse at trace level, the nanoMIP EIS affinity sensors have to achieve excellent sensitivity and specificity. Both these features were explored by performing cumulative assays. This work offers the first attempt in the integration of nanoMIP with an EIS electrochemical platform and, therefore, optimisation studies were carried out on SPE electrodes as their application in EIS biosensor arena is more consistent and better recognised (Rushworth *et al.*, 2013).

According to the achieved results (summarised in **Table 6-1**), both cocaine nanoMIP and morphine nanoMIP EIS sensors, developed on SPE, and were able to specifically detect the related analyte at a very low concentrations. Cocaine nanoMIP EIS sensor was not responsive against morphine and morphine nanoMIP EIS was not responsive against cocaine, while the assay conditions were kept constant. These results suggest a possible integration of the two nanoMIPs EIS sensors in a multiplex and selective platform for the

simultaneous detection of cocaine and morphine at trace level.-Additionally, each sensor can be used as the negative control of the other in the final device.

Table 6-1: Summary of the cocaine nanoMIP and morphine nanoMIP EIS sensors features and performances.

Electrode	WE Area (mm^2)	NanoMIP type	nanoMIP ($mg\ mL^{-1}$)	LOD ($ng\ mL^{-1}$)	Linear range ($ng\ mL^{-1}$)	Specificity
DropSens SPE	12.56	C	5	0.240 (0.71 nM)	0.1 – 50 (0.29 - 147 nM)	Levamisole, caffeine, mannitol, morphine
		M	1.2	0.323 (0.85 nM -)	0.1 – 50 (0.26 – 132 nM)	-
		M	2.4	0.109 (0.29 nM))	0.1 – 10 (0.26 – 26.39 nM)	Paracetamol, cocaine
DropSens IDE	16.9	C	5	2.54 (7.47 nM)	2.5 – 50 (7.36 - 147 nM)	-
		M	2.4	0.114 (0.30 nM))	0.01 – 5 (0.03 – 13.2 nM)	-

C = cocaine; M = morphine.

Concerning the specificity, the cocaine nanoMIP EIS sensor was assessed against levamisole, caffeine and mannitol. All these substances occur the composition of the street sample of cocaine hydrochloride (Grobério *et al.*, 2015; Pichini *et al.*, 2017). A blocking agent optimisation study was required to eliminate the cross-reactivity against caffeine, which was successfully minimised. Thus, no cross-reactivity towards caffeine and levamisole were detected. On the other hand, mannitol was found to bind non-specifically toward the control surface (electrodes functionalised without attaching the nanoMIP). However the sensor response was lower compared to the response towards cocaine.

The specificity of morphine nanoMIP EIS sensor was tested against paracetamol and the ability of the sensor to discriminate morphine from paracetamol was successfully proved.

Paracetamol is one of the major heroin and morphine cutting agents (Broséus *et al.*, 2015). However, the discrimination between paracetamol and morphine also has an implication in monitoring of athletic doping as paracetamol is a painkiller accepted in sports competition, whereas morphine is a banned substance (WADA, 2017). Nevertheless, the cutting agents may change over the time and across different countries as reported in retrospective studies (Broséus, Gentile and Esseiva, 2016). Therefore, the nanoMIP EIS sensor specificity should be reassessed accordingly and further blocking agent optimisation studies should be carried out, if needed.

Finally, both the optimised cocaine nanoMIP and morphine nanoMIP EIS sensors were respectively replicated onto IDEs and the sensitivity performances were tested. The sensor surface chemistry and fabrication process was kept consistent, thus allowing the comparison of the nanoMIP sensors onto the two type of electrodes (SPE and IDE). Notably, the LODs of morphine nanoMIP EIS sensor developed onto SPE (0.108 ng mL^{-1}) was nearly equal to the LOD achieved when the same sensor was fabricated on IDE (114 ng mL^{-1}). By contrast, the LOD achieved when the cocaine nanoMIP was fabricated on SPE (0.240 ng mL^{-1}) was one order of magnitude lower than the LOD achieved when the sensor was fabricated on IDE (2.5 ng mL^{-1}). However, the results were probably affected by the lack of stability at the connector and IDE electrode interface. Furthermore, the performances of the cocaine nanoMIP EIS sensor fabricated onto DropSens IDE may improve by working under a microfluidic condition, changing the cocaine nanoMIP concentration to use and blocking the glass substrate surface.

The data do not provide the evidence of higher performances in using IDE electrodes as reported in the literature. However, the linear ranges of both the nanoMIP sensor fabricated on IDE occurrd at lower concentrations than the linear ranges of the sensors fabricated on SPE. Thus, it is likely that the sensitivity of the sensor fabricated on IDE may improve by performing further optimisation studies, such as trying a different nanoMIP concentration or blocking the glass substrate of the IDE.

6.3 NanoMIP QCM Sensors for Drugs of Abuse Detection

The QCM sensor platform is a piezoelectric based sensor and the signal arises from a resonant frequency shift due to the viscosity and density changes at the sensor interface, such as due to the receptor-analyte binding. Quartz crystal microbalance (QCM) is a piezoelectric biosensor platform widely used both at research and commercial level. QCM biosensors devices with a fully embedded microfluidic system are already available on the market since many years, such as QCMA-1 (Sierra Sensor GmbH Hamburg, Germany) and QSense (Biolin Scientific Gothenburg, Sweden). At the same time, research works have been focusing on the QCM device miniaturisation and portability (Thies *et al.*, 2017). Although the QCM portability seems to be achievable, the theoretical limit of detection of this device has been reported to be in the range of ng cm^{-2} (Garcia *et al.*, 2011).

In this work, the QCM platform has been applied for the fabrication of a nanoMIPs based sensor able to specifically detect cocaine and morphine. The QCM sensor platform (QCMA-1, Sierra Sensors GmbH, Hamburg, Germany) has a fully embedded microfluidic and allowed to work on two sensing spot at the same time. The QCM also allowed a real-time visualisation of the sensor response (F (Hz)). Both the real-time and the microfluidic system allowed a fast workflow, although extensive time is required for the routine maintenance procedure of the machine. The raw data process required minimal data analysis, which was carried out by the integrated software Sierra Sensor Analyser. Although the miniaturised and portable formats are under development, the QCM sensor platform is not portable and, therefore, are used to develop in-lab analytical methods. Furthermore, the target analyte needs to have a detectable mass, such as the mass of protein. Among others nanotechnology-based expedients, the conjugation of the analyte with the gold nanoparticles (AuNPs) have been successfully applied to enhance the sensor sensitivity and has been exploited in this work to increase the mass of cocaine and morphine. Therefore, the drugs of abuse investigated in this work were conjugated to gold nanoparticles (AuNPs).

The nanoMIP were covalently attached onto the MUDA activated self-assembly monolayer (SAM) until the saturation was reached. Then, the surface of the nanoMIP

QCM sensor was investigated by AFM before and after the nanoMIP attachment and results showed a homogeneous nanoMIPs deposition onto the gold surface. The obtained AFM 3D images of the surface topography were comparable to AFM 3D images reported by previous studies related to nanoMIP onto similar gold sensor surface (Ashley *et al.*, 2018). Concerning the development of the nanoMIPs QCM sensor performances, results showed that the drugs were adsorbed onto the gold nanoparticles and were specifically detected by the nanoMIP covalently immobilised onto the gold QCM surface, with LODs equal to 0.191 µg mL^{-1} (morphine) and 0.360 µg mL^{-1} (cocaine). The affinity between the morphine nanoMIP and the morphine conjugated-AuNPs was evaluated performing KD and was found to be equal to 6.47 x 10^{-8} ± 3.40 x10^{-8}. The affinity between the cocaine nanoMIP and cocaine conjugated-AuNPs was in the one order of magnitude higher, i.e. 2.25 x 10^{-7} ± 1.9 x 10^{-7}. Despite the LODs valued are higher compared to other biosensors and analytical tools, the specific, environmentally stable and cheap receptors offer advantages for the fabrication of a low cost and rapid biosensor able to identify and quantify drugs of abuse.

Overall, the nanoMIPs QCM sensor was successfully developed and proved to detect of cocaine and morphine conjugated AuNPs. This affinity sensor promise to be a valuable lab- based methods for detecting drugs of abuse occurring in seized suspected materials.

6.4 Final Conclusion

In this work, the integration of two recent and cutting-edge technologies, such as the EIS sensor platform and the nanoMIP receptor, was achieved and allowed the development of a sensitive (sub-ppb), yet specific, sensors for the detection of cocaine and morphine in traces. Although further development is needed, the sensor platform promises to be a valuable candidate for the design of a portable sensor device able to replace police dogs and other portable, but more expensive devices employed by LEA in counteracting the illicit drugs of abuse activities.

The nanoMIP QCM sensor corroborated the previous results while providing a quick easy-to-perform analytical tool for the identification and quantification of cocaine and morphine in seizures comprising large quantity of suspected materials. The LOD was in

the sub-ppm range and the biosensor platform overcome limitations due to the lack of specificity owned by other analytical tools in detecting the selected illicit drugs (such as the immunobased kit or the IMS). Overall, the work has developed two biosensor platforms which promises to aid the forensic investigators and laboratories in answering to the following questions:

- Does the suspected material contain an illicit drug?
- If so, which one?
- How much pure drug does the seized material contain?

Currently, the developed sensors can discriminate and quantified only cocaine and morphine, but a possible extension to other drugs can be reasonably achieved with further developments, thus providing multiplexing, environmentally stable and easy to use nanoMIP based sensors platform for both on-site (EIS sensor) and in-lab (QCM sensor) applications.

6.5 Future work

The nanoMIP based sensors achieved in this work showed excellent performances in terms of sensitivity and specificity in detecting morphine and cocaine. However, several suggestions can be outlined to improve the development of each group of nanoMIP sensors:

NanoMIP EIS sensors:

- Optimisation study of the nanoMIP concentrations to be use in the fabrication of the EIS sensor.
- Optimisation study of nanoMIP EIS developed on DropSens IDE. Future works should cover the development of *ad-hoc* blocking of the IDE glass substrate and the optimisation of the nanoMIP concentration to be used during the sensor surface fabrication. This investigation aims to explore any possible improvement of the sensor sensitivity. The cumulative assay with the optimised condition needs to be replicated on cocaine nanoMIP EIS sensor fabricated on IDE using the developed 3D printed cable holder.

- Thermal regeneration studies is a desirable strategy to renew the sensor surface and allow its reusability. Therefore, the regeneration protocol needs to be replicated and the number of regeneration cycles has to be assessed.
- Durability and stability studies are needed to assess the storage time of both cocaine and morphine nanoMIPs EIS sensor. This study should first assess how stable is the sensor surface over the time and, when developed, how stable is the surface over temperature fluctuation.
- Validation in the real sample is required before reaching the commercialisation step, at least of the sensor surface chemistry. This study should be carried out by analysing the real sample by the EIS sensor and a benchmark instrument (such as IMS or MS hyphenated methods), as reported in previous studies (Moore, Kelley-Baker and Lacey, 2013; Musshoff *et al.*, 2014; Erol Öztürk, Yeter and Alpertunga, 2015).
- Design and development of a real-time EIS sensor platform equipped with a fully embedded microfluidic system. Preferably, the development should be done in collaboration with industrial partners who already commercialised the FRA/EIS potentiostat and with proved ability in the development of IDE electrodes for the bio-nano-sensor application. To speed the data analysis, a partnership with bioinformatics groups with a proved expertise in EIS biosensor and bioassay data analysis is also desirable.

NanoMIP QCM sensor:

- Specificity studies against current cutting cocaine and morphine agents should be investigated by blocking the surface with the optimised protocol developed onto the nanoMIP EIS sensor.
- Although promising regeneration protocol were achieved, chemical and thermal regeneration protocols have to be further investigated, thus allowing the chip reusability. Also, the number of regeneration cycles has to be assessed.
- Durability and stability studies of the QCM functionalised chip should be carried out and possible stabilisers should be explored for the QCM chip storage.

- Validation in the real sample should be carried out as outlined for the nanoMIP EIS sensors, thus providing the full dataset required to move into the commercialisation step.

REFERENCES

Abdin, M. J., Altintas, Z. and Tothill, I. E. (2015) 'In silico designed nanoMIP based optical sensor for endotoxins monitoring', *Biosensors and Bioelectronics*. Elsevier, 67, pp. 177–183. doi: 10.1016/j.bios.2014.08.009.

Acevska, J., Dimitrovska, A., Stefkov, G., Brezovska, K., Karapandzova, M. and Kulevanova, S. (2012) 'Development and Validation of a Reversed-Phase HPLC Method for Determination of Alkaloids from <I>Papaver somniferum</I> L. (Papaveraceae)', *Journal of AOAC International*, 95(2), pp. 399–405. doi: 10.5740/jaoacint.11-102.

Adnane, A. (2011) 'Electrochemical Biosensors for Virus Detection', in *Biosensors for Health, Environment and Biosecurity*. InTech. doi: 10.5772/17620.

Agius, R. and Kintz, P. (2010) 'Guidelines for European workplace drug and alcohol testing in hair.', *Drug testing and analysis*, 2(8), pp. 367–76. doi: 10.1002/dta.147.

Ahmed, A., Rushworth, J. V., Hirst, N. A. and Millner, P. A. (2014) 'Biosensors for whole-cell bacterial detection', *Clinical Microbiology Reviews*. American Society for Microbiology, 27(3), pp. 631–646. doi: 10.1128/CMR.00120-13.

Ahmed, A., Rushworth, J. V., Wright, J. D. and Millner, P. A. (2013) 'Novel Impedimetric Immunosensor for Detection of Pathogenic Bacteria *Streptococcus pyogenes* in Human Saliva', *Analytical Chemistry*, 85(24), pp. 12118–12125. doi: 10.1021/ac403253j.

Ahmed, A., Rushworth, J. V, Wright, J. D. and Millner, P. A. (2013) 'Novel impedimetric immunosensor for detection of pathogenic bacteria Streptococcus pyogenes in human saliva.', *Analytical chemistry*. American Chemical Society, 85(24), pp. 12118–25. doi: 10.1021/ac403253j.

Altintas, Z., Fakanya, W. M. and Tothill, I. E. (2014) 'Cardiovascular disease detection using bio-sensing techniques', *Talanta*, 128, pp. 177–186. doi: 10.1016/j.talanta.2014.04.060.

Altintas, Z., France, B., Ortiz, J. O. and Tothill, I. E. (2016) 'Computationally modelled receptors for drug monitoring using an optical based biomimetic SPR sensor', *Sensors and Actuators, B: Chemical*. Elsevier, 224, pp. 726–737. doi: 10.1016/j.snb.2015.10.075.

Altintas, Z., Gittens, M., Guerreiro, A., Thompson, K. A., Walker, J., Piletsky, S. and Tothill, I. E. (2015) 'Detection of Waterborne Viruses Using High Affinity Molecularly Imprinted Polymers', *Analytical Chemistry*. American Chemical Society, 87(13), pp. 6801–6807. doi: 10.1021/acs.analchem.5b00989.

Altintas, Z., Guerreiro, A., Piletsky, S. A. and Tothill, I. E. (2015) 'NanoMIP based optical sensor for pharmaceuticals monitoring', *Sensors and Actuators, B: Chemical*, 213, pp. 305–313. doi: 10.1016/j.snb.2015.02.043.

Altintas, Z., Kallempudi, S. S. and Gurbuz, Y. (2014) 'Gold nanoparticle modified capacitive sensor platform for multiple marker detection.', *Talanta*, 118, pp. 270–6. doi: 10.1016/j.talanta.2013.10.030.

Altintas, Z., Pocock, J., Thompson, K.-A. and Tothill, I. E. (2015) 'Comparative investigations for adenovirus recognition and quantification: Plastic or natural antibodies?', *Biosensors and Bioelectronics*. Elsevier, 74, pp. 996–1004. doi: 10.1016/j.bios.2015.07.076.

Altintas, Z. and Tothill, I. E. (2012) 'DNA-based biosensor platforms for the detection of TP53 mutation', *Sensors and Actuators B: Chemical*. Elsevier Science B.V., Amsterdam., 169, pp. 188–194. doi: 10.1016/j.snb.2012.04.064.

Altintas, Z. and Tothill, I. E. (2013) 'Biomarkers and biosensors for the early diagnosis of lung cancer', *Sensors and Actuators, B: Chemical*, 188, pp. 988–998. doi: 10.1016/j.snb.2013.07.078.

Altintas, Z., Uludag, Y., Gurbuz, Y. and Tothill, I. E. (2012) 'Development of surface chemistry for surface plasmon resonance based sensors for the detection of proteins and DNA molecules', *Analytica Chimica Acta*. Elsevier Science B.V., Amsterdam., 712, pp. 138–44. doi: 10.1016/j.aca.2011.11.026.

Ambrosini, S., Beyazit, S., Haupt, K. and Tse Sum Bui, B. (2013) 'Solid-phase synthesis of molecularly imprinted nanoparticles for protein recognition', *Chemical Communications*, 49(60), p. 6746. doi: 10.1039/c3cc41701h.

Analysis, I. (2011) 'Review of Transducer Principles for Label-Free Biomolecular Interaction Analysis', *Biosensors*, 1(3), pp. 70–92. doi: 10.3390/bios1030070.

Ansari, S. and Karimi, M. (2017) 'Novel developments and trends of analytical methods for drug analysis in biological and environmental samples by molecularly imprinted polymers', *TrAC - Trends in Analytical Chemistry*. Elsevier, pp. 146–162. doi: 10.1016/j.trac.2017.02.002.

Arntson, A., Ofsa, B., Lancaster, D., Simon, J. R., McMullin, M. and Logan, B. (2013) 'Validation of a novel immunoassay for the detection of synthetic cannabinoids and metabolites in urine specimens.', *Journal of analytical toxicology*, 37(5), pp. 284–90. doi: 10.1093/jat/bkt024.

Arroyo, A., Sanchez, M., Barberia, E., Barbal, M., Marrón, M. T. and Mora, A. (2013) 'Comparison of the Cozart DDS 801 on-site drug test device and gas chromatography/mass spectrometry (GC/MS) confirmation results of cannabis and cocaine in oral fluid specimens', *Australian Journal of Forensic Sciences*. Taylor and Francis Ltd., 46(3), pp. 272–281. doi: 10.1080/00450618.2013.832796.

Arya, S. K., Chornokur, G., Venugopal, M. and Bhansali, S. (2010) 'Antibody functionalized interdigitated μ-electrode (IDμE) based impedimetric cortisol biosensor', *The Analyst*. The Royal Society of Chemistry, 135(8), p. 1941. doi: 10.1039/c0an00242a.

Arya, S. K., Zhurauski, P., Jolly, P., Batistuti, M. R., Mulato, M. and Estrela, P. (2018) 'Capacitive aptasensor based on interdigitated electrode for breast cancer detection in undiluted human serum', *Biosensors and Bioelectronics*. Elsevier, 102, pp. 106–112. doi: 10.1016/J.BIOS.2017.11.013.

Ashley, J., Piekarska, M., Segers, C., Trinh, L., Rodgers, T., Willey, R. and Tothill, I. E. (2017) 'An SPR based sensor for allergens detection', *Biosensors and Bioelectronics*.

Elsevier, 88, pp. 109–113. doi: 10.1016/j.bios.2016.07.101.

Ashley, J., Shukor, Y., D'Aurelio, R., Trinh, L., Rodgers, T. L., Temblay, J., Pleasants, M. and Tothill, I. E. (2018) 'Synthesis of MIP Nanoparticles for α-Casein Detection using SPR as a Milk Allergen Sensor', *ACS Sensors*. American Chemical Society, p. acssensors.7b00850. doi: 10.1021/acssensors.7b00850.

Asturias-Arribas, L., Alonso-Lomillo, M. A., Domínguez-Renedo, O. and Arcos-Martínez, M. J. (2013) 'Electrochemical determination of cocaine using screen-printed cytochrome P450 2B4 based biosensors', *Talanta*, 105, pp. 131–134. doi: 10.1016/j.talanta.2012.11.078.

Atta, N. F., Galal, A., Wassel, A. A. and Ibrahim, A. H. (2012) 'Sensitive Electrochemical Determination of Morphine Using Gold Nanoparticles – Ferrocene Modified Carbon Paste Electrode', *International Journal of Electrochemical Science*, 7(11), pp. 10501–10518.

Atta, N. F., Hassan, H. K. and Galal, A. (2014) 'Rapid and simple electrochemical detection of morphine on graphene-palladium-hybrid-modified glassy carbon electrode.', *Analytical and bioanalytical chemistry*, 406(27), pp. 6933–42. doi: 10.1007/s00216-014-7999-x.

Baker, B. R., Lai, R. Y., Wood, M. S., Doctor, E. H., Heeger, A. J. and Plaxco, K. W. (2006) 'An electronic, aptamer-based small-molecule sensor for the rapid, label-free detection of cocaine in adulterated samples and biological fluids.', *Journal of the American Chemical Society*, 128(10), pp. 3138–9. doi: 10.1021/ja056957p.

Bănică, F.-G. (2012) *Chemical Sensors and Biosensors*, *Chemical Sensors and Biosensors: Fundamentals and Applications*. Chichester, UK: John Wiley & Sons, Ltd. doi: 10.1002/9781118354162.

Bell, S. (2009) 'Forensic chemistry.', *Annual review of analytical chemistry (Palo Alto, Calif.)*, 2, pp. 297–319. doi: 10.1146/annurev-anchem-060908-155251.

Berbel Manaia, E., Paiva Abuçafy, M., Chiari-Andréo, B. G., Lallo Silva, B., Oshiro-Júnior, J. A. and Chiavacci, L. (2017) 'Physicochemical characterization of drug nanocarriers', *International Journal of Nanomedicine*. Dove Press, Volume 12, pp. 4991–5011. doi: 10.2147/IJN.S133832.

Bhalla, V., Carrara, S., Stagni, C. and Samorì, B. (2010) 'Chip cleaning and regeneration for electrochemical sensor arrays', *Thin Solid Films*, 518(12), pp. 3360–3366. doi: 10.1016/j.tsf.2009.10.022.

Bhattacharjee, S. (2016) 'DLS and zeta potential – What they are and what they are not?', *Journal of Controlled Release*. Elsevier B.V., 235, pp. 337–351. doi: 10.1016/j.jconrel.2016.06.017.

Blencowe, T., Pehrsson, A., Lillsunde, P., Vimpari, K., Houwing, S., Smink, B., Mathijssen, R., Van der Linden, T., Legrand, S. A., Pil, K. and Verstraete, A. (2011) 'An analytical evaluation of eight on-site oral fluid drug screening devices using laboratory confirmation results from oral fluid', *Forensic Science International*, 208(1–3), pp. 173–179. doi: 10.1016/j.forsciint.2010.11.026.

Bondarenko, A. S., Ragoisha, G. A. and Pomerantsev, A. L. (2005) 'Progress in Chemometrics Research', *Nova Science Publication, NY*. Edited by E. Pomerantsev A. L. Nova Science Publishers, pp. 89–102.

Borsdorf, H. and Eiceman, G. A. (2006) 'Ion Mobility Spectrometry: Principles and Applications', *Applied Spectroscopy Reviews*. Taylor & Francis Group, 41(4), pp. 323–375. doi: 10.1080/05704920600663469.

Botelho, É. D., Cunha, R. B., Campos, A. F. C. and Maldaner, A. O. (2014) 'Chemical Profiling of Cocaine Seized by Brazilian Federal Police in 2009-2012: Major Components', *Journal of the Brazilian Chemical Society*, 25(4), pp. 611–618. doi: 10.5935/0103-5053.20140008.

Bozokalfa, G., Akbulut, H., Demir, B., Guler, E., Gumus, Z. P., Odaci Demirkol, D., Aldemir, E., Yamada, S., Endo, T., Coskunol, H., Timur, S. and Yagci, Y. (2016) 'Polypeptide Functional Surface for the Aptamer Immobilization: Electrochemical Cocaine Biosensing', *Analytical Chemistry*. American Chemical Society, 88(7), pp. 4161–4167. doi: 10.1021/acs.analchem.6b00760.

Broséus, J., Gentile, N., Bonadio Pont, F., Garcia Gongora, J. M., Gasté, L. and Esseiva, P. (2015) 'Qualitative, quantitative and temporal study of cutting agents for cocaine and heroin over 9 years.', *Forensic science international*. Elsevier Ireland Ltd, 257, pp. 307–13. doi: 10.1016/j.forsciint.2015.09.014.

Broséus, J., Gentile, N. and Esseiva, P. (2016) 'The cutting of cocaine and heroin: A critical review', *Forensic Science International*. Elsevier, 262, pp. 73–83. doi: 10.1016/J.FORSCIINT.2016.02.033.

Broséus, J., Huhtala, S. and Esseiva, P. (2015) 'First systematic chemical profiling of cocaine police seizures in Finland in the framework of an intelligence-led approach', *Forensic Science International*, 251. doi: 10.1016/j.forsciint.2015.03.026.

Buckley, K. and Matousek, P. (2012) *Non-Invasive Detection of Illicit Drugs Using Spatially Offset Raman Spectroscopy*, *Infrared and Raman Spectroscopy in Forensic Science*. Edited by J. M. Chalmers, H. G. M. Edwards, and M. D. Hargreaves. Chichester, UK: John Wiley & Sons, Ltd. doi: 10.1002/9781119962328.

Burnett, A. D., Edwards, H. G. M., Hargreaves, M. D., Munshi, T. and Page, K. (2011) 'A forensic case study: the detection of contraband drugs in carrier solutions by Raman spectroscopy.', *Drug testing and analysis*, 3(9), pp. 539–43. doi: 10.1002/dta.169.

Caddy, B. (2003) *Drugs of abuse*, *Science* . Springfield, Virginia, United States. doi: 10.1016/S1355-0306(03)71753-5.

Cai, Q., Chen, L., Luo, F., Qiu, B., Lin, Z. and Chen, G. (2011) 'Determination of cocaine on banknotes through an aptamer-based electrochemiluminescence biosensor', *Analytical and Bioanalytical Chemistry*, 400(1), pp. 289–294. doi: 10.1007/s00216-011-4739-3.

Canfarotta, F., Poma, A., Guerreiro, A. and Piletsky, S. (2016) 'Solid-phase synthesis of molecularly imprinted nanoparticles.', *Nature protocols*, 11(3), pp. 443–55. doi: 10.1038/nprot.2016.030.

Casale, J. and Klein, R. (1993) 'Illicit Production of Cocaine', *Forensic Science Review*, 5, pp. 95–107.

Cecinato, A., Balducci, C. and Perilli, M. (2016) 'Illicit psychotropic substances in the air: The state-of-art.', *The Science of the total environment*. Elsevier, 539, pp. 1–6. doi: 10.1016/j.scitotenv.2015.08.051.

Cecinato, A., Romagnoli, P., Perilli, M., Patriarca, C. and Balducci, C. (2014) 'Psychotropic substances in indoor environments.', *Environment international*. Elsevier Ltd, 71, pp. 88–93. doi: 10.1016/j.envint.2014.06.008.

Cela-Pérez, M. C., Bates, F., Jiménez-Morigosa, C., Lendoiro, E., de Castro, A., Cruz, A., López-Rivadulla, M., López-Vilariño, J. M. and González-Rodríguez, M. V. (2016) 'Water-compatible imprinted pills for sensitive determination of cannabinoids in urine and oral fluid.', *Journal of chromatography. A*, 1429, pp. 53–64. doi: 10.1016/j.chroma.2015.12.011.

Cerreta, M. M. and Furton, K. G. (2015) 'An assessment of detection canine alerts using flowers that release methyl benzoate, the cocaine odorant, and an evaluation of their behavior in terms of the VOCs produced', *Forensic Science International*. Elsevier, 251, pp. 107–114. doi: 10.1016/j.forsciint.2015.03.021.

Chandler, C. (2005) *Animal Assisted Therapy in Counselling*. 2 edition. Routledge.

Chantada-Vázquez, M. P., Sánchez-González, J., Peña-Vázquez, E., Tabernero, M. J., Bermejo, A. M., Bermejo-Barrera, P. and Moreda-Piñeiro, A. (2016) 'Synthesis and characterization of novel molecularly imprinted polymer - coated Mn-doped ZnS quantum dots for specific fluorescent recognition of cocaine', *Biosensors and Bioelectronics*. Elsevier Ltd, 75, pp. 213–221. doi: 10.1016/j.bios.2015.08.022.

Chardin, H., Mercier, K., Frydman, C. and Vollmer, N. (2014) 'Surface Plasmon Resonance imaging: A method to measure the affinity of the antibodies in allergy diagnosis', *Journal of Immunological Methods*. Elsevier, 405, pp. 23–28. doi: 10.1016/J.JIM.2013.12.010.

Chen, A. and Yang, S. (2015) 'Replacing antibodies with aptamers in lateral flow immunoassay', *Biosensors and Bioelectronics*. Elsevier Ltd, 71, pp. 230–242. doi: 10.1016/j.bios.2015.04.041.

Chen, J. Y., Penn, L. S. and Xi, J. (2018) 'Quartz crystal microbalance: Sensing cell-substrate adhesion and beyond', *Biosensors and Bioelectronics*, pp. 593–602. doi: 10.1016/j.bios.2017.08.032.

Cheraghi, S., Taher, M. A. and Karimi-Maleh, H. (2016) 'A Novel Strategy for Determination of Paracetamol in the Presence of Morphine Using a Carbon Paste Electrode Modified with CdO Nanoparticles and Ionic Liquids', *Electroanalysis*. WILEY-VCH Verlag, 28(2), pp. 366–371. doi: 10.1002/elan.201500357.

Chianella, I., Guerreiro, A., Moczko, E., Caygill, S., Piletska, E., De Vargas Sansalvador, I., Whitcombe, M. J. and Piletsky, S. (2013) 'Direct replacement of antibodies with molecularly imprinted polymer nanoparticles in ELISA - Development of a novel assay for vancomycin', *Analytical Chemistry*. American Chemical Society, 85(17), pp. 8462–

8468. doi: 10.1021/ac402102j.

Chianella, I., Lotierzo, M., Piletsky, S. A., Tothill, I. E., Chen, B., Karim, K. and Turner, A. P. F. (2002) 'Rational Design of a Polymer Specific for Microcystin-LR Using a Computational Approach', *Analytical Chemistry*. American Chemical Society, 74(6), pp. 1288–1293. doi: 10.1021/ac010840b.

Choodum, A. and Daeid, N. N. (2011) 'Rapid and semi-quantitative presumptive tests for opiate drugs.', *Talanta*, 86(1), pp. 284–92. doi: 10.1016/j.talanta.2011.09.015.

Choodum, A., Parabun, K., Klawach, N., Daeid, N. N., Kanatharana, P. and Wongniramaikul, W. (2014) 'Real time quantitative colourimetric test for methamphetamine detection using digital and mobile phone technology.', *Forensic science international*, 235, pp. 8–13. doi: 10.1016/j.forsciint.2013.11.018.

Christodoulides, N., De La Garza, R., Simmons, G. W., McRae, M. P., Wong, J., Newton, T. F., Smith, R., Mahoney Iii, J. J., Hohenstein, J., Gomez, S., Floriano, P. N., Talavera, H., Sloan, D. J., Moody, D. E., Andrenyak, D. M., Kosten, T. R., Haque, A. and McDevitt, J. T. (2015) 'Application of programmable bio-nano-chip system for the quantitative detection of drugs of abuse in oral fluids.', *Drug and alcohol dependence*, 153, pp. 306–13. doi: 10.1016/j.drugalcdep.2015.04.026.

Cowen, T., Karim, K. and Piletsky, S. (2016) 'Computational approaches in the design of synthetic receptors – A review', *Analytica Chimica Acta*, 936. doi: 10.1016/j.aca.2016.07.027.

Craven, B. A., Paterson, E. G. and Settles, G. S. (2010) 'The fluid dynamics of canine olfaction: unique nasal airflow patterns as an explanation of macrosmia.', *Journal of the Royal Society, Interface*. The Royal Society, 7(47), pp. 933–43. doi: 10.1098/rsif.2009.0490.

Cruces-Blanco, C. and García-Campaña, A. M. (2012) 'Capillary electrophoresis for the analysis of drugs of abuse in biological specimens of forensic interest', *TrAC - Trends in Analytical Chemistry*, 31, pp. 85–95. doi: 10.1016/j.trac.2011.06.019.

Cumeras, R., Figueras, E., Davis, C. E., Baumbach, J. I. and Gràcia, I. (2015) 'Review on ion mobility spectrometry. Part 1: current instrumentation.', *The Analyst*. The Royal Society of Chemistry, 140(5), pp. 1376–90. doi: 10.1039/c4an01100g.

Cuypers, E., Bonneure, A.-J. and Tytgat, J. (2016) 'The use of presumptive color tests for new psychoactive substances.', *Drug testing and analysis*. John Wiley and Sons Ltd, 8(1), pp. 137–41. doi: 10.1002/dta.1847.

D'Avila, F. B., Limberger, R. P. and Fröehlich, P. E. (2016) 'Cocaine and crack cocaine abuse by pregnant or lactating mothers and analysis of its biomarkers in meconium and breast milk by LC-MS-A review.', *Clinical biochemistry*. doi: 10.1016/j.clinbiochem.2016.01.019.

D'Elia, V., Montalvo García, G. and García Ruiz, C. (2015) 'Spectroscopic Trends for the Determination of Illicit Drugs in Oral Fluid', *Applied Spectroscopy Reviews*. Taylor and Francis Inc., 50(9), pp. 775–796. doi: 10.1080/05704928.2015.1075206.

Daniels, J. S. and Pourmand, N. (2007) 'Label-Free Impedance Biosensors: Opportunities and Challenges.', *Electroanalysis*, 19(12), pp. 1239–1257. doi: 10.1002/elan.200603855.

Davis, J. J. (2009) *Engineering the Bioelectronic Interface: Applications to Analyte Biosensing and Protein Detection*. RSC Pub.

Dehdashtian, S., Gholivand, M. B., Shamsipur, M. and Kariminia, S. (2016) 'Construction of a sensitive and selective sensor for morphine using chitosan coated Fe3O4 magnetic nanoparticle as a modifier', *Materials Science and Engineering: C*. Elsevier, 58, pp. 53–59. doi: 10.1016/J.MSEC.2015.07.049.

Dong, H., Tong, A. and Li, L. (2003) 'Syntheses of steroid-based molecularly imprinted polymers and their molecular recognition study with spectrometric detection', *Spectrochimica Acta Part A: Molecular and Biomolecular Spectroscopy*, 59(2), pp. 279–284. doi: 10.1016/S1386-1425(02)00179-8.

Du, F., Guo, L., Qin, Q., Zheng, X., Ruan, G., Li, J. and Li, G. (2015) 'Recent advances in aptamer-functionalized materials in sample preparation', *TrAC - Trends in Analytical Chemistry*, 67, pp. 134–146. doi: 10.1016/j.trac.2015.01.007.

Dunn, M. and Degenhardt, L. (2009) 'The use of drug detection dogs in Sydney, Australia.', *Drug and alcohol review*, 28(6), pp. 658–62. doi: 10.1111/j.1465-3362.2009.00065.x.

Ebrahimi, M., Johari-Ahar, M., Hamzeiy, H., Barar, J., Mashinchian, O. and Omidi, Y. (2012) 'Electrochemical impedance spectroscopic sensing of methamphetamine by a specific aptamer.', *BioImpacts : BI*, 2(2), pp. 91–5. doi: 10.5681/bi.2012.013.

Eissa, S., Tlili, C., L'Hocine, L. and Zourob, M. (2012) 'Electrochemical immunosensor for the milk allergen β-lactoglobulin based on electrografting of organic film on graphene modified screen-printed carbon electrodes', *Biosensors and Bioelectronics*. Elsevier, 38(1), pp. 308–313.

Eltzov, E., Guttel, S., Low Yuen Kei, A., Sinawang, P. D., Ionescu, R. E. and Marks, R. S. (2015) 'Lateral Flow Immunoassays - from Paper Strip to Smartphone Technology', *Electroanalysis*. Wiley-VCH Verlag, 27(9), pp. 2116–2130. doi: 10.1002/elan.201500237.

EMCDDA; Europol (2013) *EU Drug Market Report: A strategic analysis*. Lisbon.

Emcdda (2010) *Cocaine: A European Union perspective in the global context*. Lisbon. doi: 10.2810/16059.

EMCDDA (2005) *Illicit Drug Use in the Eu : Legislative Approach*. Lisbon.

EMCDDA (2012) *European Drug Report 2012*, *Euro surveillance : bulletin europ??en sur les maladies transmissibles = European communicable disease bulletin*. Luxembourg. doi: 10.2810/64775.

EMCDDA (2016) *European Drug Report 2016: Trends and Developments*, *European Monitoring of Drugs and Drugs Addiction*. Luxembourg. doi: 10.2810/88175.

Emcdda and Union, P. O. of the E. (2015) *New Psychoactive Substances in Europe. An*

update from the EU Early Warning System (March 2015)., *Publications Office of the European Union*. Luxembourg. doi: 10.2810/372415.

Emrani, A. S., Danesh, N. M., Ramezani, M., Taghdisi, S. M. and Abnous, K. (2016) 'A novel fluorescent aptasensor based on hairpin structure of complementary strand of aptamer and nanoparticles as a signal amplification approach for ultrasensitive detection of cocaine', *Biosensors and Bioelectronics*, 79, pp. 288–293. doi: 10.1016/j.bios.2015.12.025.

ENFSI (2014) 'Guidelines on Sampling of Illicit Drugs for Quantitative Analysis', pp. 1–82.

Erol Öztürk, Y., Yeter, O. and Alpertunga, B. (2015) 'Validation of JWH-018 and its metabolites in blood and urine by UPLC-MS/MS: Monitoring in forensic cases', *Forensic Science International*, 248, pp. 88–93. doi: 10.1016/j.forsciint.2014.12.029.

Farka, Z., Juřík, T., Kovář, D., Trnková, L. and Skládal, P. (2017) *Nanoparticle-Based Immunochemical Biosensors and Assays: Recent Advances and Challenges*, *Chemical Reviews*. American Chemical Society. doi: 10.1021/acs.chemrev.7b00037.

Favretto, D., Castagna, F., Maietti, S., Boscolo-Berto, R. and Ferrara, S. D. (2013) 'When color fails: illicit blue tablets containing anabolic androgen steroids.', *Journal of pharmaceutical and biomedical analysis*, 83, pp. 260–4. doi: 10.1016/j.jpba.2013.05.024.

Fei, W., Chen, F., Sun, L., Li, Q., Yang, J. and Wu, Y. (2013) 'Ultrasensitive electrochemiluminescent immunoassay for morphine using a gold electrode modified with CdS quantum dots, polyamidoamine, and gold nanoparticles', *Microchimica Acta*, 181(3–4), pp. 419–425. doi: 10.1007/s00604-013-1130-4.

Fenton, V. (1992) 'The use of dogs in search, rescue and recovery', *Journal of Wilderness Medicine*, pp. 292–300. doi: 10.1580/0953-9859-3.3.292.

Fenzl, C., Hirsch, T. and Baeumner, A. J. (2016) 'Nanomaterials as versatile tools for signal amplification in (bio)analytical applications', *TrAC - Trends in Analytical Chemistry*, pp. 306–316. doi: 10.1016/j.trac.2015.10.018.

Fernandes, L. S., Homem-De-Mello, P., De Lima, E. C. and Honorio, K. M. (2015) 'Rational design of molecularly imprinted polymers for recognition of cannabinoids: A structure-property relationship study', *European Polymer Journal*, 71, pp. 364–371. doi: 10.1016/j.eurpolymj.2015.08.005.

Ferreira, G. N. M., da-Silva, A. C. and Tomé, B. (2009) 'Acoustic wave biosensors: physical models and biological applications of quartz crystal microbalance', *Trends in Biotechnology*. Elsevier Current Trends, 27(12), pp. 689–697. doi: 10.1016/j.tibtech.2009.09.003.

Fischer, K. and Schmidt, M. (2016) 'Pitfalls and novel applications of particle sizing by dynamic light scattering', *Biomaterials*. Elsevier, 98, pp. 79–91. doi: 10.1016/j.biomaterials.2016.05.003.

Fischer, L. M., Tenje, M., Heiskanen, A. R., Masuda, N., Castillo, J., Bentien, A., Émneus, J., Jakobsen, M. H. and Boisen, A. (2009) 'Gold cleaning methods for

electrochemical detection applications', *Microelectronic Engineering*, 86(4–6), pp. 1282–1285. doi: 10.1016/j.mee.2008.11.045.

Fogel, R., Limson, J. and Seshia, A. A. (2016) 'Acoustic biosensors', *Essays In Biochemistry*. Portland Press Ltd, 60(1), pp. 101–110. doi: 10.1042/EBC20150011.

Forbes, T. P. and Najarro, M. (2016) 'Ion mobility spectrometry nuisance alarm threshold analysis for illicit narcotics based on environmental background and a ROC-curve approach', *The Analyst*. Royal Society of Chemistry, 141(14), pp. 4438–4446. doi: 10.1039/C6AN00844E.

Gambaro, V., Casagni, E., Dell'Acqua, L., Roda, G., Tamborini, L., Visconti, G. L. and Demartin, F. (2015) 'Identification and characterization of a new designer drug thiothinone in seized products', *Forensic Toxicology*. Springer-Verlag Tokyo, 34(1), pp. 174–178. doi: 10.1007/s11419-015-0289-2.

Gandhi, S., Banga, I., Maurya, P. K. and Eremin, S. A. (2018) 'A gold nanoparticle-single-chain fragment variable antibody as an immunoprobe for rapid detection of morphine by dipstick', *RSC Advances*. Royal Society of Chemistry, 8(3), pp. 1511–1518. doi: 10.1039/C7RA12810J.

Gandhi, S., Suman, P., Kumar, A., Sharma, P., Capalash, N. and Suri, C. R. (2015) 'Recent advances in immunosensor for narcotic drug detection.', *BioImpacts : BI*. Tabriz University of Medical Sciences, 5(4), pp. 207–13. doi: 10.15171/bi.2015.30.

Gao, S., Zheng, X. and Wu, J. (2017) 'A biolayer interferometry-based competitive biosensor for rapid and sensitive detection of saxitoxin', *Sensors and Actuators B: Chemical*. Elsevier, 246, pp. 169–174. doi: 10.1016/J.SNB.2017.02.078.

Garcia, J. V, Jimenez, Y., March, C., Montoya, A. and Arnau, A. (2011) 'QCM technology in biosensors', in *Biosensors - Emerging Materials and Applications*. InTech, pp. 153–178. doi: 10.5772/17991.

Garcia, Y., Smolinska-Kempisty, K., Pereira, E., Piletska, E. and Piletsky, S. (2017) 'Development of competitive 'pseudo'-ELISA assay for measurement of cocaine and its metabolites using molecularly imprinted polymer nanoparticles', *Analytical Methods*, 9(31). doi: 10.1039/c7ay01523b.

Goode, J. A., Rushworth, J. V. H. and Millner, P. A. (2015) 'Biosensor Regeneration: A Review of Common Techniques and Outcomes', *Langmuir*, pp. 6267–6276. doi: 10.1021/la503533g.

Goode, J., Dillon, G. and Millner, P. A. (2016) 'The development and optimisation of nanobody based electrochemical immunosensors for IgG', *Sensors and Actuators, B: Chemical*. Elsevier, 234, pp. 478–484. doi: 10.1016/j.snb.2016.04.132.

Grange, A. H. and Sovocool, G. W. (2011) 'Detection of illicit drugs on surfaces using direct analysis in real time (DART) time-of-flight mass spectrometry.', *Rapid communications in mass spectrometry : RCM*, 25(9), pp. 1271–81. doi: 10.1002/rcm.5009.

Grobério, T. S., Zacca, J. J., Botelho, É. D., Talhavini, M. and Braga, J. W. B. (2015)

'Discrimination and quantification of cocaine and adulterants in seized drug samples by infrared spectroscopy and PLSR.', *Forensic science international*. Elsevier Ireland Ltd, 257, pp. 297–306. doi: 10.1016/j.forsciint.2015.09.012.

Gross, J. H. (2013) 'Direct analysis in real time—a critical review on DART-MS', *Analytical and Bioanalytical Chemistry*, 406(1), pp. 63–80. doi: 10.1007/s00216-013-7316-0.

Guo, X. (2012) 'Surface plasmon resonance based biosensor technique : A review', *Journal of Biophotonics*, 19(7), pp. 1–19. doi: 10.1002/jbio.201200015.

Halámek, J., Makower, A., Skládal, P. and Scheller, F. W. (2002) 'Highly sensitive detection of cocaine using a piezoelectric immunosensor', *Biosensors and Bioelectronics*, 17(11–12), pp. 1045–1050. doi: 10.1016/S0956-5663(02)00098-2.

Hammond, J. L., Formisano, N., Estrela, P., Carrara, S. and Tkac, J. (2016) 'Electrochemical biosensors and nanobiosensors', *Essays In Biochemistry*, 60(1), pp. 69–80. doi: 10.1042/EBC20150008.

Han, L., Liu, P., Petrenko, V. A. and Liu, A. (2016) 'A Label-Free Electrochemical Impedance Cytosensor Based on Specific Peptide-Fused Phage Selected from Landscape Phage Library', *Scientific Reports*. Nature Publishing Group, 6(1), p. 22199. doi: 10.1038/srep22199.

Hao, H., Zhou, H., Zeng, L., Liu, J. and Liu, Y. (2014) 'Highly sensitive detection of morphine based on molecular imprinting polymers using surface plasmon resonance', *Journal of Chemical and Pharmaceutical Research*, 6(6), pp. 1699–1708.

Harper, L., Powell, J. and Pijl, E. M. (2017) 'An overview of forensic drug testing methods and their suitability for harm reduction point-of-care services', *Harm Reduction Journal*. BioMed Central, 14(1), p. 52. doi: 10.1186/s12954-017-0179-5.

Harris, D. C. (2010) *Quantitative Chemical Analysis*. 8th edn. New York: W. H. Freeman.

He, J.-L., Wu, Z.-S., Zhou, H., Wang, H.-Q., Jiang, J.-H., Shen, G.-L. and Yu, R.-Q. (2010) 'Fluorescence aptameric sensor for strand displacement amplification detection of cocaine.', *Analytical chemistry*, 82(4), pp. 1358–64. doi: 10.1021/ac902416u.

He, J., Wei, J., Rizak, J. D., Chen, Y., Wang, J., Hu, X. and Ma, Y. (2015) 'An odor detection system based on automatically trained mice by relative go no-go olfactory operant conditioning.', *Scientific reports*. Nature Publishing Group, 5, p. 10019. doi: 10.1038/srep10019.

Heuett, N. V, Ramirez, C. E., Fernandez, A. and Gardinali, P. R. (2015) 'Analysis of drugs of abuse by online SPE-LC high resolution mass spectrometry: communal assessment of consumption.', *The Science of the total environment*, 511, pp. 319–30. doi: 10.1016/j.scitotenv.2014.12.043.

Heurich, M., Altintas, Z. and Tothill, I. E. (2013) 'Computational design of peptide ligands for ochratoxin A', *Toxins*. Multidisciplinary Digital Publishing Institute, 5(6), pp. 1202–1212. doi: 10.3390/toxins5061202.

Hickey, S., McIlwraith, F., Bruno, R., Matthews, A. and Alati, R. (2012) 'Drug detection dogs in Australia: more bark than bite?', *Drug and alcohol review*, 31(6), pp. 778–83. doi: 10.1111/j.1465-3362.2012.00431.x.

Hilton, J. P., Nguyen, T. H., Pei, R., Stojanovic, M. and Lin, Q. (2011) 'A microfluidic affinity sensor for the detection of cocaine', *Sensors and Actuators A: Physical*, 166(2), pp. 241–246. doi: 10.1016/j.sna.2009.12.006.

Hinman, S. S., McKeating, K. S. and Cheng, Q. (2018) 'Surface Plasmon Resonance: Material and Interface Design for Universal Accessibility', *Analytical Chemistry*, 90(1), pp. 19–39. doi: 10.1021/acs.analchem.7b04251.

Hua, M., Tao, M., Wang, P., Zhang, Y., Wu, Z., Chang, Y. and Yang, Y. (2010) 'Label-free Electrochemical Cocaine Aptasensor Based on a Target-inducing Aptamer Switching Conformation', *Analytical Sciences*, 26(12), pp. 1265–1270. doi: 10.2116/analsci.26.1265.

Huang, X., Xu, Z., Mao, Y., Ji, Y., Xu, H., Xiong, Y. and Li, Y. (2015) 'Gold nanoparticle-based dynamic light scattering immunoassay for ultrasensitive detection of Listeria monocytogenes in lettuces', *Biosensors and Bioelectronics*. Elsevier, 66, pp. 184–190. doi: 10.1016/J.BIOS.2014.11.016.

Ilkhani, H., Ravalli, A. and Marrazza, G. (2016) 'Design of an Affibody-Based Recognition Strategy for Human Epidermal Growth Factor Receptor 2 (HER2) Detection by Electrochemical Biosensors', *Chemosensors*. Multidisciplinary Digital Publishing Institute, 4(4), p. 23. doi: 10.3390/chemosensors4040023.

Jaffrezic-Renault, N. (2013) 'Label-free affinity biosensors based on electrochemical impedance spectroscopy', in *Neuromethods*. Humana Press, Totowa, NJ, pp. 295–318. doi: 10.1007/978-1-62703-370-1-14.

Jagtap Ambre, A. H., R. N. (2006) 'Overview literature on atomic force microscopy (AFM): Basics and its important applications for polymer characterization', *Indian journal of Engineering & Materials Science*, pp. 368–384.

Jain, R. and Singh, R. (2016) 'Applications of dispersive liquid-liquid micro-extraction in forensic toxicology', *TrAC - Trends in Analytical Chemistry*. Elsevier, 75, pp. 227–237. doi: 10.1016/j.trac.2015.07.007.

Jezierski, T., Adamkiewicz, E., Walczak, M., Sobczyńska, M., Górecka-Bruzda, A., Ensminger, J. and Papet, E. (2014) 'Efficacy of drug detection by fully-trained police dogs varies by breed, training level, type of drug and search environment', *Forensic Science International*, 237, pp. 112–118. doi: 10.1016/j.forsciint.2014.01.013.

Justino, C. I. L., Freitas, A. C., Pereira, R., Duarte, A. C. and Rocha, T. A. P. (2015) 'Trends in Analytical Chemistry Recent developments in recognition elements for chemical sensors and biosensors', *Trends in Analytical Chemistry*, 68, pp. 2–17. doi: 10.1016/j.trac.2015.03.006.

Kadehjian, L. J. (2005) 'Chapter 2. Specimens for Drugs-of-Abuse Testing', in *Drugs of Abuse Body Fluid Testing*. Totowa: Humana Press Inc., pp. 11–29.

Kaushik, A., Shah, P., Vabbina, P. K., Jayant, R. D., Tiwari, S., Vashist, A., Yndart, A. and Nair, M. (2016) 'A label-free electrochemical immunosensor for beta-amyloid detection', *Anal. Methods*. The Royal Society of Chemistry, 8(31), pp. 6115–6120. doi: 10.1039/C6AY01910B.

Kerrigan, S., Mellon, M. B., Banuelos, S. and Arndt, C. (2011) 'Evaluation of commercial enzyme-linked immunosorbent assays to identify psychedelic phenethylamines', *Journal of Analytical Toxicology*, 35(7), pp. 444–451. doi: 10.1093/anatox/35.7.444.

Kim, I., Moon, J.-S. and Oh, J.-W. (2016) 'Recent advances in M13 bacteriophage-based optical sensing applications', *Nano Convergence*. Korea Nano Technology Research Society, 3(1), p. 27. doi: 10.1186/s40580-016-0087-5.

Klenkar, G. and Liedberg, B. (2008) 'A microarray chip for label-free detection of narcotics', *Analytical and Bioanalytical Chemistry*, 391(5), pp. 1679–1688. doi: 10.1007/s00216-008-1839-9.

Kontomaris, S. V and Stylianou, A. (2017) 'Atomic force microscopy for university students: applications in biomaterials', *European Journal of Physics*. IOP Publishing, 38(3), p. 033003. doi: 10.1088/1361-6404/aa5cd6.

Korpi, E. R., den Hollander, B., Farooq, U., Vashchinkina, E., Rajkumar, R., Nutt, D. J., Hyytiä, P. and Dawe, G. S. (2015) 'Mechanisms of Action and Persistent Neuroplasticity by Drugs of Abuse.', *Pharmacological reviews*. American Society for Pharmacology and Experimental Therapeutics, 67(4), pp. 872–1004. doi: 10.1124/pr.115.010967.

Korposh, S., Chianella, I., Guerreiro, A., Caygill, S., Piletsky, S., James, S. W. and Tatam, R. P. (2014) 'Selective vancomycin detection using optical fibre long period gratings functionalised with molecularly imprinted polymer nanoparticles', *The Analyst*. Royal Society of Chemistry, 139(9), pp. 2229–2236. doi: 10.1039/C3AN02126B.

Krauss, S. T., Remcho, T. P., Lipes, S. M., Aranda, R., Maynard, H. P., Shukla, N., Li, J., Tontarski, R. E. and Landers, J. P. (2016) 'Objective Method for Presumptive Field-Testing of Illicit Drug Possession Using Centrifugal Microdevices and Smartphone Analysis', *Analytical Chemistry*, 88(17), pp. 8689–8697. doi: 10.1021/acs.analchem.6b01982.

de la Rica, R., Fernández-Sánchez, C. and Baldi, A. (2006) 'Polysilicon interdigitated electrodes as impedimetric sensors', *Electrochemistry Communications*. Elsevier, 8(8), pp. 1239–1244. doi: 10.1016/j.elecom.2006.05.028.

Lai, C.-Y., Foot, P., Brown, J. and Spearman, P. (2017) 'A Urea Potentiometric Biosensor Based on a Thiophene Copolymer', *Biosensors*. Multidisciplinary Digital Publishing Institute, 7(4), p. 13. doi: 10.3390/bios7010013.

Lapachinske, S. F., Okai, G. G., dos Santos, A., de Bairros, A. V. and Yonamine, M. (2015) 'Analysis of cocaine and its adulterants in drugs for international trafficking seized by the Brazilian Federal Police.', *Forensic science international*. Elsevier Ireland Ltd, 247, pp. 48–53. doi: 10.1016/j.forsciint.2014.11.028.

Leffler, A. M., Smith, P. B., de Armas, A. and Dorman, F. L. (2014) 'The analytical investigation of synthetic street drugs containing cathinone analogs.', *Forensic science*

international, 234, pp. 50–6. doi: 10.1016/j.forsciint.2013.08.021.

Leitch, O., Anderson, A., Kirkbride, K. P. and Lennard, C. (2013) 'Biological organisms as volatile compound detectors: a review.', *Forensic science international*, 232(1–3), pp. 92–103. doi: 10.1016/j.forsciint.2013.07.004.

Lendoiro, E., de Castro, A., Fernández-Vega, H., Cela-Pérez, M. C., López-Vilariño, J. M., González-Rodríguez, M. V, Cruz, A. and López-Rivadulla, M. (2014) 'Molecularly imprinted polymer for selective determination of Δ9-tetrahydrocannabinol and 11-nor-Δ9-tetrahydrocannabinol carboxylic acid using LC-MS/MS in urine and oral fluid.', *Analytical and bioanalytical chemistry*. Springer Verlag, 406(15), pp. 3589–97. doi: 10.1007/s00216-013-7599-1.

Lesiak, A. D., Musah, R. A., Domin, M. A. and Shepard, J. R. E. (2014) 'DART-MS as a preliminary screening method for "herbal incense": chemical analysis of synthetic cannabinoids.', *Journal of forensic sciences*, 59(2), pp. 337–43. doi: 10.1111/1556-4029.12354.

Li, M., Zhang, J., Jiang, J., Zhang, J., Gao, J. and Qiao, X. (2014) 'Rapid, in situ detection of cocaine residues based on paper spray ionization coupled with ion mobility spectrometry.', *The Analyst*. The Royal Society of Chemistry, 139(7), pp. 1687–91. doi: 10.1039/c3an02198j.

Li, X., Yu, M., Chen, Z., Lin, X. and Wu, Q. (2017) 'A sensor for detection of carcinoembryonic antigen based on the polyaniline-Au nanoparticles and gap-based interdigitated electrode', *Sensors and Actuators B: Chemical*. Elsevier B.V., 239, pp. 874–882. doi: 10.1016/j.snb.2016.08.101.

Li, Y., Ji, X. and Liu, B. (2011) 'Chemiluminescence aptasensor for cocaine based on double-functionalized gold nanoprobes and functionalized magnetic microbeads.', *Analytical and bioanalytical chemistry*, 401(1), pp. 213–9. doi: 10.1007/s00216-011-5064-6.

Li, Y., Qi, H., Peng, Y., Yang, J. and Zhang, C. (2007) 'Electrogenerated chemiluminescence aptamer-based biosensor for the determination of cocaine', *Electrochemistry Communications*, 9(10), pp. 2571–2575. doi: 10.1016/j.elecom.2007.07.038.

Li, Y., Zou, L., Li, Y., Li, K. and Ye, B. (2014) 'A new voltammetric sensor for morphine detection based on electrochemically reduced MWNTs-doped graphene oxide composite film', *Sensors and Actuators, B: Chemical*, 201, pp. 511–519. doi: 10.1016/j.snb.2014.05.034.

Li, Z., Yu, Y., Li, Z., Wu, T. and Yin, J. (2015) 'The art of signal transforming: electrodes and their smart applications in electrochemical sensing', *Analytical Methods*. Royal Society of Chemistry, 7(23), pp. 9732–9743. doi: 10.1039/C5AY02373D.

Lian, Y., He, F., Wang, H. and Tong, F. (2015) 'A new aptamer/graphene interdigitated gold electrode piezoelectric sensor for rapid and specific detection of Staphylococcus aureus', *Biosensors and Bioelectronics*. Elsevier Ltd, 65, pp. 314–319. doi: 10.1016/j.bios.2014.10.017.

Lisdat, F. and Schäfer, D. (2008) 'The use of electrochemical impedance spectroscopy for biosensing.', *Analytical and bioanalytical chemistry*, 391(5), pp. 1555–67. doi: 10.1007/s00216-008-1970-7.

Liu, H. C., Lee, H. T., Hsu, Y. C., Huang, M. H., Liu, R. H., Chen, T. J. and Lin, D. L. (2015) 'Direct injection LC-MS-MS analysis of opiates, methamphetamine, buprenorphine, methadone and their metabolites in oral fluid from substitution therapy patients', *Journal of Analytical Toxicology*. Oxford University Press, 39(6), pp. 472–480. doi: 10.1093/jat/bkv041.

Liu, X., Zhong, J., Rao, H., Lu, Z., Ge, H., Chen, B., Zou, P., Wang, X., He, H., Zeng, X. and Wang, Y. (2017) 'Electrochemical dipyridamole sensor based on molecularly imprinted polymer on electrode modified with Fe<inf>3</inf>O<inf>4</inf>@Au/amine-multi-walled carbon nanotubes', *Journal of Solid State Electrochemistry*. doi: 10.1007/s10008-017-3650-z.

Liuni, P., Romanov, V., Binette, M. J., Zaknoun, H., Tam, M., Pilon, P., Hendrikse, J. and Wilson, D. J. (2014) 'Unambiguous characterization of analytical markers in complex, seized opiate samples using an enhanced ion mobility trace detector-mass spectrometer', *Analytical Chemistry*. American Chemical Society, 86(21), pp. 10772–10779. doi: 10.1021/ac502676d.

Lorenzo, N., Wan, T., Harper, R. J., Hsu, Y.-L., Chow, M., Rose, S. and Furton, K. G. (2003) 'Laboratory and field experiments used to identify Canis lupus var. familiaris active odor signature chemicals from drugs, explosives, and humans.', *Analytical and bioanalytical chemistry*, 376(8), pp. 1212–24. doi: 10.1007/s00216-003-2018-7.

Lvovich, V. F. (2012) *Impedance spectrocopy-Applications to Electrochemical and Dielectric Phenomena*. Wiley.

Ma, C., Wang, W., Yang, Q., Shi, C. and Cao, L. (2011) 'Cocaine detection via rolling circle amplification of short DNA strand separated by magnetic beads', *Biosensors and Bioelectronics*. Elsevier, 26(7), pp. 3309–3312. doi: 10.1016/j.bios.2011.01.003.

Ma, Q., Bai, H., Li, W., Wang, C., Cooks, R. G. and Ouyang, Z. (2015) 'Rapid analysis of synthetic cannabinoids using a miniature mass spectrometer with ambient ionization capability.', *Talanta*. Elsevier, 142, pp. 190–6. doi: 10.1016/j.talanta.2015.04.044.

Macias, M. S., Guerra-Diaz, P., Almirall, J. R. and Furton, K. G. (2010) 'Detection of piperonal emitted from polymer controlled odor mimic permeation systems utilizing Canis familiaris and solid phase microextraction-ion mobility spectrometry.', *Forensic science international*, 195(1–3), pp. 132–8. doi: 10.1016/j.forsciint.2009.12.006.

Mackuľak, T., Staňová, A. V., Gál, M., Híveš, J., Grabic, R. and Tichý, J. (2015) 'Determination of illicit drugs and their metabolites contamination on banknotes', *Monatshefte für Chemie - Chemical Monthly*. Springer-Verlag Wien, 147(1), pp. 39–43. doi: 10.1007/s00706-015-1610-9.

Mali, N., Karpe, M. and Kadam, V. (2011) 'A review on biological matrices and analytical methods used for determination of drug of abuse', *Journal of Applied Pharmaceutical ...*, 1(06), pp. 58–65.

Mark, D., Haeberle, S., Roth, G., von Stetten, F. and Zengerle, R. (2010) 'Microfluidic lab-on-a-chip platforms: requirements, characteristics and applications', *Chemical Society Reviews*. Royal Society of Chemistry, 39(3), p. 1153. doi: 10.1039/b820557b.

Masdor, N. A., Altintas, Z. and Tothill, I. E. (2016) 'Sensitive detection of Campylobacter jejuni using nanoparticles enhanced QCM sensor', *Biosensors and Bioelectronics*, 78, pp. 328–336. doi: 10.1016/j.bios.2015.11.033.

Masdor, N., Altintas, Z. and Tothill, I. E. (2017) 'Surface Plasmon Resonance Immunosensor for the Detection of Campylobacter jejuni', *Chemosensors*. Multidisciplinary Digital Publishing Institute, 5(2), p. 16. doi: 10.3390/chemosensors5020016.

Mastroianni, N., Postigo, C., López de Alda, M., Viana, M., Rodríguez, A., Alastuey, A., Querol, X. and Barceló, D. (2015) 'Comprehensive monitoring of the occurrence of 22 drugs of abuse and transformation products in airborne particulate matter in the city of Barcelona', *Science of the Total Environment*. Elsevier, 532, pp. 344–352. doi: 10.1016/j.scitotenv.2015.06.027.

Mazzotta, E., Turco, A., Chianella, I., Guerreiro, A., Piletsky, S. A. and Malitesta, C. (2016) 'Solid-phase synthesis of electroactive nanoparticles of molecularly imprinted polymers. A novel platform for indirect electrochemical sensing applications', *Sensors and Actuators, B: Chemical*, 229, pp. 174–180. doi: 10.1016/j.snb.2016.01.126.

Mcquillan, J. S. and Shaw, A. M. (2013) 'Whole-cell Escherichia coli-based bio-sensor assay for dual zinc oxide nanoparticle toxicity mechanisms', *Biosensors and Bioelectronic*, 51, pp. 274–279. doi: 10.1016/j.bios.2013.07.024.

Meyer, M. R. (2014) 'Trends in analyzing emerging drugs of abuse--from seized samples to body samples.', *Analytical and bioanalytical chemistry*. Springer Verlag, 406(25), pp. 6105–10. doi: 10.1007/s00216-014-8082-3.

Michen, B., Geers, C., Vanhecke, D., Endes, C., Rothen-Rutishauser, B., Balog, S. and Petri-Fink, A. (2015) 'Avoiding drying-artifacts in transmission electron microscopy: Characterizing the size and colloidal state of nanoparticles', *Scientific Reports*, 5. doi: 10.1038/srep09793.

Miočević, O., Cole, C. R., Laughlin, M. J., Buck, R. L., Slowey, P. D. and Shirtcliff, E. A. (2017) 'Quantitative Lateral Flow Assays for Salivary Biomarker Assessment: A Review', *Frontiers in Public Health*. Frontiers, 5, p. 133. doi: 10.3389/fpubh.2017.00133.

Moczko, E., Poma, A., Guerreiro, A., Perez De Vargas Sansalvador, I., Caygill, S., Canfarotta, F., Whitcombe, M. J. M. J. and Piletsky, S. (2013) 'Surface-modified multifunctional MIP nanoparticles.', *Nanoscale*. Royal Society of Chemistry, 5(9), pp. 3733–41. doi: 10.1039/c3nr00354j.

Mohr, A. L. A., Ofsa, B., Keil, A. M., Simon, J. R., McMullin, M. and Logan, B. K. (2014) 'Enzyme-linked immunosorbent assay (ELISA) for the detection of use of the synthetic cannabinoid agonists UR-144 and XLR-11 in human urine', *Journal of Analytical Toxicology*, 38(7), pp. 427–431. doi: 10.1093/jat/bku049.

Mokhtarzadeh, A., Ezzati Nazhad Dolatabadi, J., Abnous, K., de la Guardia, M. and

Ramezani, M. (2015) 'Nanomaterial-based cocaine aptasensors', *Biosensors and Bioelectronics*, 68, pp. 95–106. doi: 10.1016/j.bios.2014.12.052.

Monošík, R., Stred'anský, M. and Šturdík, E. (2012) 'Application of electrochemical biosensors in clinical diagnosis.', *Journal of clinical laboratory analysis*, 26(1), pp. 22–34. doi: 10.1002/jcla.20500.

Moore, C., Kelley-Baker, T. and Lacey, J. (2013) 'Field testing of the Alere DDS2 mobile test system for drugs in oral fluid', *Journal of Analytical Toxicology*, 37(5), pp. 305–307. doi: 10.1093/jat/bkt022.

Moreno, V. M., López-López, M., Atoche, J.-C. and García-Ruiz, C. (2014) 'Raman identification of drug of abuse particles collected with colored and transparent tapes.', *Science & justice : journal of the Forensic Science Society*. Forensic Science Society, 54(2), pp. 164–9. doi: 10.1016/j.scijus.2013.12.003.

Munoz, E. M., Lorenzo-Abalde, S., González-Fernández, Á., Quintela, O., Lopez-Rivadulla, M. and Riguera, R. (2011) 'Direct surface plasmon resonance immunosensor for in situ detection of benzoylecgonine, the major cocaine metabolite', *Biosensors and Bioelectronics*, 26(11), pp. 4423–4428. doi: 10.1016/j.bios.2011.04.056.

Muñoz, J., Montes, R. and Baeza, M. (2017) 'Trends in electrochemical impedance spectroscopy involving nanocomposite transducers: Characterization, architecture surface and bio-sensing', *TrAC - Trends in Analytical Chemistry*. Elsevier, 97, pp. 201–215. doi: 10.1016/j.trac.2017.08.012.

Musshoff, F., Hokamp, E. G., Bott, U. and Madea, B. (2014) 'Performance evaluation of on-site oral fluid drug screening devices in normal police procedure in Germany', *Forensic Science International*. Elsevier Ireland Ltd, 238, pp. 120–124. doi: 10.1016/j.forsciint.2014.02.005.

Musshoff, F., Kirschbaum, K. M., Graumann, K., Herzfeld, C., Sachs, H. and Madea, B. (2012) 'Evaluation of two immunoassay procedures for drug testing in hair samples.', *Forensic science international*, 215(1–3), pp. 60–3. doi: 10.1016/j.forsciint.2011.03.030.

Nagel, B., Dellweg, H. and Gierasch, L. (1992) *Glossary for chemists of terms used in biotechnology (IUPAC Recommendations 1992)*, *Pure and Applied Chemistry*. doi: 10.1351/pac199264010143.

Nestić, M., Babić, S., Pavlović, D. M. and Sutlović, D. (2013) 'Molecularly imprinted solid phase extraction for simultaneous determination of δ9-tetrahydrocannabinol and its main metabolites by gas chromatography-mass spectrometry in urine samples', *Forensic Science International*, 231(1–3), pp. 317–324. doi: 10.1016/j.forsciint.2013.06.009.

Neves, M. A. D., Blaszykowski, C., Bokhari, S. and Thompson, M. (2015) 'Ultra-high frequency piezoelectric aptasensor for the label-free detection of cocaine', *Biosensors and Bioelectronics*, 72, pp. 383–392. doi: 10.1016/j.bios.2015.05.038.

Nguyen, H. H., Park, J., Kang, S. and Kim, M. (2015) 'Surface plasmon resonance: A versatile technique for biosensor applications', *Sensors (Switzerland)*, 15(5), pp. 10481–10510. doi: 10.3390/s150510481.

Nguyen, T. H., Sun, T. and Grattan, K. T. V. (2016) 'Surface plasmon resonance based fibre optic chemical sensor for the detection of cocaine', in Lewis, E. (ed.). International Society for Optics and Photonics, p. 991612. doi: 10.1117/12.2236938.

Nieddu, M., Burrai, L., Trignano, C. and Boatto, G. (2014) 'Cross-reactivities of 39 new amphetamine designer drugs on three abuse drugs urinary screening tests', *Forensic Toxicology*, 32(1), pp. 132–138. doi: 10.1007/s11419-013-0198-1.

Ohno, R., Ohnuki, H., Wang, H., Yokoyama, T., Endo, H., Tsuya, D. and Izumi, M. (2013) 'Electrochemical impedance spectroscopy biosensor with interdigitated electrode for detection of human immunoglobulin A', *Biosensors and Bioelectronics*, 40(1), pp. 422–426. doi: 10.1016/j.bios.2012.07.052.

De Oliveira, R. R. L., Albuquerque, D. a. C., Cruz, T. G. S. and Leite, F. M. Y. and F. L. (2012) 'Measurement of the Nanoscale Roughness by Atomic Force Microscopy: Basic Principles and Applications', *Atomic Force Microscopy - Imaging, Measuring and Manipulating Surfaces at the Atomic Scale*, 3, p. 256. doi: DOI: 10.5772/37583.

Ozturk, S., Ozturk, Y. E., Yeter, O. and Alpertunga, B. (2015) 'Application of a validated LC–MS/MS method for JWH-073 and its metabolites in blood and urine in real forensic cases', *Forensic Science International*, 257, pp. 165–171. doi: 10.1016/j.forsciint.2015.08.013.

Parker, C. O. and Tothill, I. E. (2009) 'Development of an electrochemical immunosensor for aflatoxin M1in milk with focus on matrix interference', *Biosensors and Bioelectronics*. Elsevier Science B.V., Amsterdam., 24(8), pp. 2452–2457. doi: 10.1016/j.bios.2008.12.021.

Pawula, M., Altintas, Z. and Tothill, I. E. (2016) 'SPR detection of cardiac troponin T for acute myocardial infarction', *Talanta*, 146, pp. 823–830. doi: 10.1016/j.talanta.2015.06.006.

Pawula, M., Altintas, Z. and Tothill, I. E. (2016) 'Talanta SPR detection of cardiac troponin T for acute myocardial infarction', *Talanta*, 146, pp. 823–830. doi: 10.1016/j.talanta.2015.06.006.

Petersen, R. and L., R. (2017) 'Strategies Using Bio-Layer Interferometry Biosensor Technology for Vaccine Research and Development', *Biosensors*. Multidisciplinary Digital Publishing Institute, 7(4), p. 49. doi: 10.3390/bios7040049.

Pichini, S., Busardò, F. P., Gregori, A., Berretta, P., Gentili, S. and Pacifici, R. (2017) 'Purity and adulterant analysis of some recent drug seizures in Italy', *Drug Testing and Analysis*, 9(3), pp. 485–490. doi: 10.1002/dta.2134.

Piletska, E. V., Guerreiro, A. R., Romero-Guerra, M., Chianella, I., Turner, A. P. F. and Piletsky, S. A. (2008) 'Design of molecular imprinted polymers compatible with aqueous environment', *Analytica Chimica Acta*, 607(1), pp. 54–60. doi: 10.1016/j.aca.2007.11.019.

Piletska, E. V., Romero-Guerra, M., Chianella, I., Karim, K., Turner, A. P. F. and Piletsky, S. A. (2005) 'Towards the development of multisensor for drugs of abuse based on molecular imprinted polymers', *Analytica Chimica Acta*, 542(1 SPEC. ISS.), pp. 111–

117. doi: 10.1016/j.aca.2005.03.067.

Piro, B., Shi, S., Reisberg, S., Noël, V. and Anquetin, G. (2016) 'Comparison of Electrochemical Immunosensors and Aptasensors for Detection of Small Organic Molecules in Environment, Food Safety, Clinical and Public Security.', *Biosensors*, 6(1). doi: 10.3390/bios6010007.

Polet, M., Van Gansbeke, W., Van Eenoo, P. and Deventer, K. (2016) 'Gas chromatography/chemical ionization triple quadrupole mass spectrometry analysis of anabolic steroids: Ionization and collision-induced dissociation behavior', *Rapid Communications in Mass Spectrometry*. John Wiley and Sons Ltd, 30(4), pp. 511–522. doi: 10.1002/rcm.7472.

Poma, A., Brahmbhatt, H., Pendergraff, H. M., Watts, J. K. and Turner, N. W. (2015) 'Generation of Novel Hybrid Aptamer – Molecularly Imprinted Polymeric Nanoparticles', *Advanced Materials*, 27(4), pp. 750–758. doi: 10.1002/adma.201404235.

Poma, A., Guerreiro, A., Caygill, S., Moczko, E. and Piletsky, S. (2014) 'Automatic reactor for solid-phase synthesis of molecularly imprinted polymeric nanoparticles (MIP NPs) in water', *RSC Adv.*, 4(8), pp. 4203–4206. doi: 10.1039/C3RA46838K.

Poma, A., Guerreiro, A., Whitcombe, M. J., Piletska, E. V., Turner, A. P. F. and Piletsky, S. A. (2013) 'Solid-Phase Synthesis of Molecularly Imprinted Polymer Nanoparticles with a Reusable Template-"Plastic Antibodies"', *Advanced Functional Materials*, 23(22), pp. 2821–2827. doi: 10.1002/adfm.201202397.

Poma, A., Turner, A. P. F. and Piletsky, S. A. (2010) 'Advances in the manufacture of MIP nanoparticles', *Trends in Biotechnology*, 28(12), pp. 629–637. doi: 10.1016/j.tibtech.2010.08.006.

Prodromidis, M. I. (2010) 'Impedimetric immunosensors—A review', *Electrochimica Acta*, 55(14), pp. 4227–4233. doi: 10.1016/j.electacta.2009.01.081.

PubChem (2018) *Morphine Hydrochloride*, *National Center for Biotechnology Information*. Available at: https://pubchem.ncbi.nlm.nih.gov/compound/5492889 (Accessed: 21 January 2018).

Pujol, M. L., Cirimele, V., Tritsch, P. J., Villain, M. and Kintz, P. (2007) 'Evaluation of the IDS One-Step™ ELISA kits for the detection of illicit drugs in hair', *Forensic Science International*, 170(2–3), pp. 189–192. doi: 10.1016/j.forsciint.2007.02.032.

Pyrz, W. D. and Buttrey, D. J. (2008) 'Particle Size Determination Using TEM: A Discussion of Image Acquisition and Analysis for the Novice Microscopist', *Langmuir*. American Chemical Society, 24(20), pp. 11350–11360. doi: 10.1021/la801367j.

Quesada-González, D. and Merkoçi, A. (2015) 'Nanoparticle-based lateral flow biosensors', *Biosensors and Bioelectronics*. Elsevier Ltd, 73, pp. 47–63. doi: 10.1016/j.bios.2015.05.050.

Raab, N. and Bachelet, I. (2017) 'Resolving biofilm topography by native scanning electron microscopy', *Journal of Biological Methods*, 4(2), p. 70. doi: 10.14440/jbm.2017.173.

Ram, Y., Yoetz-Kopelman, T., Dror, Y., Freeman, A. and Shacham-Diamand, Y. (2016) 'Impact of Molecular Surface Charge on Biosensing by Electrochemical Impedance Spectroscopy', *Electrochimica Acta*. Pergamon, 200, pp. 161–167. doi: 10.1016/J.ELECTACTA.2016.03.162.

Ramachandran, R., Chen, S. M., Gnana Kumar, G. P., Gajendran, P. and Devi, N. B. (2015) 'An overview of fabricating nanostructured electrode materials for biosensor applications', *International Journal of Electrochemical Science*. Electrochemical Science Group, pp. 8607–8629.

Rana, S., Garg, R. K. and Singla, A. (2014) 'Rapid analysis of urinary opiates using fast gas chromatography-mass spectrometry and hydrogen as a carrier gas', *Egyptian Journal of Forensic Sciences*, 4(3), pp. 100–107. doi: 10.1016/j.ejfs.2014.03.001.

Randviir, E. P. and Banks, C. E. (2013) 'Electrochemical impedance spectroscopy: an overview of bioanalytical applications', *Analytical Methods*. Royal Society of Chemistry, 5(5), p. 1098. doi: 10.1039/c3ay26476a.

Rezaei, B., Foroughi-Dehnavi, S. and Ensafi, A. A. (2015) 'Fabrication of electrochemical sensor based on molecularly imprinted polymer and nanoparticles for determination trace amounts of morphine', *Ionics*. Institute for Ionics, 21(10), pp. 2969–2980. doi: 10.1007/s11581-015-1458-3.

Rice, S. and Koziel, J. A. (2015) 'The relationship between chemical concentration and odor activity value explains the inconsistency in making a comprehensive surrogate scent training tool representative of illicit drugs.', *Forensic science international*. Elsevier Ireland Ltd, 257, pp. 257–70. doi: 10.1016/j.forsciint.2015.08.027.

Riquelme, M. V., Zhao, H., Srinivasaraghavan, V., Pruden, A., Vikesland, P. and Agah, M. (2016) 'Optimizing blocking of nonspecific bacterial attachment to impedimetric biosensors', *Sensing and Bio-Sensing Research*, 8, pp. 47–54. doi: 10.1016/j.sbsr.2016.04.003.

Romero Guerra, M., Chianella, I., Piletska, E. V., Karim, K., Turner, A. P. F. and Piletsky, S. A. (2009) 'Development of a piezoelectric sensor for the detection of methamphetamine', *The Analyst*. Royal Society of Chemistry, 134(8), p. 1565. doi: 10.1039/b819351g.

Ronkainen, N. J., Halsall, H. B. and Heineman, W. R. (2010) 'Electrochemical biosensors.', *Chemical Society reviews*, 39(5), pp. 1747–63. doi: 10.1039/b714449k.

Rouessac, F. and Rouessac, A. (2013) *Chemical Analysis: Modern Instrumentation Methods and Techniques*.

Roushani, M. and Shahdost-fard, F. (2016) 'An aptasensor for voltammetric and impedimetric determination of cocaine based on a glassy carbon electrode modified with platinum nanoparticles and using rutin as a redox probe', *Microchimica Acta*. Springer-Verlag Wien, 183(1), pp. 185–193. doi: 10.1007/s00604-015-1604-7.

Rudnicka, J. and Mochalski, P. (2010) 'Application of ion mobility spectrometry for the detection of human urine', *Caspian J. Chem*, 2, pp. 2031–2038. doi: 10.1007/s00216-010-4147-0.

Rushworth, J., Hirst, N., Goode, J., Pike, D., Ahmed, A. and Millner, P. A. (2013) *Impedimetric Biosensors for Medical Applications*, *Asme*. ASME Press. doi: 10.1115/1.860243.

Ruzilawati, A. B., Yusuf, W. N. W., Ramli, N., Hussain, Z. and Rasool, A. H. G. (2013) 'Determination of Morphine in Human Urine by A Simple Reverse Phase High-Performance Liquid Chromatography Method with UV Detection', *International Journal of Pharmaceutical Sciences and Drug Research*, 5(1), pp. 18–22.

Salam, F., Uludag, Y. and Tothill, I. E. (2013) 'Real-time and sensitive detection of Salmonella Typhimurium using an automated quartz crystal microbalance (QCM) instrument with nanoparticles amplification', *Talanta*, 115, pp. 761–767. doi: 10.1016/j.talanta.2013.06.034.

Santos, A. (2014) 'Fundamentals and Applications of Impedimetric and Redox Capacitive Biosensors', *Journal of Analytical & Bioanalytical Techniques*. OMICS International, S7(012). doi: 10.4172/2155-9872.S7-016.

Sarkar, S., Mathwig, K., Kang, S., Nieuwenhuis, A. F. and Lemay, S. G. (2014) 'Redox cycling without reference electrodes', *The Analyst*. NIH Public Access, 139(22), pp. 6052–6057. doi: 10.1039/C4AN01287A.

Schott, M., Klein, B. and Vilcinskas, A. (2015) 'Detection of illicit drugs by trained honeybees (Apis mellifera)', *PLoS ONE*. Public Library of Science, 10(6), p. e0128528. doi: 10.1371/journal.pone.0128528.

Schott, M., Wehrenfennig, C., Gasch, T. and Vilcinskas, A. (2013) 'Insect antenna-based biosensors for in situ detection of volatiles', *Advances in Biochemical Engineering/Biotechnology*. Springer Science and Business Media Deutschland GmbH, 136, pp. 101–122. doi: 10.1007/10_2013_210.

Shang, Z. Y., Han, C. F. and Song, Q. J. (2014) 'An electrochemiluminescence sensor with molecularly imprinted polymer for heroin detection', *Fenxi Huaxue/ Chinese Journal of Analytical Chemistry*, 42(6), pp. 904–908. doi: 10.1016/S1872-2040(14)60748-9.

Shcherbakova, E. G., Zhang, B., Gozem, S., Minami, T., Zavalij, P. Y., Pushina, M., Isaacs, L. D. and Anzenbacher, P. (2017) 'Supramolecular Sensors for Opiates and Their Metabolites', *Journal of the American Chemical Society*. American Chemical Society, 139(42), pp. 14954–14960. doi: 10.1021/jacs.7b06371.

Sheng, Q., Liu, R., Zhang, S. and Zheng, J. (2014) 'Ultrasensitive electrochemical cocaine biosensor based on reversible DNA nanostructure', *Biosensors and Bioelectronics*, 51, pp. 191–194. doi: 10.1016/j.bios.2013.07.053.

Shi, Y., Dai, H., Sun, Y., Hu, J., Ni, P. and Li, Z. (2013) 'Fluorescent sensing of cocaine based on a structure switching aptamer, gold nanoparticles and graphene oxide.', *The Analyst*. The Royal Society of Chemistry, 138(23), pp. 7152–6. doi: 10.1039/c3an00897e.

Singh, K. V., Bhura, D. K., Nandamuri, G., Whited, A. M., Evans, D., King, J. and Solanki, R. (2011) 'Nanoparticle-Enhanced Sensitivity of a Nanogap-Interdigitated Electrode Array Impedimetric Biosensor', *Langmuir*, 27(22), pp. 13931–13939. doi:

10.1021/la202546a.

Skládal, P. (2016) 'Piezoelectric biosensors', *TrAC - Trends in Analytical Chemistry*, 79, pp. 127–133. doi: 10.1016/j.trac.2015.12.009.

Smith, J. P., Metters, J. P., Irving, C., Sutcliffe, O. B. and Banks, C. E. (2014) 'Forensic electrochemistry: the electroanalytical sensing of synthetic cathinone-derivatives and their accompanying adulterants in "legal high" products.', *The Analyst*, 139(2), pp. 389–400. doi: 10.1039/c3an01985c.

Smolinska-Kempisty, K., Ahmad, O. S. S., Guerreiro, A., Karim, K., Piletska, E. and Piletsky, S. (2017) 'New potentiometric sensor based on molecularly imprinted nanoparticles for cocaine detection', *Biosensors and Bioelectronics*. Elsevier Ltd, 96, pp. 49–54. doi: 10.1016/j.bios.2017.04.034.

Sonnberg, S., Armenta, S., Garrigues, S. and de la Guardia, M. (2015) 'Detection of tetrahydrocannabinol residues on hands by ion-mobility spectrometry (IMS). Correlation of IMS data with saliva analysis', *Analytical and bioanalytical chemistry*. Springer Verlag, 407(20), pp. 5999–6008. doi: 10.1007/s00216-015-8784-1.

Stephanson, N., Sandqvist, S., Lambert, M. S. and Beck, O. (2015) 'Method validation and application of a liquid chromatography-tandem mass spectrometry method for drugs of abuse testing in exhaled breath.', *Journal of chromatography. B, Analytical technologies in the biomedical and life sciences*, 985, pp. 189–96. doi: 10.1016/j.jchromb.2015.01.032.

Strano-Rossi, S., Castrignanò, E., Anzillotti, L., Serpelloni, G., Mollica, R., Tagliaro, F., Pascali, J. P., Di Stefano, D., Sgalla, R. and Chiarotti, M. (2012) 'Evaluation of four oral fluid devices (DDS®, Drugtest 5000®, Drugwipe 5+® and RapidSTAT®) for on-site monitoring drugged driving in comparison with UHPLC-MS/MS analysis', *Forensic Science International*, 221(1–3), pp. 70–76. doi: 10.1016/j.forsciint.2012.04.003.

Su, Y., Wang, H., Liu, J., Wei, P., Cooks, R. G. and Ouyang, Z. (2013) 'Quantitative paper spray mass spectrometry analysis of drugs of abuse.', *The Analyst*, 138(16), pp. 4443–7. doi: 10.1039/c3an00934c.

Sun, B., Qi, H., Ma, F., Gao, Q., Zhang, C. and Miao, W. (2010) 'Double covalent coupling method for the fabrication of highly sensitive and reusable electrogenerated chemiluminescence sensors', *Analytical Chemistry*, 82(12), pp. 5046–5052. doi: 10.1021/ac9029289.

Swiss Guidelines Committee for Drugs of Abuse Testing (2012) *Guidelines for Drugs of Abuse Testing*.

Taghdisi, S. M., Danesh, N. M., Emrani, A. S., Ramezani, M. and Abnous, K. (2015) 'A novel electrochemical aptasensor based on single-walled carbon nanotubes, gold electrode and complimentary strand of aptamer for ultrasensitive detection of cocaine', *Biosensors and Bioelectronics*, 73, pp. 245–250. doi: 10.1016/j.bios.2015.05.065.

Talemi, R. P. and Mashhadizadeh, M. H. (2015) 'A novel morphine electrochemical biosensor based on intercalative and electrostatic interaction of morphine with double strand DNA immobilized onto a modified Au electrode', *Talanta*. Elsevier, 131, pp. 460–

466. doi: 10.1016/J.TALANTA.2014.08.009.

Temerdashev, A. Z., Grigoriev, A. M. and Rybalchenko, I. V. (2015) 'Narcotic substances of natural origin and methods of their determination', *Journal of Analytical Chemistry*. Maik Nauka Publishing / Springer SBM, 71(1), pp. 1–21. doi: 10.1134/S1061934816010135.

Thanh Ngo, V. K., Nguyen, D. G., Uyen Nguyen, H. P., Man Tran, V., My Nguyen, T. K., Phat Huynh, T., Vinh Lam, Q., Dat Huynh, T. and Lien Truong, T. N. (2014) 'Quartz crystal microbalance (QCM) as biosensor for the detecting of Escherichia coli O157:H7', *Advances in Natural Sciences: Nanoscience and Nanotechnology*. IOP Publishing, 5(4), p. 045004. doi: 10.1088/2043-6262/5/4/045004.

Thies, J. W., Kuhn, P., Thürmann, B., Dübel, S. and Dietzel, A. (2017) 'Microfluidic quartz-crystal-microbalance (QCM) sensors with specialized immunoassays for extended measurement range and improved reusability', *Microelectronic Engineering*. Elsevier, 179, pp. 25–30. doi: 10.1016/j.mee.2017.04.023.

Tothill, I. E. (2001) 'Biosensors developments and potential applications in the agricultural diagnosis sector', *Computers and Electronics in Agriculture*, 30(1–3), pp. 205–218. doi: 10.1016/S0168-1699(00)00165-4.

Tothill, I. E. (2010) *Peptides as molecular receptors*, *Recognition Receptors in Biosensors*. doi: 10.1007/978-1-4419-0919-0_6.

Tothill, I. E. (2011) 'Biosensors and nanomaterials and their application for mycotoxin determination', *World Mycotoxin Journal*. Wageningen Academic Publishers, 4(4), pp. 361–374. doi: 10.3920/WMJ2011.1318.

Tothill, I. E. and Turner, A. P. F. (2003) 'Biosensors', *Encyclopaedia of food sciences and nutrition*. Academic Press Salt Lake City, UT, USA, pp. 489–499.

Tsai, J. S.-C. and Lin, G. L. (2005) 'CHAPTER 3 Drug-Testing Technologies and Applications', in Wong, Raphael C.; Harley, Y. T. (ed.) *Drugs of Abuse Body Fluid Testing*. Humana Press Inc., pp. 1–308.

Turner, A. P. F. (2013) 'Biosensors: sense and sensibility.', *Chemical Society reviews*, 42(8), pp. 3184–96. doi: 10.1039/c3cs35528d.

Uludag, Y. and Tothill, I. E. (2012) 'Cancer biomarker detection in serum samples using surface plasmon resonance and quartz crystal microbalance sensors with nanoparticle signal amplification', *Analytical Chemistry*. American Chemical Society, 84(14), pp. 5898–5904. doi: 10.1021/ac300278p.

UNODC (1995) 'Rapid testing methods of drugs of abuse'. New York, pp. 1–116.

UNODC (2003) *Terminology and information on drugs*. New York.

UNODC (2009a) *Guidance for the Validation of Analytical Methodology and Calibration of Equipment used for Testing of Illicit Drugs in Seized Materials and Biological Specimens*. New York.

UNODC (2009b) *Recommended methods for the identification and analysis of cannabis*

and cannabis products. New York.

UNODC (2012) *Recommended methods for the Identification and Analysis of Cocaine in Seized Materials*, *United Nations of Drugs and Crime*.

UNODC (2013) *The International Drug Control Conventions*. New York.

UNODC (2015) *World Drug Report 2015*. Vienna.

UNODC (2016) *World drug report 2016*, *United Nations publication*. Vienna. doi: 10.1007/s13398-014-0173-7.2.

UNODC (2017a) *Afghanistan Opium Survey 2017*. Vienna.

UNODC (2017b) *World Drug Report 2017*. Vienna.

Uygun, H. D. E. and Z. O. (2013) *State of the Art in Biosensors - General Aspects*. Edited by T. Rinken. InTech. doi: 10.5772/45832.

Uygun, Z. O. and Ertuğrul Uygun, H. D. (2014) 'A short footnote: Circuit design for faradaic impedimetric sensors and biosensors', *Sensors and Actuators, B: Chemical*. Elsevier, 202, pp. 448–453. doi: 10.1016/j.snb.2014.05.029.

Veitenheimer, A. M. and Wagner, J. R. (2017) 'Evaluation of Oral Fluid as a Specimen for DUID', *Journal of Analytical Toxicology*, 41(6), pp. 517–522. doi: 10.1093/jat/bkx036.

Vergara, A. V., Pernites, R. B., Tiu, B. D. B., de Leon, A. C. C., Mangadlao, J. D., Binag, C. A. and Advincula, R. C. (2016) 'Capacitive Detection of Morphine via Cathodically Electropolymerized, Molecularly Imprinted Poly(*p* -aminostyrene) Films', *Macromolecular Chemistry and Physics*, 217(16), pp. 1810–1822. doi: 10.1002/macp.201600127.

Verkouteren, J. R. and Staymates, J. L. (2011) 'Reliability of ion mobility spectrometry for qualitative analysis of complex, multicomponent illicit drug samples', *Forensic Science International*, 206(1–3), pp. 190–196. doi: 10.1016/j.forsciint.2010.08.005.

Vidal, J. C., Bertolín, J. R., Bonel, L., Asturias, L., Arcos-Martínez, M. J. and Castillo, J. R. (2016) 'A Multi-electrochemical Competitive Immunosensor for Sensitive Cocaine Determination in Biological Samples', *Electroanalysis*, 28(4), pp. 685–694. doi: 10.1002/elan.201500517.

Wackerlig, J. and Lieberzeit, P. A. (2015) 'Molecularly imprinted polymer nanoparticles in chemical sensing–Synthesis, characterisation and application', *Sensors and Actuators B: Chemical*. Elsevier, 207, pp. 144–157.

WADA (2017) *The World Anti-Doping Code Prohibited List Non-Approved Substances Anabolic Agents*. Montreal, Canada.

Wade, L. G. (2010) *Organic chemistry*. 7th Editio. Pearson Prentice Hall.

Wen, T., Wang, R., Sotero, A. and Li, Y. (2017) 'A portable impedance immunosensing system for rapid detection of Salmonella Typhimurium', *Sensors (Switzerland)*.

Multidisciplinary Digital Publishing Institute, 17(9), p. 1973. doi: 10.3390/s17091973.

Wetter, O. E. (2013) 'Imaging in airport security: Past, present, future, and the link to forensic and clinical radiology', *Journal of Forensic Radiology and Imaging*, 1(4), pp. 152–160. doi: 10.1016/j.jofri.2013.07.002.

Weyermann, C., Mimoune, Y., Anglada, F., Massonnet, G., Esseiva, P. and Buzzini, P. (2011) 'Applications of a transportable Raman spectrometer for the in situ detection of controlled substances at border controls', *Forensic Science International*, 209(1–3), pp. 21–28. doi: 10.1016/j.forsciint.2010.11.027.

Whitcombe, M. J. J., Chianella, I., Larcombe, L., Piletsky, S. A. A., Noble, J., Porter, R. and Horgan, A. (2011) 'The rational development of molecularly imprinted polymer-based sensors for protein detection', *Chemical Society Reviews*, 40(3), pp. 1547–1571. doi: 10.1039/c0cs00049c.

WHO (2004) *Neuroscience of Psychoactive Substance Use and Dependence*, *Addiction*. Geneve. doi: 10.1111/j.1360-0443.2004.00906.x.

Wille, S. M. R., Samyn, N., Ramírez-Fernández, M. del M. and De Boeck, G. (2010) 'Evaluation of on-site oral fluid screening using Drugwipe-5+®, RapidSTAT® and Drug Test 5000® for the detection of drugs of abuse in drivers', *Forensic Science International*, 198(1–3), pp. 2–6. doi: 10.1016/j.forsciint.2009.10.012.

Wilson, W. D. (2002) 'Analyzing biomolecular interactions', *Science*. American Association for the Advancement of Science, pp. 2103–2105. doi: 10.1126/science.295.5562.2103.

Wren, S. P., Nguyen, T. H., Gascoine, P., Lacey, R., Sun, T. and Grattan, K. T. V. (2014) 'Preparation of novel optical fibre-based Cocaine sensors using a molecular imprinted polymer approach', *Sensors and Actuators B: Chemical*, 193(193), pp. 35–41. doi: 10.1016/j.snb.2013.11.071.

Wulff, G. (2013) 'Fourty years of molecular imprinting in synthetic polymers: Origin, features and perspectives', *Microchimica Acta*. Springer, 180(15–16), pp. 1359–1370. doi: 10.1007/s00604-013-0992-9.

Yáñez-Sedeño, P., Agüí, L., Villalonga, R. and Pingarrón, J. M. (2014) 'Biosensors in forensic analysis. A review', *Analytica Chimica Acta*, 823, pp. 1–19. doi: 10.1016/j.aca.2014.03.011.

Yang, D., Singh, A., Wu, H. and Kroe-Barrett, R. (2016) 'Comparison of biosensor platforms in the evaluation of high affinity antibody-antigen binding kinetics', *Analytical Biochemistry*. Academic Press, 508, pp. 78–96. doi: 10.1016/J.AB.2016.06.024.

Yang, Y., Pan, J., Hua, W. and Tu, Y. (2014) 'An approach for the preparation of highly sensitive electrochemical impedimetric immunosensors for the detection of illicit drugs', *Journal of Electroanalytical Chemistry*. Elsevier, 726, pp. 1–6. doi: 10.1016/j.jelechem.2014.04.022.

Yang, Z., Castrignanò, E., Estrela, P., Frost, C. G. and Kasprzyk-Hordern, B. (2016) 'Community Sewage Sensors towards Evaluation of Drug Use Trends: Detection of

Cocaine in Wastewater with DNA-Directed Immobilization Aptamer Sensors', *Scientific Reports*, 6, p. 21024. doi: 10.1038/srep21024.

Yeh, W. M. and Ho, K. C. (2005) 'Amperometric morphine sensing using a molecularly imprinted polymer-modified electrode', *Analytica Chimica Acta*, 542(1 SPEC. ISS.), pp. 76–82. doi: 10.1016/j.aca.2005.01.071.

Yoon, J.-Y. (2013) *Chapter 10 Electrochemical Sensors*, *Introduction to Biosensors: From Electric Circuits to Immunosensors*. New York, NY: Springer New York. doi: 10.1007/978-1-4419-6022-1.

Yüce, M. and Kurt, H. (2017) 'How to make nanobiosensors: surface modification and characterisation of nanomaterials for biosensing applications', *RSC Adv.* The Royal Society of Chemistry, 7(78), pp. 49386–49403. doi: 10.1039/C7RA10479K.

Zhang, C.-Y. and Johnson, L. W. (2009) 'Single quantum-dot-based aptameric nanosensor for cocaine.', *Analytical chemistry*. American Chemical Society, 81(8), pp. 3051–5. doi: 10.1021/ac802737b.

Zhang, D., Jiang, J., Chen, J., Zhang, Q., Lu, Y., Yao, Y., Li, S., Logan Liu, G. and Liu, Q. (2015) 'Smartphone-based portable biosensing system using impedance measurement with printed electrodes for 2,4,6-trinitrotoluene (TNT) detection', *Biosensors and Bioelectronics*, 70, pp. 81–88. doi: 10.1016/j.bios.2015.03.004.

Zheng, T., Bott, S. and Huo, Q. (2016) 'Techniques for Accurate Sizing of Gold Nanoparticles Using Dynamic Light Scattering with Particular Application to Chemical and Biological Sensing Based on Aggregate Formation', *ACS Applied Materials & Interfaces*. American Chemical Society, 8(33), pp. 21585–21594. doi: 10.1021/acsami.6b06903.

Zhou, L., Cai, M., Tong, T. and Wang, H. (2017) 'Progress in the Correlative Atomic Force Microscopy and Optical Microscopy', *Sensors*. MDPI AG, 17(4), p. 938. doi: 10.3390/s17040938.

Zhou, W., Su, M. and Cai, X. (2017) 'Advances in nanoparticle sizing in suspensions: Dynamic light scattering and ultrasonic attenuation spectroscopy', *KONA Powder and Particle Journal*. Hosokawa Powder Technology Foundation, 2017(34), pp. 168–182. doi: 10.14356/kona.2017022.

WEB REFERENCES

MCDDA website

http://www.emcdda.europa.eu/countries

UNODC website

https://www.unodc.org/

IONSCAN500DT

https://www.smithsdetection.com/index.php?option=com_k2&view=item&id=115:ionscan-500dt&Itemid=1427#.VxELN_krLq6

BIOSENS®

http://biosensor.se/drugs/

UK Law

http://www.cps.gov.uk/

SupelMIP ® SPE cartridge (Sigma-Aldrich Company Ltd, Dorset, UK))

http://www.sigmaaldrich.com/analytical-chromatography/sample-preparation/spe/supelmip.html

APPENDICES

Appendix A Commercially available Immune Device

Table_Apx A-1: Overview of commercially and under development on-site immune-based screening kits and devices.

Image	Immuno-Assay	Type	Sample matrix	Ligand	Assay principle	Targets	Time (minutes)	UK approved	Ref
	Bio-nano-chip system	Optical sensor	Oral fluids	Ab	competitive immunoassay	Tetrahydrocannabinol, Morphine, Amphetamine, Methamphetamine, Cocaine, Methadone And Benzodiazepines	10	N	(Christodoulides *et al.*, 2015)
	Alere DDS2 Mobile Test System (DDS2)	Strip device (strip kit and reader)	Oral fluids	Ab	chromatographic competitive inhibition immunoassay	Amphetamine	8-10	N	(Moore, Kelley-Baker and Lacey, 2013)
						Benzodiazepines		N	
						tetrahydrocannabinol (THC)		N	
						Cocaine		N	
						Methamphetamine		N	
						Opiates		N	
						Methadone		N	
	Cozart Cocaine test kit (Cozart Bioscience Ltd)	Strip kit	Suspected substances	Ab	chromatographic competitive inhibition immunoassay	Cocaine and crack cocaine.		Y	Home Office Circular 015/2012
	Drug-ID® cocaine test kit	Strip kit	Suspected substances	Ab	chromatographic competitive inhibition immunoassay	Cocaine		Y (cocaine only)	Home Office Circular 015/2012
	Draäger DrugTest®5000	Analyser and test kit.	Oral fluids	Ab	chromatographic competitive inhibition immunoassay	Amphetamine	8-10	N	(Musshoff *et al.*, 2014)
						Benzodiazepines			
						tetrahydrocannabinol (THC)			
						Cocaine			
						Methamphetamine			
						Opiates			

Image	Immuno-Assay	Type	Sample matrix	Ligand	Assay principle	Targets	Time (minutes)	UK approved	Ref
	Mavand RapidSTAT®	Strip device (strip kit and reader)	Oral fluids		chromatographic competitive inhibition immunoassay		6 - 8	N	(Wille *et al.*, 2010)
	Cozart DDS 801 test®	Strip test with reader	Oral fluids	Ab	chromatographic competitive inhibition immunoassay	Amphetamines, Methamphetamine, Cannabinoids, Opiates And Cocaine	10	N	(Arroyo *et al.*, 2013)
	Securetec Drugwipe-5®	Strip kit	Oral fluids	Ab	chromatographic competitive inhibition immunoassay	Cannabis (Marihuana/Hashish/THC), Amphetamines/Methamphetamines/ Ecstasy, Cocaine/Crack, Opiates (Morphine/Heroin)	3 to 8	N	(Wille *et al.*, 2010)
	DrugScreen	Strip test	Urine	Ab	chromatographic competitive inhibition immunoassay	Amphetamine, Benzodiazepines, Cocaine, Morphine, tetrahydrocannabinol (THC).	5 to 10	N	(Musshoff *et al.*, 2014)

Appendix B Electrodes Specifications

This Appendix provides the specifications of each electrode used in this work and as issued by the retailer.

B.1 DropSens SPE (DPR C220AT)

Figure_Apx B-1: DPR C220AT electrode specification as provided by DropSens.

B.2 DropSens IDE (DPR IDEAu5)

Figure_Apx B-2: DPR IDEAu5 electrode specification as provided by DropSens.

B.3 Micrux IDE (ED IDE 3 Au)

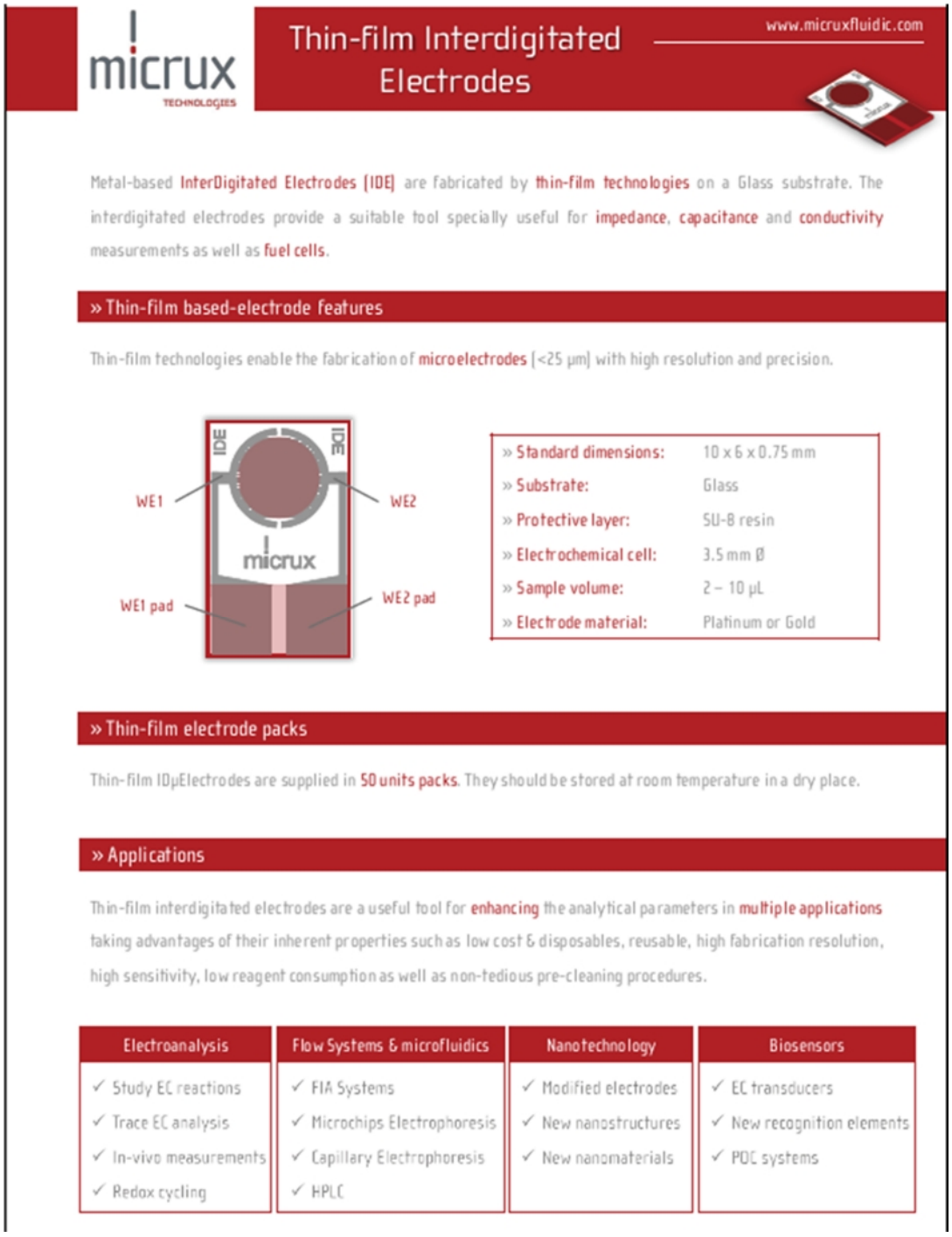

Figure_Apx B-3: Micrux ED IDE 3 Au electrode specification as provided by Micrux (page 1).

micrux TECHNOLOGIES

Thin-film Interdigitated Electrodes

www.micruxfluidic.com

» Electrochemical cell

The most basic **interdigitated electrodes** (IDE) consist of **two individually addressable microelectrode array strips with an interdigitated approach**. Non additional reference and auxiliary electrodes are included on the device.

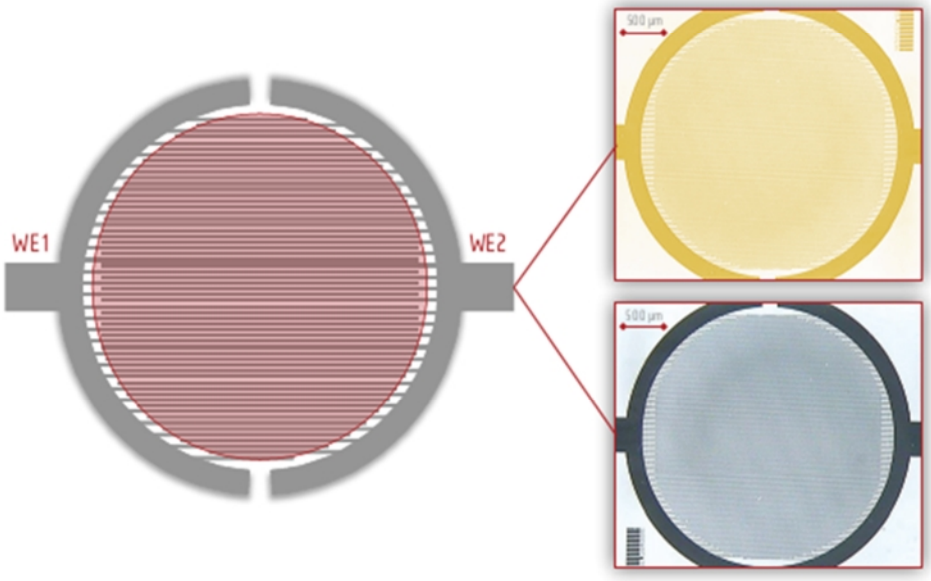

These lineal-band electrodes have been specially designed in a circular cell to work with very small sample drops (< 10 µL). The sample drop shape is well-adapted to the electrode cell in order to get the maximum performance and precision.

» Interdigitated electrodes

InterDigitated Electrode (IDE) designs are available in platinum or gold with different widths and gaps.

Reference	Material	µElectrode width	µElectrode gap	Number of feet	Thickness
» *ED-IDE1-Pt*	Ti/Pt	10 µm	10 µm	90 pairs	50/150 nm
» *ED-IDE2-Pt*	Ti/Pt	10 µm	5 µm	120 pairs	50/150 nm
» *ED-IDE3-Pt*	Ti/Pt	5 µm	5 µm	180 pairs	50/150 nm
» *ED-IDE1-Au*	Ti/Au	10 µm	10 µm	90 pairs	50/150 nm
» *ED-IDE2-Au*	Ti/Au	10 µm	5 µm	120 pairs	50/150 nm
» *ED-IDE3-Au*	Ti/Au	5 µm	5 µm	180 pairs	50/150 nm

Figure_Apx B-4: Micrux ED IDE 3 Au electrode specification as provided by Micrux (page 2).

Appendix C DLS Size Intensity Graphs

This appendix provide the DLS quality report related to each nanoMIPs analysed within the characterisation study.

C.1 Cocaine nanoMIP

C.1.1 Batch 2

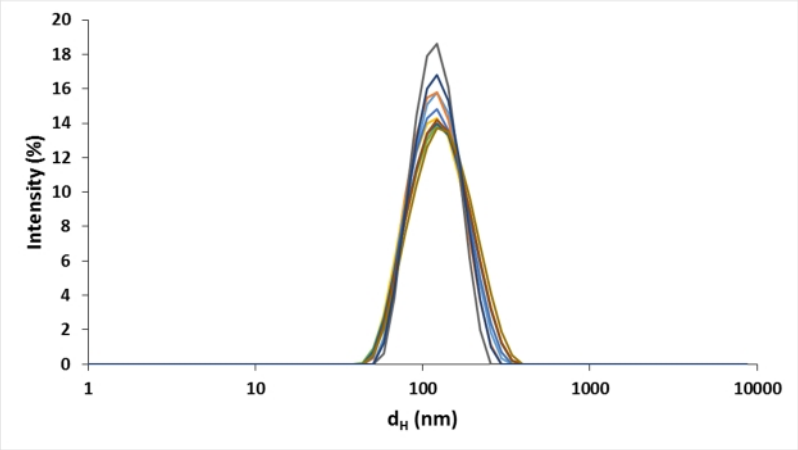

Figure_Apx C-1: Size distribution by intensity of 10 DLS records of cocaine nanoMIP batch 2.

C.1.2 Batch 3

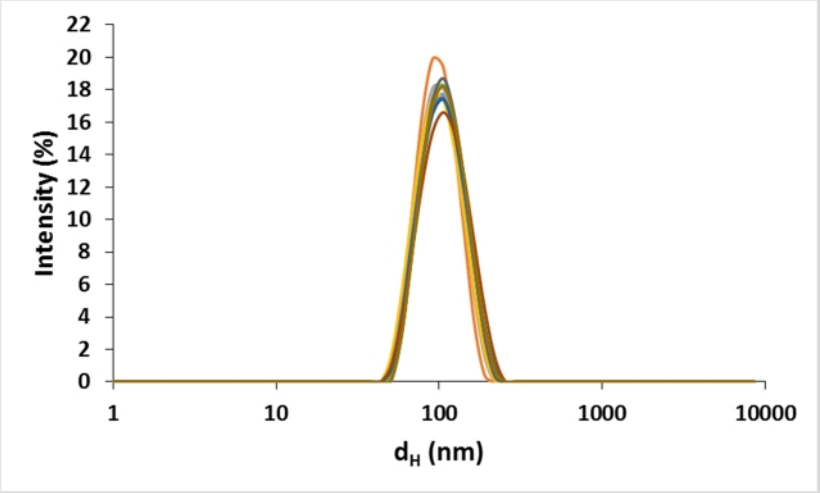

Figure_Apx C-2: Size distribution by intensity of 10 DLS records of cocaine nanoMIP batch 3.

C.1.3 Batch 4

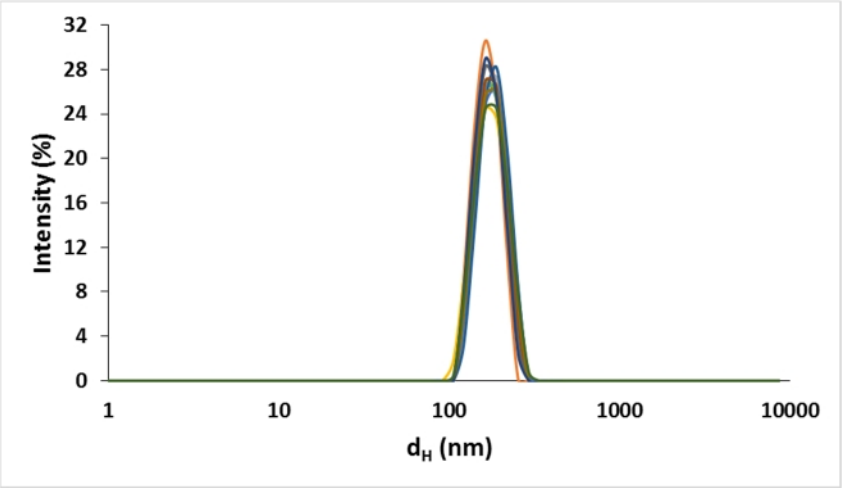

Figure_Apx C-3: Size distribution by intensity of 10 DLS records of cocaine nanoMIP batch 4.

C.1.4 Batch 5

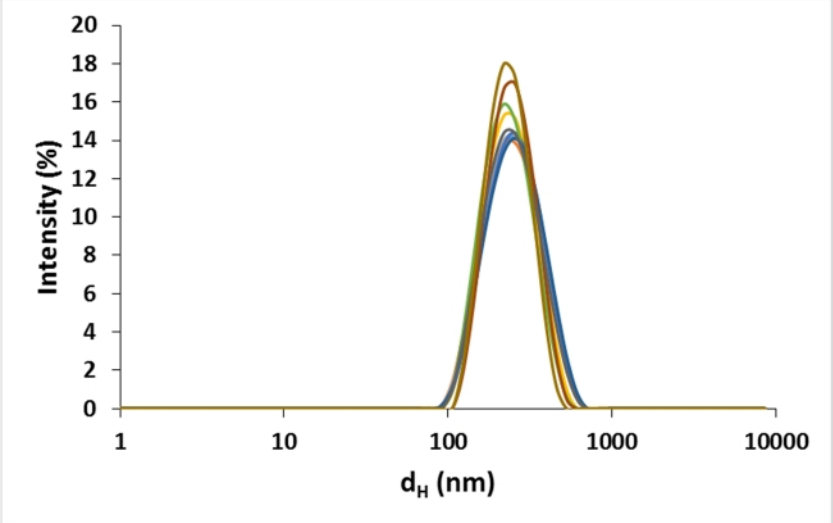

Figure_Apx C-4: Size distribution by intensity of 10 DLS records of cocaine nanoMIP batch 4.

C.2 Morphine nanoMIP

C.2.1 Batch 2

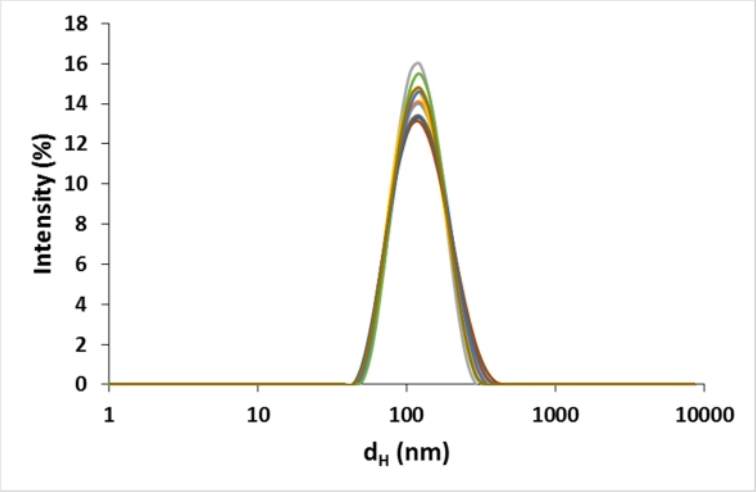

Figure_Apx C-5: Size distribution by intensity of 10 DLS records of morphine nanoMIP batch 2.

C.2.2 Batch 3

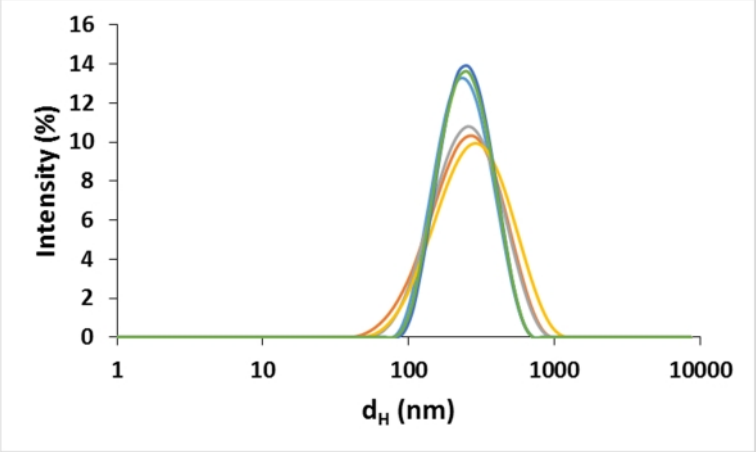

Figure_Apx C-6: Size distribution by intensity of 6 DLS records of morphine nanoMIP batch 3.

C.2.3 Batch 4

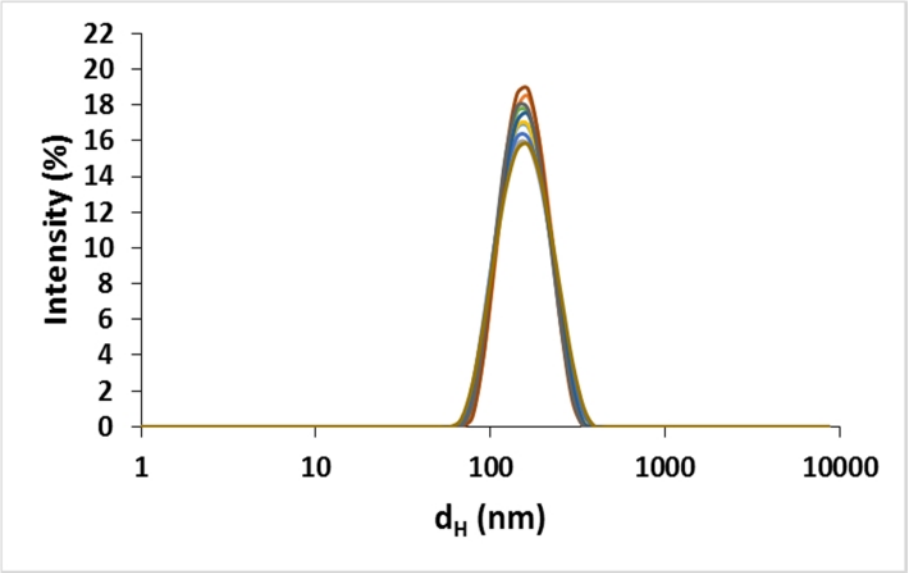

Figure_Apx C-7: Size distribution by intensity of 10 DLS records of morphine nanoMIP batch 4.

C.2.4 Batch 5

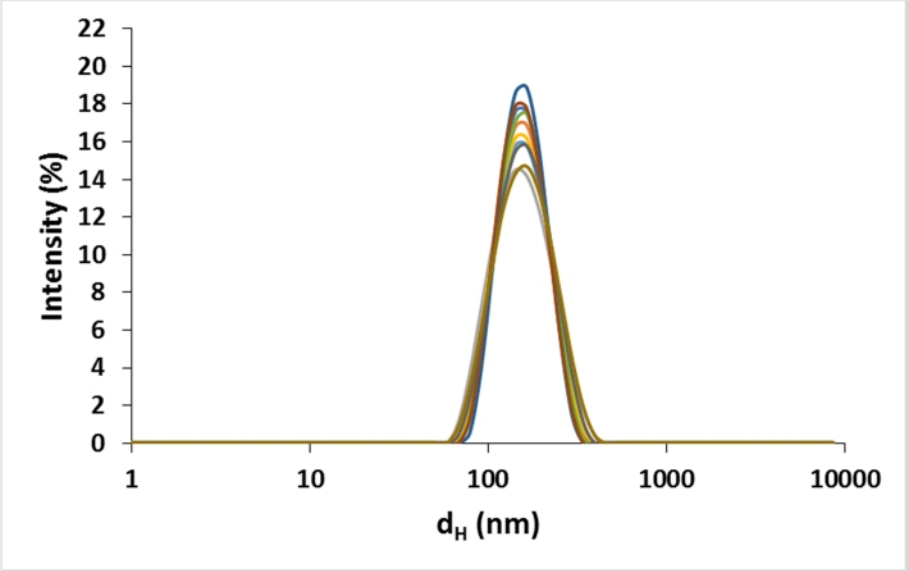

Figure_Apx C-8: Size distribution by intensity of 10 DLS records of morphine nanoMIP batch 5.

Appendix D Conferences, Posters and Publications

D.1 List of Conferences

- Rapid Method Europe 2016 (**RME 2016**). Amsterdam, The Netherlands. 7 – 9 November 2016.
- 5th International Conference on Bio-Sensing Technology (**BITE 2017**). Riva del Garda, Italy. 7 - 10 May 2017
- Female Researcher Network Lecture 2017. Cranfield University, United Kingdom. 19 June 2017.
- 28th Anniversary World Congress on Biosensors (**BIOS 2018**). Miami, Florida, USA. 12-15 June 2018.

D.2 Posters

NanoMIP-EIS Sensor: A Fast Method to Detect Traces of Drugs of Abuse

R. D'Aurelio[1], I. Chianella[1], K. Smolinska-Kempisty[2], E. Piletska[2], S. Piletsky[2], I.E. Tothill[1*]*

[1]Cranfield University, Cranfield, Bedfordshire, MK43 0AL, England, UK
[2]University of Leicester, Leicester LE1 7RH, England, UK

Introduction

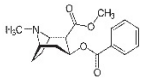

Cocaine
MW=303

Among all drugs of abuse, cocaine is the most commonly illicit stimulant used in European Countries. From security outlook, cocaine illicit market is worth around 6 billion Euros yearly. In order to prevent illicit cocaine trafficking and their use, it is vital to identify and to promptly screen suspected items/substances. Currently, on-site screening methods rely on Ion mobility spectroscopy (IMS), competitive inhibition immunoassay in lateral flow format, and colorimetric tests. Nevertheless, these methods provide only qualitative or semi-quantitative results and require trained personnel to conduct the assay.
Presently, electrochemical impedance spectroscopy (EIS) is gaining popularity, due to the outstanding performance in detecting target molecules at very low concentrations. At the same time, nanoscale molecular imprinting polymers (nanoMIPs) are considered highly sensitive receptor molecules, hence, this work combines the two technologies in order to construct a NanoMIP-EIS-Sensor able to detect cocaine at trace levels.

Methodology

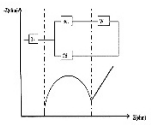

Equivalent circuit used to fit the EIS experimental data.

Cocaine nanoMIP and nanoNIP were synthesised according to a solid phase method. Transmission electron microscopy (TEM) was used to characterise the nanoMIPs. Both nanoMIP/nanoNIP surfaces were functionalised with amino group, thus allowing their attachment onto the gold working electrode, as schematically illustrated in **Fig 1.**

Cocaine hydrochloride (HCl) solutions were then incubated onto both sensors in an cumulative assay (n=3). EIS experimental data, fitted in an equivalent circuit, were used to evaluated the sensor assembly process and the cumulative assays outcomes. Atomic force microscopy (AFM) was also used to characterised the sensor surface.

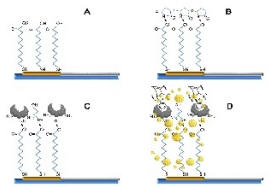

Fig 1. Schematic representation of the sensor surface assembly (A,B,C) and the analyte detection via Faradaic EIS technique (D).

Results

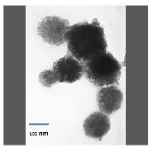

Fig 2. TEM image of cocaine nanoMIP. The average size is around 148 ±3.98 nm.

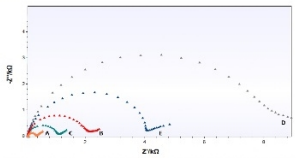

Fig 3. Nyquist plots obtained during Cocaine nanoMIP EIS sensor fabrication. A) bare electrode; B) SAM; C) EDC NHS activation; D) NanoMIP attachment; E) ethanolamine blocking.

Table 1. Cocaine HCl dilutions.

Label	ng mL^{-1}
a	BLANK
b	0.3
c	0.75
d	0.5
e	5
f	10
g	25

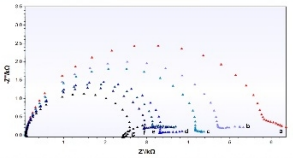

Fig 4. Nyquist plots gathered during the cumulative assay over nanoMIP EIS sensor. Cocaine is an electroactive substance, hence when the cocaine concertation increase (**Table 1**) the Rct decrease.

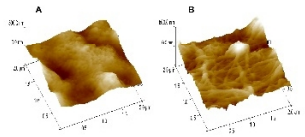

Fig 5. AFM 3D images related to WE of the SPE before (**A**) and after (**B**) the cocaine nanoMIP sensor construction onto the WE surface.

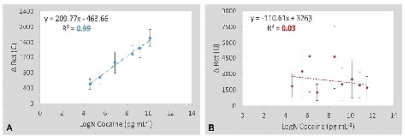

Fig 6. Linear regression plots related to the processed data of the cumulative assays performed onto three cocaine nanoMIP sensors (**A**) and three nanoNIP EIS sensors (**B**). The error bars refer to the SD (±) of the triplicates.

Conclusion

The work shows preliminary results of the construction and development of a cocaine nanoMIP sensor based on an EIS readout. The sensor has shown reproducible data in detecting the cocaine HCl in water solution when compared to nanoNIP sensor. Further investigations and optimisations have to be carried out to confirm the results and stabilise the nanoNIP sensor results. In comparison to existing screening immunoassays (i.e. ELISA and lateral flow devices), the presented nanoMIP EIS sensor has been developed in a direct and real-time platform, thus being faster than these methods. Furthermore, the LOD of the cocaine nanoMIP EIS sensor was as low as 0.52 ng mL^{-1}, which is similar to the LODs reported by the majority of current screening methods.

*Corresponding Authors:
i.tothill@cranfield.ac.uk
i.chianella.1998@cranfield.ac.uk
www.cranfield.ac.uk

Acknowledgement
This research is financially supported by European Commission under the project number 653839

Presented at:

Rapid Method Europe 2016 (**RME 2016**). Amsterdam, The Netherlands. 7 – 9 November 2016.

NanoMIP-EIS- Sensor for Cocaine Detection

R. D'Aurelio[1], I. Chianella[1*], K. Smolinska-Kempisty[2], E. Piletska[2], S. Piletsky[2], I.E. Tothill[1*]

[1]Cranfield University, Cranfield, Bedfordshire, MK43 0AL, England, UK
[2]University of Leicester, Leicester LE1 7RH, England, UK

Introduction

Among all drugs of abuse, cocaine is the most commonly illicit stimulant used in European Countries. From security outlook, cocaine illicit market is worth around 6 billion Euros yearly. In order to prevent illicit cocaine trafficking and their use, it is vital to identify and to promptly screen suspected items/substances. Currently, on-site screening methods rely on Ion mobility spectroscopy (IMS), competitive inhibition immunoassay in lateral flow format, and colorimetric tests. Nevertheless, these methods provide only qualitative or semi-quantitative results and require trained personnel to conduct the assay.
Presently, electrochemical impedance spectroscopy (EIS) is gaining popularity, due to the outstanding performance in detecting target molecules at very low concentrations. At the same time, nanoscale molecular imprinting polymers (nanoMIPs) are considered highly sensitive receptor molecules, hence, this work combines the two technologies in order to construct a NanoMIP-EIS-Sensor able to detect cocaine at trace levels.

Methodology

Cocaine nanoMIPs were synthesised according to a solid phase method. Transmission electron microscopy (TEM) was used to characterise the nanoMIPs. The nanoMIPs surface was functionalised with amino group, thus allowing their attachment onto the gold working electrode, as schematically illustrated in **Fig 1.**

Cocaine hydrochloride (HCl) solutions were then incubated onto the sensor in an cumulative assay (n=3). The specificity of the sensor surface was tested against two common cutting agents, i.e. caffeine and levamisole. EIS experimental data, fitted in an equivalent circuit, were used to evaluate the sensor assembly process and the cumulative assays outcomes. Atomic force microscopy (AFM) was also used to characterise the sensor surface.

Results

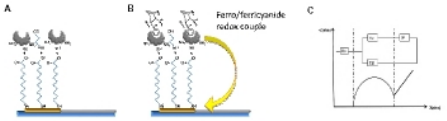

Fig 1. Schematic representation of the sensor surface assembly (A) and the analyte detection via Faradaic EIS technique (B). Equivalent circuit used to fit the EIS experimental data (C).

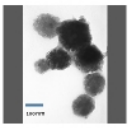

Fig 2. TEM image of cocaine nanoMIP. The average size is around 148 ±3.98 nm.

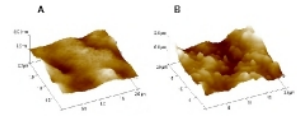

Fig 3. AFM 3D images related to WE of the SPE before (**A**) and after (**B**) the cocaine nanoMIP sensor construction onto the WE surface.

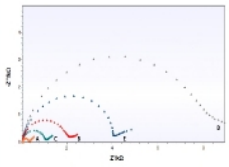

Fig 4. Nyquist plots obtained during Cocaine nanoMIP EIS sensor fabrication. A) bare electrode; B) SAM; C) EDC NHS activation; D) NanoMIP attachment; E) ethanolamine blocking.

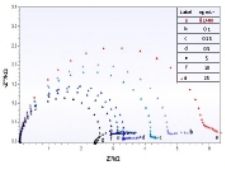

Fig 5. Nyquist plots gathered during the cocaine cumulative assay over nanoMIP EIS sensor. Cocaine is an electroactive substance, hence when the cocaine concertation increases (inlet **Table**) the Rct decreases.

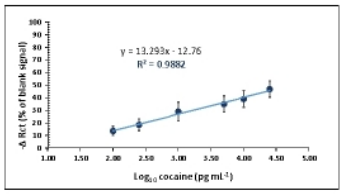

Fig 6. Linear regression plots related to the processed data of the cumulative assays performed onto three cocaine nanoMIP sensors. The LOD was calculated to be as low as 0.52 ng mL^{-1}. The error bars refer to the SD (±) of the triplicates.

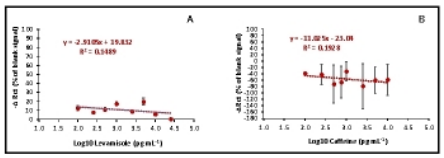

Fig 7. Linear regression plots related to the specificity assay performed with levamisole (A) and caffeine (B) onto three cocaine nanoMIP sensors. The error bars refer to the SD (±) of the triplicates. Notably, all the %Rct values achieved during the specificity assays are below the %Rct of the LOD value.

Conclusion

The work shows the results of the construction and development of a cocaine nanoMIP sensor based on an EIS readout. The sensor has shown reproducible data in detecting the cocaine HCl. The NanoMIP EIS based sensor was also able to discriminate the cocaine from two actual major cutting agents, specifically levamisole and caffeine.
In comparison to existing screening immunoassays (i.e., ELISA and lateral flow devices), the presented nanoMIP EIS sensor has been developed in a direct and real-time platform, thus being faster than these methods. Furthermore, the LOD of the cocaine nanoMIP EIS sensor was as low as 0.52 ng mL^{-1}, which is similar to the LODs reported by the majority of current lab-based screening methods.

Corresponding Authors:

i.tothill@cranfield.ac.uk

i.chianella.1998@cranfield.ac.uk

www.cranfield.ac.uk

Acknowledgement
This research is financially supported by European Commission under the project number 653839

Presented at:

5th International Conference on Bio-Sensing Technology (**BITE 2017**). Riva del Garda, Italy. 7 - 10 May 2017.

Development of nanoMIP-SPR sensor for milk allergens detection

R. D'Aurelio[1], J. Ashley[1], T. Rodgers[2], J. Temblay[3], R. Willey[3], I.E. Tothill[1]*

[1]Cranfield University, UK; [2]University of Manchester, UK; [3]SEAC, Unilever plc, UK

Introduction

Due to the increase in incidence of milk allergy and the possible severe clinical problems associated with it, industries urges for an effective and rapid analytical tools to detect milk allergens cross-contamination during dairy free products processing.
This work illustrates the development of an innovative, yet specific and sensitive SPR affinity sensor, designed in a label-free direct assay for milk proteins analysis. Nanoscale molecular imprinting polymers (nanoMIPs) were synthesised and used as the receptor particles to overcome the limitations posed by biological receptor (i.e., antibody). The whey protein, β-lactoglobulin (BLG), was used as a target analyte, since it is a good indicator of both milk and whey contaminations and it is also most frequently reported in allergic responses.

Methods

BLG nanoMIP were synthesised according to the solid phase method. Freeze drying was used to evaluate the nanoMIPs production yield. Dynamic Light Scattering (DLS) and Transmission electron microscopy (TEM) were used for the nanoMIPs size characterisation study. The nanoMIPs surfaces were functionalised with amino group asa core shell synthesis, thus allowing direct immobilisation of the MIP onto the SPR sensor surface. Cumulative assay was performed by injecting increasing concentration of BLG (1 ng – 100 µg mL^{-1}). Vancomycin nanoMIP were used as the control MIP. The BLG nanoMIP SPR sensor specificity was evaluated by injecting other milk allergens (α-casein, k-casein, Lactoferrin) onto the BLG nanoMIP SPR sensor and by comparing the related dissociation constant (K_D) values.

Results

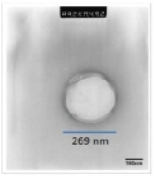

Fig 1. Typical TEM image of the BLG nanoMIP. The nanoMIP average size was 252 ±4.5 nm, in agreement with DLS results.

A)

Batch	Average size (nm)	SD (±)	PDI	SD (±)
1	287.03	9.42	0.30	0.01
2	264.88	3.81	0.20	0.02
3	293.7	12.05	0.14	0.12

B)

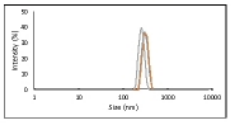

Fig 2. A) DLS Average sizes (±SD) and Polydispersity Index (±SD) for each batch production have been reported in the table. The overall average among the three batch was 281.87 (± 4.20). **B)** A typical DLS graph of size distribution by intensity of the BLG nanoMIP.

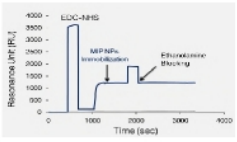

Fig 3. A sensorgram of the BLG nanoMIPs immobilisation onto the gold SPR sensor chip.
The nanoMIPs were immobilised through an amine coupling method on the sensor surfaces. The average of the RU value achieved over three replicates was 1320 (± 221).

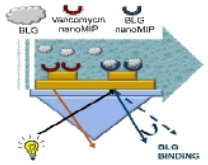

Fig 4. A schematic of the MIP assay on the SPR sensor. BLG nanoMIP and Vancomycin nanoMIP were covalently attached via amine coupling onto the SPR active and control spots, respectively. The surface was blocked using ethanolamine.
Cumulative assay were performed injecting several concentrations of BLG onto both spots, ranging from 1 ng to 1 100 µg mL^{-1}.

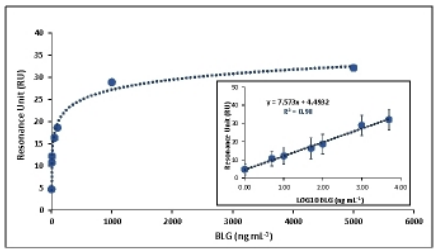

Fig 5. Non-linear and linear regression curves of the BLG cumulative assay. Resonance Unit (RU) values were obtained by subtracting the blank and the control RU signals. The error bars refer to the SD(±) of three replicates. The achieved LOD was as low as 3.10 ng mL^{-1}.

A)

Milk Allergens	Binding affinity K_D (M) BLG MIP-NPs
β-lactoglobulin	7.454×10^{-9}
Lactoferrin	2.08×10^{-4}
α-casein	3.175×10^{-4}
k-casein	3.061×10^{-4}

B)

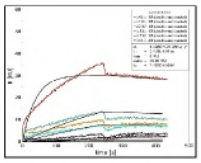

Fig 6. A) The dissociation constant (K_D) values obtained from kinetic studies, showing that the BLG nanoMIPs have higher affinity for BLG compared to the others milk allergens proteins. **B)** The sensorgram in the form of overlay plot and the results obtained by fitting the data to 1:1 Langmuir binding model.

Conclusion

This work shows the results of the development of an SPR based nanoMIP sensor specifically designed to detect BLG whey protein. BLG nanoMIP were designed and successfully synthesised using solid phase synthesis, with good quality production. Furthermore, the nanoMIP were used to develop the SPR affinity sensor achiving an LOD of 3.10 ng mL^{-1}. This is well below the actual required detection level of 2 ppm. Kinetic study results suggest that the sensor has the ability to selectively bind BLG, thus discriminating it from other whey protein (Lactoferrin) and from the casein milk fraction (α-casein, k-casein). Compare to other technologies, the developed BLG nanoMIP SPR sensor offers a valid, fast and real-time analytical platform for allergens analysis in a range of products and for unintentional cross-contamination events.

*Corresponding Authors: Prof Ibtisam E. Tothill

i.tothill@cranfield.ac.uk

www.cranfield.ac.uk

Acknowledgement
This research was partially financially supported by Innovate UK

Presented at:

5th International Conference on Bio-Sensing Technology (**BITE 2017**). Riva del Garda, Italy. 7 - 10 May 2017.

D.3 Publications

- Roberta D'Aurelio, Iva Chianella, Katarzyna Smolinska-Kempisty, Elena Piletska, Sergey Piletsky, Jack Goode, Ibtisam E. Tothill. *NanoMIPs – Electrochemical Impedance Spectroscopy based Sensor for Cocaine Detection. (*On-going submission).
- Roberta D'Aurelio, Iva Chianella, Keith Rogers, Ibtisam E. Tothill. *Analytical Tools for Drugs of Abuse Detection: a Review*. (In preparation).
- Roberta D'Aurelio, Iva Chianella, Katarzyna Smolinska-Kempisty, Elena Piletska, Sergey Piletsky, Jack Goode, Ibtisam E. Tothill. *Morphine Detection through NanoMIPs – Electrochemical Impedance Spectroscopy Based Sensor. (*In preparation).
- Roberta D'Aurelio, Maria Salbini, Iva Chianella, Francesca Calò, Cosimino Malitesta, Ibtisam E. Tothill. *AuNPs Enhanced NanoMIPs QCM Sensor For Drugs of Abuse Detection*. (In preparation).